FORSCHUNGSZENTRUM ROSSENDORF
WISSENSCHAFTLICH-TECHNISCHE BERICHTE
**FZR-285**
März 2000

# Annual Report 1999
# Institute of Radiochemistry

**Editor:** Prof. Dr. G. Bernhard

**Editorial staff:** Dr. H.-J. Engelmann
Prof. Dr. G. Bernhard

# Foreword

Remarkable progress was achieved in the reported period with regard to the Institute´s goal of contributing through basic and applied research to a better understanding of radionuclide migration in the environment.
The following original papers illustrate our scientific progress in our research topics:

- speciation and migration of radionuclides
- organic matter and its interaction with radionuclides
- interaction of microorganisms with radionuclides
- application of X-ray absorption spectroscopy
- behavior of colloids
- chemistry of the heaviest elements.

The first XAFS measurements of aqueous solutions containing plutonium were an important milestone for the beamline ROBL and a highlight of our research work. The goal of these measurements was twofold:

1) We wanted to demonstrate that it is possible to prepare and transport plutonium solutions from our radiochemical laboratories to the ESRF and to carry out high-quality measurements of XANES and EXAFS spectra of these samples. This was to encourage scientists in other institutions worldwide to experiment with radioactive samples in cooperation with us.
2) The hydrate is the simplest chemical form of plutonium in aqueous solution. Knowledge of the structural parameters of the hydration sphere is important for the interpretation of EXAFS results on complicated aqueous plutonium complexes or sorbates where the water molecules are partly or fully replaced by other ligands.

We extended our experimental capabilities for EXAFS measurements at ROBL by installing a helium cryostat for actinide compounds inside the glovebox. At low temperatures of 20 K the EXAFS oscillations due to the thermal vibrations are greatly reduced. This makes it possible to measure the EXAFS over a larger *k* range and to determine interatomic uranium-uranium distances of up to 7 Å.

We made further progress with our synthetic humic acid model substances by preparing humic acids (HAs) with varying concentrations of functional groups, e.g., HAs with blocked carboxylic and phenolic OH groups. We synthesized various chemically modified $^{13}$C-labeled HAs, using $^{13}$C-diazomethane as a methylation agent. The recorded $^{13}$C-CP/MAS-NMR spectra showed that during this reaction carboxylic and acidic OH groups of the HAs are methylated. The methyl ester groups formed are hydrolyzed into carboxyl groups by treatment with NaOH, while the phenolic OH groups remain blocked. In continuation of our work we studied the influence of phenolic OH groups on the complexation of HAs with uranium, using chemically modified synthetic and natural HAs. Laser spectroscopic measurements provided evidence that the loading capacity of HAs with blocked phenolic OH groups to uranium is lower than that of unmodified HAs.

The lower oxidation states of the actinide elements are predominant under reducing conditions in geochemical systems such as aquifers. In the future we will increasingly focus our investigations on these conditions. During the reported period we investigated the chemistry of uranium(IV). As a result the complex formation constant of U(IV) with phosphoric acid was determined for the first time.

The experiments and the modeling of uranium (VI) sorption onto phyllite are now completed. We modeled the sorption of U(VI) with the Diffuse Double Layer Model (DDLM), using the primary main mineralogical constituents of phyllite, i.e. quartz, chlorite muscovite, and albite and, as an additional component, the formed iron oxide hydroxide mineral ferrihydrite. The modeling indicated that the uranyl sorption onto ferrihydrite dominated the sorption onto phyllite. This result shows the great importance of secondary iron phases for sorption processes under environmentally relevant conditions.
We obtained some first results concerning the influence of organic coatings and microorganisms (biofilms) on actinide sorption. Ferrihydrite dominates the sorption of uranium (VI) onto phyllite also in presence of humic acids. We successfully prepared *a Thiobacillus ferrooxidans* film on the phyllite surface.
Bacterial diversity was studied in water samples from various uranium mill-tailings and uranium mining disposal sites. The composition of the bacterial communities differs significantly between the environments studied. The predominant bacterial groups studied in the water samples were site specific. A microdiversity between the natural *Thiobacillus ferrooxidans* uranium waste pile isolates was found for the first time. This microdiversity is not only reflected in the 16S rRNA gene structure but also in the interactions (biosorption and tolerance) of the various *Thiobacillus ferrooxidans* eco types with U(VI). The results obtained by the use of laser fluorescence and infrared spectroscopy demonstrate that the nature and the strength of the uranium complexes formed with the cell wall polymers of the *Thiobacillus ferrooxidans* isolates are type-specific. One of the uranium mining waste *Bacillus* isolates (*B. sphaericus* JG-A12) possesses a surface S-layer with a novel protein structure. The formation of metal clusters on this S-layer was demonstrated. The intact cells of the *Bacillus* uranium waste

isolates, *B. sphaericus* and *B. cereus*, can bind much larger amounts of U (VI) than *T. ferrooxidans*. However, the complexes formed are weaker than those formed with *Thiobacillus ferrooxidans*. Using laser fluorescence and X-ray absorption methods we found that in the case of *Bacilli* uranium is bound mainly by the phosphate groups of the cell walls.

The behavior of environmental colloids was studied in an acid rock drainage (ARD) solution from an abandoned mine at Freiberg. We found that the water contained two kinds of colloid particles of different size: a population of 70 to 250 nm in a concentration of less than 50 mg/L, and a population of ultra fine particles smaller than 5 nm in a concentration of 1g/L. About 80% of the lead, 50% of the arsenic and 15% of the iron were in colloidal form. The number of possible minerals forming the particles was limited by geochemical modeling calculations. These results provide the basis for future X-ray absorption measurements for the characterization of minerals in these colloids.

Although research into the chemistry of the heaviest elements is not in the mainstream of our Institute, staff members made a significant contribution to a large international project (PSI Villigen, CH; LBNL, USA; FZR, D; GSI Darmstadt, D; JINR, RU).
The element bohrium (Z=107) was chemically characterized for the first time.
Bohrium forms a volatile oxychloride, presumably $BhO_3Cl$. From the experimental data it was concluded that this heaviest element can be placed in the expected position in group seven of the Periodic Table. The Rossendorf group prepared the detection system ROMA for the exacting demands of this experiment (detection of only six Bh-267 atoms) and participated in the four-week experimental run.

During the reported period we submitted seven additional EU projects. The EU projects “HUMICS” and “RESTRAT“ were successfully finished. Three specific projects received financial support from the Federal Ministry for Education and Research (BMB+F) and the German Research Community (DFG).

It was a great honor and pleasure for us that Professor U. Abram from our Institute was offered a professorship in radiochemistry at the Freie Universität Berlin.

The Institute would like to thank all friends and organizations that supported its advance. We would also like to thank all visitors and scientific collaborators for their interest in and support of our research.

Dresden, January 2000

Prof. Dr. habil. Gert Bernhard
Acting Director

# CONTENTS

# I. SCIENTIFIC CONTRIBUTIONS

# Speciation and Migration of Radionuclides

# COMPLEX FORMATION OF URANIUM (IV) STUDIED BY LASER-INDUCED PHOTOACOUSTIC SPECTROSCOPY (LIPAS)

G. Geipel, G. Bernhard

*In continuation of the studies of the complex formation of uranium(IV) in the phosphate system we used the LIPAS technique for studies at lower uranium and acid concentrations. Isosbestic points were found at the same wavelength as in the UV-vis measurements. The complex formation constant at an ionic strength of 0.1 M was calculated to be log $k_1$ = 4.83 ± 0.12.*

We studied the complex formation between uranium(IV) and phosphate in the concentration range from $2 \cdot 10^{-4}$ to $5 \cdot 10^{-4}$ M using conventional UV-vis spectroscopy /1/. A relatively high acid concentration was necessary in this system to avoid precipitation of uranium phosphates. The ionic strength of the solution was therefore 0.5 M and higher. Lower concentrations of uranium(IV) cannot be studied by this technique because the spectra already show background noise. To get the complex formation reaction and the formation constant at infinite solution it is necessary to study the complex formation in this system depending on the pH and on the ionic strength. Studies at lower uranium concentrations had to be carried out. Some first results will be given.

The design of LIPAS is described in /2/. In addition, we measured the fluorescence spectra of all prepared solutions to determine the amount of reoxidized uranium(VI). For our calculations we used only spectra where the amount of reoxidized uranium(VI) was less than 5% of the total uranium. The concentration of uranium(IV) was corrected by the data obtained for uranium(VI).

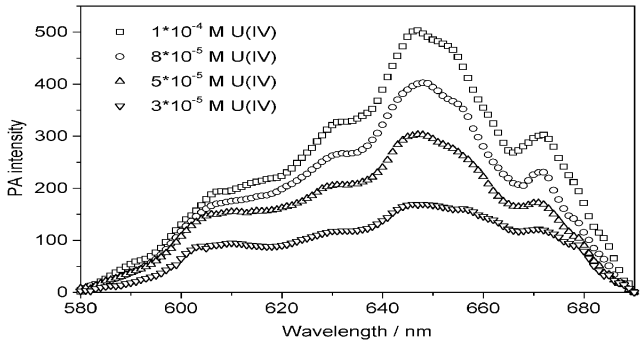


Fig. 1: Spectra of $U^{4+}$ in 0.1 M $HClO_4$

We measured the LIPAS spectra of uranium(IV) in 0.1 M $HClO_4$ depending on the uranium concentration. These spectra are shown in Fig. 1. We find the typical absorption spectrum in the wavelength range from 580 nm to 690 nm.

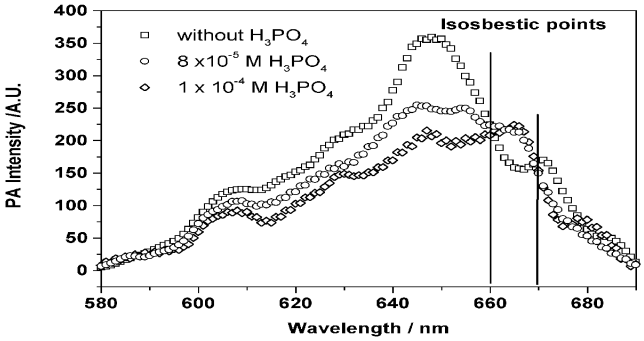


Fig. 2: Spectra of 5 x $10^{-5}$ M $U^{4+}$ in 0.1 M $HClO_4$ with $H_3PO_4$

Fig.2 shows the LIPAS spectra of a $5 \cdot 10^{-5}$ M uranium(IV) solution in 0.1 M $HClO_4$ as a function of the phosphoric acid added. We find two isosbestic points at the same wavelengths as in our study using UV-vis spectroscopy. The isosbestic points are found at 660 and 669 nm. Compared with the measuring conditions applied (step width 0.1 nm for UV-vis and 1 nm for LIPAS) the agreement between the two methods is very good /1/.

The absorbance data of the isosbestic points and of the spectroscopic points at 649 nm, 664 nm and 671 nm were used to calculate the complex formation constant.

We assume that the phosphoric acid dissociates according to

$$H_3PO_4 \quad \text{ø} \quad H_2PO_4^- + H^+ \qquad \log K_1 = -2.14 \qquad (1)$$

and that the complex formation follows the reaction

$$U^{4+} + x\, H_2PO_4^- \quad \text{ø} \quad U(H_2PO_4)_x^{(4-x)+} \qquad (2)$$

The reaction (1) was used to calculate the concentration of the dihydrogen phosphate in the solution. The result of the calculation is a formation constant of log $K_2$ = 4.83 ± 0.12 when we assume that one dihydrogen phosphate (x = 1) takes part in reaction (2). For a 1:2 complex we calculate the formation constant at an ionic strength of I = 0.1 M (0.1M $HClO_4$) to be log $K_2$ = 10.20 ± 0.13. When we compare these data with the results of the study at an ionic strength of I = 0.5 M, the formation constants are smaller. This is in agreement with the predicted dependence of the formation constants on the ionic strength.

To validate the formation reaction we performed a slope analysis. We rearranged the law of mass action to fit

$$\log([U(H_2PO_4)_x^{(4-x)+}]/[U^{4+}]) = \log[H_2PO_4^{2-}] + \log K_2 \qquad (3)$$

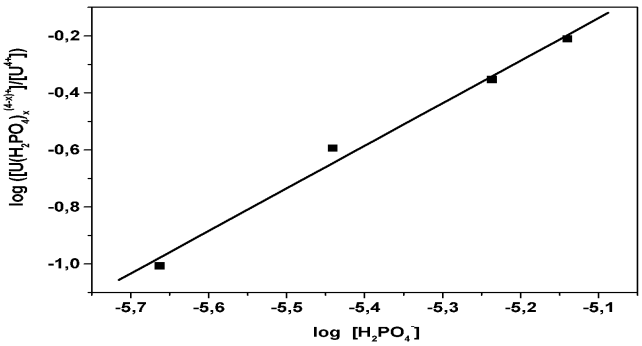


Fig. 3: Slope analysis for reaction (2)

This slope analysis is shown in Fig. 3. The slope x was found to be 1.48 ± 0.11. This result does not allow any decision about the complex formation reaction, using the actual available data. Further studies are in progress.

References

/1/ Geipel, G., Bernhard, G.; this report p. 2

/2/ Geipel, G., Bernhard, G., Brendler, V., Nitsche, H.; Complex Formation between $UO_2^{2+}$ and $CO_3^{2-}$ : Studied by Laser-Induced Photoacoustic Spectroscopy (LIPAS). Radiochim. Acta **82**, 59 (1998)

# COMPLEX FORMATION IN THE SYSTEM URANIUM(IV) - PHOSPHATE STUDIED BY UV-vis SPECTROSCOPY

G. Geipel, G. Bernhard

*A study of the complex formation of uranium (IV) in the phosphate system at uranium concentrations of $5 \cdot 10^{-4}$ M in strongly acid solution was carried out. The absorption spectra show two isosbestic points at 661.4 nm and 669.4 nm. The first formation constant at an ionic strength of 0.5 M was calculated to be log $k_1 = 5.18$.*

In the literature /1/ only few data are reported about the complex formation of uranium(IV) in the phosphate system.

The first studies in this system were carried out by conventional UV-vis spectroscopy to gain experience concerning the spectroscopic properties of uranium(IV). Fig. 1 shows the UV-vis spectra of uranium (IV) as functions of the total phosphate concentration in the solution. The solutions contain 0.5 M $HClO_4$. Precipitation occurs at total phosphate concentrations exceeding $1.5 \cdot 10^{-3}$ M.

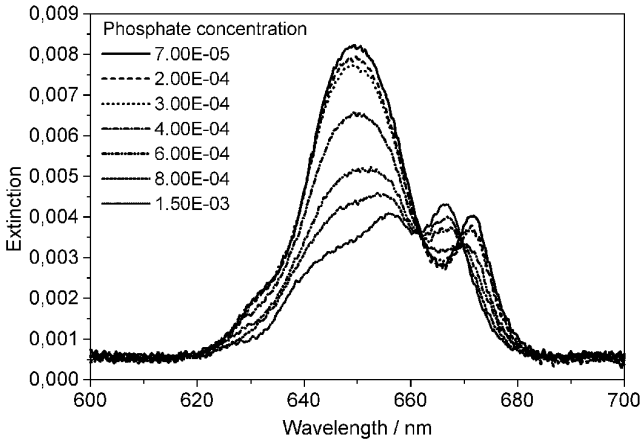


Fig. 1: UV-vis Spectra of Uranium(IV) in phosphate media

The spectra shown in Fig.1 are corrected to zero in the wavelength range below 610 nm and above 690 nm. Two isosbestic points were clearly detected at 661.4 nm and 669.4 nm. Using a Gaussian fitting algorithm, absorption maxima at 629.9 nm, 649.9 nm and 671.9 nm were calculated for uranium(IV).

Absorption maxima of the uranium phosphate complex(es) were found to be at 626.0 nm, 640.1 nm, 655.9 nm and 667.8 nm.

At the isosbestic points the absorption coefficients are the same for all species involved in the complex formation. Using this condition as a starting point, we can derive a system of equations describing the measured absorption at various wavelengths as a function of the species concentrations in the solution. It was impossible to arrive at a satisfactory solution to the equations with a two species mechanism (uranium(IV) and a uranium phosphate complex). A better solution was obtained when we introduced a third species. The result of the resolved system of equations is shown in Fig. 2. The species distribution is depicted as a function of the total phosphate concentration in the solution. At low phosphate concentrations uranium(IV) is the main species in the solution. At about $4 \cdot 10^{-4}$ M phosphate a first uranium(IV)-phosphate complex reaches its maximum in the species distribution. With increasing phosphate concentration in the solution a second uranium phosphate complex becomes the dominant species in the solution.

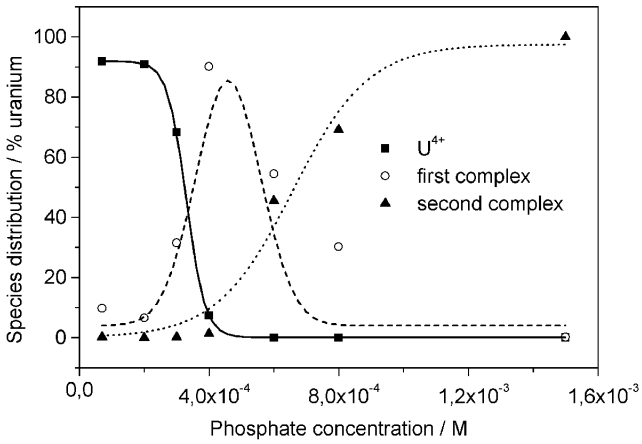


Fig. 2: Calculated species distribution of Uranium(IV) in phosphate media

Under strongly acid conditions such as 0.5 M $HClO_4$ the phosphoric acid only dissociates according to

$$H_3PO_4 \quad \text{ø} \quad H_2PO_4^- + H^+ \qquad \log K_1 = -2.14 \quad (1)$$

and we assume the first complex formation reaction is

$$U^{4+} + H_2PO_4^- \quad \text{ø} \quad UH_2PO_4^{3+} \qquad (2)$$

With the calculated concentrations for the individual species we derive a formation constant for reaction (2) of log $K_1 = 5.18 \pm 0.45$ at an ionic strength of 0.5 M (0.5 M $HClO_4$).

The second complex formation reaction is assumed to be

$$U^{4+} + 2H_2PO_4^- \quad \text{ø} \quad U(H_2PO_4)_2^{2+} \qquad (3)$$

For this complex formation reaction we derive a formation constant of log $K_2 = 11.6 \pm 2.2$, using the existing measurements.

To validate the calculated formation constants and the mechanism of complex formation reactions we measure the absorption spectra in the system uranium(IV) - phosphate at various concentrations of perchloric acid at a constant ionic strength. For these studies the ionic strength was assumed to be 1 M. Calculations are in progress.

Due to precipitation the experimental conditions are very limited. Studies of this system using LIPAS are in progress to reach lower uranium concentrations and also a decreased the acid concentration.

References

/1/ Grenthe, I., Fuger, J., Lemire, R.J., Muller, A.B., Nguyen-Trung, C., Wanner, H.; *Chemical Thermodynamics of Uranium.* 1st ed. , Elsevier Science Publishers, Amsterdam, 1992

# COMPLEX FORMATION OF URANIUM(IV) WITH PHOSPHORIC ACID DETERMINATION OF THE COMPLEX FORMATION REACTION

G. Geipel, G. Bernhard

*To determine the complex formation between uranium(IV) and phosphoric acid we carried out LIPAS and UV-vis measurements, varying the three parameters i) ionic strength, ii) concentration of phosphoric acid and iii) concentration of hydrogen ions. The stoichiometry was determined at various ionic strengths. The analysis resulted in a 1:1 complex. During its formation one proton from the reacting phosphoric acid was released.*

The complex formation between uranium(IV) and phosphoric acid was studied using LIPAS and UV-vis measurements with variation of the three parameters i) ionic strength, ii) concentration of phosphoric acid and iii) concentration of hydrogen ions. Examples of the measurements are given in /1/.
The complex formation reaction can be written as

$$U^{4+} + x\ H_3PO_4 \text{ <===> } U(H_{3-y}PO_4)_x^{(4-xy)+} + xy\ H^+ \quad (1)$$

After rearrangement and transformation in the logarithmic form, the mass action law becomes :

$$\log\frac{[U(H_{(3\&y)}PO_4)_x^{(4\&xy)\%}]}{[U^{4\%}]} = \log K\% + x\log[H_3PO_4]\& + xy\log[H^\%] \quad (2)$$

$$\log K' = \log K - xy\log[H^+] \quad (3)$$

Using the data from the hydrolysis study /2/, we were able to determine the stoichiometry of reaction (1) in combination with the measurements, including phosphoric acid and perchloric acid.
In addition to /1,2/ Fig. 1 shows a set of UV-vis spectra of $2x10^{-4}$ M $U^{4+}$ at I = 1.0 M and $8x10^{-6}$ M $H_2PO_4^-$ as a function of the perchloric acid added.

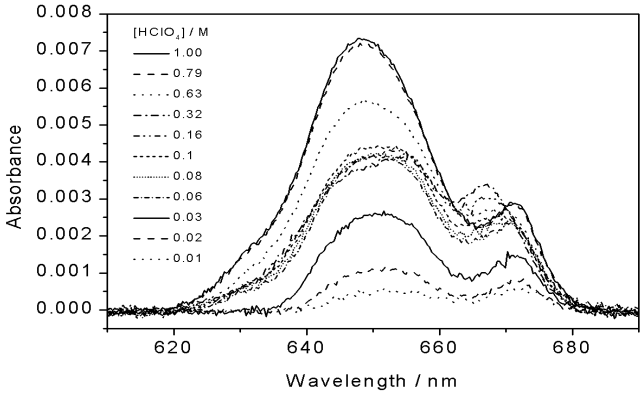


Fig. 1: UV-vis spectra of uranium(IV) as function of the concentration of $HClO_4$ at constant concentration of $H_3PO_4$

Fig. 1 demonstrates the change the uranium(IV) species in solution. The typical UV-vis spectra for uranium(IV), the phosphate complex formed and the decrease in absorption caused by the hydrolysis of uranium(IV) are shown as function of the concentration of perchloric acid.
Fig. 2 shows the plot of the log ($[U(H_{(3-y)}PO_4^{(4-xy)+}]/[U^{4+}]$) as a function of $\log[H_3PO_4]_{free}$. The plot shown in Fig. 3 is an example of the calculated formation constants log K' as function of the hydrogen concentration. The data used are from LIPAS measurements at I = 1.0 M. From the examples we obtain a slope of 1.14 ± 0.22 for the dependency on phosphoric acid and a slope of -0.77 ± 0.14 for the dependency on the concentration of $HClO_4$.The correlation coefficients were calculated to be $R^2$ = 0.84 and $R^2$ = 0.9. These analyses were carried out at various ionic strengths.

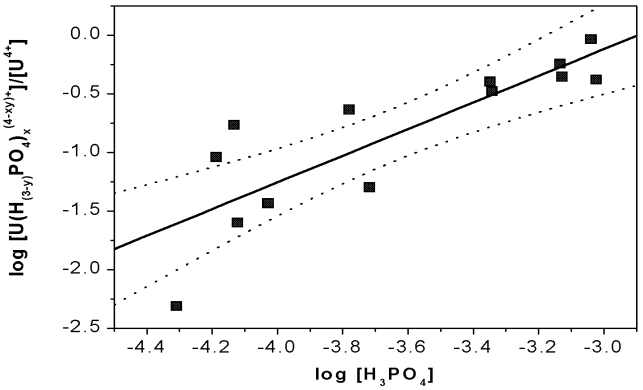


Fig. 2: Graphic analysis for determination of the number of phosphoric acid molecules.

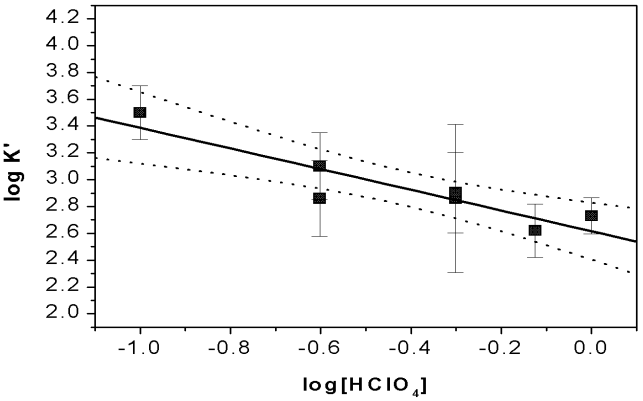


Fig. 3: Graphic analysis for determination of the number of hydrogen ions.

| Ionic strength / M | Slope analysis | |
|---|---|---|
| | $H_3PO_4$ | $H^+$ |
| 2.00 | 1.25 ± 0.34 | -0.82 ± 0.10 |
| 1.00 | 1.12 ± 0.26 | -0.77 ± 0.14 |
| 0.50 | 1.04 ± 0.27 | -1.38 ± 0.27 |
| 0.25 | 0.98 ± 0.21 | -1.08 ± 0.31 |
| 0.10 | 1.54 ± 0.16 | |

Tab. 1: Results of the slope analysis for determination of the complex formation reaction.

Tab. 1 summarizes the results of the slope analysis at various ionic strengths for the dependence of the complex formation on the concentration of phosphoric acid and on the concentration of hydrogen ions (at a constant concentration of phosphoric acid). The stoichiometry of the complex formation reaction can now be written as

$$U^{4+} + H_3PO_4 \text{ <===> } U(H_2PO_4)^{3+} + H^+ \quad (4)$$

References

/1/ Geipel, G., Bernhard, G.; this report p. 1
/2/ Geipel, G., Bernhard, G.; this report p. 2

# COMPLEX FORMATION IN THE URANIUM(IV) - PHOSPHATE SYSTEM
# EXTRAPOLATION OF THE COMPLEX FORMATION CONSTANT TO IONIC STRENGTH J = 0 M

G.Geipel, V. Brendler, G. Bernhard

*We carried out studies using LIPAS and UV-vis spectroscopy to determine the complex formation between uranium(IV) and phosphate as a function of ionic strength. Using these formation constants, we extrapolated the complex formation constant to infinite dilution by the SIT mechanism and the Davies equation. The extrapolated complex formation constant is log $K^0$ = 3.50 ± 0.20*

In previous papers /1,2/ we determined the complex formation reaction between uranium(IV) and phosphoric acid to be

$$U^{4+} + H_3PO_4 \quad <===> \quad U(H_2PO_4)^{3+} + H^+ \qquad (1)$$

Extrapolations were also carried out to estimate the complex formation constant for the reaction (1) at various ionic strengths. The data are listed in Tab. 1.

| Ionic strength / M | log $K_I$ | error |
|---|---|---|
| 2.00 | 2.75 | 0.05 |
| 1.00 | 2.52 | 0.14 |
| 0.50 | 2.70 | 0.08 |
| 0.25 | 2.59 | 0.40 |
| 0.10 | 2.65 | 0.26 |

Tab. 1: Complex formation constants as a function of ionic strength.

Ionic strength were converted from molar to molal scale. Using these data we can calculate the complex formation constant at infinite dilution. This can be done using two methods.

*1) Specific ion interaction theory /3/*

Assuming that the water activity is constant and substituting the expression of the specific ion interaction theory for the activity coefficients produces the following equation for extrapolation of the complex formation constant:

$$\log K_J - \Delta z^2 D = \log K° - \Delta\varepsilon \cdot J \qquad (2)$$

$\Delta z^2$ = difference of the square of the charges of reacting ions
$\Delta\varepsilon$ = difference of the ion interaction coefficients
J = ionic strength (molal scale) and

$$D = \frac{0.5093\,(\sqrt{J})}{1+1.5\,(\sqrt{J})} \qquad (3)$$

As $\Delta z^2 = 6$ and D can be calculated by Eqn. (3), ($\log K_J - \Delta z^2 D$) can be obtained as function of the ionic strength (Fig. 1). Extrapolation yields log K° = 3.52 ± 0.10 and $\Delta\varepsilon$ = - 0.33 ± 0.06.

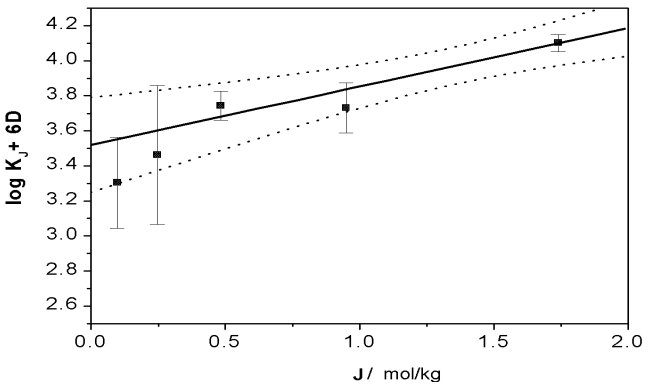


Fig. 1: Extrapolation of log K to infinite dilution according to the specific ion interaction theory

*2) Davies equation*

The complex formation constant at infinite dilution can also be calculated as a function of the formation constants at the various ionic strengths and an additive function of the ionic strength:

$$\log K° = \log K_J - 0.5093\ f(J)\ \Sigma z_i^2 \qquad (4)$$

$\Sigma z_i^2$ = product number and square of the charges of the reacting ions and

$$f(J) = \frac{\sqrt{J}}{1+\sqrt{J}} - 0.2J \qquad (5)$$

Extrapolation produces log K° =3.46 ± 0.23 (Fig. 2)

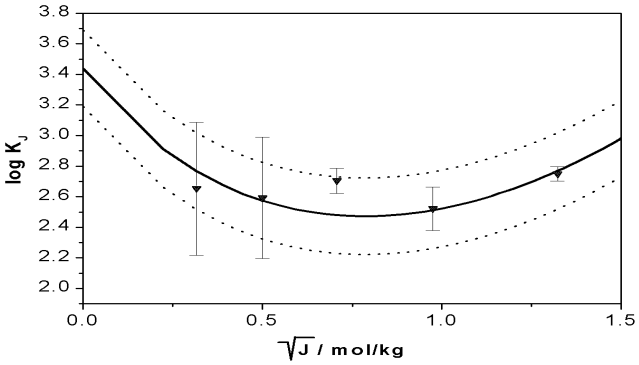


Fig. 2: Extrapolation of log K to infinite dilution according to the Davies equation.

From both methods we derive the complex formation constant at zero ionic strength for reaction (1) to be log k° = 3.50± 0.20.

Fig. 3 yields the calculated species distribution of uranium(IV) at an ionic strength of 1 mol/kg, using the derived complex formation constant for 2 x $10^{-4}$ M $U^{4+}$ and 5 x $10^{-4}$ M $H_3PO_4$.

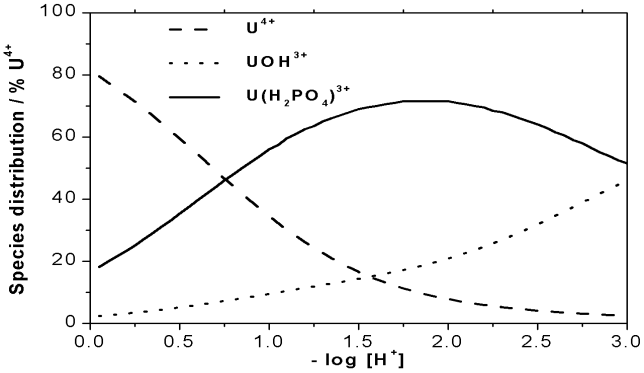


Fig. 3: Species distribution of uranium(IV) in phosphate acid media ( J = 1 M, 2x$10^{-4}$ M $U^{4+}$, 5x$10^{-4}$ M $H_3PO_4$ )

References

/1/ Geipel, G., Bernhard, G.; this report p. 1
/2/ Geipel, G., Bernhard, G.; this report p. 3
/3/ Grenthe, I., Fuger, J., Konings, R.J.M., Lemire, R.J., Muller, A.B., Nguyen-Trung Cregu, Ch., Wanner, H.; *Chemical Thermodynamics of Uranium.* NEA OECD, 1992

# HYDROLYSIS OF URANIUM(IV)

G.Geipel, V. Brendler, G. Bernhard

*To validate the experimental setup and the calculation mechanism of uranium(IV) complex formation reactions we studied the hydrolysis of uranium(IV) at two ionic strengths. The calculated hydrolysis constants of log K(I=0.5M) = -1.53 and log K(I=2.0M) = -1.64 are in very good agreement with the data provided by the NEA database.*

Complex formation reactions of uranium(IV) are often affected by the strong hydrolysis of this ion. To validate the experimental setup and the formalism of calculations we studied the hydrolysis reaction of uranium(IV). We carried out several UV-vis measurements of $2x10^{-2}$ M uranium(IV) at ionic strengths of 0.5 M and 2.0 M . The concentration of hydrogen ions in the solutions varied between 0.5 M and 0.01 M at the ionic strength I = 0.5 M and between 1.0 M and 0.01 M at the ionic strength I = 2.0 M.

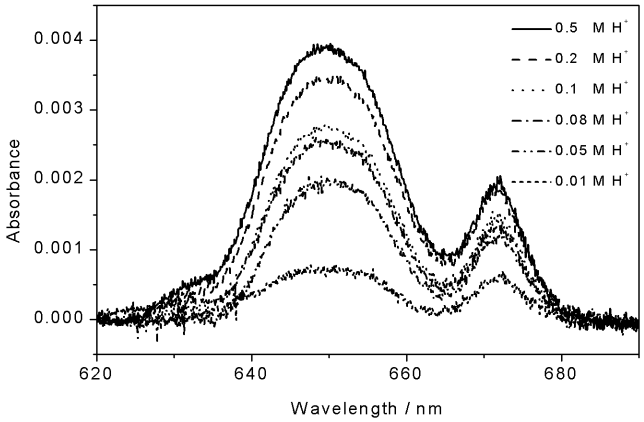


Fig. 1: UV-vis spectra of uranium(IV) as function of $H^+$ concentration at ionic strength 0.5 M.

Fig. 1 shows a set of UV-vis spectra at the ionic strength I = 0.5 M. The decreasing absorption with decreasing concentration of $H^+$ ions can be clearly seen.

For calculation of the hydrolysis constant and determination of the reaction mechanism we used the absorption maxima at 648.8 nm and 671.7 nm. The molar decadic absorption coefficients for uranium(IV) were calculated as $\varepsilon_{648.8}$ = 32.3 $LMol^{-1}cm^{-1}$ and $\varepsilon_{671.7}$ = 17.7 $LMol^{-1}cm^{-1}$.

Taking into account that the hydroxo complex does not absorb light, we can calculate both the concentration of uranium(IV) and the hydroxo complex in the solution.

The hydrolysis reaction can be written as follows:

$$U^{4+} + x\ H_2O \text{ <===> } U(OH)_x^{(4-x)+} + x\ H^+ \qquad (1)$$

The respective mass action law delives:

$$K = \frac{[U(OH)_x^{(4-x)+}]([H^+]^x}{[U^{4+}]} \qquad (2)$$

Rearranging and transforming (2) into the logarithmic expression we can write

$$\log\frac{[U(OH)_x^{(4-x)+}]}{[U^{4+}]} = \log K - x \log[H^+] \qquad (3)$$

Fig.2 and Fig.3 show the plots of $\log([U(OH)_x^{(4-x)+}]/[U^{4+}])$ *vs.* $\log[H^+]$ at the ionic strength I = 0.5 M and I = 2.0 M.

The slope analysis results in x = 1.03 ± 0.10 at I = 0.5 M and x = 1.02 ± 0.06 at I = 2.0 M. The correlation factors $R^2$ for the two ionic strengths are 0.97 for I = 0.5 M and 0.98 for I = 2.0 M.

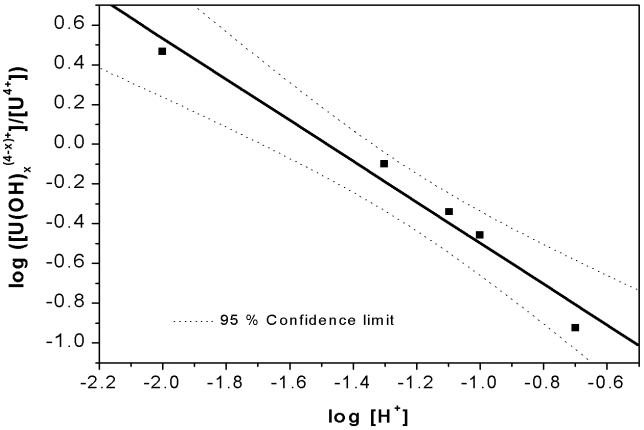


Fig. 2: Determination of the hydrolysis reaction at ionic strength I = 0.5 M.

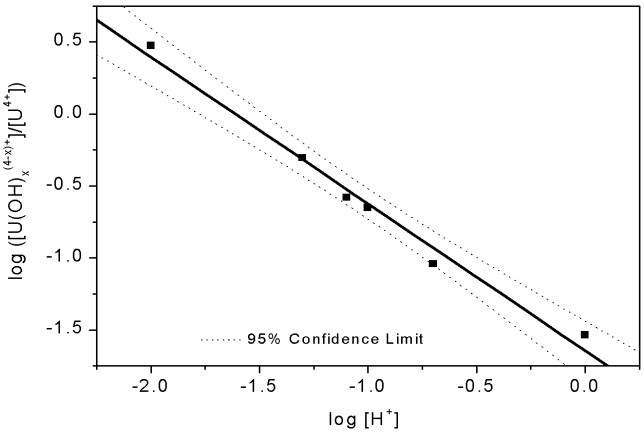


Fig. 3: Determination of the hydrolysis reaction at ionic strength I = 2.0 M.

The hydrolysis reaction can now be written as

$$U^{4+} + H_2O \text{ <===> } U(OH)^{3+} + H^+ \qquad (4)$$

The formation constant for the hydrolysis reaction (4) at ionic strength I = 0.5 M now is calculated as log K = -1.53 ± 0.13. Compared with the value referred to in /2/ (log K = -1.54 ± 0.09), we notice a very good agreement. At ionic strength I = 2.0 M we calculate the first hydrolysis constant to be log K = -1.64 ± 0.07. The NEA database /2/ refers to a value of log K = -1.63 ± 0.09. The agreement between both values is very good.

References

/1/ Kraus, K.A., Nelson, F.; J. Amer. Chem. Soc. **72**, 3901 (1950)

/2/ Grenthe, I., Fuger, J., Konings, R.J.M., Lemire, R.J., Muller, A.B., Nguyen-Trung Cregu, Ch., Wanner, H.; *Chemical Thermodynamics of Uranium.* NEA OECD, 1992

# SYNTHESIS AND CHARACTERIZATION OF BAYLEYITE, $Mg_2[UO_2(CO_3)_3] \cdot 18H_2O$

S. Amayri, M. Bubner, G. Geipel, G. Schuster, W. Matz [1], G. Bernhard
[1] Institute of Ion Beam Physics and Materials Research

*A new method for the synthesis of Bayleyite, $Mg_2[UO_2(CO_3)_3] \cdot 18H_2O$, is described. Various methods of chemical analysis, X-ray powder diffraction (XRD), thermoanalysis, and time-resolved laser-induced fluorescence spectroscopy (TRLFS) were used to characterize this substance.*

Bayleyite (B) is a secondary mineral of uranium. The aim of this study was to develop a procedure for the preparation of B. This well characterized substance will be used for the determination of its solubility and for speciation experiments.

*Experimental:* Synthesis of $Mg_2[UO_2(CO_3)_3] \cdot 18H_2O$
B was prepared by reacting stoichiometric amounts of dissolved uranyl nitrate (Merck p.a), solid basic magnesium carbonate (Merck p.a) and carbon dioxide. After dissolution of the reactants, B was precipitated by slowly evaporating the solution at room temperature. The product obtained was further purified by recrystallization from water. The transparent greenish yellow prisms were dried on exposure to air.

*Chemical analysis:* The results of the chemical analysis are compiled in Tab. 1. The chemical composition was in good agreement with the calculated values.

| Element | U | Mg | C | H |
|---|---|---|---|---|
| Found (%) | 28.92±0.60 | 5.90±0.70 | 4.34±0.01 | 3.98±0.28 |
| Calculated (%) | 28.92 | 5.91 | 4.38 | 4.41 |
| Method | ICP-MS | AAS | EA. | EA. |

Tab. 1: Chemical analysis of $Mg_2[UO_2(CO_3)_3] \cdot 18H_2O$

*X-ray crystallography:* The experimental conditions are described in /1/. Fig.1 depicts the diffractograms of B.

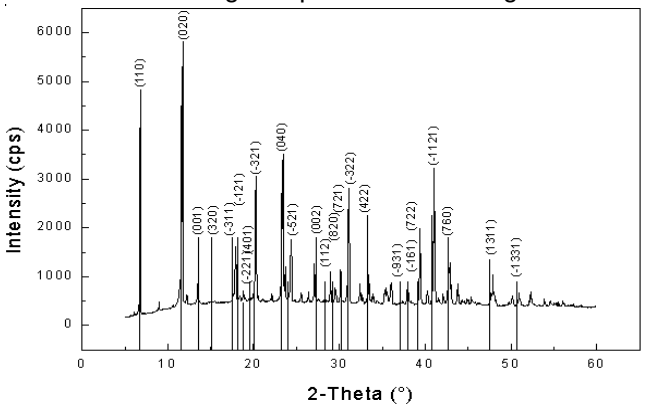


Fig. 1: X-ray diffraction pattern of synthetic bayleyite

The lattice parameters were calculated from all clearly identifiable reflections. As Tab. 2 shows, they are in good agreement with /1, 2/.

| | This work | Mereiter /2/ | PDF /3/ |
|---|---|---|---|
| a (AE) | 26.593 ± 0.101 | 26.560 (3) | 26.65 (5) |
| b (AE) | 15.263 ± 0.052 | 15.256 (2) | 15.31 (5) |
| c (AE) | 6.503 ± 0.026 | 6.505 (1) | 6.53 (2) |
| V ($AE^3$) | 26.359 ± 0.300 | 26.234 | 26.60 |

Tab. 2: Lattice constants of $Mg_2[UO_2(CO_3)_3] \cdot 18H_2O$

*Thermal behavior:* The thermal stability of B was investigated, using the thermoanalyzer STA-92 (Setaram, France) with an applied heating rate of 10°C/min and a flow of $O_2$ of 3 L/h. Fig. 2 shows the thermal decomposition of B, which is characterized by several effects. The results summarized in Tab. 3 show that B contains 17.36 ±0.52 moles of $H_2O$ and 3.17±0.10 moles of $CO_2$.

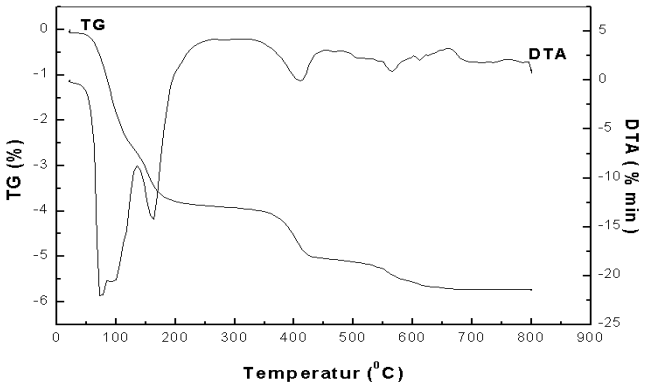


Fig. 2: TG and DTA of synthetic bayleyite

| Temp. Interval | Wt% lost | Assignment |
|---|---|---|
| 22 - 135 | 27.55 | - 12.53 $H_2O$ |
| 135 - 338 | 10.61 | - 4.83 $H_2O$ |
| 338 - 528 | 11.99 | - 2.23 $H_2O$ |
| 528 - 630 | 4.49 | - 0.83 $H_2O$ |
| 630 - 800 | 0.58 | - 0.11 $H_2O$ |

Tab. 3: Results of thermogravimetric analysis

*TRLFS measurements:* B was not investigated by TRLFS before. The TRLFS investigations, showed that the fluorescence lifetime of solid B was larger than 100 µs and the main emission wavelengths were at 470.03 nm, 486.90 nm, 505.80 nm, 526.35 nm, 550.22 nm, 576.24 nm and 601.88 nm (Fig.3). The characteristic fluorescence was induced by exciting the solid sample with a 266 nm laser beam (Nd-YAG-laser system) /4/.

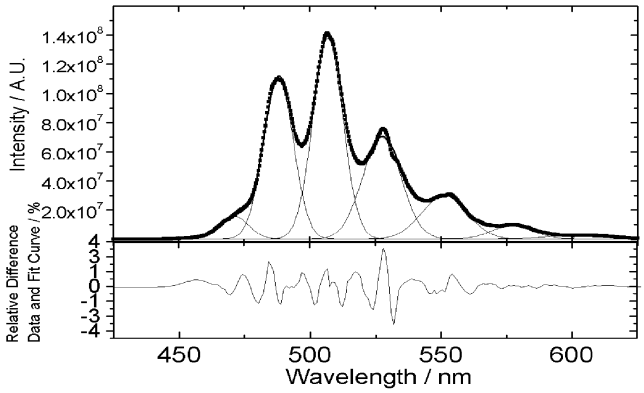


Fig. 3: TRLFS spectrum of solid synthetic bayleyite

*Conclusion:* The results of our analysis confirm the identity of our product with the mineral Bayleyite. The first solubility experiments (0.1 M $NaClO_4$ , under air, 25°C, pH 8.0) show, that the solubility of B is 190 g/L.

References

/1/ Amayri, S.; PhD thesis at TU Dresden in preparation
/2/ Mayer, H., Mereiter, K., Tschermaks Min. Petr. Mitt. **35**, 133-146 (1986)
/3/ *Powder Diffraction File*, Inter. Center of Diffraction Data, New town Square, Pennsylvania, USA
/4/ Brachmann, A., PhD Thesis TU Dresden (1997)

# CHARACTERIZATION OF AMMONIUM URANYL CARBONATE $(NH_4)_4[UO_2(CO_3)_3]$

S. Amayri, G. Geipel, G. Bernhard, W. Matz[1] , G. Schuster
[1]Institute of Ion Beam Physics and Materials Research

*Chemical analysis, X-ray powder diffraction (XRD), thermoanalysis, and time-resolved laser-induced fluorescence spectroscopy (TRLFS) were used to characterize the synthesized $(NH_4)_4[UO_2(CO_3)_3]$. It is an initial substance for the synthesis of other uranyl carbonate complexes.*

Our goal was to synthesize and characterize $(NH_4)_4[UO_2(CO_3)_3]$ (AUC) in order to use it as a starting material for the preparation of other alkali and alkaline earth metal uranyl carbonates. Another aspect was the study of the complexation behavior of the uranyl ions with ammonium and carbonate species by TRLFS.

*Chemical analysis:* AUC was prepared according to /1/. Concerning the formula $(NH_4)_4[UO_2(CO_3)_3]$, the determined chemical composition was in good agreement with the calculated values (Tab.1).

| | Found (%) | Calculated (%) |
|---|---|---|
| U | 45.52 ± 0.5 | 45.58 |
| N | 10.75 ± 0.02 | 10.73 |
| C | 6.89 ± 0.02 | 6.90 |
| H | 3.11 ± 0.01 | 3.09 |
| $NH_4^+$ | 13.4 ± 0.5 | 13.82 |
| $CO_3^{2-}$ | 34.5 ± 0.4 | 34.47 |

Tab.1: Chemical analysis of AUC

*X-ray powder diffraction:* The diffraction pattern was obtained, using a universal X-ray diffractometer (URD-6, Freiberger Präzisionsmechanik, Germany) in Bragg-Brentano geometry with CuK„ radiation. The diffractograms were recorded in the range from 8E to 60E (Fig. 1). The peaks were identified using a diffraction data pool and taking into account the monoclinic structure. The results (Tab.2) are in good agreement with published data /2,3/.

| | This work | Malcic /2/ | Bachmann/3/ |
|---|---|---|---|
| a (D) | 12.824 ± 0.001 | 12.845 ± 0.015 | 12.824 ± 0.002 |
| b (D) | 9.358 ± 0.001 | 9.360 ± 0.015 | 9.356 ± 0.001 |
| c (D) | 10.653 ± 0.001 | 10.650 ± 0.015 | 10.654 ± 0.001 |
| V ($D^3$) | 12.705 ± 0.001 | 12.725 | 12.70 ± 0.3 |

Tab. 2: Lattice constants of $(NH_4)_4[UO_2(CO_3)]$

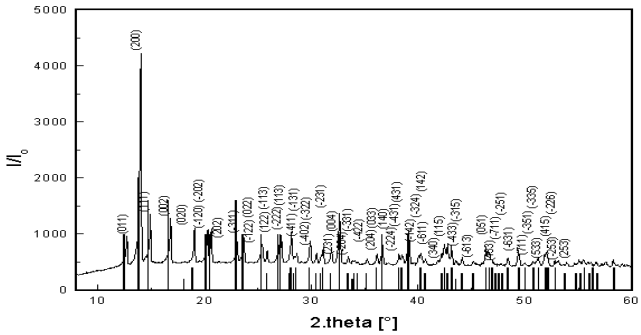


Fig. 1: X-ray powder diagrams of $(NH_4)_4[UO_2(CO_3)_3]$

*Thermoanalysis:* Thermoanalysis was carried out, using the thermoanalyzer STA-92 (Setaram, France) in the range from 20 to 800EC with a heating rate of 10EC/min under oxygen. As reported by Jinder and Skramovsky /4/, the thermal decomposition of AUC occurs in a single step and can be described by the following equation:

$$(NH_4)_4[UO_2(CO_3)_3] = 4NH_3 + 3CO_2 + UO_3 + 2H_2O$$

Diagrams (Fig. 2) showed a single endothermic effect between 165 and 185 EC. At this temperature AUC disintegrates. Uranium oxide is formed by generating ammonia, carbon dioxide and water vapor. A weight loss of 47.53 % (calc. 45.22%) is measured by thermogravimetry.

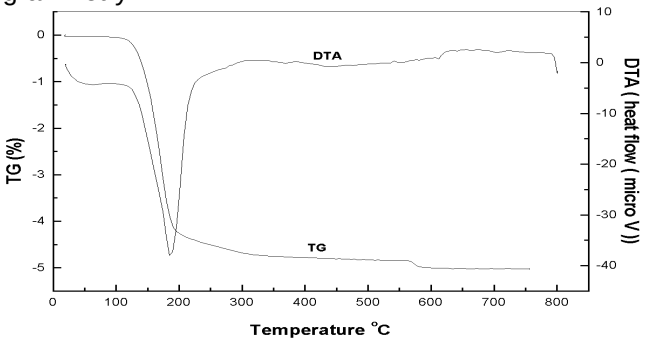


Fig. 2: TG and DTA diagrams of $(NH_4)_4[UO_2(CO_3)_3]$

*Fluorescence spectroscopy:* The fluorescence lifetime of solid AUC was determined to be 10.45 µs and the main emission wavelengths were at 451.6 nm, 465.8 nm, 483.6 nm, 503.3 nm, 524.4 nm, 547.6 nm, 572.9 nm and 596.6 nm. The characteristic fluorescence was induced by exciting the solid sample with a 266 nm laser beam (Nd-YAG-laser system: Spectra Physics, Mountain View, CA, USA).

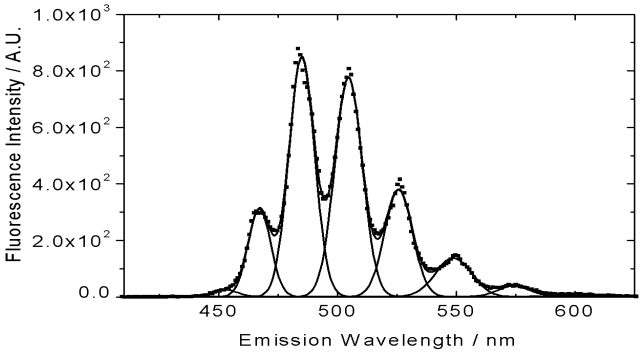


Fig. 3: TRLFS spectrum of $(NH_4)_4[UO_2(CO_3)_3]$

Solid AUC (see Fig.3) shows a fluorescence pattern different from that of solid uranyl carbonate (rutherfordine). The results of the various characterization methods shows that pure ammonium uranyl carbonate was synthesized. It can be used as a starting material for the preparation of other uranyl carbonate complexes.

Acknowledgments
The authors would like to thank Dr. W. Wiesener for performing the chemical analysis and A. Scholz for the X-ray diffraction measurements.

References

/1/ Amayri, S.; PhD thesis at TU Dresden in preparation
/2/ Malcic, S.; Bull. Inst. Nucl. Sci. **8**, 95-97 (1958)
/3/ Bachmann, H., Seibold, K.; J. Inorg. Nucl. Chem. **37**, 735 (1975)
/4/ Jindra J., Skramovesky, S.; Coll. Czech. Chem. Comm. **31**, 2639-2645 (1966)

## LASER-INDUCED PHOTOACOUSTIC SPECTROSCOPIC STUDIES OF NEPTUNIUM

G. Geipel, G. Bernhard, G. Grambole

*We installed the LIPAS equipment for studies in a glove box. Some first photoacoustic spectra of neptunium were compared with normal UV-vis spectra.*

In the new radiochemistry building /1/ a laboratory for laser induced spectroscopy was set up. From this laboratory we can transmit laser pulses with fibre optics into the other laboratories where glove boxes are installed. In this way we can apply laser-induced spectroscopic methods to transuranium elements.

As a first step of operation of the Nd:YAG pumped OPO system in the new laboratory we measured the wavelength of the signal output of the OPO. The result for the spectral range from 580 nm to 590 nm is shown in Fig. 1. As expected, a straight dependence exists

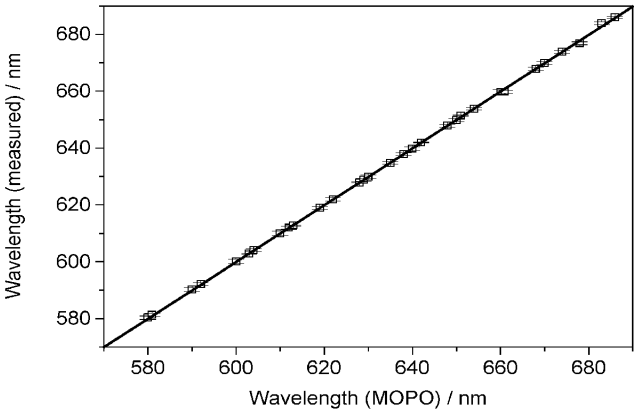


Fig. 1: Dependence of wavelength output of the OPO-System on the set wavelength

between the OPO output and the measured wavelength. The linearity is 0.999 ± 0.002. The correlation factor $R^2$ was calculated as $0.9998_7$. The difference between the set OPO output and the measured wavelength was smaller than the error of the spectrographic arrangement (0.2 nm).

The power of the OPO output was lowered by an attenuator (Newport Model 850) to an average pulse power of about 5 mJ and was then coupled to a fibre optic. The length of this fiber optic was about 50 m transmitting the laser pulse into laboratories with glove boxes for Np experiments. The measured power in the glove box was about 2 mJ (~40% of the input into the fiber). In the glove box we have the same equipment for LIPAS as described in /2/. The electrical signals of the power meter head and of the piezoceramic detector were conveyed out of the glove box, using BNC-cables. The preamplifier was set directly on the BNC connector of the glove box. The signal was measured, using an oscilloscope in the laser laboratory. The signal of the power detector was conveyed to the power meter in the laser laboratory. All settings and data storage were computer controlled in the laser laboratory.

Fig. 2 shows the UV-vis spectrum of a $5 \cdot 10^{-3}$ M solution of $NpO_2^+$ in 0.1 M $HNO_3$ in the spectral range from 580 nm to 650 nm. By curve fitting we calculate three absorption maxima in the range at 592.0 nm, 616.4 nm and 625.9 nm. The main absorption in this range was found at 616.4 nm. The molar extinction coefficient for $NpO_2^+$ at this wavelength was calculated as 13.2 L $mol^{-1}cm^{-1}$. Assuming the lowest detectable absorption to be $10^{-2}$ units, we calculated a detection limit of $7 \cdot 10^{-4}$ mol/L for UV-vis spectroscopy with 1 cm cuvettes.

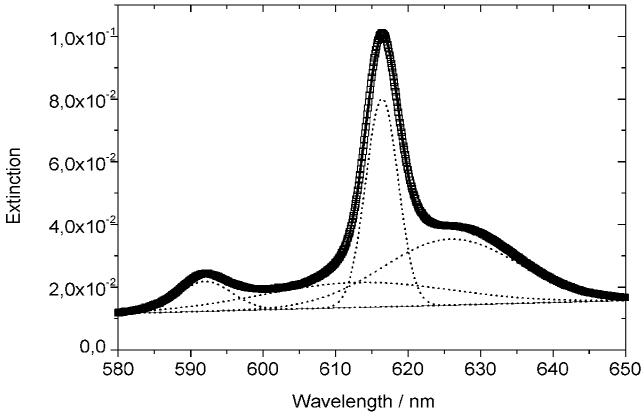


Fig. 2: UV-vis spectrum of $NpO_2^+$ in 0.1 M $HNO_3$

Adding 0.1 M $HNO_3$ we diluted this $NpO_2^+$ solution to a $5 \cdot 10^{-4}$ M $NpO_2^+$ solution. This solution was measured in the same wavelength range by the described LIPAS technique.

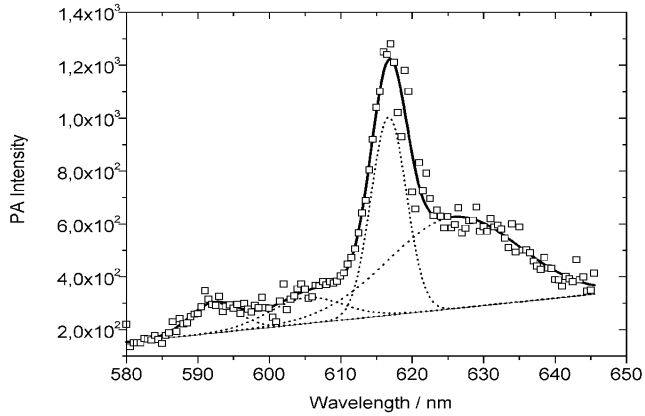


Fig. 3: LIPAS spectrum of $NpO_2^+$ in 0.1 M $HNO_3$

The spectrum is shown in Fig. 3. The absorption maxima were calculated as 592.2 nm, 616.7 nm and 625.5 nm by fitting the measured absorption with a Gaussian peak fit algorithm. These absorption maxima are in excellent agreement with the maxima found by UV-vis spectroscopy. Using the threefold noise of the spectrum as the detection limit we calculated the lowest detectable $NpO_2^+$ concentration to be $5 \cdot 10^{-6}$ M. This is more than two orders of magnitude smaller than the results of conventional UV-vis spectroscopy.

References

/1/ Friedrich, H., Bernhard, G., Nitsche, H.; Report FZR-247 (1999) p.1

/2/ Geipel, G., Bernhard, G., Brendler, V., Nitsche, H.; Complex Formation between $UO_2^{2+}$ and $CO_3^{2-}$ : Studied by Laser-Induced Photoacoustic Spectroscopy (LIPAS). Radiochim. Acta **82**, 59 (1998)

/3/ Keller, C.: *The Chemistry of the Transuranium Elements*. Verlag Chemie, Weinheim (1971) p.294

# TIME-RESOLVED LASER-INDUCED FLUORESCENCE SPECTROSCOPY WITH ULTRA-SHORT PULSES - PART III: A NEW FIT ROUTINE FOR SPECTRA EVALUATION

M. Rutsch, G. Geipel

*A new evaluation routine has been developed for computing the fluorescence lifetimes from time-resolved fluorescence measurements with ultrashort excitation pulses over the whole emissions wavelength range. The routine is demonstrated by the example of a time-resolved fluorescence spectrum of a humic acid.*

## Methodology

To obtain fluorescence lifetimes, the fluorescence decay is fitted as a function of time on a sum of exponential decay functions (Eq. 1):

$$A(t) = A_0 + \sum A_i \cdot e^{-(t/J)} \quad \text{with } i = 1, 2, 3, 4... \quad (1)$$

Previously only a limited number of emissions wavelengths or the integral of the whole spectrum (or a part of it) were used for a fit with Eq. (1), particularly for organic ligands (humic acid). Based on the program Igor Pro 3.1 (WaveMetrics, Inc.) we developed a fit routine that fits the fluorescence lifetime and fluorescence yields of each wavelength separately step by step, using the Levenberg-Marquardt non-linear least squares algorithm.

The user has to define the number of lifetimes i and to enter estimated values for the lifetimes and fluorescence yields. The program also makes it possible to put constraints on selected parameters, e.g. a constant value for $A_0$ can be chosen as background value. Furthermore, the user can involve the whole spectrum or parts of it, e.g. selected wavelengths, in the fit procedure. The program is not limited in therms of a maximum of lifetimes, wavelength or delay time steps. During fitting the adjustment progress can be observed in a separate graph window. The program generates an output table with the following values: selected wavelength, chi$^2$, $A_0$, error of $A_0$, $A_1$, error of $A_1$, $J_i$, error of $J_i$, $A_2$, error of $A_2$...

## Example

A typical fluorescence spectrum of Aldrich humic acid (5 mg/l, pH=11), measured immediately after the excitation pulse ($8_{ex}$ =400 nm, <130 fs), is shown in Fig. 1 (see /1/ for experimental details). Three characteristic features are observed: i) the excitation pulse at 400 nm, ii) an unexpectedly high background and iii) a Raman band from water at 460 nm. The features i) and ii) are caused by light scattering from the cuvette and colloid particles in the sample. These features influence calculation of the fluorescence lifetimes and falsify the result. An application of our new fit routine for calculation of the fluorescence decay (Eq.1) for each emission wavelength without correction of i) and ii) yields three lifetime ranges $J_1$ from 0.3 to 0.8 ns, $J_2$ from 1.4 to 3 ns and $J_3$ from 4 to 7 ns with $A_1$ from 60 to 70 %, $A_2$ from 15 to 25% and $A_3$ from 10 to 15%. Caused by i) and ii) the intensity of $A_1$ is extremely high. Errors for $J_i$ and $A_i$ are very high (>30%) and no calculated fluorescence spectra are obtained (for i = 2, 3). Up to now we are unable to separate the fluorescence of the humic acid from the impairing features. We therefore compute the TRLFS spectra approximately 2 ns after the laser excitation pulse (Fig. 2).

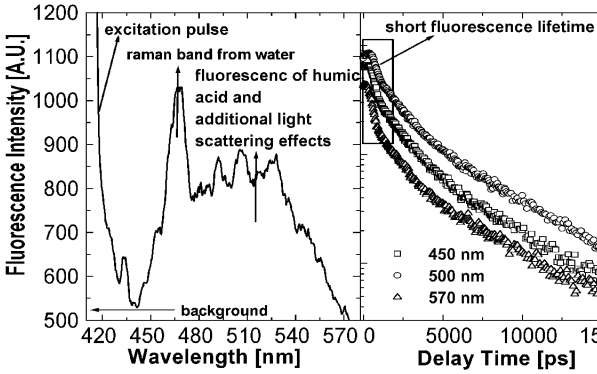


Fig. 1: Fluorescence spectra and decay curves of Aldrich HA at 0.2 ns after pulse excitation ($8_{ex}$ = 400 nm).

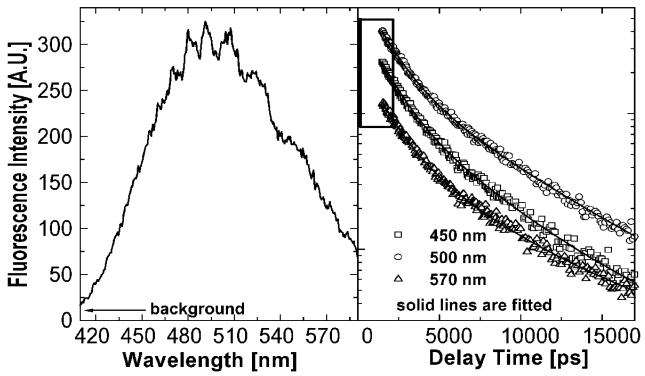


Fig. 2: Fluorescence spectra and decay curves of Aldrich HA at 2 ns after pulse excitation ($8_{ex}$ = 400 nm).

The spectra are not influenced by light scattering. The results of such a fit are shown in Fig. 3.

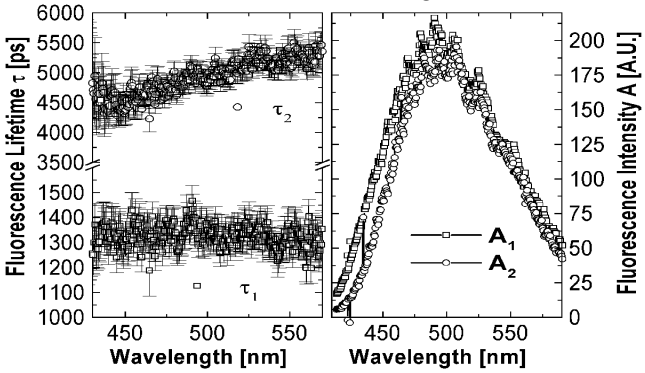


Fig. 3: Fluorescence lifetime and intensity as a function of the emissions wavelength ($8_{ex}$ = 400 nm, Aldrich Ha).

Two lifetimes ($J_1$ from 1.2 to 1.5 ns and $J_2$ from 4 to 5.5 ns) were found and a single fluorescence spectrum was obtained for each lifetime range. The errors for $J_i$ and $A_i$ are smaller than 20%. The results obtained with other humic acids, such as natural and synthetic humic acid, are briefly discussed in /2/.

## Acknowledgments

The authors are grateful to John Weeks (WaveMetrics, Inc.) for his help in programming the fit routine.

## References

/1/ Rutsch, M., et al., Report FZR-247 (1999) p.14, 15
/2/ Rutsch, M., et al., this report p. 11

# TIME-RESOLVED LASER-INDUCED FLUORESCENCE SPECTROSCOPY WITH ULTRA-SHORT PULSES - PART IV: VARIATION OF THE EXCITATION WAVELENGTH

M. Rutsch, G. Geipel, G. Bernhard

*An ultrafast kHz optical parametrical amplifier (OPA) was installed in our pico- and femtosecond laser system for TRLFS in order to select various excitation wavelengths. Some first measurements of a humic acid sample were performed with three excitation wavelengths.*

## Experimental

Our pico- and femtosecond laser system for TRLFS, described in /1/, was extended by an optical parametrical amplifier (OPA) system to generate a tunable wavelength range between 290 nm and 10 µm.

The wavelengths are generated by nonlinear frequency processes on beta-barium (BBO) crystals. The OPA is pumped by femtosecond laser pulses (<130 fs, 800 nm) which are generated in a mode-locked Ti: sapphire oscillator (Tsunamie, Spectra Physics). First these pulses are amplified to 1 mJ in the regenerative Ti:sapphire amplifier consisting of two Pockells cells which select a train of a number of individual pulses. For an output energy higher than 1 mJ, the selected pulse train is injected into an additional newly installed multipass Ti : sapphire amplifier (with four mirrors, Superspitfire, Spectra Physics) which makes it possible to achieve an output energy of 3 mJ for pumping the OPA. The output energy of the OPA is nominally 30 µJ at 320 nm.

Investigations of the fluorescence properties of a humic acid were the first series of measurements carried out with the OPA system. The aim of this work was to obtain an overview of the changes in the fluorescence emission spectra of humic acid in a broad emission wavelength range as a function of the excitation wavelength.

The time-resolved fluorescence spectra of Aldrich humic acid (pH=11, 5 mg/l) were recorded at three excitation wavelengths (338, 360 and 400nm) and evaluated by the method described in /2/. Each decay curve in the wavelength range from 430 to 570 nm was fitted with a di-exponential decay function (300 single decay functions for excitation wavelengths at 338 nm and 400 nm, 90 for 360 nm). A reliable description of the decay curves is only possible in therms of di-exponential decay. Errors in the calculated lifetimes and fluorescence intensities are less than 20 %. Higher decay orders lead to unacceptable errors in lifetimes and amplitudes.

## Example

The lifetime as a function of the emission wavelength depending on the excitation wavelength is shown in Fig. 1. The fluorescence kinetics depends on the excitation wavelength. Compared with 360 and 338 nm the fluorescence lifetimes at 400 nm are slightly smaller. Despite considerable differences between the excitation wavelengths, the fluorescence lifetimes have the same magnitude, $J_1$ from 1.1 to 1.7 ns and $J_2$ from 4.2 to 8 ns. The normalized spectra, calculated from the computed fluorescence intensities $A_1$ and $A_2$ are depicted in Fig.2. The shape of the spectra remains unchanged. A characteristic increase in the emission maximum with increasing excitation wavelength is observed for $A_1$. For $A_2$ the emission spectra excited with

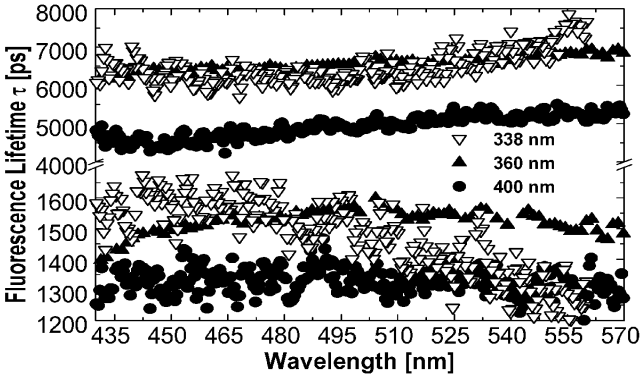


Fig. 1: Fluorescence lifetime as a function of the emissions wavelength for three excitation wavelength.

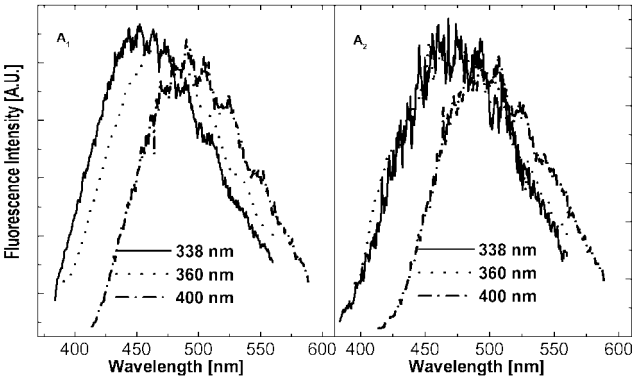


Fig. 2: Calculated fluorescence spectra of Aldrich humic acid (normalized intensity)

338 nm and 360 nm are almost identical. A significant shift occurs at an excitation wavelength of 400 nm (Fig. 2). The ratios of the amplitudes $A_1$ and $A_2$ are given in Tab. 1.

| Excitation wavelength [nm] | Amplitude $A_1$ [%] | Amplitude $A_2$ [%] |
|---|---|---|
| 338 | 68 ± 4 | 32 ± 4 |
| 360 | 84 ± 5 | 16 ± 5 |
| 400 | 53 ± 3 | 47 ± 3 |

Tab. 1: Dependence of the relative fluorescence intensity (from 440 to 560 nm) on the excitation wavelength

For the first time the fluorescence kinetics of a humic acid was studied and calculated over a broad emission wavelength range with a high density of measurement points at three excitation wavelengths. Comprehensive investigations are necessary in view of the complexity of the humic acid systems and for a thorough discussion of the first results. These Investigations can be conducted by excitation in a broad wavelength range thanks to the new OPA system, by recording the whole emission spectra and evaluating the decay kinetics of the whole emission spectra.

## References

/1/ Rutsch, M., et al., Report FZR-247 (1999) p. 14
/2/ Rutsch, M., et al., this report p. 9

# THE FLUORESCENCE LIFETIME AS A KEY TO A "FINGER PRINT" CHARACTERISTIC OF HUMIC ACID?

M. Rutsch, G. Geipel, G. Bernhard

*The fluorescence decay processes of five humic acid samples were studied. The results were to be related to the structural properties of the humic acids.*

## Experimental

The following humic acid samples were investigated:

I) purified Aldrich HA
ii) a synthetic humic acid (Maillard reaction type M42 /1/)
iii) Aldrich HA with blocked phenolic groups /2/
iv) a natural humic acid (extracted from the "Kleiner Kranichsee" Bog in Saxony /3/)
v) a natural fulvic acid (extracted from the "Kleiner Kranichsee" Bog in Saxony /3/)

Experimental conditions of fluorescence measurements:
Excitation wavelength - 400 with an energy of 30 µJ, pulse duration < 130 fs, gate time of the CCD camera - 2 ns and slit of the spectrograph - 100 µm. 1,000 laser shots were collected and averaged per spectrum. The spectra were recorded from 409 to 590 nm in steps of 0.473 nm and from 0 to 17 ns after laser pulse excitation in delay time steps of 25, 50 and 100 ps. The starting point of the measurement was set at approximately 500 ps before excitation. The concentration of the humic acid solutions was 5 mg/l, the pH was adjusted to 6.5 and 11.5.
All spectra were evaluated by the method described in /4/.

## First results

The averaged fluorescence lifetimes of the single lifetimes between 460 nm and 540 nm (210 single decay curves) at pH 6.5 and 11.5 are listed in Tab. 1. All humic acids investigated show two lifetimes, $J_1$ mainly in the region between 1.2 and 1.5 and $J_2$ between 4 and 5.6 ns. The first lifetime $J_1$ is almost constant for all examined humic acids. For lifetime $J_2$ the differences between the samples are more significant.

| Sample | pH = 6.5 | | pH = 11.5 | |
|---|---|---|---|---|
| | $J_1$ [ps] | $J_2$ [ps] | $J_1$ [ps] | $J_2$ [ps] |
| i) | 1406± 63 | 5375± 42 | 1345± 15 | 4967± 19 |
| ii) | 1403± 101 | 4607± 428 | 1431± 77 | 4549± 299 |
| iii) | 1545± 93 | 5601± 259 | 1331± 68 | 4672± 206 |
| iv) | 1295± 174 | 3774± 471 | 1318± 13 | 4249± 129 |
| v) | 1372± 160 | 4038± 394 | 1319± 43 | 4167± 129 |

Tab 1: Fluorescence lifetime of the humic acid samples at pH=6.5 and pH=11.5

In all samples the fluorescence lifetime $J_2$ depends very slightly on the emission wavelength in the emission wavelength range considered. The fluorescence lifetimes increase continuously from 460 nm to 540 nm and reach values that are 10 to 15% higher compared with 460 nm (Fig. 1).

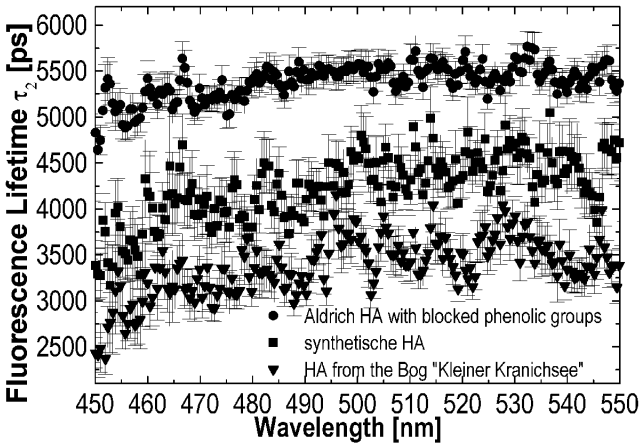


Fig. 1: Fluorescence lifetime $J_2$ as a function of the emissions wavelength ($8_{ec}$ = 400 nm).

The fluorescence spectra, calculated from the amplitudes $A_1$ and $A_2$, are almost identical for all samples. The ratios between the amplitudes $A_1$ and $A_2$ vary, depending on the various humic acid samples (Tab. 2). $J_i$ and $A_i$ are found to be slightly influenced by the pH.

| Sample | pH = 6.5 | | pH = 11.5 | |
|---|---|---|---|---|
| | $A_1$ [%] | $A_2$ [%] | $A_1$ [%] | $A_2$ [%] |
| i) | 49±2 | 51±2 | 52±1 | 48±1 |
| ii) | 58±7 | 42±7 | 67±5 | 32±5 |
| iii) | 54±2 | 46±2 | 49±4 | 51±4 |
| iv) | 57±8 | 43±8 | 63±1 | 37±1 |
| v) | 59±5 | 41±25 | 55±10 | 45±10 |

Tab 2: Relative fluorescence intensity of the humic acid sample at pH=6.5 and pH =11.5

The content of carboxylic and alcoholic groups provides structural information about the examined humic acids /1-3/. In general there is no significant correlation between the lifetimes $J_i$, amplitudes $A_i$ and the structural characteristics of the humic acids at an excitation wavelength of 400 nm. It is shown that the blocked phenolic groups (methyl ether groups) have no significant influence on the fluorescence properties of a humic acid.
But with a shift of the excitation wavelength towards the absorption maxima (330<8<370 nm) of the humic acids, more fluorescence decay processes might become detectable and more differences might occur.

## References

/1/ Pompe, S., et al., Radiochim. Acta **74**, 135 (1996)
/2/ Pompe, S., et al., Radiochim. Acta **82**, 89 (1998)
/3/ Schmeide, K., et al., Report FZKA 6124 (1998) p. 161
/4/ Rutsch, M., et al., this report p. 9

# GEOHISTORIC SIGNIFICANCE OF MARINE HUMIC COMPOUNDS AS RELATED TO THE FORMATION OF MICROCRYSTALLINE, AUTHIGENIC CA-CARBONATES: FIRST RESULTS FROM THE SEDIMENTARY ROCK RECORD (LOWER CRETACEOUS)

F. Neuweiler, A. Reimer, M. Rutsch, G. Geipel, K.H. Heise

*Qualitative and semi-quantitative analysis of intra- versus extracrystalline humic compounds from authigenic versus allogenic microcrystalline carbonate (marine Cretaceous sediment, ca. 100 million year old) was proceeded applying TRLFS. Our first results suggest that marine polymer gels acted as substrates for the in-situ precipitation of marine calcite, whereas allomicrite was preferentially covered by humic compounds via multiple deposit feeding.*

## Introduction

50 to 80 % of the total organic material in marine waters consists of water humus, humic substances or gelbstoff /1/. This fraction makes up the majority of the colloidal organic carbon in seawater. Accumulation at the sea floor is controlled, e.g. by sediment grain size and mineralogy well expressed by preferential adsorption of humic compounds upon clay minerals /2/. Microaggregates of marine organic polymers may also serve as nuclei for Ca-carbonate precipitation through complexation of divalent cations such as $Ca^{2+}$ and $Mg^{2+}$ /3/. The latter mechanism may lead to long-term, intracrystalline preservation of polymers, thus providing a tool to trace authigenic Ca-carbonate precipitation in ancient reef rocks and lithified surface sediments or hardgrounds. Our first studies focused on the identification of loci (intra- versus extracrystalline) and related semi-quantification of fossil humic compounds from automicrite and allomicrite.

## Material and Methods

Samples (calcite) were collected from a Cretaceous (Upper Albian) mud bank exposed near Iraneta, Navarra Province, N Spain. Rock thin sections were used for fluorescence microscopy, excite. 395-440 nm; em. >470 nm. By selective extraction we differentiated between two extracrystalline fractions (NaOH > 1-10 kD and > 10 kD) and two intracrystalline fractions (HCl > 1 kD and NaOH > 1 kD). Aqueous solutions were measured using time-resolved laser-induced fluorescence spectroscopy (TRLFS, excite. 400 nm, em. 430-610 nm, laser pulse <130 fs).

## Results

Total organic carbon content ranges from 0.3 to 0.7 weight-%. Fluorescence microscopy reveals that fluorescence occurs highly selective (Fig.1) as related to automicrite, faecal pellets, geopetal allomicrite (pars), some skeletal components (e.g. sponges), and rim cement (weak fluorescence). The spar mosaic and most of the skeletal debris is non-fluorescent as well as microcrystalline sediment which became strongly recrystallized towards microspar. Emission spectra of subsamples of authigenic and allogenic microcrystalline sediment is shown in Fig. 2. Humic compounds are significantly enriched within automicrite (intracrystalline sink), whereas humic compounds of allomicrite are mainly extracrystalline, thus predominantly localized upon crystal surfaces. Albeit, we have to check for such a systematic relationship other examples from the rock record, we suggest that polymeric marine gels of humic compounds served as an organic substrate for the in-situ precipitation of marine calcite. Concerning allomicrite, a successive enrichment of refractory organic matter during ingestion and re-ingestion is likely. TRLFS is a promising tool in order to elucidate cycling and burial of marine organic carbon within the sedimentary rock record. It also provides important data for our understanding of the origin and history of marine, microcrystalline carbonates.

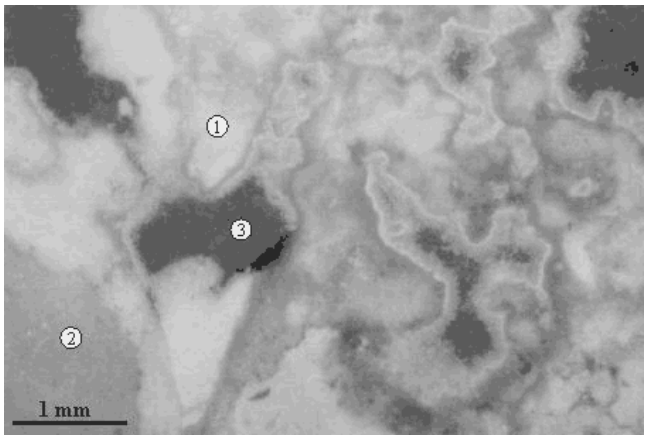


Fig. 1: Fluorescence micrograph of a Cretaceous mud bank rock, 1=automicrite, 2=allomicrite, 3=cement.

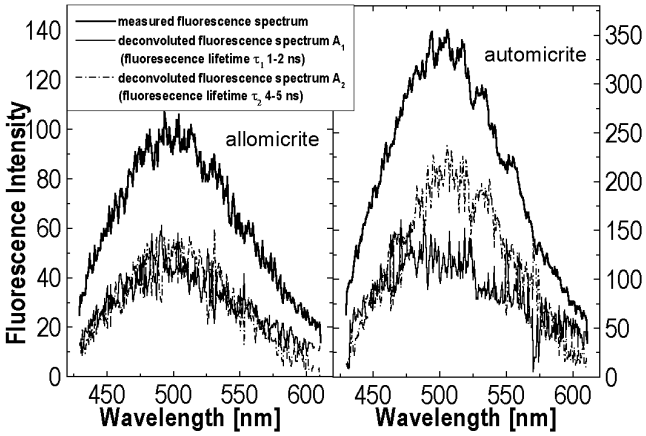


Fig. 2: Fluorescence emission spectra obtained from allo- and automicrite, HCl-soluble intracrystalline fraction.

## References

/1/ Hayes, M.H.B., Humic substances: progress towards more realistic concepts of structures. Royal Soc. Chemistry, Spec. Publ. **228**, 1-27 (1998)

/2/ Meyers, P.A., Organic geochemical proxies of paleocanographic, paleolimnologic, and paleoclimatic processes. Org. Geochem. **27**, 213-250 (1997)

/3/ Chin, W.-C., et al., Spontaneous assembly of marine dissolved organic matter into polymer gels, Nature **391**, 568-572 (1998)

# ABSORPTION SPECTROSCOPY OF PLUTONIUM AT LOW CONCENTRATIONS

S. Taut, H. Nitsche [1]
[1] Lawrence Berkeley National Laboratory, Glenn T. Seaborg Center

*We measured the absorption spectra of Pu(VI) perchlorate in concentrations as low as $2x10^{-7}$ M. Model experiments with Nd perchlorate solutions indicate that Pu(III), Pu(IV), and Pu(V) should be detectable in at least $5x10^{-7}$ M solutions, presumably also in $2x10^{-7}$ M solutions.*

The Pu oxidation state in solutions at low concentrations is usually determined with a chemical separation procedure or LIPAS /1, 2/. We tested the detection limit for Pu and Nd of an conventional absorption spectrometer using a one-meter path length cell.

From $^{239}$Pu(VI) /3/ a dilution series from $7x10^{-8}$ M to $1.8x10^{-6}$ M Pu in 0.3 M $HClO_4$ was prepared. The Pu concentration was determined by LSC. A Nd dilution series in 0.1 M $HClO_4$ was prepared with concentrations from $5x10^{-7}$ M to $2.5x10^{-6}$ M. Three samples per concentration were measured. The absorption spectra were recorded with an OceanOptics S2000 spectrometer coupled to a OceanOptics LPC-1 cell with one meter path length.

We first determined the instrument's spectral translucence with water. A good signal to-noise ratio was obtained in the region between 540 and 700 nm. Then, we tested the spectrometer with $Nd^{3+}$. It has an adsorption band at 575.5 nm with $\varepsilon$ = 6.93 $M^{-1}$ $cm^{-1}$ /4/. Fig. 1 shows the linearity between the absorption band areas and the Nd concentration.

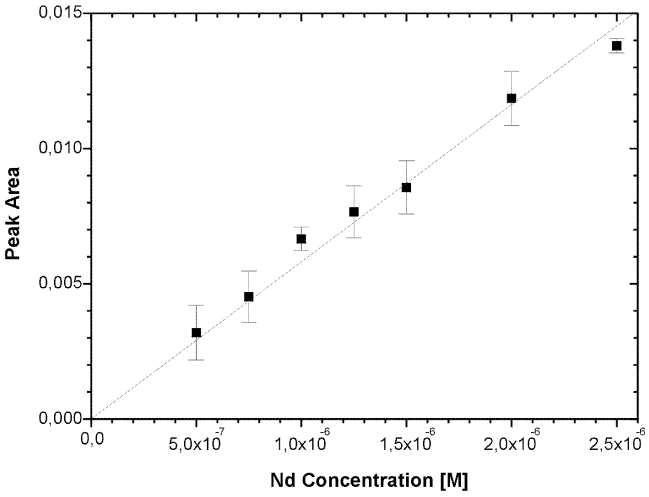


Fig. 1: Absorption peak area as function of Nd concentration; $Nd^{3+}$ in 0.1 M $HClO_4$, peak at 575.5 nm

The characteristic absorption peak of Pu(VI) is at 830 nm with $\varepsilon$ = 550 $M^{-1}$ $cm^{-1}$ /5/. This is in a region with very low spectral translucence, about 3 % of the maximum. Therefore, we substantially increased the light intensity to obtain a spectrum in this region. Unfortunately, this leads to spectrometer saturation below 750 nm, and a strong increase of noise above 870 nm. Fig. 2 shows the spectrum of a $3.61x10^{-7}$ M Pu(VI) solution together with the fitted peak area. Fig. 3 shows the linearity between the concentration and the absorption peak area. We encountered baseline instabilities in the Pu experiments due to small gas bubbles in the cell. This could be a reason for the fact that the fitted straight line does not intersect with zero.

Pu(III), Pu(IV), and Pu(V) have absorption maxima between 560 nm and 700 nm with $\varepsilon > 17$ /5/, i.e., $\varepsilon$ is at least 2.5 times higher than the $\varepsilon$ for the $Nd^{3+}$ peak at 575.5 nm. This should enable us to detect Pu in these oxidation states at concentrations of about $2x10^{-7}$ M Pu, 2.5 times lower than the detection limit of $5x10^{-7}$ M that we determined for $Nd^{3+}$.

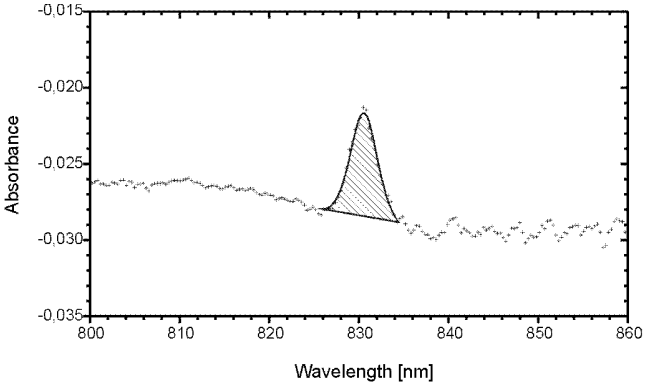


Fig. 2: Absorption spectrum of $3.61x10^{-7}$ M Pu(VI) in 0.3 M $HClO_4$, peak at 830 nm

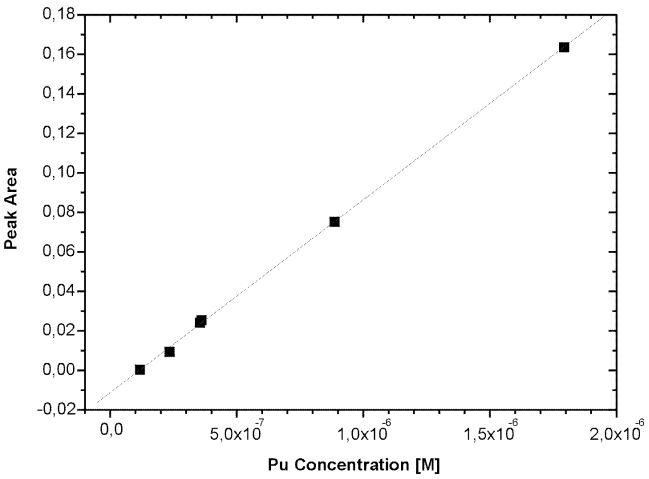


Fig. 3: Absorption peak area as function of Pu concentration; Pu(VI) in 0.3 M $HClO_4$, peak at 830 nm

Acknowledgments

S. Taut gratefully acknowledges the Glenn T. Seaborg Center of the Lawrence Berkeley National Laboratory for a Visiting Scientist Fellowship.

References

/1/ Neu, M.P., et al., Radiochim. Acta **66/67**, 265 (1994)
/2/ Kim, J.-I., et al., *Topics in Current Chemistry*, Berlin, 1990, p. 131 ff
/3/ Taut, S., et al., Sorption of hexavalent Plutonium onto Goethite, this report p. 14
/4/ Ryabchikov, D.I., et al., *Analytical Chemistry of Yttrium and the Lanthanides*, London, 1970, p. 160
/5/ Cohen, D., J. Inorg. Nucl. Chem. **18**, 211 (1961)

# SORPTION OF HEXAVALENT PLUTONIUM ONTO GOETHITE

S. Taut, K. Pecher [1], H. Nitsche [1]
[1] Lawrence Berkeley National Laboratory, Glenn T. Seaborg Center

*The sorption of hexavalent plutonium onto goethite was studied with batch experiments in aqueous solution as a function of time and pH ranging from 3 to 6.3. The sorption behavior is similar to U(VI) and Pu(V).*

## Introduction

We investigated the adsorption of Pu(VI) onto synthetic goethite as a first part of a larger program for Pu adsorption onto iron oxides. Until now, no data about Pu(VI) adsorption onto goethite are reported in the literature. First results are reported here.

## Experimental

$^{239}$Pu was purified by anion exchange /1/. Pu(VI) was prepared by oxidation with hot conc. $HClO_4$. The hexavalent oxidation state was verified by Vis/near-IR absorption spectroscopy. A stock solution was prepared by adding 25 µL of this solution to 5 mL water.

Bayferrox 910 goethite was used as adsorbent material ($pH_{ZPC}$ 7.8; BET surface 17.5 $m^2g^{-1}$; surface hydroxyl groups density 5.5 $nm^{-2}$; geometry: needles with ~0.4 µm length and ~0.1 µm diameter).

Adsorption samples were prepared in 50 mL polypropylene vials: 10 mg goethite, 4 mL 1 M $NaClO_4$ solution and 100 µL Pu stock solution were added to 30 mL water. The initial sample pH was adjusted during three days. Then, the solution volume was filled to a total of 40 mL, and the pH was recorded. Similar reference solutions without goethite were prepared in the same way. The total plutonium concentration in all samples was $5.4x10^{-7}$ M. The various samples had initial pH values between 3.1 to 6.3. In this region $PuO_2^{2+}$ and $PuO_2(OH)^+$ are the predominant species, and the formation of carbonate complexes is negligible.

All samples were gently agitated to avoid an increase in surface area due to abrasion. No further pH adjustments were carried out during the equilibration. After different times, the pH was measured and samples were taken from adsorption and reference experiments. The samples were counted for plutonium by liquid scintillation counting (LSC). To exclude the presence of colloidal goethite in the LSC samples, each sample taken from the supernatant solution was filtered through a Microcon YM-30 filter (experiments proved that no Pu(VI) sorption occurred on the filters in the pH range 3–6.3). Five 100 µL aliquots per sample were measured in a LKB Wallace 1219 counter. The adsorption was calculated as the Pu concentration ratio of sample and corresponding reference solution.

## Results

Fig. 1 shows the adsorption curves as a function of pH and time.

Within 624 h, the pH values of all samples with pH above 4 had shifted slowly to lower values, e.g., from 6.2 to 5.4. In the reference solutions with initial pH values from 3 to 4.5 the pH remained nearly constant, in the reference solution with higher pH values the pH shifted slowly (from 4.8 to 4.7, and from 6.3 to 5.3). No sorption of Pu occurred onto the vial walls in the reference solutions in this time interval. For the adsorption samples having a pH greater than 4.5, the Pu sorption increased with time.

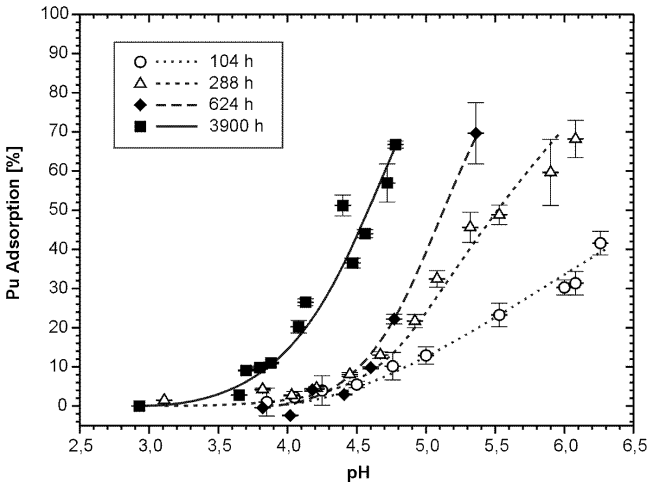


Fig. 1: Adsorption of Pu(VI) in 0.1 M $NaClO_4$ solution onto goethite as function of pH and time.

Between 624 and 3900 hours, the pH shift to lower values in the adsorption and reference samples continued. The loss of Pu in the reference solutions after 3900 h was 6 % (vial sorption). The 3900 hour-sorption curve has a shape similar to the adsorption curve of Pu(V) which may indicate that a (partial) reduction may have occurred /2/. Unfortunately, the plutonium concentration in the batch experiments was too low to verify this change of oxidation state by absorption spectroscopy. The loss of Pu in the reference solutions (possibly caused by Pu(IV) sorption onto the vial walls) may be an indiction that even a reduction to Pu(IV) may have taken place.

Pu(V) /2/, Np(V) /3/, and U(VI) /4/ have very similar sorption curves thus indicating comparable actinide binding on goethite. Further studies on the oxidation state of the Pu and the bonding to goethite are underway.

## Acknowledgments

S. Taut gratefully acknowledges the Glenn T. Seaborg Center of the Lawrence Berkeley National Laboratory for a Visiting Scientist Fellowship.

## References

/1/ Katz, J.J., et al. (eds.), *The Chemistry of the Actinide Elements*, London 1986, vol. 1, p. 550 ff
/2/ Sanches, A.L., et al., Geochim. Cosmochim. Acta **49**, 2297 (1985)
/3/ Kohler, M., et al., Radiochim. Acta **85**, 33 (1999)
/4/ Hsi, C.-K.D., et al., Geochim. Cosmochim. Acta **49**, 1931 (1985)

# SORPTION BEHAVIOR OF U(VI) ON PHYLLITE: EXPERIMENTS AND MODELING

T. Arnold, T. Zorn, H. Zänker, G. Bernhard, H. Nitsche [1]
[1] Lawrence Berkeley National Laboratory, The Glenn T. Seaborg Center, Berkeley, CA 94720, USA

*The sorption of U(VI) onto low-grade metamorphic rock phyllite was modeled with the Diffuse Double Layer Model (DDLM) using the primary main mineralogical constituents of phyllite, i.e. quartz, chlorite, muscovite, and albite as input components and, as additional component, the poorly ordered Fe oxide hydroxide mineral ferrihydrite.*

## Hypothesis

We hypothesize that the sorption behavior of uranium onto rocks can be described in an additive fashion to the sorption onto its mineralogical components and onto possibly forming secondary minerals. To verify this hypothesis, we carried out a large number of batch sorption experiments with U(VI), acid base titration, and adsorption isotherms with phyllite, quartz, chlorite, muscovite, albite, and ferrihydrite. Furthermore, we probed for the possible formation of secondary Fe phases by Moessbauer spectroscopy and centrifugation experiments. A detailed description of the experimental conditions is given in /1/.

## Results and Discussion

The basis for the successful interpretation of the experimental sorption data of uranyl(VI) on phyllite, which is composed of 48 Vol % quartz, 25 Vol. % chlorite, 20 Vol % muscovite, 5 Vol.% albite feldspar, and 2 Vol. % opaqueous material, mostly rutile, magnetite, and traces of hematite, were:

(1.) the determination of surface complex formation constants of uranyl with quartz, chlorite, muscovite, albite, and ferrihydrite, respectively, in individual batch sorption experiments, shown in Tab. 1;

| Mineral | Reaction | log K | Ref |
|---|---|---|---|
| Quartz | $X(OH)_2 + UO_2^{2+} = (XO_2UO_2) + 2H^+$ | -5.51 | /1/ |
| Chlorite | $XOH + UO_2^{2+} = (XO^-UO_2^{2+}) + H^+$ | 4.71 | /1/ |
| Muscovite | $X(OH)_2 + UO_2^{2+} = (XO_2UO_2) + 2H^+$ | -0.55 | /1/ |
| | $XOH + UO_2^{2+} = (XO^-UO_2^{2+}) + H^+$ | -5.75 | /1/ |
| Albite | $XOH + UO_2^{2+} = (XO^-UO_2^{2+}) + H^+$ | 1.54 | /1/ |
| Ferrihydrite | $Fe_s(OH)_2 + UO_2^{2+} = Fe_sO_2UO_2 + 2H^+$ | -3.18 | /1/ |
| | $Fe_s(OH)_2 + UO_2^{2+} = Fe_sO_2UO_2 + 2H^+$ | -6.31 | /1/ |
| | $Fe_s(OH)_2 + UO_2^{2+} + CO_3 = Fe_sO_2UO_2CO_3 + 2H^+$ | 3.67 | /4/ |
| | $Fe_s(OH)_2 + UO_2^{2+} + CO_3 = Fe_sO_2UO_2CO_3 + 2H^+$ | -0.42 | /4/ |

Tab. 1: Surface complex formation constants (I = 0) of uranyl(VI) with mineralogical components of phyllite.

(2.) the determination of surface acidity constants of quartz, chlorite, muscovite, and albite, obtained from separate acid base titration, /1,2/;

(3.) the determination of surface site densities of quartz, chlorite, muscovite and albite evaluated independently of each other with adsorption isotherms, and

(4.) the quantification of the secondary phase ferrihydrite, which formed during the batch sorption experiments with phyllite.

The surface complex formation constants and the protolysis constants were optimized by using the experimentally obtained data sets and the computer code FITEQL /3/. Surface site densities were evaluated from adsorption isotherms at pH 6.5 and a total uranium concentration of $1\times10^{-4}$ M. The formation of ferrihydrite during the batch sorption experiment was identified by Moessbauer spectroscopy, showing a 2.8 percent increase of $Fe^{3+}$ in the phyllite powder. The newly formed ferrihydrite was present as Fe nano-particles or agglomerates with diameters ranging from 6-25 nm.

FITEQL calculations were carried out for a composite phyllite which was assembled from the respective mineral components quartz, chlorite, muscovite, and albite in their relative proportion within the phyllite, and in addition with the newly forming phase ferrihydrite.

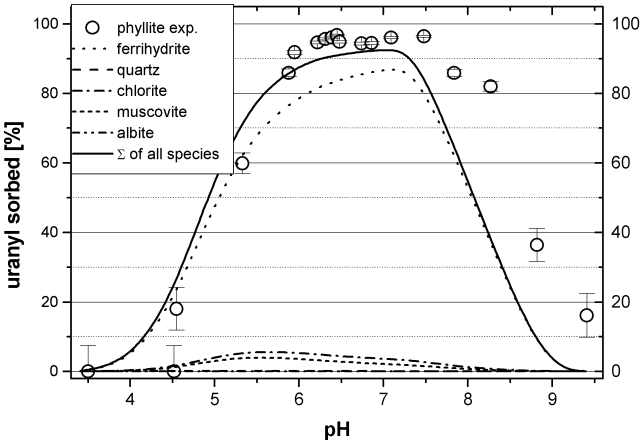


Fig. 1: Modeled uranyl(VI) sorption on phyllite together with experimental uranyl(VI) sorption data on phyllite.

Fig. 1 shows the modeled sorption curve together with the experimental sorption data of phyllite. It is noteworthy that the calculated sorption curve of the phyllite is based exclusively on surface complex formation and surface acidity constants obtained from individual batch experiments with pure mineral phases. No experimental data of phyllite were used for the optimization procedure.

## Conclusions

The modeling indicated that uranyl sorption to ferrihydrite clearly dominates the uranyl sorption on phyllite showing the great importance of secondary iron phases for sorption studies.

## Acknowledgments

The studies were funded by the Deutsche Forschungsgemeinschaft (DFG) under the project number Ni 210/ 6-1.

## References

/1/ Arnold, T. et al., subm. to J. of Contam. Hydrol.

/2/ Zorn, T.; *Untersuchungen zur Sorption von U(VI) an das Gestein Phyllit zur Bestimmung von Oberflächenkomplexbildungskonstanten*. PhD. Thesis, TU Dresden (2000)

/3/ Herbelin, A., Westall, J.; *FITEQL* Report 96-01, Oregon State University, Oregon (1996)

/4/ Waite, T.D. et al., Geochim. Cosmochim. Acta **58**, 5465 (1994)

# MODELING THE SORPTION OF URANIUM(VI) ONTO ALBITE FELDSPAR

T. Arnold, T. Zorn, G. Bernhard, H. Nitsche

*A surface complexation constant for uranyl sorbing onto albite and two protonation reactions on the albite surface were determined by applying the Diffuse Double Layer Model together with the computer code FITEQL*

## Experimental

Acid base titration of albite feldspar were performed under nitrogen atmosphere. One gram of albite (grain size 63 - 200 µm) was titrated with acid and base in 80 mL 0.1 M $NaClO_4$ - solution. Sixty µL of $1 \cdot 10^{-3}$ M NaOH or HCl were added to the albite suspension in intervals of two minutes. Batch sorption experiments in the pH range of 3.5 to 9.5 were carried out in equilibrium with atmospheric $P_{CO2}$ a solid to solution ratio of 0.5g/40 mL and an uranium concentration of $1 \cdot 10^{-6}$ M uranium(VI).

## Results and discussion

The specific surface area, the surface site density and the protolysis constants of the albite feldspar was determined prior to applying the Diffuse Double Layer Model (DDLM) to the sorption data. The specific surface area of the albite powder (grain size 63-200 µm) was determined with the BET method as 0.2 $m^2/g$. The surface site density of albite and the respective protolysis constants were determined with data derived from acid-base titration. The point of zero charge ($pH_{pzc}$) is known to be at pH 2.0 /1/. From this the surface site density was determined at pH 9.47, a pH at which almost all surface species should exist as deprotonated $XO^-$ species. The surface site density is then calculated from:

$$F = F/A \times S\ [c_A - c_B - (H^+) + (OH^-)]$$

$c_A$ is the molar concentration of added acid, $c_B$ the molar concentration of added base, $(H^+)$ and $(OH^-)$ are the molar concentration of $H^+$ and $OH^-$,calculated from the pH measurement, F is the Faraday constant, A is the specific surface area and S the solid solution ratio. At pH 9.47 a surface site density of 3.10 sites/$nm^2$ was determined. It was expected that at pH values higher than the $pH_{pzc}$ the predominant surface species on albite is the negatively charged $XO^-$ species. However, using only one surface reaction, $XOH = XO^- + H^+$, to model the titration data was unsuccessful. In contrast, it was found that there is already an excess of protons. This clearly indicates that an additional proton consuming reaction should occur. In various mineral dissolution experiments with albite Hellmann et al. /2/ and Wollast and Chou /3/ found out that a hydrogen enriched surface layer forms during the early stages of chemical weathering. They both related this behavior to a cation exchange reaction in which $Na^+$ from the albite surface is replaced by $H^+$ from solution. Despite the presence of 0.1 M $NaClO_4$ which should suppress the ion exchange between $Na^+$ and $H^+$ at the albite surface, this additional cation exchange reaction seems to occur and was therefore included in the modeling. The titration data was modeled with the following two reactions:

$$XOH = XO^- + H^+ \qquad \log K_{XO-}$$

$$NaXOH + H^+ = XOH_2^+ + Na^+ \qquad \log K_{XOH2+}$$

Both formation constants were optimized simultaneously with FITEQL /4/ and the following constants were determined at an ionic strength of I = 0.1 M: $\log K_{XO-} = -7.87$ and $\log K_{XOH2+} = 6.34$ with WSOS/DF = 9.89. WSOS/DF stands for "weighted square of sums divided by degree of freedom" and is an indicator of the goodness of fit /4/. However, the WSOS/DF value is highly dependent on the error assigned to the experimental data and therefore should not be over interpreted.

With these two constants the sorption results of the uranium(VI) albite system were modeled with the DDLM by using a partial pressure of $P_{CO2}$ of $10^{-3.5}$ and including all known aqueous uranium species. The experimental data was best fitted with the monodentate mononuclear surface complex:

$$XOH + UO_2^{2+} = (XOUO_2)^+ + H^+ \qquad \log K_{(XOUO2)+}$$

Despite showing a high WSOS/DF value of 23.30 this species with $\log K_{(XOUO2)+} = 1.22$ (I = 0.1 M) was chosen, because it represents the best description of the experimental data. However, both modeled adsorption edges, as shown in Fig. 1, are too wide.

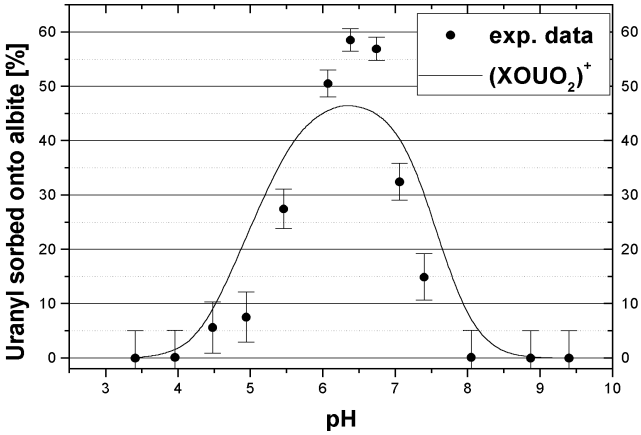


Fig. 1: Exp. and calc. data of U(VI) sorption onto albite

As this species is purely postulated, spectroscopic evidence is urgently required to identify the local environment of sorbed uranium on the surface. Furthermore, additional reactions, e.g. cation exchange and/ or chemical weathering may alter the albite surface and thus influence the sorption of uranyl onto albite.

## Acknowledgments

G. Grambole is thanked for conducting acid - base titration, W. Wiesener and her team for performing ICP-MS analysis, and G. Schuster for BET measurements.

## References

/1/ Stumm, W.; *Chemistry of the solid-water interface*. Wiley (1992).

/2/ Hellmann, R., et al.; Geochimica Cosmochimica Acta **61** (8), 1575-1594 (1997)

/3/ Wollast, R., Chou, L.; Geochimica et Cosmochimica Acta **56**, 3113-3121 (1992)

/4/ Herbelin, A., Westall, J.; *FITEQL Version 3.2.* Report 96-01, Dep. of Chem., Oregon State University, (1996)

# APPLYING THE DDLM TO MODEL THE SORPTION OF URANIUM(VI) ONTO QUARTZ AND MUSCOVITE

T. Arnold, T. Zorn, G. Bernhard, H. Nitsche

*The DDLM Model was used with sorption data to calculate surface complexation constants for uranyl sorbed onto quartz and muscovite, respectively. Furthermore, one deprotonation reaction for the quartz surface and two protonation reactions for muscovite were calculated.*

## Experimental

Batch sorption experiments with uranyl and the minerals quartz and muscovite, respectively, were carried out under ambient temperature and pressure in the pH range from 3.5 to 9.5 in 0.1 M $NaClO_4$ solution. An U(VI) concentration of $1 \cdot 10^{-6}$ M, a size fraction of 63-200 µm, and a solid solution ratio of 0.5 g/40 mL was used. Acid base titrations with muscovite and quartz were carried out under $N_2$ atmosphere and the above specified experimental conditions. The titrations were performed with $CO_2$-free NaOH and $CO_2$-free deionized water. The specific surface area of both mineral surfaces (63-200 µm) was determined with the BET method. For quartz 0.2 $m^2/g$ and for muscovite 1.4 $m^2/g$ was found.

## Results and discussion

The point of zero charge ($pH_{pzc}$) of quartz is reported to range between pH 2.0 /1/ and pH 2.9 /2/. Conclusively, the quartz surface in our sorption experiments is negatively charged and $XO^-$ species should predominate. Therefore, only one acidity constant for the reaction $XOH = XO^- + H^+$ was determined. By using the titration data and FITEQL /3/ the acidity constant for quartz was determined to be $\log K_{XO^-} = -5.62$ at an ionic strength of I = 0.1 M. The value for weighted square of sums divided by degree of freedom (WSOS/DF), an indicator of the goodness of fit, was equal to 19.32. In contrast to quartz, the $pH_{pzc}$ of muscovite is at 6.6 /4/. This indicates that both positively and negatively charged surface species occur and thus, two acidity constants were determined. Again, titration data and FITEQL were used to calculate these constants. The resulting log K values for muscovite are listed below.

$XOH = XO^- + H^+$ $\quad \log K_{XO^-} = -7.81$ (I = 0.1 M)

$XOH_2^+ = XOH + H^+$ $\quad \log K_{XOH2+} = 6.06$ (I = 0.1 M)

The WSOS/DF value was 12.01. Using these acidity constants together with the sorption data obtained in batch experiments and the computer code FITEQL, surface complex formation constants for uranyl sorbing onto quartz and muscovite, respectively, were calculated. The surface complex which best modeled the sorption results with the Diffuse Double Layer Model in the quartz system was a bidentate mononuclear surface complex shown in the following equation:

$X(OH)_2 + UO_2^{2+} = (XO_2^{2-}UO_2^{2+}) + 2\,H^+ \quad \log K_{(XO2UO2)}$

EXAFS analysis /5/ indicated the formation of such a bidentate mononuclear surface species. The formation constant $\log K_{(XO22\text{-}UO22+)}$ of this species was calculated to be -5.72 (WSOS/DF = 2.66) at an ionic strength of I = 0.1 M. Using this calculated uranyl-quartz surface complex to model the sorption of uranyl onto quartz, it was found that there was a good agreement with the experimentally derived sorption data, as shown in Fig. 1. In the case of muscovite, however, the modeling favors the formation of two uranyl surface complexes. Both surface complex were simultaneously calculated

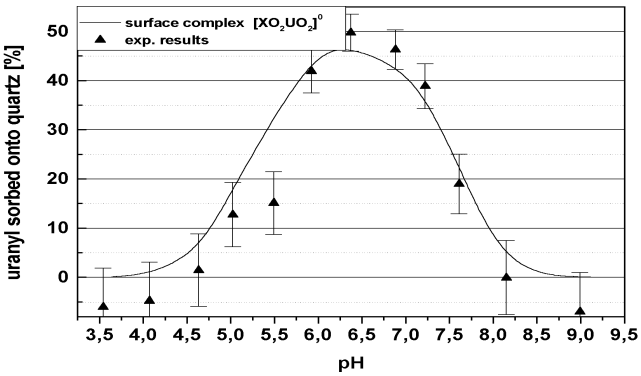


Fig. 1: Exp. and calc. data of U(VI) sorbed onto quartz.

with FITEQL. The first one is the monodentate mononuclear surface complex:

$XOH + UO_2^{2+} = (XO^-UO_2^{2+})^+ + H^+ \quad \log K_{(XOUO2)+}$

The second surface complex is a bidentate mononuclear surface complex:

$X(OH)_2 + UO_2^{2+} = (XO_2^{2-}UO_2^{2+}) + 2\,H^+ \quad \log K_{(XO2UO2)}$

For the first uranyl muscovite surface species the formation constant $\log K_{(XO\text{-}UO22+)+}$ was calculated to be - 0.86 (I = 0.1 M). The second one was determined to be -5.97 (I = 0.1 M). The WSOS/DF value was 5.73. The fitted data together with the experimental sorption results are shown in Fig.2.

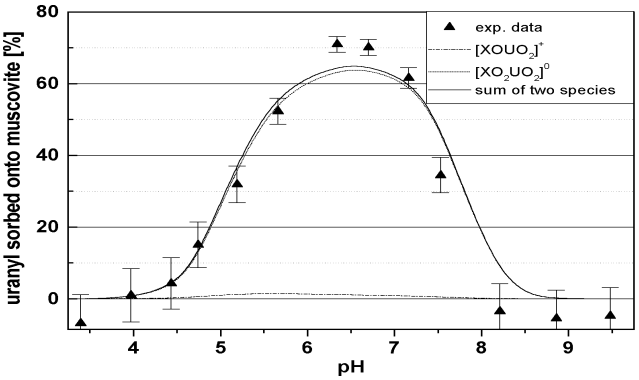


Fig. 2: Exp. and calc. data of U(VI) sorbed onto muscovite.

## Acknowledgments

G. Grambole is thanked for conducting acid - base titrations, W. Wiesener and her team for performing ICP-MS analysis, and G. Schuster for BET measurements.

## References

/1/ Stumm, W.; *Chemistry of the solid-water interface.* Wiley (1992).

/2/ Sposito, G.; *The surface chemistry of soils*. Oxford University Press, New York (1984)

/3/ Herbelin, A., Westall, J.; *FITEQL Version 3.2.* Report 96-01, Dep. of Chem., Oregon State University, (1996)

/4/ Sverjensky, D.A.: Geochim. Cosmochim. Acta **58**, 3123-3129.

/5/ Reich et al.: J. Elec. Spec. Rel. Phe. **96**, 237-243 (1998)

# THERMODYNAMIC DATABASE FOR SURFACE COMPLEXATION MODELS

V. Brendler, T. Arnold, G. Bernhard

*Surface complexation models (SCM) are in increasing use to substitute simplistic approaches such as the $K_d$ concept for the description of sorption processes. To apply such SCM in geochemical speciation modeling, a thermodynamic database containing published complexation constants and surface characteristics was established.*

## Surface Complexation Models

Modern concepts treat surface reactions as complexation reactions analogous to such reactions in homogeneous aqueous solutions. Therefore these models are called Surface Complexation Models (SCM), for details refer to, e.g., /1/. This requires the definition of surface sites with a finite concentration. Usually such surface sites are represented as =SOH groups with S denoting a metal from the solid structure, located at the solid-liquid interface. Many mineral surfaces, but especially colloids carry a significant surface charge, creating an electrostatic potential extending into the aqueous solution. To account in a proper way for this charge effect, additional terms have been introduced into adsorption models, modifying the activity of sorbate ions. These terms describe the electrical work necessary to penetrate the zone of electrostatic potentials, resulting in a difference between the activity of ions $\mathbf{M_s}$ with the charge $z^+$ near the surface and the same ions **M** in the bulk solution.

The main models used at present are sorted according to the increasing number of required electrostatic model parameters:

- the Diffuse Double Layer Model (DDL): Here, the total charge of the double layer is defined as a function only of charge and ionic strength. Thus, an important advantage of this rather simple approach is, that there are no electrostatic parameters required at all. This reduces data needs and consequently data uncertainty.
- the Constant Capacitance Model (CC): The constant capacitance model assumes only one layer or plane between surface and bulk solution. All specifically adsorbed ions contribute to the surface charge in this layer. Actually, this model is just a special case of the diffuse layer model for solutions of higher ionic strength ( I > 0.01 mol/L ) and surfaces of low potential. It is strongly dependent on the ionic strength, and requires one electrostatic parameter, the capacity **C**.
- the Triple Layer Model (TL): Two different planes are assumed for the surface: The innermost or o-plane does only incorporate protonation or deprotonation of surface sites. All other specifically adsorbed ions are assigned to the outer or b-plane. Therefore, each plane has its own charge and potential. The third layer (to justify the name of the model) is as in the above models the diffuse layer. In summary, this would give two electrostatic parameters (Capacities $\mathbf{C_1}$ and $\mathbf{C_2}$), but to reduce further the number of variable model parameters, $\mathbf{C_2}$ is generally fixed to 0.2, whereas $\mathbf{C_1}$ is a fitting parameter inside a range between 0.1 and 2.0, which is supported by theoretical considerations.

## Database Implementation and Content

The database is implemented in MS Excel 5.0, it is foreseen to be transferred as a relational database into MS Access. The data structure consists of three tables, with the first one containing the intrinsic surface properties such as the specific surface area, the number of distinct site types, surface site densities for each site type, the up to two constants for surface protolysis reactions, and electrostatic parameters (the capacities $\mathbf{C_n}$ of the various surface layers in the TL and CC models). The second table consists of the surface complexation constants, including the chemical reaction equation and the applied SCM type. The third table is the bibliography, with both original citations and secondary literature references.

Presently, the database contains 135 datasets for the following minerals / solid phases: ferrihydrite ($Fe_2O_3 \cdot H_2O$), goethite ($\alpha$-FeOOH), hematite ($\alpha$-$Fe_2O_3$), quartz ($SiO_2$), amorphous silica, pyrolusite ($MnO_2$), kaolinite, montmorillonite, $TiO_2$ (anatase), $Al_2O_3$, calcite($CaCO_3$), chlorite, cement, and fluorapatite. Most of them originate from publications in *Geochimica et Cosmochimica Acta* and in the *Journal of Colloid and Interface Science*. If available, data uncertainties are included.

This project is a steadily ongoing effort. In case of data gaps the database is supplemented by data estimation methods such as Linear Free Energy Relationships (see /2/). An important application of the SCM database was in the EU project RESTRAT /3/ to include surface phenomena into radiological risk assessment software. For this purpose, a subset of the database related to the DDL SCM was incorporated into the thermodynamic database of the geochemical speciation software MINTEQA2 /4/.

Acknowledgments

Financial support from the Nuclear Fission Safety Programme of the European Commission under contract F14P-CT95-0021a is gratefully acknowledged.

References

/1/ Stumm, W.; *Chemistry of the solid-water interface*. Wiley, New York, 1992

/2/ Dzombak, D.A., Morel, F.M.M.; *Surface complexation modeling*. Hydrous ferric oxide, Wiley, New York (1990)

/3/ http://www.fz-rossendorf.de/RESTRAT/

/4/ Allison, J.D., Brown, D.S., Novo-Gradac, K.J.; U.S. EPA, Environ. Res. Lab., Report EPA/600/3-91/021 (1991)

# DISTRIBUTION COEFFICIENTS FOR RISK ASSESSMENT OF THE DRIGG SITE

V. Brendler, A.Bousher [1], T. Arnold
[1] Westlakes Scientific Consulting, Moor Row, Cumbria, GB

*Distribution coefficients ($K_d$) for uranium, plutonium and americium with hydrous ferric oxides were computed for the British Low Level Waste Disposal Site at Drigg / Cumbria. The Diffuse Double Layer Surface Complexation Model (SCM) is used to describe the sorption behavior.*

## Modeling

A newly developed approach to incorporate physico-chemical phenomena into risk assessment modeling /1/ is applied to the Drigg Site in Cumbria/Great Britain, a low level radioactive waste disposal operated by BNFL.

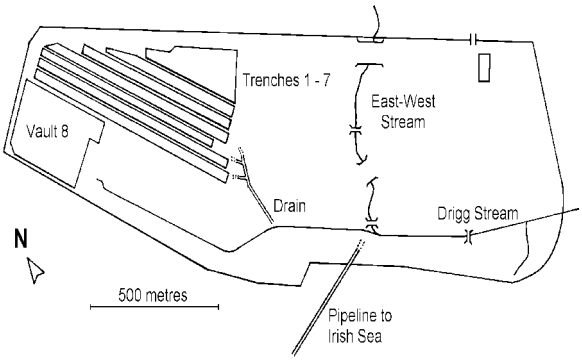


Fig. 1: Schematic view on the Drigg Site

A schematic overview is shown in Fig. 1, whereas Fig. 2 indicates the compartments used for the contaminant transport modeling, together with the major exposure pathways.

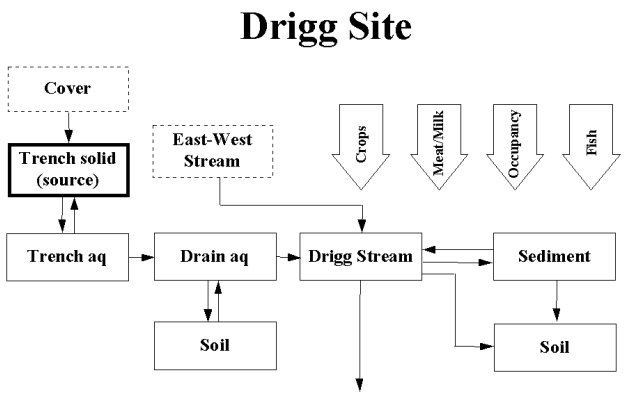


Fig. 2: Compartment scheme for the Drigg Site

The present model assumes two compartments with solid-water equilibria, the Drain (Box **D**) and the Drigg Stream (Box **S**).

The main contaminants are uranium, plutonium, americium and caesium. Based on sample analysis from the site, ferrihydrite was chosen as the major adsorbing surface. The Diffuse Double Layer model /2/ is selected to describe surface complexation. The respective intrinsic surface parameters and the reaction constants for the ions competing with the contaminants for sorption sites were taken from a database described earlier in this report, at page 30. The caesium sorption could not be described by an SCM, here ion exchange processes seem to be more appropriate.

## Results

Tab. 1 is based on runs with 1000 varied parameter sets. The computed $K_d$ values for all contaminants exhibit a clear lognormal distribution. They fall well into the range used so far for modeling of this site /3/, but exhibit much smaller uncertainties. Moreover, applying ranked regression analysis those parameters were identified contributing most to the uncertainty of the various computed $K_d$ values: pH, the carbonate content $C_{HCO3-}$, and the solid concentration $C_{solid}$. The first two parameters determine the contaminant speciation in solution, controlling the amount of hydrolysis species and carbonate complexes that reduce the respective sorbed portion. The uncertainty in the solid concentration is mainly assigned to the sediment composition (ferrihydrite content).

| Box | log $K_d$ ± s | 1st Factor | 2nd Factor |
|---|---|---|---|
| | *Uranium* | | |
| **D** | -0.42±0.38 | $C_{HCO3-}$: 71.7 % | pH: 8.9 % |
| **S** | 0.29±0.32 | pH: 36.1 % | $C_{solid}$: 27.4 % |
| | *Americium* | | |
| **D** | 1.81±0.66 | pH: 66.9 % | $C_{solid}$: 11.9 % |
| **S** | 1.59±0.48 | $C_{solid}$: 21.5 % | $C_{HCO3-}$: 14.1 % |
| | *Plutonium* | | |
| **D** | 1.94±0.12 | $C_{HCO3-}$: 63.6 % | $C_{solid}$: 10.9 % |
| **S** | 2.38±0.19 | $C_{solid}$: 67.0 % | $C_{HCO3-}$: 8.8 % |

Tab. 1: Computed log $K_d$ values for the Drigg Site compartments (for box labels see above) with those parameters contributing most to the overall uncertainty.

These results for the Drigg Site / Great Britain prove the applicability of the concept of unfolding the $K_d$ and its software implementation.

Acknowledgments
Financial support from the Nuclear Fission Safety Programme of the European Commission under contract F14P-CT95-0021a is gratefully acknowledged.

References

/1/ http://www.fz-rossendorf.de/RESTRAT/
/2/ Dzombak, D.A., Morel, F.M.M.; *Surface complexation modeling*. Hydrous ferric oxide, Wiley, New York (1990)
/3/ Bousher, A.; *Drigg Site: Basic characteristics and evaluation of restoration options*. RESTRAT Report TD 9, Westlakes Scientific Consulting, Cumbria, UK (1999)

# CRYSTAL STRUCTURE OF COPPER URANYL ARSENATE I: META-ZEUNERITE

C. Hennig, G. Reck [1], J. Sieler [2]
[1] Bundesanstalt für Materialforschung und Materialprüfung, D-12489 Berlin
[2] Universität Leipzig, Institut für Anorganische Chemie, D-04103 Leipzig

*The crystal structure of meta-zeunerite has been re-determined. The uranyl arsenate layers are linked by an inner-layer and an outer-layer axial uranyl oxygen atom and are bridged by square planar coordinated copper atoms.*

X-ray diffraction measurements showed that a crystal, which was considered as meta-zeunerite in a previous EXAFS investigation /1/, is an intergrown mineral of zeunerite and meta-zeunerite.

Zeunerite is the fully hydrated phase, meta-zeunerite(I) is the next lower hydration state, and meta-zeunerite (II) is in the lowest hydration state (not found occurring naturally). The EXAFS measurements have shown strong differences in the average bond lengths in comparison to literature data /2/ (Tab. 1).

| bond type | bond length RXD /2/ | bond length EXAFS /1/ |
|---|---|---|
| U-$O_{ax}$ | 1.94 Å<br>1.78 Å | 1.79 Å, U $L_{III}$-EXAFS |
| U-$O_{eq}$ | 2.18 Å | 2.28 Å, U $L_{III}$-EXAFS |
| As-$O_{eq}$ | 1.77 Å | 1.68 Å, As K-EXAFS |
| Cu-O | 2.14 Å | 1.95 Å, Cu K-EXAFS |

Tab. 1: Bond length comparison for zeunerite/metazeunerite

To clarify this structural problem, single-crystal analyses were carried out. In the result of these measurements it was found that the natural material is very complex which may be one of the reasons for the inaccurate structural data of meta-zeunerite given in the literature. The unit cell data measured by Hanic /2/ are a=7.10(5) Å and c=17.70(4) Å and the proposed space group is P $4_2$/nmc. Later, Ross et al. /3/ repeated the lattice-constant analysis and found a=7.12(5) Å and c=17.45(4) Å. They found a reflexion condition of hk0:h+k=2n, which is evident for a 4/m Laue symmetry and the proposed space group is P4/n, the same as in meta-torbernite, what makes it possible, that meta-zeunerite and meta-torbernite are isostructural. We determined the lattice constants of a=7.058 Å and c=8.666 Å and the space group P4/nmm (Tab. 2). X-ray Weißenberg photographs of a very small crystal shows two types of intensity reflections. One type consists of very sharp reflections whereas the reflections of the second type are strongly broadened. The sharp reflections belong to zeunerite, the broad ones origin from meta-zeunerite. Meta-zeunerite and zeunerite crystallize in two structurally related groups.

From the chemical point of view the main difference of both minerals is the water content. The significant structural features in both crystal structures are two-dimensional layers of distorted $UO_6$ octahedra, which are connected monodentately by $AsO_4$ tetrahedra. Perpendicular to the layers, two symmetry independent axial uranyl oxygen atoms ($O_{ax}$) are arranged having different bond lengths. The distance between two $[UO_2AsO_4]$ layers amounts to 8.666 Å. They are linked together by $(Cu(H_2O)_4)^{2+}$ cations.

| Mineral | Meta-Zeunerite | Zeunerite |
|---|---|---|
| Formula | $Cu[UO_2AsO_4]_2$ 8 $H_2O$ | $Cu[UO_2AsO_4]_2$ 12 $H_2O$ |
| Space group | P4/nmm (129) | I 4/mmm (139) |
| a [Å] | 7.058(1) | 7.1635(7) |
| c [Å] | 8.666(2) | 20.851(2) |
| Z, V [$Å^3$] | 1, 431.7(2) | 2, 1070.0(2) |
| Dx [$Mg/m^3$] | 3.944 | 3.407 |
| μ [$mm^{-1}$] | 25.031 | 19.255 |
| F(000) | 455 | 990 |
| 2 $2_{max}$ | 52° | 46.83° |
| refl. collected<br>refl. unique | 2335<br>286 | 2055<br>271 |

Tab. 2: Crystal and experimental data.

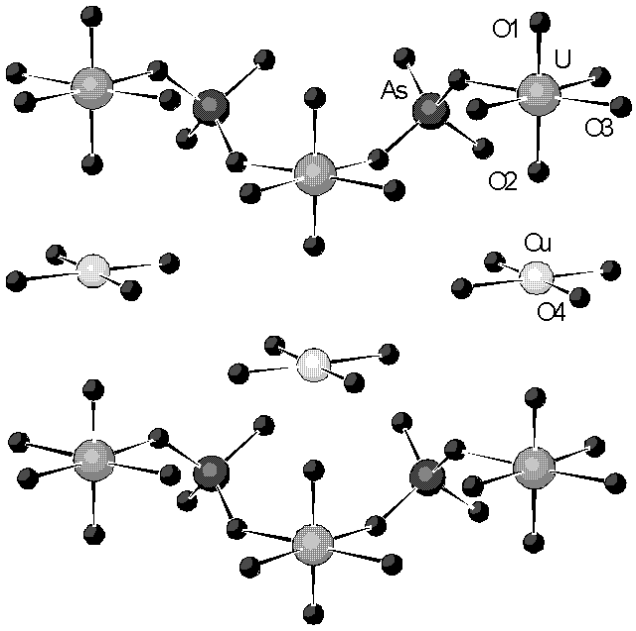


Fig. 1: Projection of a segment from the meta-zeunerite structure near at the [110] direction.

References

/1/ Hennig, C., et al., Report FZR-247 (1999) p. 55
/2/ Hanic, F., Czech. J. Phys. **10**, 169 (1960)
/3/ Ross, M. et al., Am. Min. **49**, 1603 (1964)

# CRYSTAL STRUCTURE OF COPPER URANYL ARSENATE II: ZEUNERITE

G. Reck [1], C. Hennig, W. Kraus [1]
[1] Bundesanstalt für Materialforschung und Materialprüfung, D-12489 Berlin

*The crystal structure of zeunerite was determined for the first time. The uranyl arsenate sheets are linked by two inner-layer and two outer-layer axial uranyl oxygen atoms and are bridged by square planar and fivefold coordinated copper atoms.*

The crystal structure of zeunerite hitherto has not been determined. Merely the unit cell data were determined until now to a=7.18 Å and c=21.06 Å /1/. The present study indicates unit cell data, which are in good agreement with these values (see previous contribution).

In contrast to meta-zeunerite adjacent $[UO_2AsO_4]$ layers are related by a translation vector [1/2 1/2 1/2], whereby two uranyl arsenate layers are bridged with $(Cu(H_2O)_4)^{2+}$ units via two inner-layer oxygen atoms giving a long distance of 8.94 Å and about two outer-layer oxygen atoms giving a short distance of 4.93 Å (Fig.1). This arrangement of the uranyl arsenate layers leads to an increase of the uranyl arsenate layer distance to 10.426 Å and to a doubling of the c lattice constant in comparison to meta-zeunerite.

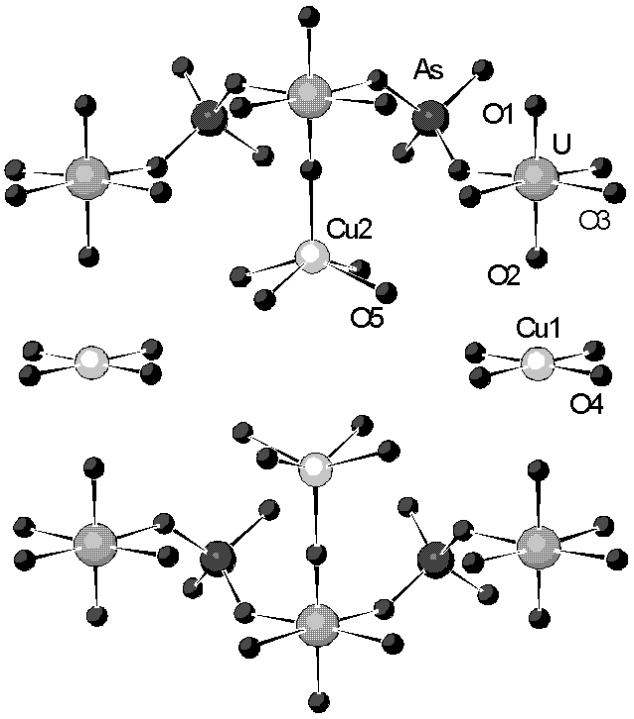


Fig. 1: Projection of a segment from the zeunerite structure near at the [110] direction.

The interlayer is built up by two different copper polyhedra: in the first one the copper is square planar coordinated by water molecules, in the second one four water molecules and an inner-layer oxygen atom form a tetragonal pyramid.

The long distance between the inner-layer oxygen atoms is bridged by two groups of the fivefold coordinated copper atoms, whereas the outer-layer oxygen atoms are bridged by the copper atom with the square plane coordinated water molecules. Whereas the water molecules fully occupy their positions, the occupation of the copper positions is different. The distance between the copper atom and each of the square coordinated water molecule represented by Cu1-O4 is 1.92 Å, similar to the bond length of the interlayer copper coordination center in meta-zeunerite. In comparison, the bond length of the fivefold coordinated copper atoms is longer (Cu2-O5: 2.08 Å and Cu2-O1: 1.99 Å). Meta-torbernite, the copper uranyl phosphate analogous mineral, shows a Cu-O bond length of 1.91 Å /2/. Because of the low copper occupation only few water molecules belonging to the tetragonal pyramid are connected with copper at a distance of 2.075 Å. The average of this occupation factor weighted distances is in good agreement with the bond length of 1.95 Å of the EXAFS measurements on the Cu K edge (previous contribution, Tab. 1). The arsenic-oxygen distance (As-O3) within the arsenate tetrahedra is with 1.649 Å equivalent to the data measured by EXAFS.

References

/1/ Berman, R., Am. Min. **42**, 905 (1957)
/2/ Ross, M., Am. Min. **49**, 1603 (1964)

# THE STABILITY OF CONCRETE SUSPENSIONS FOR PREPARATION OF THIN "-SOURCES

C. Nebelung, B. Barz

*Direct "-spectrometry of thin and large-area concrete sources is a fast and accurate method for determination of actinides up to 0.02 Bq/g in concrete /1/. Stable concrete suspensions without agglomeration are required for the preparation of the sources. The stability of the suspensions is measured by the streaming potential, using a particle charge detector (PCD).*

## Experimental

The preparation of the thin (0.6 - 6.0 µm) and large (314 $mm^2$) "-sources for direct "-spectrometry consists in spraying the concrete suspensions (particle size 0.5 µm) onto plates and than drying them. During this process agglomeration of the particles has to be prevented to obtain homogenous thin sources. The stability of a suspension depends on the particle charge in the electrochemical double layer. This particle charge can be measured by the relative movement of the solid and liquid phases. By generating this movement with a drive-out piston in the measuring cylinder of the PCD, part of the diffuse layer is sheared off. At the shearing plane the so-called zeta or PCD potential /2/ can be measured. If this potential near zero, the suspension begins to agglomerate.

## Results

Fig. 1 shows the PCD potential versus pH of suspensions of four concretes (BGI: Greifswald, nuclear power plant; RRR: Rossendorf, zero energy research reactor; WAK: Karlsruhe, reprocessing plant; RCNS: Rossendorf, radiochemical laboratory) during the titration with 0.01 n HCl. The RCNS concretes were measured in three versions: the complete concrete, the fine grained cement particles and the coarse grained additive particles. All concretes were milled to 0.5 µm particle suspensions. The original (not titrated) suspensions (highest pH of the curves) of the WAK concrete and the coarse RCNS concretes are the most stable ones. The addition of HCl decreases the stability of the suspensions in all cases. The comparison of the PCD results with the elemental composition of the concretes (measured by X-ray fluorescence analysis) shows that oxides or carbonates of the alkaline-earth elements have most influence of the U-pH curves.

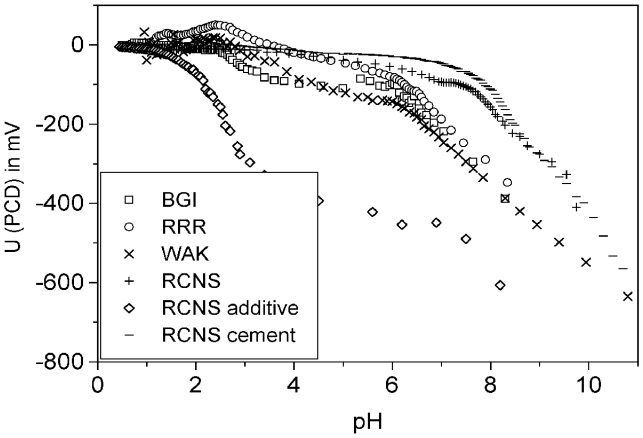


Fig. 1: Variation of the PCD potential of various concretes

A number of tensides were tested for their influence on the concrete suspensions. Four examples are given in Fig. 2. Most of the tensides are decreasing the PCD potentials and stabilize the concrete suspensions. Only ethoxyled nonylphenol (x in Fig. 2) and ammonia water reduce the stability of the concrete suspensions. The tenside concentration which is most effective for the suspension stability was determined by titration of the concrete suspensions with solutions of tensides.

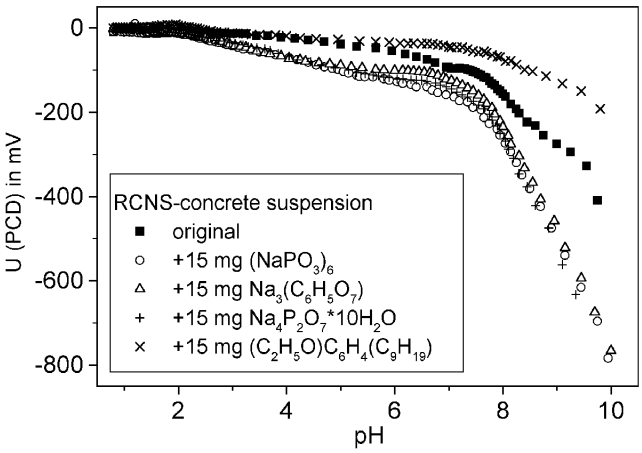


Fig. 2: Influence of tensides on the PCD potential

Fig. 3 shows the influence of particle concentration on the PCD potential. During the drying process (drying for source preparation) we get increasing particle concentrations. The higher the concrete content of the suspension (respectively the drier the source), the more probable becomes agglomeration.

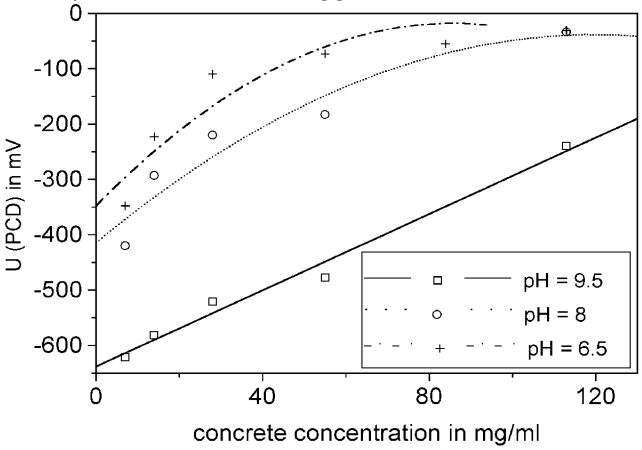


Fig. 3: Variation of the PCD potential of RCNS concrete during the drying process

## Acknowledgments

This work was supported by the Bundesministerien BMWi and BMBF of the Federal Republic of Germany under the contract number 02 S 7768.

## References

/1/ Nebelung, C., Nitsche, H., *Stilllegung und Rückbau: Direktmessung alpha-aktiver Nuklide in Bauschutt zur Freigabeentscheidung*, Schlussbericht BMBF Fördervorhaben 02 S 7655 / 02 S 7655A8 (1999)

/2/ Müller, R.H., *Zetapotential und Partikelladung in der Laborpraxis*. Wissenschaftliche Verlagsgesellschaft mbH Stuttgart, Band 37, 1996

# ANALYSIS OF " - SPECTRA OF THIN CONCRETE SAMPLES

C. Nebelung, J. Henniger [1], G. Mann [1]
[1] TU Dresden, Institute of Physics of Radiation Protection

*The direct alpha-spectrometry of thin and large-area concrete samples is a fast and accurate method for determining actinides in concrete during the decommissioning of nuclear installations /1/. The calculation of the "- spectra depends on the structure of the sample layers and the self-absorption of the "-radiation in these sources. Using the calculated peak shape, it is possible to fit and deconvolute spectra of an unknown number and amount of actinides up to 0.02 Bq $g^{-1}$ for each nuclide.*

The "-spectra of concrete samples of thicknesses between 0.62 and 5.0 µm differ from “massless” samples after electrodeposition.
We used two methods to analyze the "-spectra:
*1. Peak fitting with self-defined functions*
This method is based on measurement of standard concretes with added actinides. The peak shape, the self-absorption and the effectivity of the "-spectrometer (the grid ionization chamber) are determined depending on the thickness of the layer. The peak shape is a combined Gaussian (at the high energy side of the peak) and exponential curve (towards low energies) /1/.
2. *WINKRUM - a program using the calculation of the radiation transport*
These calculations consider a geometrical model of the layers in agreement with the particle size distribution, the packing density in the dried layer, the specific density, the thickness of the layer, the spectrometer parameter and the actinide energy. The calculations are performed with the multi-purpose radiation transport model /2/.

Results
The figures show measured (Fig. 1) and calculated "-spectra (Fig. 2) of a 50 mg standard concrete.

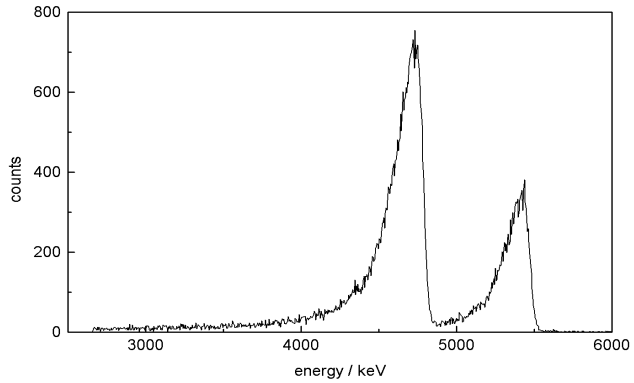


Fig. 1: Measured "-spectrum

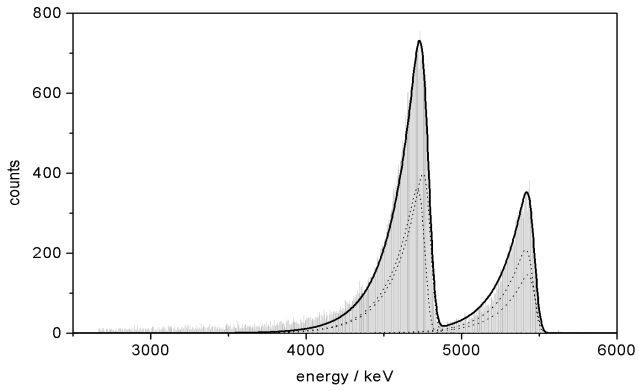


Fig. 2: "-spectrum calculated by the peak fitting method

The samples of a diameter of 20 cm and various masses were measured for 20 h in the grid ionization chamber.
Calculation of the thin-layer spectra by the peak-fitting method shows good agreement with the doted activities or the results by chemical analysis (Tab. 1).

| Nuclide | Doted activity /3/ | Chem. analysis /3/ | Peak fitting | | WINKRUM |
|---|---|---|---|---|---|
| $^{237}$Np | 16.4 | 16.6 | 15.3 | 32.7 | 36.2 |
| $^{233}$U | 18.3 | 17.9 | 17.4 | | |
| $^{241}$Am | 9.0 | 9.2 | 9.1 | 14.9 | 13.7 |
| $^{238}$Pu | 6.0 | 6.1 | 5.8 | | |

Tab. 1: Specific "-activity in Bq $g^{-1}$

The calculation with WINKRUM (Fig. 3) yields a higher activity for the peak at lower energies caused by a relatively high zero effect in this range. Peak shapes calculated by WINKRUM agree better with the measured "-peaks than the calculation using the self-defined peak fitting curves. Further developments of the program WINKRUM are planned to consider the zero effect and the actual calibration of the spectra.

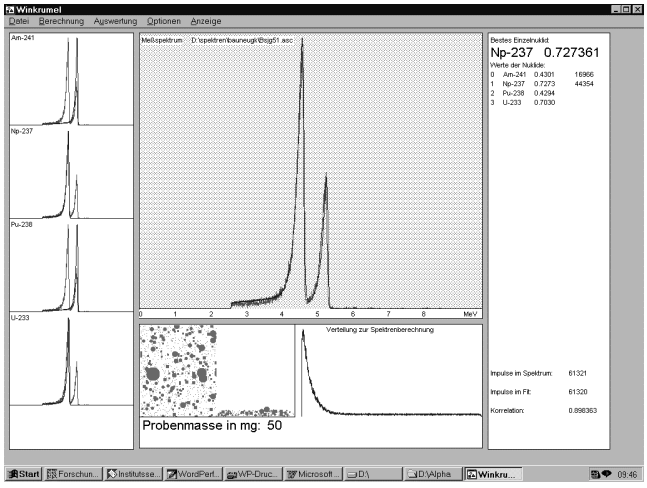


Fig. 3: "-spectrum calculated by the program WINKRUM

Acknowledgments
This work was supported by the Bundesministerium für Bildung, Wissenschaft, Forschung und Technologie of the Federal Republic of Germany under the contract number 02 S 7655A8.

References
/1/ Nebelung, C., Nitsche, H.; Schlussbericht, Fördervorhaben BMBF 02 S 7655 / 02 S 7655A (1999)
/2/ Henniger, J.; *Strahlenschutz, Physik und Meßtechnik*, Bd. 1, S.145-150, 26. Jahrestagung des Fachverbandes für Strahlenschutz e.V., Karlsruhe, 24.-26. Mai 1994
/3/ Küppers, G., Erdtmann, G.; J. Radioanal. Nucl. Chem. **260**, 65-77 (1986)

# Organic Matter and its Interaction with Radionuclides

# COMPARISON OF THE SORPTION BEHAVIOR OF TWO DIFFERENT HUMIC ACIDS ONTO PHYLLITE AND THEIR INFLUENCE ON THE URANIUM(VI) SORPTION

K. Schmeide, S. Pompe, M. Bubner, K.H. Heise, G. Bernhard

*Two different humic acids, a natural humic acid Kranichsee HA and a synthetic humic acid $^{14}$C-M1, were compared with regard to their sorption onto phyllite and their influence on uranium(VI) sorption in the pH range from 3.5 to 9.5 by batch experiments.*

## Introduction

Adsorption of humic material onto mineral surfaces can significantly alter the sorption of organic and inorganic contaminants by these minerals, the stability of colloids and their transport. In continuation of our sorption studies /1/, we compared the sorption of two different humic acids (HAs) onto phyllite in order to identify structural elements of the HAs that affect their sorption behavior and the sorption of uranium onto phyllite. We used natural Kranichsee HA and $^{14}$C-labeled synthetic HA $^{14}$C-M1.

## Experimental

The experimental conditions were: [$UO_2^{2+}$] = 1 µM, [HA] = 5 mg/L, I = 0.1 M ($NaClO_4$), m/V = 500 mg phyllite/40 mL, pH 3.5-9.5, aerobic conditions, 60 h reaction period. The 450 nm filtrates were analyzed for Kranichsee HA by UV/Vis spectroscopy, for $^{14}$C-M1 by LSC after combustion of the samples and for uranium by ICP-MS.

## Results

In Fig. 1 the HA uptake by phyllite is shown for Kranichsee HA and for $^{14}$C-M1 as a function of pH.

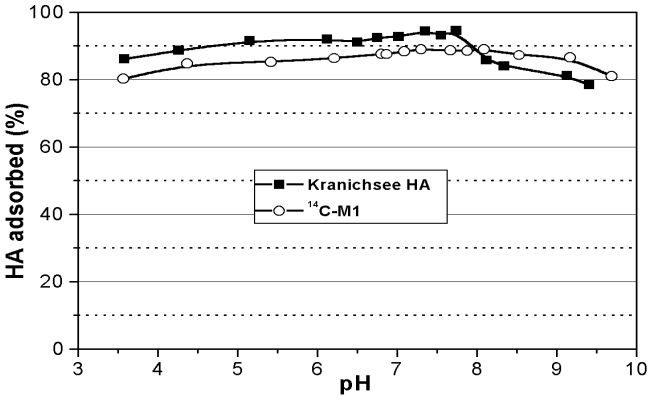


Fig. 1: Humic acid uptake by phyllite

Both HAs are strongly taken up over the entire pH range studied. The sorption of $^{14}$C-M1 between pH 3.5 to 7.7 is 4 to 6 % lower and above pH 8, 2 to 5 % higher than that of Kranichsee HA. The adsorption of HAs onto minerals is primarily determined by their functional group content. Mainly carboxylic groups and also hydroxyl groups (in ortho-position to carboxylic groups) bind to the oxide surface sites by ligand exchange and surface complexation. Kranichsee HA has a higher carboxylic and phenolic OH group content (3.88 and 3.87 meq/g) than $^{14}$C-M1 (1.34 and 2.4 meq/g). This should result in a considerably lower sorption of $^{14}$C-M1. However, the differences in the sorption of the two HAs are relatively small compared with the differences in the functional group contents. From the literature it follows that the sorption of HAs increases with their molecular size, their content of aromatic moieties and amino acid groups. $^{14}$C-M1 has both a larger molecular size and more aromatic structural elements than Kranichsee HA as was shown by capillary electrophoresis, IR and NMR spectroscopy /2,3/. This explains the high sorption of $^{14}$C-M1 despite its low functional group content.

Fig. 2 shows that compared with the uranium sorption onto phyllite in the absence of HA /4/, uranium sorption between pH 3.5 and 6 is increased by both HAs. This implies that although sorbed HA reduces direct uranium sorption onto phyllite surface groups, the total number of binding sites for uranyl ions is increased. For $^{14}$C-M1 we assume that comparatively fewer carboxylic groups are involved in the adsorption reactions, since functional groups on the larger molecules should be more sterically hindered from reacting with surface sites. Comparatively more unreacted functional groups of $^{14}$C-M1 are therefore available for binding uranium. This leads to a comparable enhancement of uranium sorption by both HAs between pH 3.5 to 6. The apparent enhancement of uranium sorption together with the high sorption of $^{14}$C-M1 above pH 7.5 is caused by the low solubility of uranyl humate complexes formed by $^{14}$C-M1 due to a low content of free carboxylic groups compared with complexes formed by Kranichsee HA.

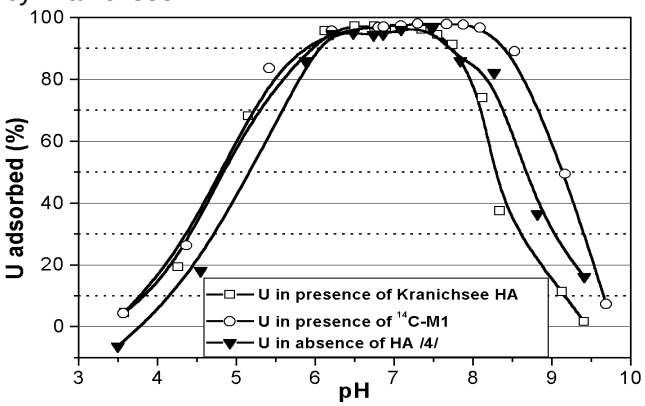


Fig. 2: Uranium uptake by phyllite

## Conclusion

The total content of HA functional groups and the fraction that is actually available for binding uranyl ions, the molecular size and the amount of aromatic structural elements of the HAs were found to affect the sorption of HAs and their influence on uranium sorption.

## Acknowledgment

This work was supported by the EC Commission under contract no. F14W-CT96-0027.

## References

/1/ Schmeide, K., et al., submitted to Radiochim. Acta
/2/ Schmeide, K., et al., Report FZKA 6324 (1999) p.177
/3/ Pompe, S., et al., Final Report, BMBF Project No. 02E88150 (1999)
/4/ Arnold, T., et al., Chem. Geology **151**, 129 (1998)

# SORPTION OF HUMIC ACID AND URANIUM ON THE CRYSTAL FACES OF BIOTITE AND MUSCOVITE

E. Krawczyk-Bärsch, K. Schmeide, T. Arnold, G. Bernhard

*Sheets of biotite and muscovite were brought into contact with a humic acid (HA) solution at pH values of 4.5 and 8.5 for 1 hour. FE-SEM investigations showed individual spherical particles of HA as well as agglomerates sorbed on the crystal face ⟨001⟩ of biotite and muscovite at pH 4.5. At a pH of 8.5 no sorbed HA particles were seen.*

## Introduction

In nature the sorption process of uranium onto geological materials is influenced by the presence of humic acid and its ability to form humic-metal complexes. In batch experiments the effects of humic acid (HA) on the sorption of U(VI) were examined on pulverized biotite and muscovite /1/ in the pH range from 3.5 to 9.5. The results show that the sorption of HA strongly depends on the pH value. The HA sorption on biotite reached a maximum of 77 % at pH 4.5 to 5.0 (Fig. 1). At the same pH HA sorption on muscovite reached its maximum of 83 %. At higher pH values HA sorption decrease. These results provided the basis for field emission scanning electron microscopy (FE-SEM) investigations on biotite and muscovite crystals. The goal was a better understanding of the sorption behavior of HA on the various crystal faces, especially the ⟨001⟩ and ⟨hk0⟩ faces.

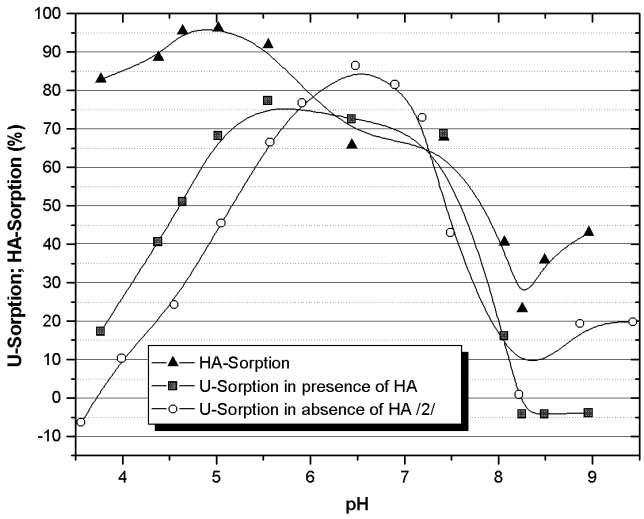


Fig. 1: Humic acid and uranium uptake on biotite in batch experiments. Added: HA = 5 mg/L; U = $10^{-6}$ M

## Experimental

Individual sheets of biotite and muscovite were brought into contact with a 40 mg/L HA (Aldrich) solution for one hour. The HA solution was filtered through a 50 nm Nuclepore filter to remove bacteria from the solution prior to bringing it into contact with biotite and muscovite. This was necessary to avoid any misinterpretation of the FE-SEM pictures. HA, on the other hand, passes through the micropores because of its typical size of 1-10 nm diameter /3/. In previous batch experiments the ionic strength was kept constant at 0.1 M, adjusted with $NaClO_4$ solution. However, by forming a precipitated sodium salt, $NaClO_4$ covered the mineral surface and with it the sorbed HA. Hence, the addition of $NaClO_4$ solution was discontinued. On the basis of the results of the batch experiments with pulverized biotite and muscovite, pH 4 was chosen for high adsorption and pH 8 for low adsorption of HA. The samples were intensively washed with deionized $H_2O$ and dried. To avoid misinterpretations caused by Au coating, the samples were not sputtered with Au.

## Results and discussion

Sorbed HA is visualized by FE-SEM as individual spherical particles or as agglomerates. The size of the particles ranges from 5 to 10 nm in diameter (Fig. 2). They are sorbed irregularly onto the surfaces of the samples. HA sorption greatly depends on pH. Sorbed particles were detected by FE-SEM on biotite and muscovite samples which had been in contact with HA solution at pH of 4. At a pH of 8.5 no sorbed HA particles were visualized. This result confirms previous batch experiments.

There are some indications that the reactivity of the ⟨001⟩ and ⟨hk0⟩ faces differs. Sorbed HA particles were detected by FE-SEM only on the ⟨001⟩ faces. However, these observations have to be confirmed in further FE-SEM investigations.

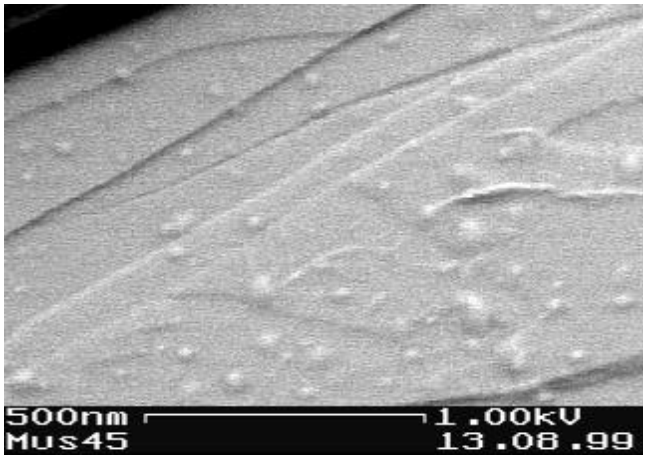


Fig. 2: Individual spherical particles of HA and as agglomerates sorbed on muscovite. - FE-SEM picture

## Acknowledgments

This work was supported by the DFG (Ni 210/5-1). The authors wish thank the Fraunhofer Institute for the FE-SEM investigations.

## References

/1/ Schmeide, K., et al.: Uranium(VI) Sorption onto Phyllite and Selected Minerals in the Presence of Humic Acid. Radiochim. Acta (submitted)

/2/ Arnold, T., et al.: Sorption of Uranium(VI) onto Phyllite. Chemical Geology **151**, 129 (1998b)

/3/ Zänker, H., et al.: The Colloidal States of Humic Acid. In: Report FZKA 6324, FZ Karlsruhe (1999) p.155-175

# KINETIC STUDIES OF THE URANIUM(VI) AND HUMIC ACID SORPTION ONTO FERRIHYDRITE

K. Schmeide, S. Pompe, M. Bubner, S. Wallner, R. Jander, K.H. Heise, G. Bernhard

*The kinetics of uranium(VI) and humic acid adsorption by ferrihydrite was studied at pH 6.5 under aerobic conditions. For the sorption experiments various experimental modes were applied to obtain information on the sorption mechanisms.*

## Introduction

Ferrihydrite (FH) is formed as a secondary mineral phase due to the weathering of rock materials, such as phyllite /1/, forming coatings on the surface of other minerals. It has a high sorption potential for contaminants and organic materials. In previous batch experiments it was found that both the uranium and humic acid (HA) sorption onto FH has its maximum in the neutral pH range.

## Experimental

The experimental conditions were: $[UO_2^{2+}]$ = 1 µM, [HA] = 5 mg/L, [FH] = $3 \cdot 10^{-4}$ M Fe, I = 0.1 M ($NaClO_4$), V = 400 mL, pH 6.5, aerobic conditions. A $^{14}C$-labelled synthetic HA type M1 was used /2/. The HA and uranyl sorption onto the mineral was followed by measuring the corresponding concentrations in solution (450 nm filtrate) over time by Liquid Scintillation Counting after combustion of the samples and ICP-MS, respectively. Five experimental modes were applied:

1. addition of U without HA;
2. addition of HA without U;
3. preequilibration of the mineral with HA, then addition of U;
4. simultaneous addition of U and HA;
5. addition of U and HA after preequilibration for 48h.

## Results

The kinetics of uranium sorption onto FH as a function of the various experimental modes is shown in Fig. 1.

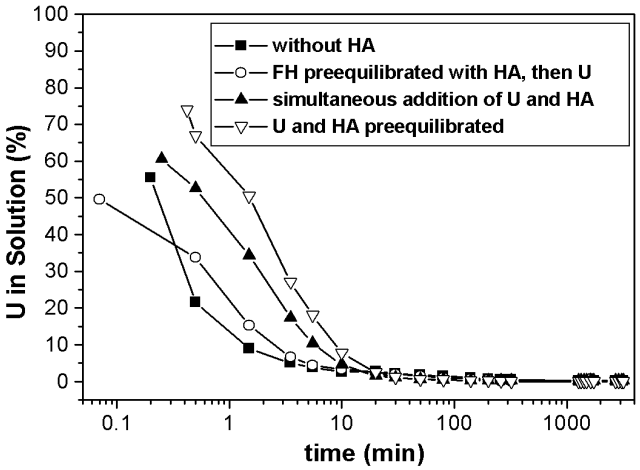


Fig. 1: Kinetics of uranium sorption onto ferrihydrite at pH 6.5

It is obvious that uranium sorption is very fast. This can be attributed to the high specific surface area of FH, which is 600 $m^2/g$ /3/. The differences in the sorption kinetics depending on various experimental modes are small. In the absence of HA uranium has the highest sorption rate. When FH is first coated with HA due to its preequilibration with HA, the uranium sorption is slightly slower. Some strong sorption sites of FH are probably blocked by the sorbed HA and are no longer accessible to uranium. The complexation and/or sorption sites that are additionally provided by the sorbed HA bind uranium more slowly than the strong sorption sites of FH. When uranium and HA are added simultaneously, the uranium sorption is again slightly retarded as FH and HA compete for uranium. Uranyl humate complexes formed in solution have either to dissociate again before the uranium can sorb onto FH or the sorption rate of the uranyl humate complex is slower. The latter seems to be more probable due to the very high sorption rates. When aliquots of preformed uranyl humate complexes are added to start the experiment, the uranium sorption takes place at the slowest rate compared with other experimental modes.

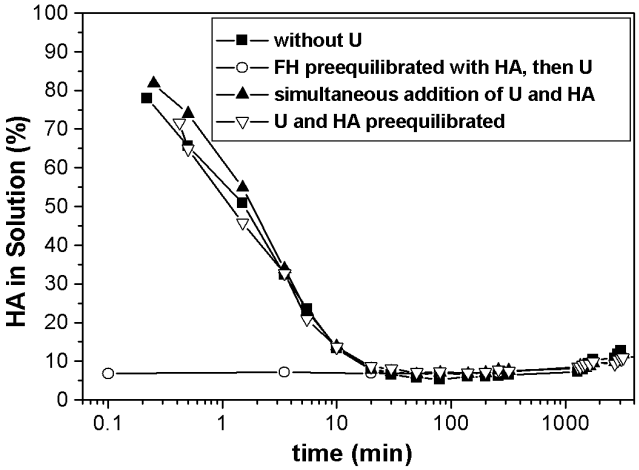


Fig. 2: Kinetics of HA sorption onto ferrihydrite at pH 6.5

The rate of HA sorption, shown in Fig. 2, was also observed to be very fast but in contrast to the uranium sorption almost unaffected by the various experimental modes. About 7 % of the initially added HA remain in solution whereas the initially added uranium is completely sorbed. Furthermore, after the rapid HA sorption onto FH a slight increase in the HA concentration in solution was observed in all experiments although the pH was constant (cf. Fig. 2). This release of sorbed HA might be caused by a slight dissolution of the FH mineral caused by formation of dissolved iron humate complexes.

It can be concluded that FH strongly adsorbs both uranium and HA due to its high specific surface area. The kinetics of uranium sorption onto FH is slightly influenced by HA.

## Acknowledgment

This work was supported by the EC Commission under contract no. F14W-CT96-0027.

## References

/1/ Arnold, T., et al., Chem. Geology **151**, 129 (1998)
/2/ Bubner, M., et al., Report FZR-247 (1999) p. 25
/3/ Dzomback, D.A., et al., *Surface Complexation Modeling*. Hydrous Ferric Oxide. Wiley, NY, (1990)

# INFLUENCE OF SULFATE ON THE KINETICS OF URANIUM(VI) SORPTION ONTO FERRIHYDRITE IN THE ABSENCE AND PRESENCE OF HUMIC ACID

K. Schmeide, V. Brendler, S. Pompe, M. Bubner, K.H. Heise, G. Bernhard

*We studied the influence of sulfate on the kinetics of uranium(VI) sorption onto ferrihydrite both in the absence and presence of humic acid at pH 6.5 under aerobic conditions. The sequence in which the components were added was varied.*

## Introduction

In continuation of the kinetic studies of uranium and humic acid (HA) sorption onto ferrihydrite (FH) /1/, we studied the effect of sulfate on the uranium and HA sorption onto FH at pH 6.5, since seepage waters from uranium mine tailing piles in Saxony contain up to $3 \cdot 10^{-2}$ M sulfate. The materials and experimental conditions were the same as described in /1/, with the exception that two sulfate concentrations were applied (0.005 and 0.02 M $Na_2SO_4$). The total ionic strength was always 0.1 M. Sulfate was added to FH prior to the addition of uranium and HA.

## Results

Experiments without HA:

According to speciation calculations, the uranium in solution occurs as $UO_2(OH)_{2\,(aq)}$, no uranyl sulfate complexes are formed at pH 6.5. With increasing total sulfate concentration and thus, with increasing sulfate sorption onto FH, the initial uranium sorption rate decreases (Fig. 1). This is attributed to partial blocking of strong FH sorption sites by presorbed sulfate, which has two effects on uranium sorption: first, uranyl ions have to diffuse to more internal FH sorption sites; second, uranyl ions displace sorbed sulfate ions due to their higher sorption affinity. Both effects become stronger with increasing total sulfate concentration.

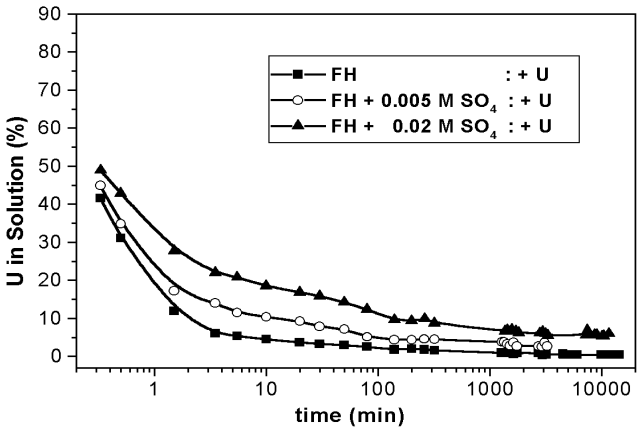


Fig. 1: Effect of sulfate on uranium sorption in absence of HA

The total uranium sorption onto FH decreases with increasing sulfate concentration, since the number of strong surface sites that are accessible to uranium is reduced. Direct competition between uranium and sulfate for strong sorption sites of FH predominates electrostatic effects due to the change in the net surface charge of FH upon sulfate sorption.

Experiments with HA ($^{14}$C-M1):

When uranium and HA are simultaneously added to FH suspensions (not shown), the uranium sorption rate and the total uranium sorption decrease with increasing sulfate concentration.

When aliquots of preformed uranyl humate complexes are added (Fig. 2), the initial uranium sorption rates are almost unchanged by the presorbed sulfate. The decrease in the total uranium sorption as a result of increasing sulfate concentration is slightly smaller than in the preceding experimental mode. Compared with experiments in which uranium and HA were added simultaneously, the initial uranium sorption rates are lower. This confirms previous experiments /1/ and is attributed both to a lower sorption rate of uranyl humate complexes and to the partial redistribution of uranyl ions to FH binding sites.

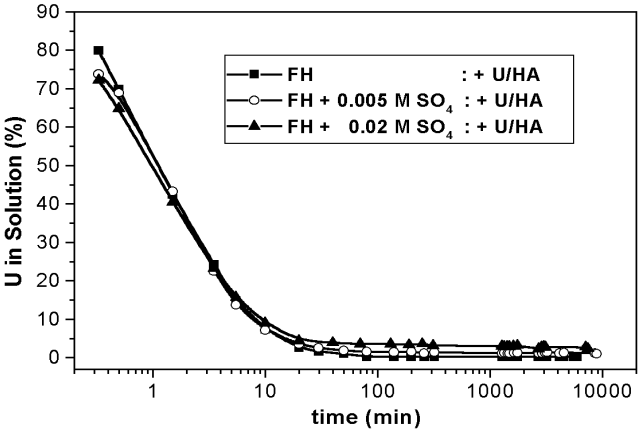


Fig. 2: Effect of sulfate on uranium sorption in presence of HA

The initial HA sorption rate (not shown) is also hardly influenced by presorbed sulfate. Only the total HA sorption decreases slightly with increasing sulfate concentration. That means that despite the large excess of sulfate (4 and 16 meq/400 mL) compared with HA carboxylic and phenolic OH groups (2.7 and 4.8 µeq/400 mL), the competitive effect of sulfate on the total HA sorption at pH 6.5 is small . This reflects a higher sorption affinity of HA for FH surface sites compared with that of sulfate.

Since sorbed HA molecules have a number of carboxylate groups that are not involved in sorption reactions, the total number of potential binding sites for uranyl ions is higher in the presence of HA, which leads to a higher uranium sorption (Fig. 2) compared with uranium sorption in the absence of HA (Fig. 1).

## Conclusion

In the absence of HA, the availability of uranium is increased by sulfate. In the presence of HA, the influence of sulfate on uranium sorption is smaller. Especially in the presence of larger amounts of uranyl humate complexes, the reducing effect of sulfate on the total uranium sorption is almost counterbalanced by HA.

## Acknowledgment

This work was supported by the EC Commission under contract no. F14W-CT96-0027.

## References

/1/ Schmeide, K., et al., this report p. 27

# THE INFLUENCE OF PHENOLIC HYDROXYL GROUPS ON THE COMPLEXATION BEHAVIOR OF HUMIC SUBSTANCES WITH URANYL(VI) IONS: I. SYNTHESIS AND CHARACTERIZATION OF NATURAL AND SYNTHETIC HUMIC ACIDS WITH BLOCKED PHENOLIC HYDROXYL GROUPS

S. Pompe, M. Bubner, K. Schmeide, M. Meyer, K.H. Heise, G. Bernhard

*Various modified natural and synthetic humic acids with blocked phenolic hydroxyl groups were synthesized and characterized as regards their functional group content.*

In continuation of our investigations described in /1,2/ we synthesized modified humic acids (HA) with blocked phenolic OH groups, starting from the synthetic HA type M1 and M42 and from the purified natural HA Aldrich (A2/97) and the HA Kranichsee (KHA) /3/. These substances will be used to investigate the influence of phenolic OH groups on the metal ion complexation behavior of HA.

Synthesis and Characterization

The modification process comprised two steps: a) permethylation of carboxylic and phenolic OH groups with diazomethane, resulting in methyl ester and methyl ether groups and b) hydrolysis of the ester groups in alkaline solution.

For permethylation a suspension of the original HA in methanol was first reacted with diazomethane while stirring for three hours at -5 to 5 °C. Then the solvent was distilled. The permethylation procedure was repeated several times until no further diazomethane was incorporated into the HA. Then the HA was lyophilized. For hydrolysis of the ester groups the permethylated HA was stirred for 8 hours with 2 M NaOH in a nitrogen atmosphere at room temperature. After that the alkali insoluble residue was separated by centrifugation and the modified HA with blocked phenolic OH groups was precipitated by addition of 2 M HCl. The HA precipitate was centrifuged, washed, dialyzed using dialysis tubes and then lyophilized.

The permethylated HA and the HA with blocked phenolic OH groups were characterized as regards their functional group content, using various methods. Tab. 1 shows the phenolic OH and the carboxylic group contents of the original HA and of the modification products.

From the results in Tab. 1 it can be concluded that the phenolic OH groups of the HA are partially modified during the derivatization process. The HA with blocked phenolic OH groups show 59 - 74 % less phenolic OH groups than the original HA.

After the permethylation procedure functional groups that are capable of methylation but are not hydrolyzable, i.e. that are not carboxylic groups, were still determined by the radiometric method. However, it has not yet been confirmed whether these functional groups are unmodified phenolic OH groups or functional groups produced during the derivatization process. In some cases the number of functional groups which are capable of methylation but are not hydrolyzable obviously increases during the hydrolysis step.

A comparison of the carboxylic groups of the modified HA with blocked phenolic OH groups and the original HA shows that the modified HA have a lower carboxylic group content. Possible causes are a partial decomposition of some HA molecules in acid-soluble components, leaching of smaller HA molecules with a higher carboxylic group content from the HA mixture and/or decarboxylation reactions during the derivatization process.

| *Humic acid* | *Modification* | *Phenolic OH (meq/g)* [a] | *COOH (meq/g)* [b] |
|---|---|---|---|
| *M1* | original | 2.4 ± 0.1 | 1.3 ± 0.1 |
| *M1B* | permethylated | 0.3 | <0.1[a] |
| *M1PB* | phenol. OH blocked | 0.9 ± 0.3 | 1.2 ±0.1 |
| *M42* | original | 2.3 ± 0.4 | 4.1 ± 0.1 |
| *M42B* | permethylated | 0.6 ± 0.1 | 0.1[a] |
| *M42PB* | phenol. OH blocked | 0.6 ± 0.3 | 3.2 ± 0.1 |
| *A2/97* | original | 3.4 ± 0.5 | 4.4 ± 0.1 |
| *A2/97B* | permethylated | 0.6 ± 0.3 | <0.1[a] |
| *A2/97PB* | phenol. OH blocked | 1.1 ± 0.4 | 3.2 ± 0.1 |
| *KHA* | original | 3.9 ± 0.5 | 4.2 ± 0.2 |
| *KHAB* | permethylated | 0.3 | <0.1[a] |
| *KHAPB* | phenol. OH blocked | 1.6 ± 0.4 | 2.8 ± 0.1 |

*[a] radiometrically determined /4/; [b] determined by calcium acetate exchange*

Tab. 1: Functional group content of the original HA and the modified HA.

The blocking of the phenolic OH groups was further investigated by FTIR spectroscopy. IR absorption bands pointing to the formation of phenyl methyl ethers were identified in the spectra of the modified HA with blocked phenolic OH groups. However, a clear identification of these absorption bands is difficult because of the overlapping of IR bands of different functional groups, resulting in a few broad absorption bands.

From the characterization results it can be concluded that it is possible to synthesize HA with partially blocked phenolic OH groups.

Acknowledgment

This work was supported by the Bundesministerium für Bildung, Wissenschaft, Forschung und Technologie (BMBF) under contract number 02 E88150 and by the EC under contract No. F14W-CT96-0027.

References

/1/ Pompe, S., et al., Report FZR 218 (1998) p. 30
/2/ Pompe, S., et al., Report FZR-247(1999) p. 28
/3/ Schmeide, K., et al., Report FZKA 6124 (1998) p. 161
/4/ Bubner, M., et al., Report FZR 43 (1994) p. 22

# THE INFLUENCE OF PHENOLIC HYDROXYL GROUPS ON THE COMPLEXATION BEHAVIOR OF HUMIC SUBSTANCES WITH URANYL(VI) IONS: II. PREPARATION OF URANYL HUMATES OF VARIOUS MODIFIED AND UNMODIFIED NATURAL AND SYNTHETIC HUMIC ACIDS FOR STRUCTURAL INVESTIGATIONS

M. Bubner, K. Schmeide, S. Pompe, K.H. Heise, G. Bernhard

*Uranyl humates were synthesized with nearly twenty percent metal loading of the humic acid carboxyl groups. The humic acids used for complexation with uranium(VI) are the natural humic acid of Kranichsee, the commercial humic acid from Aldrich and the synthetic humic acids type M1 and M42 as well as their modified analogues with blocked phenolic hydroxyl groups.*

## Introduction

The goal of our syntheses was to obtain well-defined, representative and comparable solid uranyl humates from natural and synthetic humic acids and from their analogues modified by blocking the phenolic hydroxyl functionality, for structural investigations by EXAFS, FTIR and thermoanalysis. We used the natural Kranichsee humic acid (KHA), the commercial purified Aldrich humic acid (A2/97), the synthetic humic acids type M1 and M42 and their modified analogues KHAPB, A2/97PB, M1PB and M42PB /1/ for this investigation. The reaction conditions for all humates were comparable. The metal loading of all humic acids was carried out at pH 2 and was limited to 20 %. Thus, the formation of uranyl humic acid complexes with 1: 1 stoichiometry is unlikely /2/.

## Experiments

The characteristics of the humic acids (HA) used are summarized in Tab. 1. Solid uranyl(VI) humic acid complexes were prepared by reacting aqueous suspensions of previously deaerated humic acids with solutions of 0.1M uranyl perchlorate having metal ratios (meq COOH : meq $UO_2^{2+}$) of 1 : 0.2. The pH 2 of the reaction mixture was achieved by repeatedly adjusting the pH in the supernatant which had meanwhile been separated with 0.1M NaOH or 0.1M $HClO_4$, respectively. After the reaction the products were isolated by centrifugation, washed with purified water, dialyzed and lyophilized. The products were characterized by determining their elemental composition by elemental analysis and ICP-MS after digestion with $HNO_3$ in a microwave oven. The amount of bound metal was also determined by thermogravimetry.

## Results

The results are summarized in Tab. 2. The loading of the HAs with uranyl was calculated from the uranium and carbon contents of the synthesized humates in relation to the carbon content in the free humic acids. Saturated solutions of various uranyl humates with 15 to 19 % uranyl loading differ in pH although the pH of the reaction mixtures was exactly 2.0 in each case. This corresponds to the varying COOH content of the humic acids and to the solubility of the uranyl humates. In general phenol-blocked humic acids and their uranyl humates show a poorer solubility than unmodified ones. The uranyl loading of humates from phenol-blocked HAs is always slightly lower than the uranyl loading of unmodified HAs.

| HA | Functionality [meq/g] | | | C [%] |
|---|---|---|---|---|
| | COOH | phen. OH | COOH/phen.OH | |
| KHA | 4.2 | 3.9 | 1.1 | 49.9 |
| KHAPB | 2.8 | 1.6 | 1.7 | 54.9 |
| A2/97 | 4.4 | 3.4 | 1.3 | 58.7 |
| A2/97PB | 3.2 | 1.1 | 2.9 | 57.9 |
| M1 | 1.3 | 2.4 | 0.5 | 64.6 |
| M1PB | 1.2 | 0.6 | 2.0 | 63.9 |
| M42 | 4.1 | 1.8 | 2.2 | 58.4 |
| M42PB | 3.2 | 0.6 | 5.3 | 58.4 |

Tab.1: Characteristics of humic acids

| HA | C [%] | | U | loading | pH | |
|---|---|---|---|---|---|---|
| | HA | $UO_2$-HA | % | %COOH | HA | $UO_2$-HA |
| KHA | 49.9 | 44.8 | 9.7 | 18 | 2.7 | 3.0 |
| KHAPB | 54.9 | 51.6 | 4.7 | 15 | 3.4 | 3.8 |
| A2/97 | 58.7 | 52.8 | 8.9 | 19 | 2.3 | 3.3 |
| A2/97PB | 57.9 | 53.9 | 6.5 | 18 | 2.9 | 3.5 |
| M1 | 64.9 | 63.2 | 2.8 | 17 | 3.5 | 4.1 |
| M1PB | 63.9 | 62.1 | 2.3 | 17 | 3.7 | 4.2 |
| M42 | 58.4 | 53.3 | 8.1 | 18 | 3.2 | 3.5 |
| M42PB | 58.4 | 54.4 | 5.6 | 16 | 3.3 | 3.8 |

Tab. 2: Elemental composition, uranyl loading and pH of the HA and uranyl humates

## Acknowledgments

This work was supported by the Bundesministerium für Bildung, Forschung und Technologie (BMBF) under contract number 02 E88 150 and by the EC under contract number F14W-CT96-0027.

## References

/1/ Pompe, S., et al., this report p. 29
/2/ Bubner, M., et al. Report FZR-218, 44 (1998)

# THE INFLUENCE OF PHENOLIC HYDROXYL GROUPS ON THE COMPLEXATION BEHAVIOR OF HUMIC SUBSTANCES WITH URANYL(VI) IONS: III. EXAFS INVESTIGATIONS OF SOLID $UO_2^{2+}$-COMPLEXES WITH MODIFIED AND UNMODIFIED HUMIC ACIDS

S. Pompe, K. Schmeide, M. Bubner, T. Reich, A. Roßberg, C. Hennig, H. Funke, K.H. Heise, G. Bernhard

*Uranium $L_{III}$-edge EXAFS spectra of solid uranyl humates with modified humic acids containing blocked phenolic OH groups and of uranyl humates with unmodified humic acids are compared. The structural parameters for the first two uranium coordination shells show no significant differences in dependence on the phenolic OH group content of the humic acid.*

To study the influence of phenolic OH groups on the short-range order surrounding of uranium(VI) in uranyl humate complexes we investigated solid uranyl humates of the modified synthetic humic acid (HA) type M1PB and of the modified natural HA Aldrich (A2/97PB) and Kranichsee (KHAPB) /1/ with blocked phenolic OH groups. These samples were compared to uranyl humates of the original HA type M1, A2/97 and KHA.

Experimental

The preparation of the solid uranyl humates as well as their uranyl loadings are described in /2/. The samples dispersed in Teflon were pressed as 1.3 cm diameter pellets. U $L_{III}$-edge EXAFS transmission spectra were measured at room temperature at the Rossendorf Beamline at the ESRF in Grenoble. The monochromator, equipped with a Si(111) water cooled double-crystal system was used in the channel-cut mode.

Results

As examples, the $k^3$-weighted U $L_{III}$-edge EXAFS and the corresponding Fourier transforms for the investigated uranyl humates of HA type M1 and M1PB as well as HA A2/97 and A2/97PB are depicted in Fig. 1 and Fig. 2.

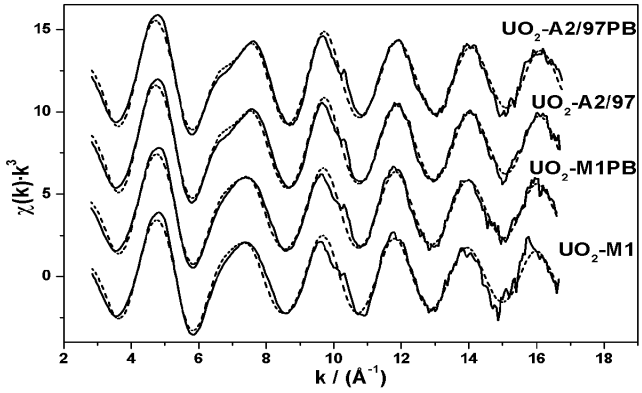


Fig. 1: $k^3$-weighted U $L_{III}$-edge EXAFS spectra of solid uranyl humates of modified and unmodified HA. Solid lines: experimental data, dashed lines: fit results.

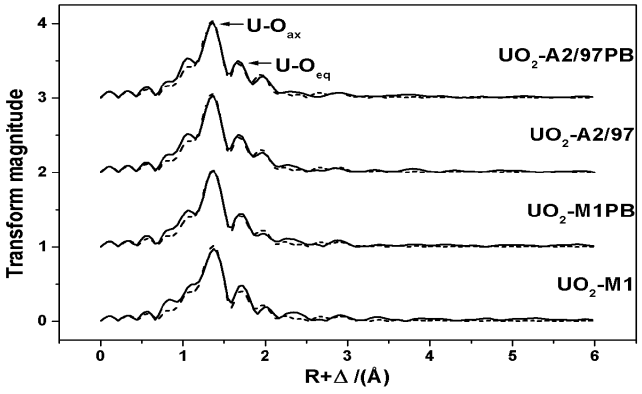


Fig. 2: Fourier transforms of the EXAFS shown in Fig. 1.

The EXAFS oscillations of all samples as well as the Fourier transforms are similar. The EXAFS oscillations were fitted to the EXAFS equation using a structural model with two coordination shells containing oxygen atoms as backscatterer and including multiple scattering effects along the uranyl unit (Tab. 1).

| Sample | *U-$O_{ax}$* | | *U-$O_{eq}$* | | |
|---|---|---|---|---|---|
| | R (Å) | $F^2$ (Å$^2$) | N | R (Å) | $F^2$ (Å$^2$) |
| $UO_2$-M1 | 1.78 | 0.002 | 5.2 | 2.38 | 0.014 |
| $UO_2$-M1PB | 1.78 | 0.001 | 5.0 | 2.38 | 0.014 |
| $UO_2$-A2/97 | 1.78 | 0.001 | 5.3 | 2.40 | 0.012 |
| $UO_2$-A2/97PB | 1.77 | 0.001 | 5.1 | 2.40 | 0.011 |
| $UO_2$-KHA | 1.78 | 0.001 | 5.2 | 2.39 | 0.012 |
| $UO_2$-KHAPB | 1.78 | 0.002 | 5.4 | 2.40 | 0.013 |

Tab. 1: EXAFS structural parameters. ) $E_0$ = -13.6 eV, $N_{ax}$=2, errors in bond length (R) and coordination numbers (N) are "0.02 Å and ~10 %, respectively.

The modified HA show a smaller amount of phenolic OH groups than the unmodified HA /1/. Therefore, the spectra of the modified HA are more dominated by the interaction of $UO_2^{2+}$ with carboxylic groups. The determined U-$O_{eq}$ bond distances correspond to monodentate coordination of the carboxylic groups /3/. The structural parameters obtained for the solid uranyl humates of the unmodified HA do not differ from that of the modified HA. This indicates a comparable short-range order surrounding of the $UO_2^{2+}$ ion. One can conclude that in the solid complexes the phenolic OH groups have only a small or no influence on the complexation of the $UO_2^{2+}$ ions.

However, a contribution of phenolic OH groups to the complexation of $UO_2^{2+}$can not fully be excluded by the EXAFS results, because the obtained structural parameters represent an average over all interactions between HA and $UO_2^{2+}$. From EXAFS investigations concerning the complexation of pyrogallol with $UO_2^{2+}$ at pH 4.8 /4/ it is known that phenolic OH groups can complex to the $UO_2^{2+}$ ion with distances of 2.40 Å, which can not be distinguished from $R_{U\text{-}Oeq}$ of the humates.

Acknowledgments

This work was supported by the BMBF under contract number 02 E88150 and by the EC under contract No. F14W-CT96-0027.

References

/1/ Pompe, S., et al., this report p. 29
/2/ Bubner, M., et al., this report p. 30
/3/ Denecke, M., et al., Radiochim. Acta **79**, 151 (1997)
/4/ Roßberg, A., et al., Report FZR-247 (1999) p. 53

# THE INFLUENCE OF PHENOLIC HYDROXYL GROUPS ON THE COMPLEXATION BEHAVIOR OF HUMIC SUBSTANCES WITH U(VI) IONS: IV. THERMOANALYTICAL INVESTIGATIONS

G. Schuster, K. Henkel, M. Bubner, S. Pompe, K. Schmeide, K.H. Heise, G. Bernhard

*Blocking phenolic OH groups by methylation produces a TG/DTA signal within the oxidative decomposition reaction at 300 - 350°C. Such methylated humic acids and, to a smaller extent their U(VI) complexes have a higher thermal stability than the unchanged substances. U(VI) binding decreases the thermal stability more for the methylated than for the unchanged HA`s.*

## Introduction

Using the natural humic acids from Aldrich (A2/97) and the Kranichsee lake (KHA) and the synthetic humic acids M1 and M42, it was to investigate wether methylation of the phenolic OH groups causes characteristic thermoanalytical effects and what DTA/TG results can be achieved by U(VI) complexation of these methylated compounds. The methylated substances have an additional index “PB” and the complexes “$UO_2$".

## Experimental

In a thermoanalyzer STA 92 from Setaram the samples were oxidatively decomposed by thermoanalytical heating up to 800°C at a rate of 10°C/min in an atmosphere of streaming oxygen (3 L/h). The TG, DTG, and DTA data were recorded for this reaction. The preparation and characterization of the samples are described in /1/ and /2/.

## Results and discussion

The DTA diagrams of this series of humic compounds of the Kranichsee humic acid KHA are shown in Fig. 1 as a typical example.

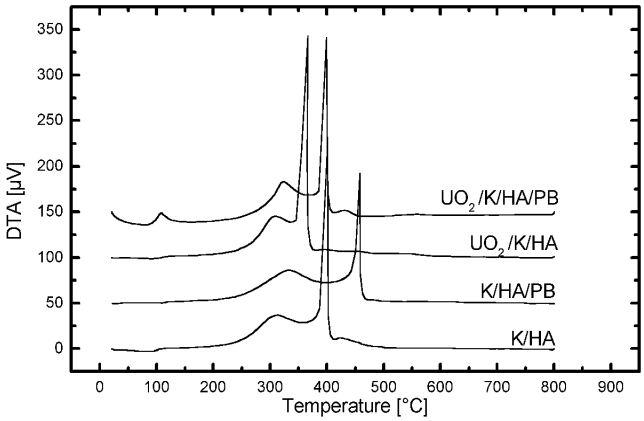


Fig. 1: DTA diagrams of the Kranichsee HA, its compound with methylated phenolic OH groups (KHAPB) and the U(VI) complexes of both. (Y axis is displaced stepwise by 50 µV)

Reaction 1 (up to 110°C) represents the endothermal vaporization of the adsorbed moisture, reaction 2 (up to 350°C) the exothermal decomposition of the reactive groups such as aliphatic and carboxylic groups, and the exothermic reaction 3 the degradation of the more resistant aromatic groups and parts of the residual carbon structure. Reaction 4 is only caused by the decomposition of the carbon structure. The degradation of all humic compounds investigated in this work with variations in temperature takes place by the same steps.

Methylation of the phenolic OH groups results in an increase in the exothermic peak of reaction 2. Consequently, the introduced methyl groups are decomposed in the temperature range up to 350°C. That is shown in Tab. 1 by the relations of the mass losses of reaction 2 to reaction 3. Investigations are under way to use this qualitative signal of methylation for a quantitative account of the methylated groups.

| Compound | $) m_{R2} / ) m_{R3}$ | Compound | $) m_{R2} / ) m_{R3}$ |
|---|---|---|---|
| A2/97 | 0.48 | $UO_2$ - A2/97 | 0.39 |
| A2/97PB | 0.62 | $UO_2$ - A2/97PB | 0.49 |
| KHA | 0.81 | $UO_2$ - KHA | 0.75 |
| KHAPB | 1.47 | $UO_2$ - KHAPB | 1.27 |
| M1 | 1.02 | $UO_2$ - M1 | 1.02 |
| M1PB | 1.09 | $UO_2$ - M1PB | 1.06 |
| M42 | 1.03 | $UO_2$ - M42 | 3.39 |
| M42PB | 1.30 | $UO_2$ - M42PB | 6.62 |

Tab. 1: Relations of the mass losses of reactions 2 to 3

At the final temperature $T_f$ of reaction 3 the organic substance of the humic compounds is completely decomposed. It was therefore used as an index of thermal stability.

From the values in Tab. 2 the following can be concluded:

The thermal stability of the humic acids and their U(VI) complexes is increased by methylation, possibly caused by the binding of the less polar methyl groups instead of the OH groups.

The thermal stability of the U(VI) complexes is decreased in comparison with the free HA`s. The reason could be the introduction of intramolecular stresses into the macromolecule by the U(VI) binding. This effect is much greater for the synthetic humic acid complexes and it is additionally increased for methylated complexes.

| Humic acid | $) T_f$ [°C] (HAPB)-HA | $) T_f$ [°C] ($UO_2$-HA)-HA | $) T_f$ [°C] ($UO_2$-HAPB)-HAPB |
|---|---|---|---|
| A2 | 16.9 | - 45.1 | - 52.1 |
| K/HA | 60.0 | - 35.6 | - 59.9 |
| M1 | 21.2 | - 122.3 | - 133.4 |
| M42 | 17.0 | - 81.9 | - 92.4 |

Tab. 2: Decreasing the thermal stability of U(VI) complexes of methylated and unchanged HA´s

## References

/1/ Pompe, S., et al.; this report p. 29
/2/ Bubner, M., et al.; this report p. 30

# $^{13}$C-CP/MAS-NMR SPECTROSCOPY WITH HUMIC ACIDS: I. INVESTIGATION OF $^{13}$C-LABELED MODIFIED HUMIC ACIDS TYPE M1

S. Pompe, M. Bubner, K.H. Heise, G.R. Choppin [1], G. Bernhard
[1] Department of Chemistry, The Florida State University, Tallahassee, Florida 32306, USA

*We synthesized site-specific $^{13}$C-labeled, chemically modified humic acids (HAs) type M1 using [$^{13}$C]diazomethane. These HAs were studied by solid state $^{13}$C-CP/MAS-NMR spectroscopy.*

## Introduction

To study the methylation process of HAs with diazomethane, which converts carboxyl groups to methyl esters and acidic (phenolic) OH groups to methyl ethers, we synthesized different chemically modified $^{13}$C-labeled HAs type M1 [$^{13}$C]diazomethane was used as methylation reagent. The $^{13}$C-labeled HAs were characterized by $^{13}$C-CP/MAS-NMR spectroscopy to verify that only carboxyl groups and acidic OH groups are methylated with diazomethane and to determine which functional groups of the HA show the highest affinity for methylation. The site-specific labeling of the HA with carbon-13 ($^{13}CH_3$ groups) simplifies the NMR spectra. Signals which are due to carbon-13 at natural abundance levels (1.1 %) are significantly reduced in intensity or only appear as noise in the baseline.

## Experimental

Starting from HA type M1 we synthesized a permethylated HA (type M1-B) as described in /1/ using an excess of [$^{13}$C]diazomethane. This permethylated HA was then saponified with NaOH resulting in a $^{13}$C-labeled synthetic HA with blocked phenolic OH groups (type M1-PB) /1/. Using a shortage of [$^{13}$C]diazomethane we synthesized a partly methylated HA (type M1-pB).

The solid state $^{13}$C-CP/MAS-NMR spectra were recorded on a Bruker WP200SY spectrometer at 50.325 MHz, a 90° pulse of 7 µs, a contact time of 1 ms and a spin rate of about 4.0 kHz.

## Results

Due to the modification, the $^{13}$C-labeled methyl groups of the methyl ester and ether groups show significant resonance signals between 50 and 60 ppm. The chemical shift assignment was performed using data for reference substances and literature data /2/.

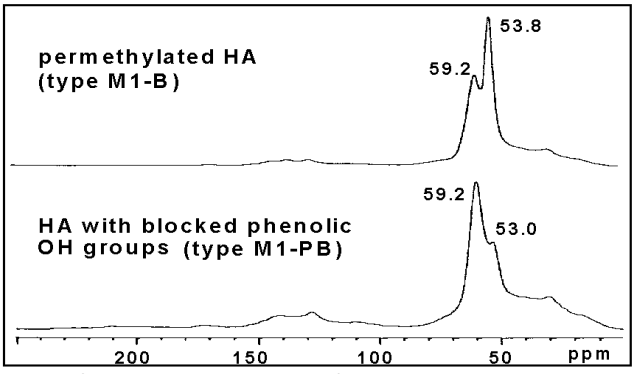


Fig. 1: $^{13}$C-NMR spectra of the $^{13}$C-labeled permethylated HA and the HA with blocked phenolic OH groups.

Fig. 1 shows a comparison of the spectra of the $^{13}$C-labeled permethylated HA (type M1-B) and the HA with blocked phenolic OH groups (type M1-PB). The spectrum of HA type M1-B shows two peaks, at 53.8 ppm and 59.2 ppm, that can be assigned to methyl esters of carboxyl groups and methyl ethers of phenolic OH groups, respectively. In the spectrum of HA type M1-PB the intensity of the peak at 53 ppm is significantly decreased. This shows that during the alkaline hydrolysis of the permethylated HA the methyl esters are hydrolyzed. However, the peak at 59.2 ppm remains unchanged which indicates that the acidic OH groups are still blocked after the hydrolysis. With these spectra we can exclude extensive insertion reactions and/or methylation of nitrogen-containing functional groups. This would be reflected in significant resonance peaks at about 30 and 40 ppm /2, 3/.

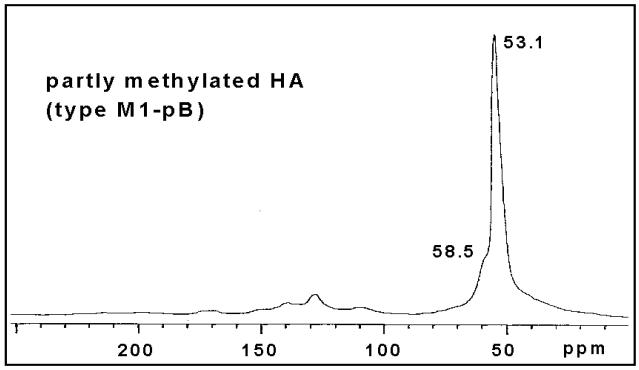


Fig. 2: $^{13}$C-NMR spectrum of the $^{13}$C-labeled partly methylated HA type M1.

Fig. 2 shows the spectrum of the partly methylated HA (type M1-pB). This spectrum shows one significant resonance signal at 53.1 ppm which can be assigned to $^{13}CH_3$ groups in ester groups. At 58.5 ppm there is only a shoulder that indicates the formation of a small amount of $^{13}$C-labeled methyl ethers. The other weak signals which can be observed in this spectrum are due to the natural abundance of $^{13}$C. It can be concluded that carboxyl groups are preferentially methylated with diazomethane in opposite to acidic OH groups. This result is very important for a selective blocking of HA functional groups.

We conclude that only carboxyl and acidic OH groups of HAs are methylated with diazomethane. The methyl ester groups are hydrolyzed during the treatment of the HAs with NaOH. Carboxyl groups show the highest affinity for methylation. Such modified HAs can be used to study the influence of various functional groups on the complexation behavior of HAs with actinides /1/.

## Acknowledgments

This work was performed during a research stay at the Florida State University (FSU). We thank FSU for financial support. In particular, we thank Dr. T. Gedris for his support during the NMR measurements.

## References

/1/ Pompe, S., et al., Radiochim. Acta, submitted
/2/ Thorn, K.A., et al., Org. Geochem. **11**, 123 (1987)
/3/ Mikita, M.A., et al., Anal. Chem. **53**, 1715 (1981)

# $^{13}$C-CP/MAS-NMR SPECTROSCOPY WITH HUMIC ACIDS: II. INVESTIGATION OF MODIFIED SYNTHETIC AND NATURAL HUMIC ACIDS

S. Pompe, M. Bubner, K. Schmeide, K.H. Heise, G.R. Choppin [1], G. Bernhard
[1] Department of Chemistry, The Florida State University, Tallahassee, Florida, 32306, USA

*Various chemically modified synthetic and natural humic acids were studied by solid-state $^{13}$C-CP/MAS-NMR spectroscopy.*

## Introduction

We studied the influence of phenolic OH groups on the complexation behavior of humic acids (HAs) with U(VI), using chemically modified synthetic and natural HAs with blocked phenolic OH groups /1/. The modified HAs were synthesized by permethylation of the original HAs with diazomethane, which converts carboxyl groups to methyl esters and acidic (phenolic) OH groups to methyl ethers. Then the permethylated HAs were saponified with NaOH, resulting in hydrolysis of the ester groups. To complete characterization of the modified HAs /1/, we performed $^{13}$C-CP/MAS-NMR measurements in order to verify whether significant structural changes had occurred in the HA during modification.

## Experimental

We studied the NMR spectra of the original synthetic HAs type M1 /2/ and type M42 /2/ as well as of the original natural HAs Aldrich /2/ and Kranichsee /3/ in comparison with the spectra of the corresponding permethylated HAs and the HAs with blocked phenolic OH groups. The synthesis of the chemically modified HAs as well as their characterization (functional groups, FTIR) is described in /1/. We also measured the NMR spectra of HAs type M1, type M42, Aldrich and Kranichsee after alkaline treatment to detect potential structural changes of the HAs following treatment with NaOH, which is one step in the preparation of HAs with blocked phenolic OH groups. These HAs were synthesized by treatment of the original HAs with 2 M NaOH for 8 hours under nitrogen and subsequent reprecipitation of the HAs. In this paper we present the results for the original and the modified HAs type M1 and Aldrich. The conditions of the NMR measurements are described in /4/.

## Results

Figs. 1 and 2 show the $^{13}$C-NMR spectra of the original and the modified HAs type M1 and Aldrich. The results of the various derivatization steps can be derived from a comparison of the spectra in the chemical shift range

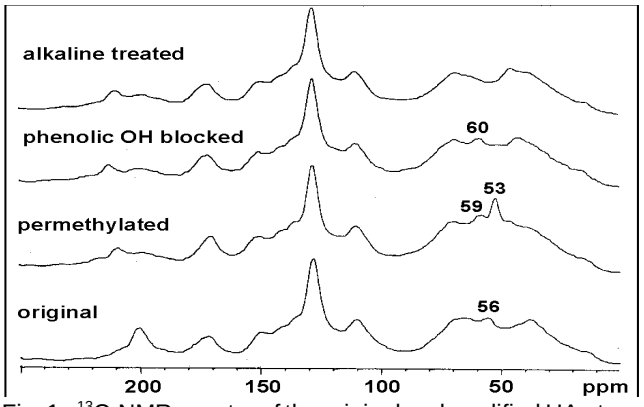


Fig. 1: $^{13}$C-NMR spectra of the original and modified HAs type M1.

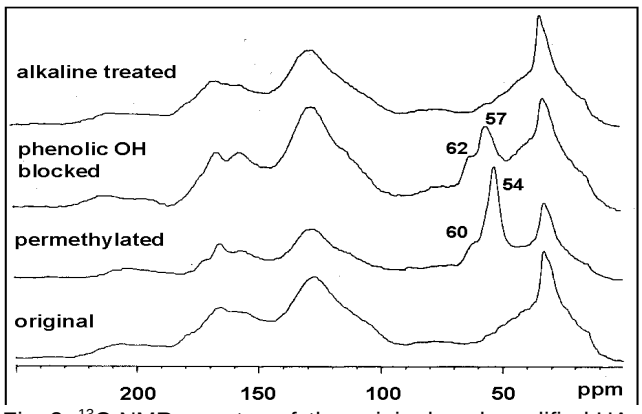


Fig. 2: $^{13}$C-NMR spectra of the original and modified HAs from Aldrich.

between 50 and 60 ppm, where the methyl groups of the methyl esters and ethers formed during modification with diazomethane show specific peaks /4/. In comparison with the original HA the permethylated HA type M1 shows new peaks at 53 and 59 ppm, which can be assigned to methyl esters and ethers, respectively. Comparable results were observed for the permethylated HA Aldrich, which shows a new peak at 54 ppm and a shoulder at 60 ppm. These signals are also due to methyl esters of carboxyl groups and methyl ethers of phenolic OH groups. After saponification of the permethylated HAs type M1 and Aldrich, the intensity of the peaks at 53 and 54 ppm decreases significantly due to hydrolysis of the ester groups. The signals at about 60 ppm are unchanged for both HAs, which indicates that the blocking of the phenolic OH groups is maintained. In addition, HA Aldrich with blocked phenolic OH groups shows a peak at 57 ppm, which can also be assigned to methyl ethers of acidic OH groups. It is to be assumed that this peak is superimposed by the peak at 54 ppm in the spectrum of the permethylated HA. Compared with the original HAs, the HAs after alkaline treatment show no or only small changes in this region. A comparison of the spectra in the range from 60 to 220 ppm shows that the original and the modified HAs have comparable structures.

It can be concluded that the derivatization of HAs with diazomethane causes only the intended structural changes on carboxyl and acidic OH groups.

## Acknowledgments

This work was performed during a research stay at the Florida State University (FSU). We thank FSU for the financial support. In particular, we thank Dr. T. Gedris for his support during the NMR measurements.

## References

/1/ Pompe, S., et al., Radiochim. Acta, submitted
/2/ Pompe, S., et al., Final Report, BMBF Project No.: 02 E 88150 (1999)
/3/ Schmeide, K., et al., Report FZKA 6124 (1998)
/4/ Pompe, S., et al., this report p. 33

# INTERACTION OF U(VI) AND FE(III) IONS WITH SOLID NATURAL AND SYNTHETIC HUMIC ACIDS IN AQUEOUS SYSTEMS

M. Bubner, S. Pompe, K. Schmeide, K.H. Heise, G. Bernhard, V.I. Nefedov [1]
[1] Kurnakov Institute of General and Inorganic Chemistry, Russian Academy of Sciences, Moscow

*The natural Kranichsee humic acid, the commercial Aldrich humic acid and the synthetic type M1 humic acid show different affinities to U(VI) and Fe(III) ions.*

## Introduction

The goal of our investigation was to gather information about the chemical affinity of U(VI) and Fe(III) ions to humic acids (HAs) of different genesis and to obtain well-defined and representative solid uranyl humates for structural investigations. We used the Kranichsee HA (KHA), the purified Aldrich HA (A2) and the synthetic type M1 HA /1/ to prepare the metal humates. Fe(III) as a ubiquitous cation seems to be able to affect the complexation behavior of the HAs with U(VI).

## Experiments and Results

Solid uranyl(VI) and iron(III) humate complexes were separately prepared according to /1/ by reacting HAs with solutions of 0.1M uranyl perchlorate or 0.1M iron(III) perchlorate. The ratios of metal to HA (meq cation : meq COOH) varied from 0.2:1 to 2:1 in the reaction mixtures. The pH values was adjusted to 2.0. The pH of the saturated solutions of the reaction products depend on the metal loading of the HA. The metal loading of the HA COOH groups was calculated from the elemental composition of the resulting solid complexes and the COOH content of each HA. The results are summarized in Tab. 1.

| HA | Cation | Cation : COOH [meq : meq] | Loading [% COOH] | pH |
|---|---|---|---|---|
| A2 | $Fe^{3+}$ | 0.2 : 1 | 17 | 3.0 |
| | $UO_2^{2+}$ | 0.2 : 1 | 17 | 3.3 |
| | $Fe^{3+}$ | 2 : 1 | 121 | 4.6 |
| | $UO_2^{2+}$ | 2 : 1 | 60 | 4.3 |
| KHA | $Fe^{3+}$ | 0.2 : 1 | 18 | 3.1 |
| | $UO_2^{2+}$ | 0.2 : 1 | 18 | 3.0 |
| | $Fe^{3+}$ | 2 : 1 | 121 | 4.0 |
| | $UO_2^{2+}$ | 2 : 1 | 50 | 3.4 |
| M1 | $Fe^{3+}$ | 0.2 : 1 | 9 | 4.0 |
| | $UO_2^{2+}$ | 0.2 : 1 | 17 | 4.0 |
| | $Fe^{3+}$ | 2 : 1 | 38 | 4.3 |
| | $UO_2^{2+}$ | 2 : 1 | 50 | 4.2 |

Tab.1: Metal loading of HAs at pH 2

Then the solid metal humates were reacted in aqueous suspensions with the competing cation - uranyl humates with iron(III) perchlorate and iron humates with uranyl perchlorate. For this cation exchange reaction stoichiometric amounts of the “free” competing cation (based on the COOH content of the humate) were used. The pH of the reaction mixture was also adjusted to 2.0. The products, mixed metal humates, were isolated as described in /1/. The metal content of the resulting solid metal complexes and of the supernatant was determined by ICP-MS. The metal loading of the HA COOH groups was calculated from the metal and carbon content of the humates. The results are shown in Tables 2 and 3.

| Loading of uranyl humate | | Loading of mixed metal humate [% COOH] | | |
|---|---|---|---|---|
| HA | [% COOH] | $UO_2^{2+}$ | $Fe^{3+}$ | 3 metal |
| A2 | 11 | 4,5 | 84 | 88,5 |
| | 60 | 20 | 68 | 88 |
| KHA | 50 | 11 | 70 | 81 |
| M1 | 15 | 11 | <2 | 13 |
| | 50 | 26 | <2 | 28 |

Tab. 2: Cation exchange of uranyl humates with $Fe^{3+}$

| Loading of iron humate | | Loading of mixed metal humate [% COOH] | | |
|---|---|---|---|---|
| HA | [% COOH] | $UO_2^{2+}$ | $Fe^{3+}$ | 3 metal |
| A2 | 12,5 | 53 | 10 | 63 |
| | 136 | 12 | 134 | 146 |
| KHA | 121 | 22 | 100 | 122 |
| M1 | 9 | 32 | <3 | 32 |
| | 38 | 29 | <3 | 29 |

Tab. 3: Cation exchange of iron humates with $UO_2^{2+}$

## Conclusions

The HAs KHA and A2 show similar affinities to $Fe^{3+}$ in comparison with $UO_2^{2+}$. High loading of the HA with $Fe^{3+}$ (up to 140 % of the COOH groups) points to the presence of hydroxylated $Fe^{3+}$. The affinity of the synthetic type M1 HA to $Fe^{3+}$ is negligible in comparison with $UO_2^{2+}$. It was shown by X-ray photoelectron spectroscopy /2/ that the HAs react with $Fe^{3+}$ and $UO_2^{2+}$ as particles. The uranyl complexes are mostly formed inside the particles whereas the iron complexes are formed on the particle surface. Loading the HAs surface with $Fe^{3+}$ prevents the further reaction with $UO_2^{2+}$. We can conclude that $Fe^{3+}$ reduces the ability of natural HAs to complex $UO_2^{2+}$.

## References

/1/ Bubner, M., et al., this report p. 30
/2/ Teterin, Yu.A., et al., J. Prakt. Chem. **341**, 773 (1999)

# URANIUM(VI) REDUCTION BY HYDROTHERMAL WOOD DEGRADATION PRODUCTS

A. Abraham, L. Baraniak, G. Bernhard, H. Nitsche

*The reduction of uranium(VI) by wood degradation products as well as by their phenolic and saccharic constituents was studied. The reducing capacities of the organic degradation product fractions were obtained from spectrophotometric determination of U(IV).*

## Introduction

The process of wood degradation in flooded uranium mines consists of hydrothermal decomposition of cellulose and lignin, with subsequent release of the breakdown products the water. The degradation products have reducing properties which are caused by phenolic units of the lignin fragments and by alcoholic groups of saccharic compounds. They are able to change the oxidation state of dissolved metals in the flood waters.

## Experimental

The hydrothermal wood degradation process was simulated out (1) by boiling wood chips in water under reflux and (2) by treating in an autoclave at 9 Mpa and 70°C under nitrogen (Institute of Plant and Wood Chemistry, Tharandt/Saxony) /1/. In treatment (1), 7 to 14 wt % of the wood was dissolved resulting in a weakly acidic hydrothermal extract with a pH of 3-4. The anaerobic treatment (2) resulted in a DOC content of up to 1400 mg/l. The leachates contained carbohydrates and phenols. Parts of the degradation products were separated in a phenolic (PHF) and a saccharic fraction (SAF) by extraction with dichlormethane. The phenolic fraction mainly consists of polymers. Monomeric compounds are formed to a lesser extent. Among them vanillin, guaiacol, coniferyl alcohol and their oxidation products (diverse hydroxybenzoic acids) were produced. The saccharic fraction contained cellulose fragments and monosaccharides such as arabinose, glucose, xylose, mannose, galactose and saccharic acids /1, 2/.

Uranium(VI) reduction was carried out by equilibrating $5.0 \cdot 10^{-5}$M U(VI) solution with different amounts of dissolved organic matter in the pH range 2-8. The samples were gently agitated over 4 to 6 weeks under nitrogen at room temperature. Then, the samples were treated with 12 M HCl to precipitate the organic compounds and dissolve the formed U(IV) hydroxide. The concentration of U(IV) was determined by spectrophotometry with arsenazo-III (666 nm) /3/. The measurements were carried out with a diode array spectrophotometer (Hewlett Packard, Type 8452A).

## Results and Discussion

About one percent of the initial uranium was reduced by both fractions of the wood degradation products.

| Sample | DOC (mg/L) | Reducing capacity (mequiv/g DOC) pH 5 | pH 8 |
|---|---|---|---|
| PHF [1)] | 38.0 | $2.08 \cdot 10^{-2}$ | $2.22 \cdot 10^{-2}$ |
| SAF [2)] | 56.3 | $1.75 \cdot 10^{-2}$ | $1.87 \cdot 10^{-2}$ |

[1)] phenolic fraction [2)] saccharic fraction

Tab. 1: Reducing capacity of phenolic and saccharic wood degradation products

The reducing capacity of the DOC was determined as $(1.7\text{-}2.2) \cdot 10^{-2}$ mequiv/g (Tab. 1).

The reducing capacity of the phenolic fraction is by a factor of 1.2 higher than that of the saccharic fraction. The results show that the total amount of reduced uranium of the wood degradation sample is about the sum of the phenolic and saccharic fractions (Fig. 1).

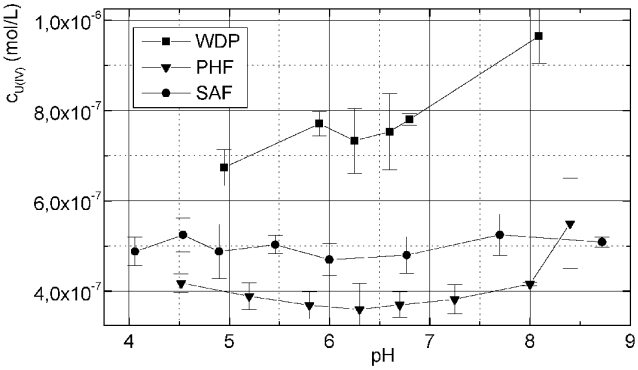


Abbr.: WDP wood degradation product, PHF phenolic fraction, SAF saccharic fraction

Fig. 1: U(VI) reduction by wood degradation products as a function of pH

For the wood degradation products the amount of reduced uranium(IV) increases with increasing pH. No significant pH dependence was found for the separated fractions.

These experiments show that not only phenolic groups but also saccharic compounds with special redox active groups, such as endiol units, are involved in the reduction of uranium. In these processes, the phenols are oxidized under radical formation that undergo coupling reactions, and the sugars are oxidized to the corresponding acids.

## Acknowledgments

This study was supported by the Sächsisches Staatsministerium für Wissenschaft und Kunst under contract no. 4-7541.83-FZR/512.

## References

/1/ Jelen, K., et al: Report FZR-123 (1996) p. 69
/2/ Jelen, K., et al: Report FZR-180 (1997) p. 30
/3/ Markow, W.K.; IAEA-Report SM-133/97

# REDOX REACTION SEQUENCE IN FLOODED WOOD-SUPPORTED MINES

L. Baraniak, A. Abraham, G. Bernhard, H. Nitsche

*The development of anoxic conditions in flooded underground uranium mines leads to the reduction of manganese(IV), iron(III) and uranium(VI). Sulfate reduction and arsenic remineralization as auripigment require more negative potential which can possibly be reached by microbial degradation of structural wood reinforcements in the uranium mines.*

## Introduction

The Schlema/Alberoda mine, one of the biggest uranium mine worldwide, is reinforced with 3-4 million $m^3$ wooden pit props. At the current stage of flooding, the mine water is contaminated with about 100 tons uranium and 60 tons arsenic.

## Discussion

The natural dampness in presence of air in underground mines leads to the oxidation of sulfidic ores, such as *pyrite, marcasite* ($FeS_2$), *skutterudite* ([Co,Ni] $As_3$), *glaucopyrite* ($FeAs_2$) to significant amounts of sulfate, uranium and arsenic which are released into the mine water.

The process of *pyrite* oxidation at pH 7

$$(FeS_2 + 8\ H_2O = Fe^{2+} + 2\ SO_4^{2-} + 16\ H^+ + 14\ e^-)$$

decreases the redox potential to -136 mV.

The microbial decomposition of organic matter

$$(CH_2O(aq) + 2\ H_2O = H_2CO_3(aq) + 4\ H^+ + 4\ e^-)$$

produces an even lower potential of -224 mV at the same pH (Fig. 1a). Furthermore, abandoned iron containing mining equipment produces an even more negative potential as the iron dissolves with time ($Fe/Fe^{2+}$ standard potential is -440 mV). The oxidation processes consume water-dissolved oxygen and generate reducing conditions, predominantly in deeper water layers. This leads to reduction processes characteristic for all natural waters (Tab. 1).

| redox reaction | log K | Eh [mV] |
|---|---|---|
| $lg[O_{2(aq)}] - lg[H_2O_{(l)}] - 4\ pH - 4\ p$, | 85.95 | 978 |
| $lg[Mn^{2+}] - lg[MnO_{2(c)}] + 4\ pH + 2\ p$, | 41.59 | 836 |
| $lg[Fe^{2+}] - lg[Fe(OH)_{3(c)}] + 3\ pH + p$, | 16.20 | 55.4 |
| $lg[UO_{2(c)}] + 2\ lg[HCO_3^-] - lg[UO_2(CO_3)_2^{2-}] + 2\ pH + 2\ p$, | 17.5 | 129 (pH 6) 69.3 (pH 7) |
| $lg[As_2O_{3(c)}] - 2\ lg[H_2AsO_4^-] + 6\ pH + 4\ p$, | 43.8 | -14.8 (pH 6) -103 (pH 7) |
| $lg[As_2S_{3(c)}] - 2\ lg[H_2AsO_4^-] - 3\ lg[H_2S] + 6\ pH + 4\ p$, | - | # - 125 (pH 7) |
| $lg[FeS_{2(c)}] - lg[Fe^{2+}] - 2\ lg[SO_4^{2-}] + 16\ pH + 14\ p$, | 87.0 | -68.5 (pH#6) -136 (pH 7) |
| $lg[HS^-] - lg[SO_4^{2-}] + 9\ pH + 8\ p$, | 34.0 | -215 |
| $lg[H_2CO_3] - lg[CH_2O_{(aq)}] - 4\ pH - 4\ p$, | -13.6 | -186 |
| $lg[CH_{4(aq)}] - lg[CH_2O_{(aq)}] + 4\ pH + 4\ p$, | 7.99 | -296 |

Tab. 1: Redox reactions sequence possible in deeper water layers of flooded wood-reinforced uranium mines /1/

After oxygen is consumed, oxides of manganese (*pyrolusite, manganite, hausmannite*) and iron (*goethite, haematite, magnetite*) are reduced. Because the mining water contains carbonate (1.2 g/L $CO_3^{2-}$), iron(II) precipitates as *siderite* (Fig. 1b). A decrease of Eh to a level of 100 mV, leads to the reduction of uranium(VI) that is present as carbonato complex (2.5•$10^{-5}$ mol/L) (Fig. 2a).

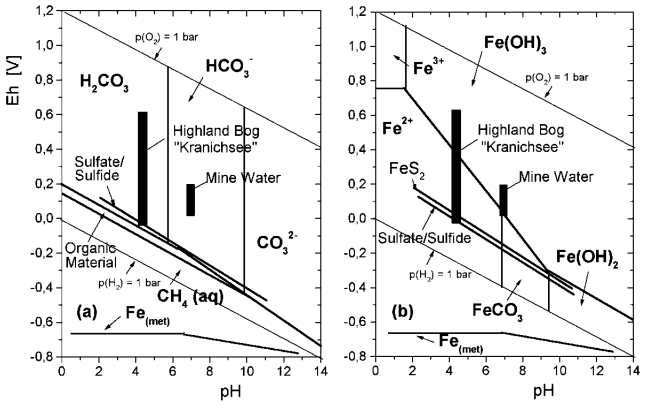


Fig. 1: Eh-pH diagram (a) for natural carbon species and (b) for iron species

This phenomenon was observed in the floodwater of the Pöhla mine where the uranium content decreased with time from 6 to 0.3 ppm. Thus large amounts of uranium were immobilized as uranium(IV) hydroxide. Arsenic(V) reduction (Fig. 2b), however, requires a more negative Eh. If the Eh decreases below -100 mV at pH 7, the reduction process may lead to the precipitation of *arsenolite* ($As_4O_6$). Microbial wood degradation leads to an even lower potential (-200 mV) where sulfate reduction occurs, thus reversing the oxidation of *pyrite*.

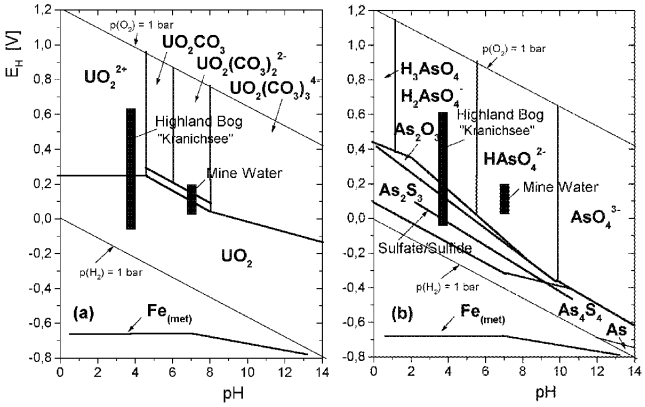


Fig. 2: Eh-pH diagram (a) for uranium species and (b) for arsenic species

This in turn leads to the precipitation of arsenic(III) sulfides as auripigment ($As_4S_6$). Such reduction processes are highly beneficial for the immobilization of uranium and arsenic in flooded uranium mines.

## References

/1/ Brookins, D.G.: *Eh-pH Diagrams for Geochemistry*, Springer-Verlag Berlin, 1988, p. 34

# BOG GAS COMPOSITION AND REDUCING CONDITIONS IN MOOR GROUND WATER

L. Baraniak, A. Abraham, G. Bernhard

*The reducing environment in the "Kranichsee" bog ground water can be characterized by an analysis of the underground bog gas and the occurrence of hydrogen sulfide in the water.*

## Introduction

The redox conditions in bog ground water can be estimated by measuring the redox potential and determining the dissolved oxygen content. The disadvantage of these direct measurements is that there are no established redox equilibria in the water and at the electrodes. It is therefore better to calculate the redox potentials from the chemical analysis of the redox active species, for example, from the pairs iron(III)/ iron(II) or sulfate/sulfide. Another possibility in strongly anoxic conditions is to analyze the bog gas that develops in the process of natural organic matter disintegration.

## Experimental

The bog gas was extracted from the moor ground by stirring deeper water layers (4° C, pH 5.3) and collecting the ascending bubbles at the water surface. The components were determined by gas chromatography using a molecular sieve column and a thermal conductivity detector /1/. In addition, the hydrogen sulfide in some subsurface water samples was analyzed by spectrophotometry with N,N-dimethyl-1.4-phenylenediamine (DIN 38 405, 1992).

## Results

Methane and nitrogen are the main components of the bog gas (Tab. 1), followed by a small amount of carbon dioxide and a trace of hydrogen sulfide. Sulfate and sulfide in the water were found to be 9.3 mg/L and 0.18±0.03 mg/L.

| gas | < [vol %] | gas | < [vol %] |
|---|---|---|---|
| $CH_4$ | 49.6±4.7 | $H_2$ | # 0.01 |
| $CO_2$ | 3.28±0.74 | $N_2$ | 44.5±1.8 |
| $H_2S$ | $1.65 \cdot 10^{-3}$ | $O_2$ | # 0.1 |

Tab. 1: Composition of the bog ground gas

*Redox equilibria:* Assuming that the potential in the subsurface water is determined by microbial wood degradation according to the equations

$$\text{native carbon} + O_2 = CO_2\,(g) + 4\,e^- \quad (1)$$

$$\text{native carbon} + 4\,H^+ + 4\,e^- = CH_4\,(g) \quad (2)$$

$$CO_2\,(g) + 8\,H^+ + 8\,e^- = CH_4\,(g) + 2\,H_2O\,, \quad (3)$$

the redox potential can be calculated from

$$lg[CH_4\,(g)] - lg[CO_2\,(g)] + 8\,pH + 8\,p\,, = lg\,K_a. \quad (4)$$

In the case of sulfate reduction Eh is obtained from

$$SO_4^{2-} + 10\,H^+ + 8\,e^- = H_2S\,(g) + 4\,H_2O \quad (5)$$

$$lg[H_2S\,(g)] - lg[SO_4^{2-}] + 10\,pH + 8\,p\,, = lg\,K_a. \quad (6)$$

Using $G^0$ and $H^0$ of the reactants, the equilibrium constant $K_a$ was calculated for 4° C, which was the bog ground temperature when the samples were taken (Tab. 2).

| reactant | $G^0$ [kJ/mol] | $H^0$ [kJ/mol] |
|---|---|---|
| $CH_4$ (g) | -50.79 | -74.80 |
| $CO_2$ (g) | -394.37 | -393.50 |
| $H_2S$ (g) | -33.56 | -20.63 |
| $H_2S$ (l) | -27.87 | -39.75 |
| $SO_4^{2-}$ | -744.6 | -909.2 |
| $H_2O$ (l) | -237.18 | -285.83 |

Tab. 2: Free energy and enthalpy of the reactants /1/

*Redox potentials in the bog ground:* The redox potential of -120 mV was calculated from the $CH_4/CO_2$ ratio using Eq. (3) (Tab. 3). Under the influence of this process the sulfate reduction was initiated, as indicated by the occurrence of hydrogen sulfide.

| | log $K_a$ | Eh [mV] |
|---|---|---|
| $CH_4/CO_2$ | 26.28 | -118.9 |
| $H_2S\,(g)/SO_4^{2-}$ | 45.04 | -60.5 |

Tab. 3: Equilibrium constant and redox potential at 4°C

That means that strongly reducing conditions were maintained as a result of microbial wood decomposition, a process consisting in the disproportionation of natural carbon into methane and carbon dioxide.

## Conclusion

Since in addition to the *pyrite* oxidation, wood decomposition in flooded mines also creates reducing conditions, it is possible to draw some conclusions concerning mine water. Considering the higher pH of about 7.5 and temperatures above 20° C in the mine water we can derive redox potentials below -200 mV. The generation of sulfide in a micromolar concentration in mine water of $2.1 \cdot 10^{-2}$ M sulfate would require a redox potential of -220 mV. That means that the anoxic environment in the mine water could be so strong that in addition to the reductive uranium immobilization it is very likely that a large amount of arsenic is reduced and precipitated as arsenic(III)-sulfide *($As_2S_3$ auripigment).*

## Acknowledgments

The gas analyses were carried out at the Fresenius Institute in Dresden and the AUA German Fuel Institute in Freiberg. We would like to thank Dr. Petra Steinbach (VKTA, Rossendorf) for the sulfide determinations.

## References

/1/ Stumm, W., Morgan, J.J.: *Aquatic Chemistry*, Wiley, 1981, p. 749.

# COMPARISON OF REDOX CONDITION IN A HIGHLAND BOG OF THE ERZGEBIRGE AND A FLOODED URANIUM MINE

L. Baraniak, A. Abraham, G. Bernhard, H. Nitsche

*Comparison of the redox conditions in the "Kranichsee" bog with deep waters of a wood reinforced flooded uranium mine shows significant similarities. The moor can be considered as a natural analogue to predict the changing of redox conditions in flooded mines.*

## Introduction

The uranium mines in Saxony and Thuringia were reinforced with large amounts of structural wood to stabilize the mining shafts and galleries. The flooding of these defunct mines by ground and surface waters exposes large amounts of wood to hydrothermal and microbial wood degradation processes. These processes generate an anoxic condition, which most likely leads to the reduction of heavy metal ions present in the water. We used the Saxon highland bog "Kranichsee" as a natural analogue to determine how the natural degradation of submerged wood influences the redox chemistry as a function of depth. The bog contains organic matter coming from submerged brush and other wood-containing vegetation.

## Results

In the bog's surface water, a mean redox potential (Eh) of 550 mV and an oxygen content of 10 mg/L (Tab. 1) was measured. In the ground at a depth of 1 meter the redox potential decreased to 156 mV and no oxygen was detected. Sampling of water from the deeper layers was accompanied by ascending gas bubbles spreading an intensive smell for hydrogen sulfide. Sulfate and sulfide in the subsurface water was found to be 9.3 mg/L and less than 0.1 mg/L, respectively.

| measuring point | pH | * [°C] | Eh [mV] | $O_2$ [mg/L] |
|---|---|---|---|---|
| **surface** | 4.3 | 8.5 | 550±3 | 10±2 |
| **marsh** | 4.9 | 8.0 | 156±5 | #0.1 |

Tab. 1: Redox potentials and oxygen content in the highland bog's surface water and in a marsh depth of 1 m

## Redox potential calculation

The water's Eh at the surface is mainly determined by the dissolved oxygen. From

$$\lg[O_2(aq)] - 4\ pH - 4\ p_{,} = -\ 93.7$$

a $p_{,}$ = 18.2 and Eh = 1002 mV was calculated, which corresponds to 950 mV at pH 7. Assuming the potential in the subsurface water is only controlled by the redox pair $SH^-/SO_4^{2-}$ and no methane formation takes place, the redox potential can be calculated from

$$\lg[HS^-] - \lg[SO_4^{2-}] + 9\ pH + 8\ p_{,} = 37.0.$$

For 1µg/L of sulfide $p_{,}$ = -0.537 and Eh = -29.4 mV are obtained. If the sulfide concentration in-creases to 10 µg/L the redox potential is decreased to -43.3 mV. That means, strongly anoxic conditions are maintained if the microbial wood decomposition (the oxidation of natural carbon to $CO_2$) causes the sulfate reduction.

## Discussion

The discrepancies between the measured and calculated Eh can be attributed to not reached equilibria in the water as well as at the electrode inter-face during the measurement. Lindberg and Runnels /2/ reviewed over 600 analysis of natural waters. They found that the potentials measured under aerobic conditions are too low by an average of half a volt and Eh values from anoxic environments are about 350 mV to high. Redox potentials should, therefore, be calculated from analytical data.

## Conclusions

Comparing the redox situation in the bog ground with that in the flooded mines (Tab. 2) a considerable decreased Eh is found in both cases. That means, iron(III) is reduced and the uranium(VI) reduction (immobilization as $U(OH)_4$) takes place in the mine water. But the Eh in the mine water is so far not low enough to reduce sulfate and arsenic(V) in order to remineralize arsenic as *auripigment* ($As_2S_3$).

| depth [m] | pH | Eh [mV] | $O_2$ [mg/L] | $Fe_{tot.}$/Fe(II) [mg/L] |
|---|---|---|---|---|
| **Schlema/Alberoda mine** | | | | |
| - 20 | 6.85 | 60-150 | 0.9-4.0 | 7.8 / 7.4 |
| - 300 | 6.75 | 24-39 | < 0.2 | 7.7 / 7.6 |
| **Pöhla mine** | | | | |
| - 20 | 7.02 | 48-54 | 1.7 | 9.2 / 7.4 |
| - 346 | 7.02 | 52-84 | 0.8-1.3 | 9.4 / 6.9 |

Tab. 2: Redox potentials and oxygen content in the watered mines of the saxon western ore mountains /3/

Until now the attainment of reducing conditions in the flood waters of uranium mines was solely attributed to the oxidation of *pyrite*. Our study of the highland bog shows that the degradation of wood causes highly anoxic conditions, indicating that the influence of the degradation of structural wood reinforcements in uranium mines must be considered when evaluating the redox processes in the mining waters.

## References

/1/ Baraniak, L., et al., Report FZR-218 (1998) p. 32
/2/ Lindberg, R.D., Runnells, D.D.: Ground Water Redox reactions: An Analysis of Equilibrium State Applied to Eh Measurements and Geochemical Modeling. Science **225**, 925-927 (1984)
/3/ VKTA-Report: Investigation of hydrochemical processes in the flooded Schlema/Alberoda and Pöhla mine. Sept. 1997 (unpublished)

# REDUCTION OF IRON(III) BY NATURAL AND SYNTHETIC MELANOIDINE-TYPE HUMIC ACIDS

B. Mack, L. Baraniak, K.H. Heise, G. Bernhard, H. Nitsche

*Iron(III) reduction by natural and synthetic humic acids was studied at pH 3.0. The reducing capacity and the content of carboxylic groups and phenolic OH groups were determined for the pure humic acids and the products resulting from methylation and saponification. The reducing properties are ascribed to the phenols in the natural humic acids and to the endiol groups in the synthetic humic acids.*

## Introduction

The reducing capacity of humic acids (HA) is commonly attributed to phenolic groups. In /1/ various HA were investigated but no direct correlation between the phenolic group content and the reducing capacity (RC) toward iron(III) was found. Therefore, we studied the influence on the iron(III) reduction by gradually blocking the functional groups. Two types of natural HA (one isolated from the bog “Kleiner Kranichsee” and a purified commercially available HA) and two synthetic HA (melanoidins M1 and M42) were examined. The HA characterization is described elsewhere /1, 2/.

## Experimental

The main functional groups such as carboxylic and phenolic hydroxyl groups, were blocked by permethylation and saponification of the resulting esters according to Bubner et al. /3/. The RC was determined at pH 3.0 at an ionic strength of 0.1 M (KCl) and an initial iron(III) concentration of 5.0 mmol/L. The HA concentrations varied from 0.1 to 0.3 g/L for the untreated and the saponified HA as well as 0.5 to 0.7 g/L for the permethylated samples. The experimental techniques used are described by Mack et al. /1/. The determined contents of carboxylic and phenolic OH groups are listed in Tab. 1.

| Humic acid | Functionality (meq/g) | |
|---|---|---|
| | COOH | phenolic OH |
| Aldrich, untreated | 3.90 ± 0.14 | 3.45 ± 0.49 |
| saponified | 3.23 ± 0.51 | 1.10 ± 0.44 |
| permethylated | 0.10 ± 0.06 | 0.64 ± 0.34 |
| Kranichsee, native | 3.88 ± 0.41 | 3.87 ± 0.52 |
| saponified | 2.38 ± 0.52 | 1.56 ± 0.39 |
| permethylated | 0.09 | 0.36 |
| M 1, untreated | 1.35 | 2.45 |
| saponified | 0.86 ± 0.23 | 0.86 ± 0.29 |
| permethylated | 0.09 | 0.32 |
| M 42, untreated | 3.72 ± 0.28 | 2.30 ± 0.36 |
| saponified | 2.74 ± 0.78 | 0.65 ± 0.29 |
| permethylated | 0.11 ± 0.01 | 0.55 ± 0.07 |

Tab. 1: Content of carboxylic and phenolic hydroxyl groups of the native and synthetic humic acids

The amount of iron(III) reduced to iron(II) was determined after a six weeks equilibration with the humic acid.

The calculated reducing capacities are shown in Tab. 2.

| Humic acid | Reducing capacity (meq/g) |
|---|---|
| Aldrich, untreated | 1.99 ± 0.07 |
| saponified | 1.38 ± 0.02 |
| permethylated | n.d. [1)] |
| Kranichsee, native | 3.14 ± 0.09 |
| saponified | 1.95 ± 0.02 |
| permethylated | 0.19 ± 0.01 |
| M 1, untreated | 3.85 ± 0.11 |
| saponified | 2.58 ± 0.01 |
| permethylated | 0.25 ± 0.01 |
| M 42, untreated | 6.14 ± 0.30 |
| saponified | 3.61 ± 0.13 |
| permethylated | 0.29 ± 0.01 |

[1)] n.d.: not detected

Tab. 2: Reducing capacity of native and synthetic humic acids after six weeks equilibration with iron(III)

## Results and Discussion

Permethylation of HA with subsequent saponification leads to free carboxylic groups and to methylethers of the phenols. The esterfication blocks the phenolic hydroxyl groups and prevents the formation of phenolate ions and phenoxy radicals.

The results show the tendency that RC of all HA decrease with decreasing phenolic group content. In case of the natural HA (Aldrich/Kranichsee) one third of the phenolic OH surprisingly remains unblocked. The RC of the same HA, however, amounts to about two third after blocking. We therefore conclude that groups other than phenolic hydroxyl are also redox active. For example, the artificial HA synthesized by Maillard reaction of phenylalanine and glycine (M 1) and glutamic acid and xylose (M 42) do not contain any phenolic groups and shows a significant RC. We believe that the reducing properties are caused by endiol groups (“reduction” groups) that are formed as a result of the amino acid degradation via formation of intermediate "-dicarbonyl compounds according to Strecker /4/. Endiol groups can easily be oxidized by iron(III) to the corresponding carbonyl compounds. L(+)-ascorbic acid represents a classic example for our assumption.

## References

/1/ Mack, B., et al.: Report FZR-247 (1999) p. 32
/2/ Pompe, S., et al.: Radiochim. Acta **74**, 136 (1996)
/3/ Bubner, M., et al.: Report FZR-43 (1994) p. 22-24
/4/ Angrick, M., Rewicki, D.: Chemie in unserer Zeit **14**, 149 (1980)

# URANIUM(VI) REDUCTION BY NATURAL ORGANIC MATTER - U(IV) DETERMINATION BY LASER-INDUCED PHOTOACOUSTIC SPECTROSCOPY

A. Abraham, L. Baraniak, G. Geipel, G. Bernhard

*The reduction of uranium(VI) by spruce-wood lignin and hydrothermal pine-wood leachate was studied. The measurements were carried out by LIPAS to validate the results of UV and visible spectrophotometry.*

## Introduction

Natural organic matter such as wood degradation products, lignins and humic acids have reducing properties. They are able to reduce Fe(III) to Fe(II) and U(VI) to U(IV). These processes are very important for flooded uranium mines that are heavily reinforced by wood. Reducing conditions that are generated by wood decomposition and pyrite oxidation cause U(IV) in the mine water to be immobilized as $U(OH)_4$. This natural purification process reduces the contamination risk posed by uranium migration to the attaching ground water table.

## Experimental

To confirm the results of the spectrophotometric determination of U(IV) by arsenazo-III /1/ we carried out measurements by laser-induced photoacoustic spectroscopy (LIPAS) as an independent method. The reduction of U(VI) by lignin and wood degradation products was carried out by equilibrating samples of $1.0 \cdot 10^{-4}$ mol/L U(VI) and 0.4 g/L organic matter at pH 9 for over four weeks under nitrogen. The photoacoustic spectra were recorded after treating the samples with 12 N HCl to dissolve the U(IV) hydroxide.

## Results

We found the typical absorbance of U(IV) in the spectrum at 630, 650 and 670 nm. The band with the highest intensity at 650 nm was used for determination. The dependence of the relative absorbance of the photoacoustic signal on the U(IV) concentration was measured first (Fig. 1).

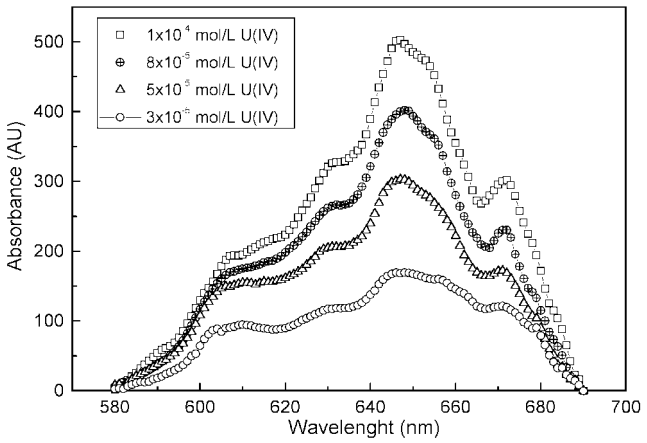


Fig. 1: Intensity of the LIPAS signal in dependency of the U(IV) concentration ($c_{U(IV)}$ from $3.0 \cdot 10^{-5}$ to $1.0 \cdot 10^{-4}$ mol/L in $HClO_4$)

After peak deconvolution we established the calibration curve (Fig. 2) and found that the intensity of the peak at 650 nm is 5.8 AU/$10^{-6}$ mol $L^{-1}$.

Then we measured the samples in the range from 610 to 690 nm and carried out the necessary basic line correction and peak deconvolution (Fig. 3).

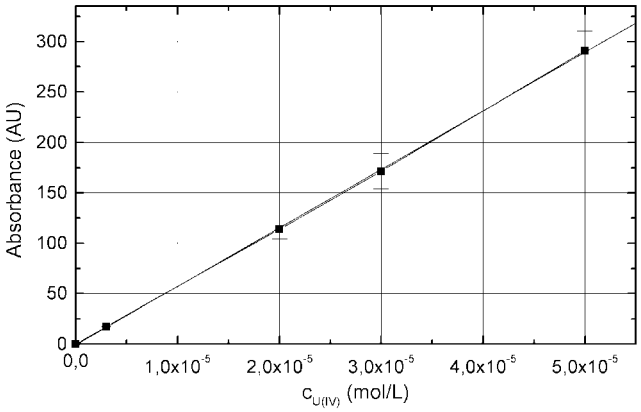


Fig. 2: Calibration curve for the U(IV) concentration range from $3.0 \cdot 10^{-6}$ to $3.0 \cdot 10^{-5}$ mol/L

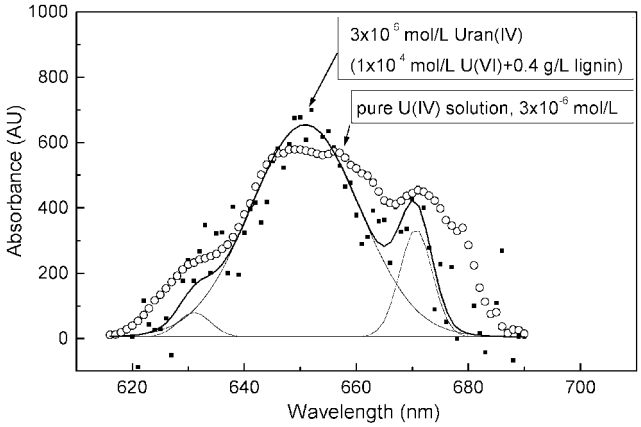


Fig. 3: Spectra of U(IV) reduced from U(VI) by lignin at pH 9 and a standard U(IV) solution.

All the U(IV) concentrations determined were in the micromolar range. The reducing capacity of the spruce-wood lignin and the hydrothermal pine-wood leachate is about $3 \cdot 10^{-2}$ meq per gram of dissolved organic carbon (DOC). These results are in agreement with the spectrophotometric measurements (Tab. 1).

| | spectrophotometry | | photoacoustics | |
|---|---|---|---|---|
| | $c_{U(IV)}$ (mol/L) | RC (meq/g DOC) | $c_{U(IV)}$ (mol/L) | RC (meq/g DOC) |
| lignin | $2.30 \cdot 10^{-6}$ $\pm 0.4 \cdot 10^{-6}$ | $2.35 \cdot 10^{-2}$ $\pm 0.2 \cdot 10^{-2}$ | $3.28 \cdot 10^{-6}$ $\pm 0.1 \cdot 10^{-6}$ | $3.20 \cdot 10^{-2}$ $\pm 0.2 \cdot 10^{-2}$ |
| wood | $1.03 \cdot 10^{-6}$ $\pm 0.7 \cdot 10^{-6}$ | $1.67 \cdot 10^{-2}$ $\pm 0.6 \cdot 10^{-2}$ | $1.88 \cdot 10^{-6}$ $\pm 0.1 \cdot 10^{-6}$ | $3.06 \cdot 10^{-2}$ $\pm 0.1 \cdot 10^{-2}$ |

Tab. 1: Comparison of the spectrophotometric and photoacoustic measurements

## References

/1/ Abraham, A., et al.; Report FZR-247 (1999) p. 30

# SAVE DISPOSAL OF CARBON-14 LABELED ORGANIC MATERIAL: I. PROCESS AND APPARATUS FOR THE ABSORPTION OF $^{14}CO_2$ AND ITS CONVERSION TO BARIUM CARBONATE-$^{14}C$

E. Förster, S. Heller, K.H. Heise

*The carbon dioxide-$^{14}C$ resulting from a mineralization process is trapped in caustic solution and finally recovered as barium carbonate-$^{14}C$ in a special apparatus.*

$^{14}CO_2$ resulting from the mineralization /1/ of the carbon-14 labeled organic compounds and waste is absorbed and precipitated as barium carbonate /2/ for disposal or recycling. A special closed apparatus was designed for this purpose. The schematic diagram of the apparatus is illustrated in Fig. 1.

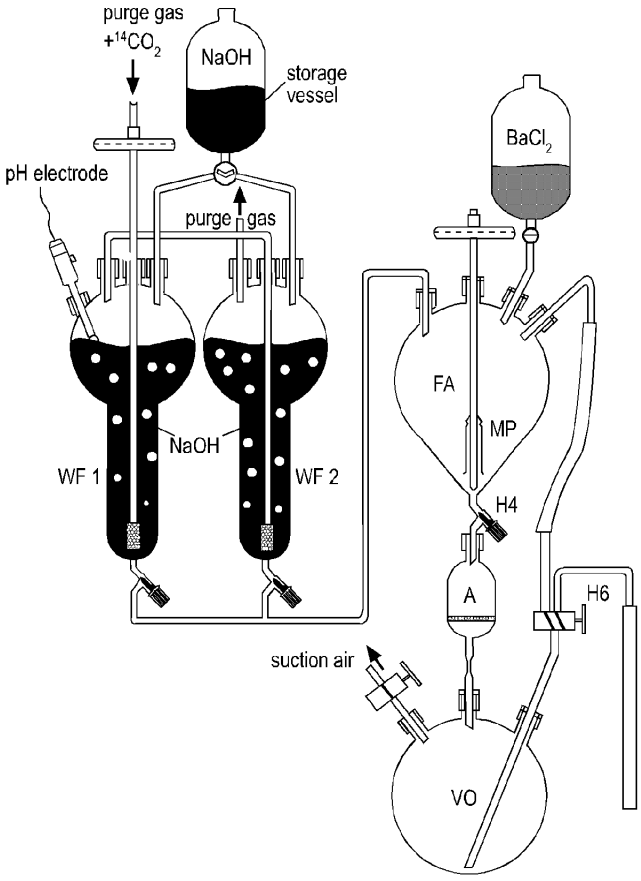


Fig. 1: Schematic diagram of the set-up for absorption of $^{14}CO_2$ and subsequent isolation of $Ba^{14}CO_3$

It is possible to combine this apparatus modular with other mineralization equipments. The set-up consists of the following components:

*Gas traps* (**WF**)
The quantitative retention of the $^{14}CO_2$ contained in the gas stream is ensured by a special design (Fig. 1) of the gas traps. No activity was detectable in the effluent purge gas stream from the outlet tube of the second gas trap. The saturation of the trapping agent (2M NaOH) is monitored by the following methods:

**S** Measuring of the pH-value: It is not necessary to determine the exact value for this purpose. The absorption curve is shown in Fig. 2. In the area of absorption the pH decreases slightly and in the area of saturation (pH <11.3) pH decreases distinctively.

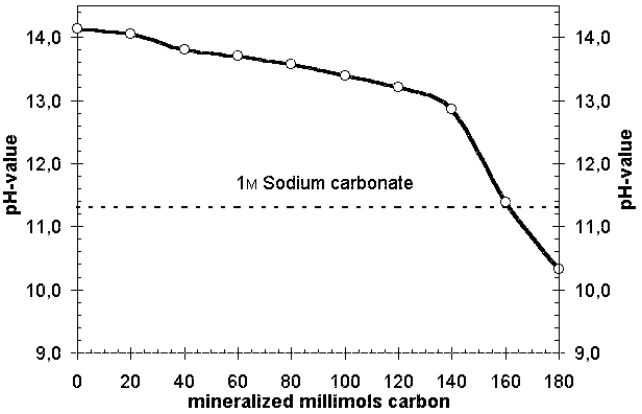


Fig. 2: pH-dependence of 2M NaOH (150 mL) on the mineralized carbon ($CO_2$-absorption)

**S** In the area of saturation the poorly soluble sodium hydrogen carbonate precipitates. The solution becomes cloudy.

*Precipitation of barium carbonate*
The saturated $Na_2{}^{14}CO_3$-containing solution is vacuum-transferred to the precipitation vessel **FA**. A freely filtrable barium carbonate-$^{14}C$ is obtained by means of the dropwise addition of an excess of 1 M barium chloride solution and subsequent Ostwald ripening. The dispersion is permanently agitated by a gas-bubble pump (**MP**). The carbon dioxide contained in the air has an advantageous effect for the complete precipitation of the barium carbonate.

*Isolation of barium carbonate*
The cock **H6** is closed and the valve **H4** is opened. Now the precipitate is collected by filtration in a special ampule **A** with a glass frit. The resulting filtrate in **VO** shows only a low activity (measuring by LSC). This ampule has on the top a screw thread (GL 18) for sealing with a plastic screw cap containing a PTFE seal. At the other end of the ampule a seal-off capillary is melted off. For final storage, the ampule is embedded in cement. Otherwise it is possible to reprocess the $Ba^{14}CO_3$ contained in the ampule.

Acknowledgment
This study was supported by the Sächsisches Ministerium für Wissenschaft und Kunst under contract No. 4-7581.312/20

References
/1/ Förster, E., Heise, K.H., Nitsche, H.: Verfahren zur elektrochemischen Mineralisierung von insbesondere C-14 markierten organischen Abfallstoffen, DE 196 46 049 A 1
/2/ Moriya, T., Motoishi, S.; in: Proceedings of the third Asian Symposium on Research Reactor. JAERI M 92 028 (Tokyo 1992), p. 367-371

# THE REACTION OF URANYL NITRATE WITH ACETYLPYRIDINE THIOSEMICARBAZONE

U. Abram

*$[UO_2(APTSC)(MeOH)(MeO)]_2$ is formed upon reaction of $UO_2(NO_3)_2$ with HAPTSC and $Et_3N$ in methanol. The solid state structure of the complex is characterized by an unusual hydrogen bonded dimer. The hydroxo-bridged dimer $[(UO_2)_2(\mu_2\text{-}OH)_2(NO_3)_4]^{2-}$ can be isolated when the same reaction is carried out without addition of a base.*

The co-ordination chemistry of uranium with sulphur-containing ligands is comparatively less developed and most structural studies deal with dithiocarbamate or dithiophosphinate ligands /1/. Complexes with thiosemicarbazones have not yet been reported whereas only one uranium semicarbazonato complex is known /2/.

A uranium(VI) complex containing a chelating thiosemicarbazone is formed when uranyl nitrate and acetylpyridine thiosemicarbazone, HAPTSC (**I**), are heated under reflux in methanol and a few drops of triethylamine are added. Red-brown crystals of $[UO_2(APTSC)(MeOH)(MeO)]_2$ deposit upon cooling.

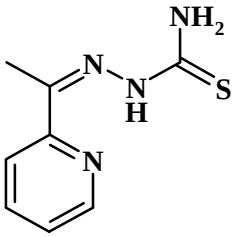

**I**

The parent ion in the FAB$^+$ mass spectrum of the complex is represented by m/z = 463 which can be assigned to the $[UO_2(APTSC)]^+$ unit. The IR spectrum clearly shows the U=O band at 910 cm$^{-1}$. This falls into the expected range for uranyl compounds. Additional bands at 2822 and 2932 cm$^{-1}$ suggest hydrogen bonds in the solid state structure of the product. This is confirmed by an X-ray structure determination.

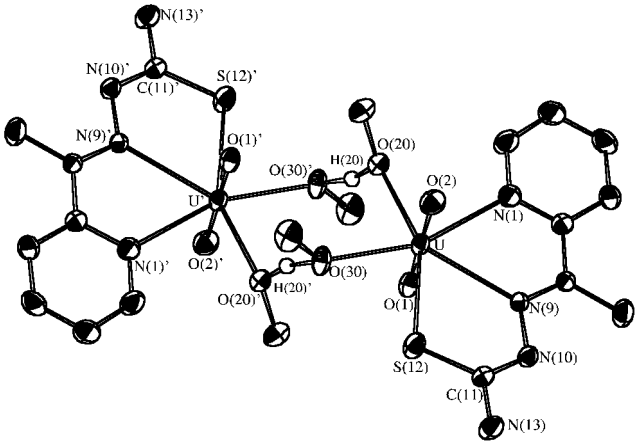


Fig. 1: Ellipsoid representation of the $[UO_2(APTSC)(MeOH)(MeO)]_2$ dimer. Hydrogen atom which do not contribute to the H bonds have been omitted for clarity. Selected bond lengths (Å): U-O(1): 1.763(3), U-O(2): 1.767(4), U-O(20): 2.263(3), U-O(30): 2.353(3), U-S(12): 2.813(1), U-N(1): 2.639(4), U-N(9): 2.622(4); U-U' distance: 5.13 Å.

$[UO_2(APTSC)(MeOH)(MeO)]_2$ crystallizes as a hydrogen bonded dimer (Fig. 1). Two $[UO_2(APTSC)(MeOH)(MeO)]$ units are linked by the H atoms of the methanol ligands which are situated between O(20) and O(30)' (O(20)-H(20): 1.16(7) Å, O(30)'-H(20): 1.33(7) Å). The environment of the uranium atom is best described as a pentagonal bipyramid. The thiosemicarbazone is deprotonated and co-ordinates via N(1), N(9) and S(12) to the metal.

Deprotonation of the thiosemicarbazone and its co-ordination to uranium is prevented when the reaction is done without addition of triethylamine. The pyridine function of the proligand is protonated as a consequence of the acidicity of the uranyl nitrate solution and $(H_2APTSC)_2[UO_2(NO_3)_2(OH)_2]_2$ is formed in almost quantitative yield (Fig. 2). The uranium atoms are bridged by OH$^-$ ligands which could doubtlessly be shown by the detection of all hydrogen atoms in the final Fourier map of the structure calculation.

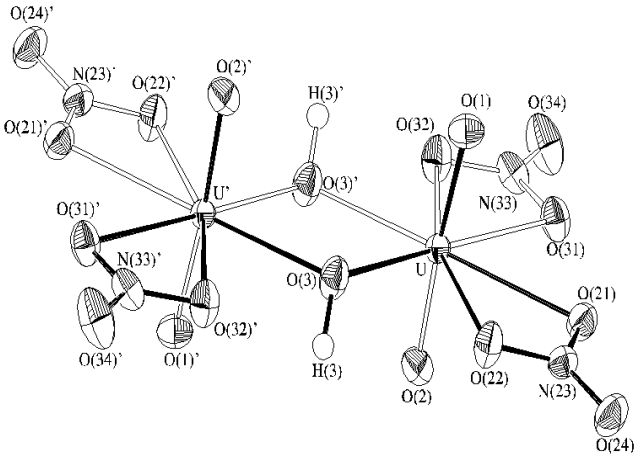


Fig. 2: Ellipsoid representation of the complex anion of $(H_2APTSC)_2[UO_2(NO_3)_2(OH)_2]_2$. Selected bond lengths (Å): U-(O1): 1.776(4), U-O(2): 1.772(4), U-O(3): 2.314(4), U-(O21): 2.540(3), U-O(22): 2.521, U-O(31): 2.524(4), U-O(32): 2.550(3), U-U': 3.892(1).

References

/1/ Bagnall, K.W. in: *Comprehensive Coordination Chemistry*, Pergamon Press, 1987

/2/ Bino, A., Inorg. Chim. Acta **127**, 95 (1987)

# BIS(TETRABUTYLAMMONIUM) (AQUA)TETRAKIS(ISOTHIOCYANATO)DIOXOURANIUM(VI)

U. Abram

*$(Bu_4N)_2[UO_2(NCS)_4(H_2O)]$ is formed in quantitative yield from $(Bu_4N)_2[UO_2Cl_4]$ and trimethylsilyl isothiocyanate. The U-N bond lengths range between 2.401(7) and 2.478(8) Å.*

Trimethylsilyl derivatives are valuable synthons in the co-ordination chemistry of numerous transition metals. In order to obtain information about their ligand exchange capabilities in the uranium(VI) chemistry, first reactions with $(Bu_4N)_2[UO_2Cl_4]$ have been performed.

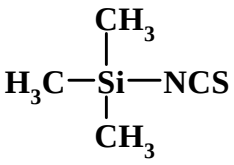

**I**

The reaction of bis(tetrabutylammonium) tetrachlorodioxouranium(VI) with $Me_3Si(NCS)$ (**I**) in dichloromethane gives yellow crystals of $(Bu_4N)_2[UO_2(NCS)_4(H_2O)]$ in almost quantitative yield. The driving force for the complete replacement of the chloro ligands is the formation of the volatile $Me_3SiCl$ which rapidly evaporates from the reaction mixture at room temperature. Moist solvents and the hygroscopic $Me_3Si(NCS)$ are sources of the co-ordinated water. No evidence was found for an attack on the tightly bound oxo ligands of the uranyl unit.

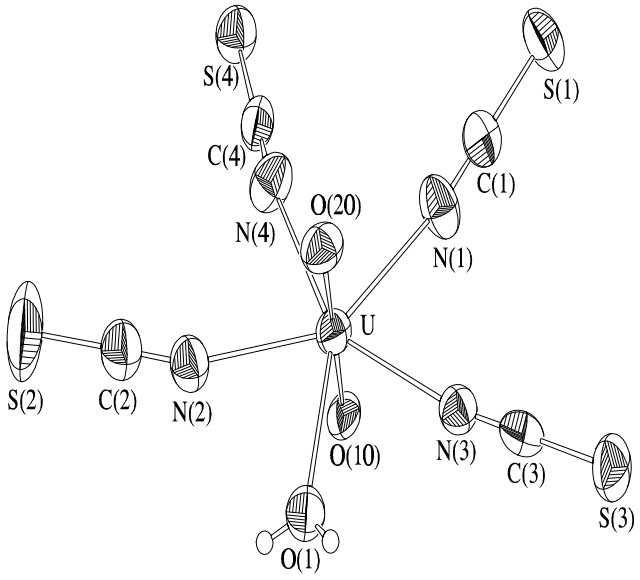


Fig. 1: Ellipsoid representation of the $[UO_2(NCS)_4(H_2O)]^{2-}$ anion. Selected bond lengths (Å): U-O(10): 1.772(7), U-O(20): 1.771(8), U-O(1): 2.475(6), U-N(1): 2.401(8), U-N(2): 2.421(8), U-N(3): 2.441(7), U-N(4): 2.478(8).

The uranium atom in the seven-coordinate $[UO_2(NCS)_4(H_2O)]^{2-}$ anion (Fig. 1) has an almost ideal pentagonal bipyramidal co-ordination environment with bond angles of 69.5(2) - 74.6(3)° between neighbouring equatorial donor atoms. The $NCS^-$ ligands are linear and the O(10)-U-O(20) angle is 179.2(3)°.

Structural data of two uranium complexes are available which can be compared with the title compound, $\{NH_4(18\text{-crown-6})\}_2[UO_2(NCS)_4(H_2O)]$ /1/ and $\{K(18\text{-crown-6})\}_2[UO_2(NCS)_4(H_2O)]$ /2/. Interactions between the sulfur sites of isothiocyanato ligands and the counter ions have been observed for both crown ether salts. This is, of course, not possible for the tetrabutylammonium compound under study. Nevertheless, intermolecular H bonds can be observed between the co-ordinated water and two isothiocyanato ligands of the neighboring molecule (H-S distances: 2.57 and 2.64 Å, O-H-S angles: 169 and 172°). This results in infinite columns of complex anions along the crystallographic b axis. Fig. 2 illustrates this arrangement which is unusual with regard to the bulky tetrabutylammonium cations.

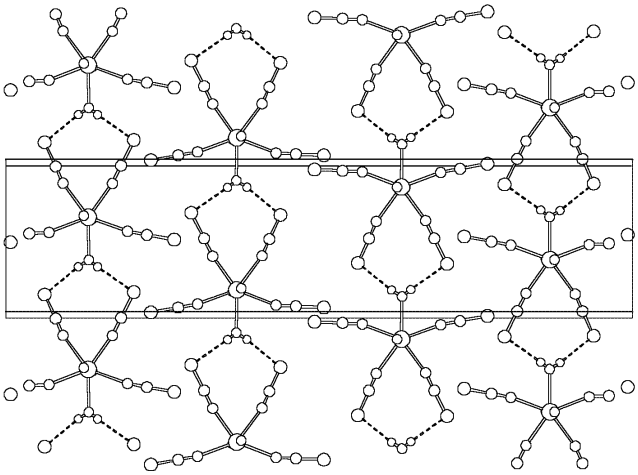

Fig. 2: Unit cell representation of the anion packing in $(Bu_4N)_2[UO_2(NCS)_4(H_2O)]$ illustrating the formation of infinite chains by H bonds along the crystallographic b axis. $Bu_4N^+$ cations have been omitted for clarity.

References

/1/ Ming Wang, et al., Acta Crystallogr. **C43**, 873 (1987)

/2/ Ming Wang, et al., Acta Crystallogr. **C43**, 1544 (1987)

# THORIUM(IV) COMPLEXES WITH CHELATING PHOSPHORYL LIGANDS: I. SYNTHESIS AND STRUCTURE OF $[Th\{Ph_2P(O)CH_2CH_2P(O)Ph_2\}_2(NO_3)_3](NO_3)$

U. Abram, E. Bonfada [1], E. Schulz-Lang [1]
[1] Universidade Federal de Santa Maria, Brazil

*A cationic thorium(IV) complex has been synthesized by the reaction of $Th(NO_3)_4 \cdot 5H_2O$ with bis(diphenylphosphino)ethane dioxide, $Ph_2P(O)CH_2CH_2P(O)Ph_2$ ($L^1$) and studied spectroscopically and by X-ray crystallography.*

Ligands containing a phosphoryl group have not only been used to study fundamental co-ordination chemistry of thorium but also to accomplish practical liquid-liquid extractions. Structural studies, however, which report details of the co-ordination environment of the metal are rare. Here we present synthesis and structural characterization of thorium(IV) complexes containing the potentially chelating ligand bis(diphenyl phosphino)ethane dioxide (**$L^1$**).

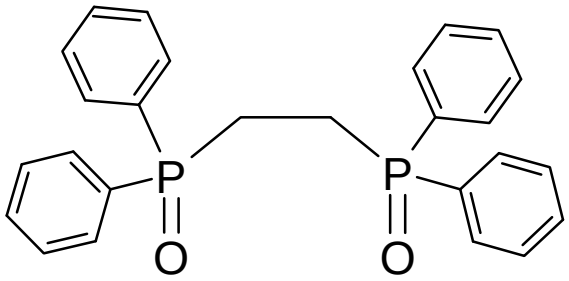


**$L^1$**

Treatment of $Th(NO_3)_4 \times 5H_2O$ with $L^1$ gives an almost colourless solid which can be recrystallized from $CH_3CN$/MeOH to yield yellow needles of $[Th(L^1)_2(NO_3)_3](NO_3)$. The formation of the bis-chelate is independent of the metal-to-ligand ratio. Infrared, NMR and mass spectra are consistent with a compound containing co-ordinated phosphine oxide and nitrate ligands. Single crystals of $[Th(L^1)_2(NO_3)_3](NO_3) \times H_2O$ can be obtained by slow evaporation of a saturated $CH_3CN$/MeOH solution. The thorium atom in the complex cation (Fig. 1) is co-ordinated with two chelating phosphine oxide and three bidentate nitrato ligands giving a co-ordination number of ten. The co-ordination polyhedron of the metal cannot be fitted into any regular geometry of this co-ordination number and may best be described as a strongly distorted bicapped square antiprism with two nitrate oxygen atoms forming the caps (Fig. 2). Main distortions origin from distinct co-ordination abilities of nitrate and $L^1$ which result in O(nitrate)-Th-O(nitrate) angles between 49.1(1) and 49.9(1)E and O($L^1$)-Th-O($L^1$) angles of 72.5(1) and 74.4(1)E. The Th-O($L^1$) bond lengths are found in the range between 2.342(3) and 2.417(3) Å. These values are substantially shorter than the Th-O(nitrate) bond lengths which have been found between 2.523(4) and 2.599(4) Å and reflect the strong basicity of the phosphoryl units.

The high co-ordination number of the metal atom may be attributed to the presence of three $NO_3^-$ ligands which compensate the steric requirements of the bulky phosphine oxide ligands.

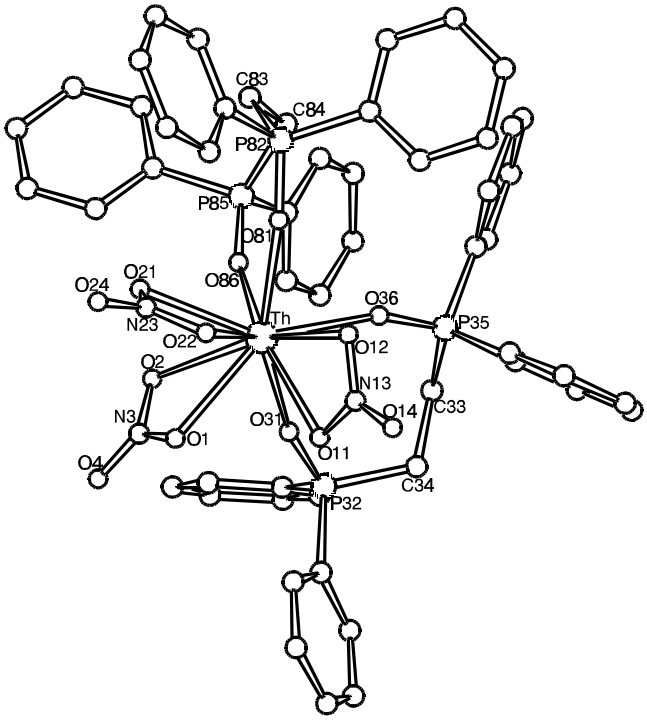


Fig. 1: Molecular structure and labeling scheme for the complex cation in $[Th(L^1)_2(NO_3)_3](NO_3) \times H_2O$.
Selected bond lengths: Th-O1 2.542(4), Th-O2 2.599(4), Th-O11 2.523(4), Th-O12 2.555(4), Th-O21 2.590(4), Th-O22 2.574(4), Th-O31 2.388(3), Th-O36 2.417(3), Th-O81 2.380(4), Th-O86 2.342(3) Å.

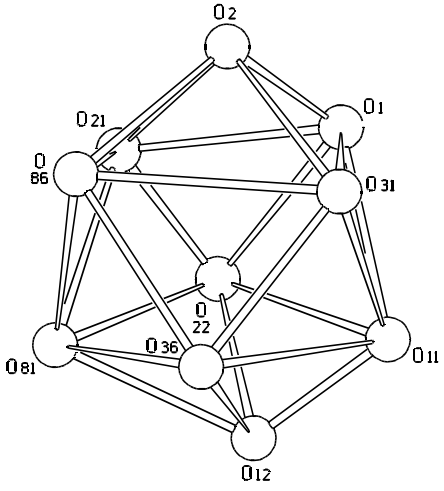


Fig. 2: Co-ordination polyhedron in $[Th(L^1)_2(NO_3)_3]^+$ representing a strongly distorted bicapped square antiprism.

# THORIUM(IV) COMPLEXES WITH CHELATING PHOSPHORYL LIGANDS: II. SYNTHESIS AND STRUCTURE OF $[Th\{Ph_2P(O)NP(O)Ph_2\}_3(dmso)_2](NO_3)$

U. Abram, E. Bonfada [1], E. Schulz-Lang [1]
[1] Universidade Federal de Santa Maria, Brazil

*A cationic thorium(IV) complex of the composition $[Th(L^2)_3(dmso)_2](NO_3)$ is formed upon the reaction of $Th(NO_3)_4 \cdot 5\,H_2O$ with ammonium bis(diphenylphosphoryl)amide and subsequent recrystallization from dimethyl sulfoxide. The thorium atom has the co-ordination number eight with an almost ideal square antiprismatic environment.*

In a previous communication we reported synthesis and structural characterization of a thorium(IV) complex containing the neutral ligand bis(diphenylphosphino)ethane dioxid $L^1$, $[Th\{Ph_2P(O)CH_2CH_2P(O)Ph_2\}_2(NO_3)_3](NO_3)$ /1/. The cationic complex containing thorium with the co-ordination number ten is formed during the reaction of thorium nitrate with $L^1$.

A thorium(IV) complex with co-ordination number eight, $[Th(L^2)_3(dmso)_2](NO_3)$, results from the reaction of $Th(NO_3)_4 \cdot 5H_2O$ with $(NH_4)L^2$ in methanol and subsequent recrystallization from dimethyl sulfoxide. The low solubility of the compound prevents from obtaining NMR and FAB mass spectra of sufficient quality. A band at 1079 $cm^{-1}$ in the IR spectrum of the complex can be assigned to the <(P=O) vibration. A band at 1384 $cm^{-1}$ can be attributed to ionic nitrate.

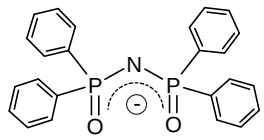

$(L^2)^-$

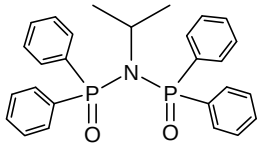

$L^3$

An X-ray structure analysis shows a square antiprismatic co-ordination environment for thorium (Fig. 1).

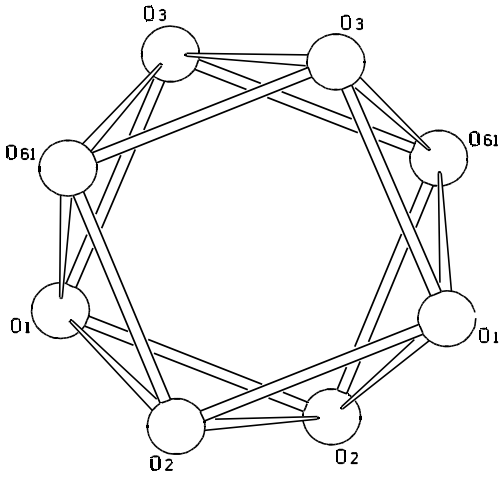


Fig. 1: Co-ordination polyhedron in $[Th(L^2)_3(dmso)_2]^+$ representing an almost ideal square antiprism.

A representation of the molecular structure is given in Fig. 2. The chelate rings only slightly deviate from planarity with maximum deviations of 0.45 Å (O1, P1, N1, P2, O2, Th) and 0.01 Å (O3, P3, N2, P3', O3', Th) from a mean least-square plane. This reflects a high extend of delocalized electron density. The Th-O($L^2$) bonds

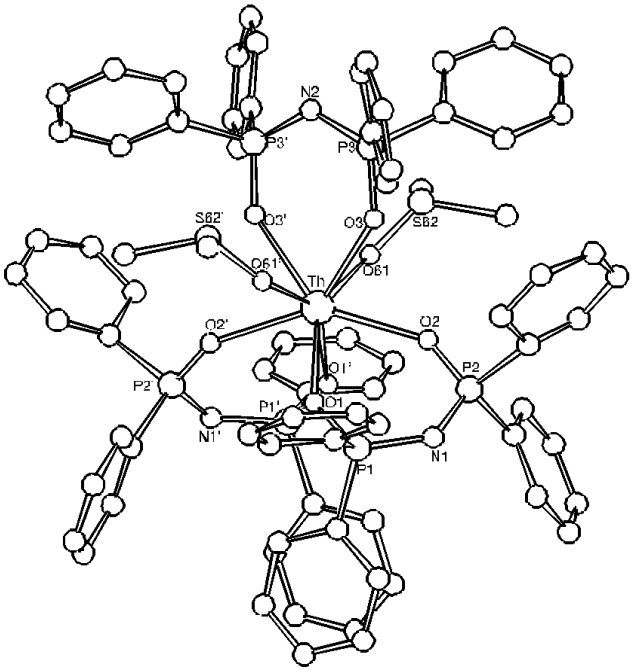


Fig. 2: Ellipsoid representation of the complex cation in $[Th(L^2)_3(dmso)_2](NO_3)$.
Selected bond lengths: Th-O1 2.363(6), Th-O2 2.376(8), Th-O3 2.379(8), Th-O61 2.392(11) Å.

are in the range between 2.363(6) and 2.379(8) Å which is shorter than in a thorium(IV) complex with the comparable neutral ligand N-isopropyl-bis(diphenyl phosphinoyl) amine ($L^3$), $[Th(L^3)_3(NO_3)_2]^{2+}$ /2/. This may be attributed to the higher coordination number in the latter compound which results in unfavourably low bite angles for $L^3$ (mean value: 65.5E, non-bonding O-O 'bite distance': mean value: 2.631 Å). The corresponding mean values for $L^2$ in $[Th(L^2)_3(dmso)_2]^+$ are 78.1E and 2.866 Å.

References

/1/ Abram, U., et al., this report p. 45
/2/ Aparna, K., et al., J. Chem. Soc., Dalton Trans. (1995) 2991

# $[Au(Et_2dtc)_2][TcNCl_4]$ - SYNTHESIS AND STRUCTURE

U. Abram

*$[Au(Et_2dtc)_2][TcNCl_4]$ ($Et_2dtc^-$ = N,N-diethyldithiocarbamate) is formed by the reaction of [Au(CO)Cl] with $[TcN(Et_2dtc)_2]$ in dichloromethane. The solid state structure of the compound is characterized by a large triclinic unit cell and shows an unusual arrangement due to long-range contacts between the technetium atoms and sulfur atoms of the $[Au(Et_2dtc)_2]^+$ units.*

The tetrachloronitridotechnetate(VI) anion, $[TcNCl_4]^-$, is of remarkable stability. The technetium-nitrogen triple bond is readily formed during reactions of oxo or halide complexes of the transition metal with azides, $NCl_3$, $PhCN(SiMe_3)N(SiMe_3)_2$ or $NH_2OSO_3H$. The $[TcNCl_4]^-$ anion is the favoured product when $Cl^-$ is present during such reactions.

The high-yield synthesis (85%) of $[Tc^{V\,I}NCl_4]^-$ during the reaction of $[Tc^{V}N(Et_2dtc)_2]$ with [Au(CO)Cl] in $CH_2Cl_2$ is surprising and requires a partial decomposition of the solvent. Atmospheric oxygen or decomposition products of dichloromethane act as oxidizing agents. This has been comfirmed by an attempted reaction in $CH_3CN$ which gives the $Tc^{V\,I}$ complex only in trace amounts.

$[Au(Et_2dtc)_2][TcNCl_4]$ crystallizes as red blocks with an unusually large triclinic unit cell (a = 9.422(2), b = 22.594(5), c = 32.153(7) Å, " = 72.64(3), $ = 85.19(1), ( = 86.15(1)E, Z = 12!!, see Fig. 1). This can be attributed to the localization of 4 gold atoms on centres of inversion (a symmetry which cannot be adopted by the anions) and weak interactions between $[TcNCl_4]^-$ anions and sulphur atoms of the $[Au(Et_2dtc)_2]^+$ cations (Tc-S distances between 3.45 und 3.56 Å). This leads to $\{[Au(Et_2dtc)_2][TcNCl_4]_2\}^-$ subunits which are shown in Fig. 2. The Tc-Cl bond lengths are comparable with those in the tetragonal $(Ph_4As)[TcNCl_4]$ /1/. The mean value for the N-Tc-Cl angles, however, is 101.9° which is between the values for $(Ph_4As)[TcNCl_4]$ (103.34°) and $Cs_2[TcNCl_5]$ (99.7°) and reflects the weak Tc...S interactions.

In solution the aggregates are dissociated. The solution EPR spectrum ($Tc^{6+}$: $d^1$) shows at ambient temperature a typical 10-line pattern due to the interaction of the unpaired electron with the nuclear spin of $^{99}Tc$ (I = 9/2). An axially symmetric EPR spectrum is obtained from frozen solutions of $[Au(Et_2dtc)_2][TcNCl_4]$. The derived spectral parameters are identical with those observed for the tetrabutylammonium or tetraphenylarsonium salts of $[TcNCl_4]^-$ which both contain isolated complex anions.

The solid state structure of $[Au(Et_2dtc)_2][TcNCl_4]$ underlines the capability of $[TcNCl_4]^-$ to form higher aggregates which has previously been demonstrated with the crystal structures of [Cs(18-crown-6][$TcNCl_4$] /1/ or $[Cs(18\text{-crown-6})]_4[(TcNCl_4)_4(OH_2)_3]$ /2/ which contain indefinite $\{TcNCl_4\}$ chains and $[N/TcCl_4...N/TcCl_4(OH_2)]^{2-}$ units, respectively.

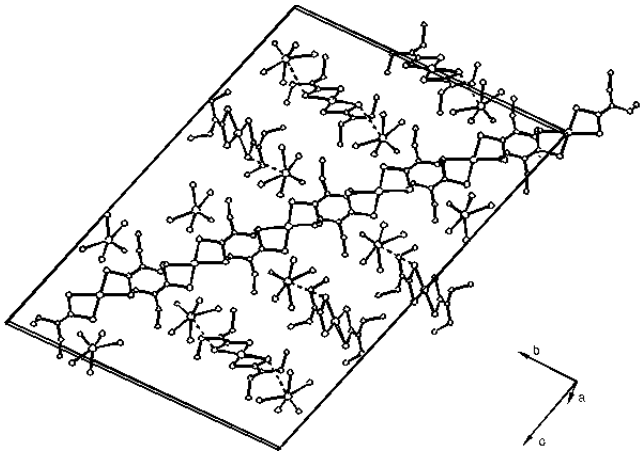


Fig. 1: Unit cell representation of $[Au(Et_2dtc)_2][TcNCl_4]$ with isolated $\{[Au(Et_2dtc)_2][TcNCl_4]_2\}^-$ subunits.

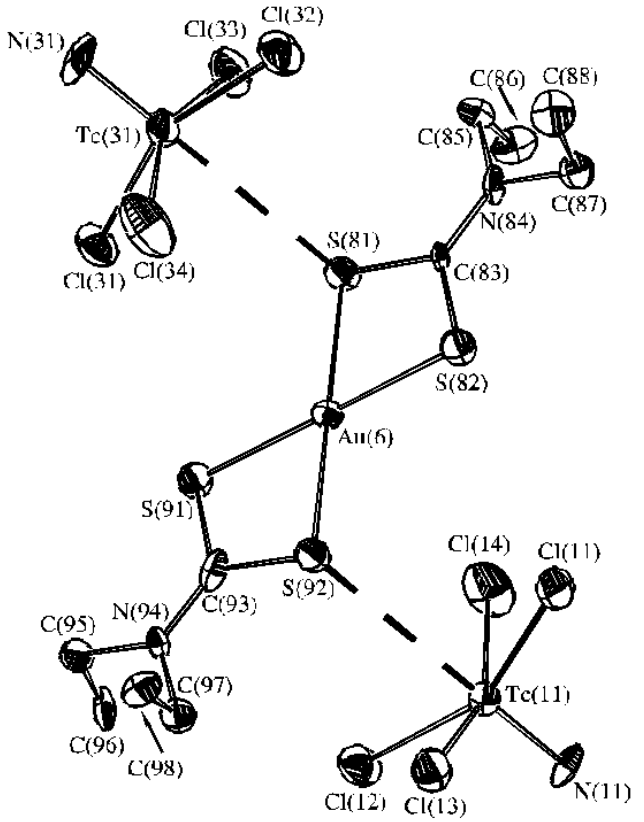


Fig. 2: Ellipsoid representation of $[TcNCl_4]^-$/ $[Au(Et_2dtc)_2]^+$ interactions. Ranges and mean values of bond lengths in the symmetry independent $\{[Au(Et_2dtc)_2][TcNCl_4]_2\}^-$ units:
Tc-N: 1.56(1) – 1.61(1) Å (mean: 1.59 Å), Tc-Cl: 2.308(4) – 2.336(4) Å (2.324 Å), Tc...S: 3.451(5) – 3.568(5) Å (3.492 Å), Au-S: 2.319 – 2.334 Å (2.327 Å), N-Tc-Cl: 100.1 – 104.7E (101.9E).

References

/1/ Baldas, J., et al., J. Chem. Soc., Chem. Commun. (1991) 954

/2/ Baldas, J., Adv. in Inorg. Chem. **41** (1994)

# $[Re(NBH_2SBH_3)(Me_2PhP)(Et_2dtc)]_2$
# A NOVEL RHENIUM DIMER WITH THE UNUSUAL BRIDGING $(NBH_2SBH_3)^{4-}$ LIGAND

U. Abram

*An unusual dimer is formed during the reaction of $[ReN(Me_2PhP)(Et_2dtc)_2]$ with excess $BH_3$ in tetrahydrofurane. Two $Re^V$ atoms are linked by two $(NBH_2SBH_3)^{4-}$ units which act as three-dentate ligands via N, S and H forming an 8-membered metallacycle with additional co-ordination of a hydrido H atom trans to the nitrogen atom.*

A variety of complexes containing a nitrido bridge between rhenium and boron has been described /1/, but in non of them the N-B-R unit acts as bridging ligand between two metal centers.

The dimeric title compound is formed from $[ReN(Me_2PhP)(Et_2dtc)_2]$ (**I**) ($Et_2dtc^-$ = diethyldithiocarbamate, $Me_2PhP$ = dimethylphenylphosphine) and $BH_3$ in THF.

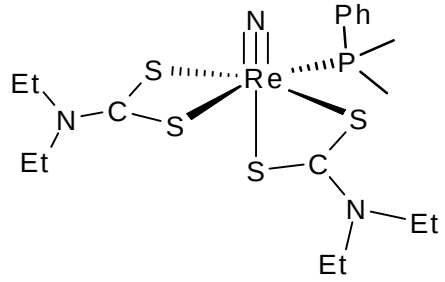


**I**

The formation of the unusual $[NBH_2SBH_3]^{4-}$ ligand can be described by an electrophilic attack of $BH_3$ at a sulfur atom of a dithiocarbamate ligand with the formation of thioformic acid diethylamide and the $[BH_2\text{-}S\text{-}BH_3]^-$ anion which rapidly reacts with the multiply bonded nitrogen atom to form the Re-N-B bridge. With this, the reported reaction is another example for a preferred attack of an electrophilic compound on sulfur /2/.

The recorded NMR spectra (in THF) agree with the structure of the compound. Hydride signals of the terminal H atoms have been observed at 1.05 ppm, whereas the signals of the co-ordinating H atoms could not be resolved. Two signals at 17.99 and -15.74 ppm have been observed in the $^{11}B$ NMR spectrum corresponding to the $N\text{-}BH_2\text{-}S$ and the $SBH_3$ moieties.

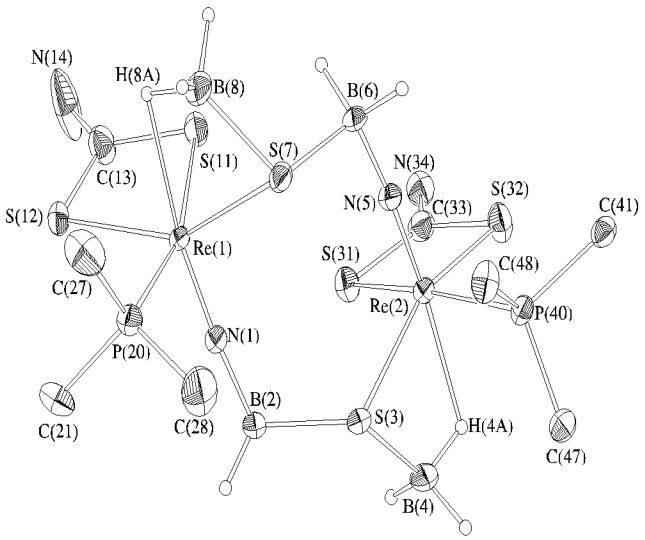


Fig. 1: Ellipsoid representation of $[Re(NBH_2SBH_3)(Me_2PhP)(Et_2dtc)]_2$. Ethyl groups, phenyl rings and CH hydrogen atoms have been omitted for clarity.

The structure of $[Re(NBH_2SBH_3)(Me_2PhP)(Et_2dtc)]_2$ (Fig. 1) shows two $[Re(Me_2PhP)(Et_2dtc)]^{4+}$ units which are linked by two $[N\text{-}BH_2\text{-}S\text{-}BH_3]^{4-}$ ligands forming a dimeric complex with an 8-membered $(ReNBS)_2$ metallacycle. The sixth co-ordination sites of the rhenium atoms are occupied by bridging hydrido ligands giving a distorted octahedral environment for the rhenium atoms. Main distortions are due to the restricting bite angle of the 4-membered dithiocarbamate chelate ring and the angles between N(1) or N(5) and the corresponding donor atoms in the equatorial co-ordination spheres of the metals which (with the exception of the N-Re-P angles) are all larger than 90°. The latter fact can be explained by the steric requirements of the multiple bond to the nitrogen atom and/or electronic repulsion between the Re/N bond and the equatorial ligands. The nitrido bridges are almost linear with Re-N-B angles of 175.4(4) and 175.9(4)°. Long distances of 2.3(1) and 2.13(6) Å have been found between Re(1) and H(8A) and Re(2) and H(4A), respectively, indicating only weak bonding interactions. This may be due to the bonds between the rhenium atoms and S(3) and S(7) which cause the 4-membered Re-S-B-H chelate rings with unusually small Re-H-B angles. Only monodentate co-ordination can be derived for both terminal $-BH_3$ units.

The short N-B bonds of 1.510(7) and 1.518(8) Å are in the range which has been previously observed for compounds containing nitrogen bridges between rhenium and boron /1/ and indicate covalent bonds between boron and nitrogen.

References

/1/ Abram, U., et al., Polyhedron **18**, 831 (1999), and references cited therein

/2/ Sellmann, D., et al., Inorg. Chem. **36**, 1397 (1997)

# SYNTHESIS, CHARACTERIZATION AND STRUCTURE OF μ-OXOBIS[BIS(PURINE-6-THIOLATO-S,N)OXORHENIUM(V)]

B. Schmidt-Brücken, U. Abram

*The title compound is formed by the reaction of $(Bu_4N)[ReOCl_4]$ with purine-6-thiole in methanol. It is the first rhenium compound containing purine-6-thiole as ligand.*

Purine-6-thiole, purinSH, is a biologically interesting ligand and shows a wide spectrum of potential applications /1/. Up to now, there are known only a few crystal structure analyses of metal complexes containing purinSH as monoanionic, chelating ligand /2,3/.

Stirring of $(Bu_4N)[ReOCl_4]$ and purinSH (molar ratio 1:2.5) in methanol at room temperature results in the formation of $\mu$-O[ReO(purinS-S,N)$_2$]$_2$ (Fig. 1) as an ocher colored powder, which is insoluble in water and most common organic solvents (yield relative to Re: 96%; elemental analysis found: C 23.7; H 1.0; N 21.8; S 13.0%; calculated for $Re_2C_{20}H_{12}N_{16}O_3S_4$: C 23.4; H 1.1; N 21.9; S 12.5%).

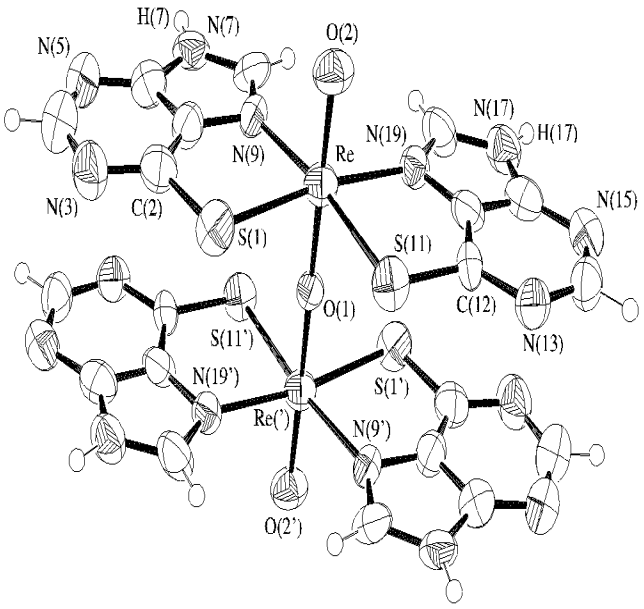


Fig. 1: Ellipsoid plot of $\mu$-O[ReO(purinS-S,N)$_2$]$_2$. Selected bond lengths [pm] and angles [°]: Re-O(1) 191.1(1), Re-O(2) 168.9(7), Re-S(1) 239.9(3), Re-S(11) 239.2(3), Re-N(9) 218.6(8), Re-N(19) 218.4(9), O(1)-Re-O(2) 167.8(2).

From the IR spectrum the following bands can be assigned: <(NH) 3392 cm$^{-1}$; <(C=C) and <(C=N) 1637, 1620 and 1591 cm$^{-1}$; <(Re=O) 977 cm$^{-1}$. The <$_{as}$(Re-O-Re) band cannot be assigned without doubt, since in the same range the *(C-H) frequencies are observed. Crystals suitable for an X-ray measurement were grown from hot dimethylsulfoxide. $\mu$-O[ReO(purinS-S,N)$_2$]$_2$ crystallizes in the monoclinic space group P2$_1$/n as dmso solvate. The bridging oxygen atom is placed on a center of inversion. The bond lengths Re-O(1) and Re-O(2) and the nearly linear angle O(1)-Re-O(2) well agree with the values observed in other oxo-bridged rhenium compounds /4,5/. The structure determination confirms that there are hydrogen atoms located at N(7) and N(17), what is assumed from the IR spectrum. All bond lengths and angles within the purine-6-thiolate are in the expected range. The bond lengths S(1)-C(2) (174(1) pm) and S(11)-C(12) (172(1) pm) are longer than the C-S double bond of purinSH (167 pm) and shorter than the distance expected for the C-S single bond (177 pm, /6/), what is expected for the delocalized system. For the sulfur and the nitrogen donor atoms a *cis* arrangement is found. The solvent molecules separate parallelly arranged layers built by the complex molecules (Fig. 2) in a way, that no stacking *via* the purine rings can be observed as is described in /2/.

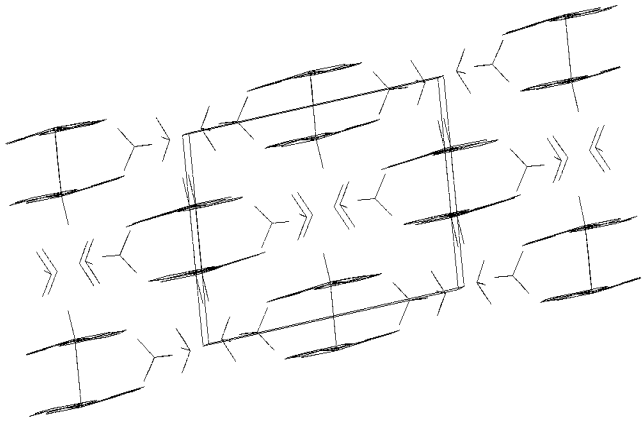

Fig. 2: Packing diagram of $\mu$-O[ReO(purinS-S,N)$_2$]$_2$.

References

/1/ Raper, E.S., Coord. Chem. Rev. **153**, 199 (1996)
/2/ Abram, U., Mack, J., Ortner, K., Müller, M.; J. Chem. Soc., Dalton Trans., 1998, 1011
/3/ Heitner, H.I., Lippard, S.J., Inorg. Chem. **13**, 815 (1974)
/4/ Conner, K.A., Walton, R.A., in: *Comprehensive Coordination Chemistry*, **Vol. 4**, Ch. 43, Pergamon Press, 1987
/5/ Abram, U., Abram, S., Mäcke, H.R., Koch, P.; Z. anorg. allg. Chem. **621**, 854 (1995)
/6/ Laverture, P., Hubert, J., Beauchamp A.L., Inorg. Chem. **15**, 322 (1976)

# Interaction of Microorganism with Radionuclides

# INTRASPECIES DIVERSITY OF *Thiobacillus ferrooxidans* STRAINS RECOVERED FROM URANIUM WASTES

K. Flemming, S. Kutschke, T. Tzvetkova [1], S. Selenska-Pobell
[1] Department of Geomicrobiology, University of Sofia, 1426 Sofia, Bulgaria

*Sequence analysis of the 16S rRNA genes of several uranium waste pile isolates of Thiobacillus ferrooxidans revealed specific signatures which distinguish three groups within the species.*

Recently, using ARDREA, we described two phylogenetic groups within the species *Thiobacillus ferrooxidans:* one related to the type strain of the species, ATCC 23270$^T$, and one represented by the uranium mining pile isolate ATCC 33020 /1/.

In this study the 16S rRNA genes of the following *T. ferrooxidans* strains were sequenced and analyzed: ATCC 33020, ATCC 23270, ATCC 21834, TFSS4, TFSS6, and TFK2. The strain 21384 has the same ARDREA patterns as the type strain 23270 /2/.

TFSS4 and TFSS6 represent two RFLP types of natural isolates recovered from the uranium mining waste pile near Johanngeorgenstadt /3/. The strain TFK2 was cultured from an oxic sediment sample of a uranium mill-tailing named Weiße Elster B1 and kindly provided to us by E. Ondruschka and H. Seidel, UFZ Leipzig. In addition, a sequence of a clone (No. 22) from the 16S rDNA clone library in the Forschungszentrum Rossendorf /4/ was included in the analysis.

The comparative analysis of the above-mentioned 16S rRNA gene sequences demonstrates intraspecies diversities called signatures.

In Fig. 1 three regions of the gene possessing specific signatures are presented. These signatures distinguish three types of *T. ferrooxidans* strains: Type I includes the type strain 23270, and the strains 21384 and TFSS4, type II the strains 33020 and TFSS6, while the strain TFK2 is discriminated in type III. Two of the signatures possess variations which influence the *Rsa*I consensus. The latter may be used for fast discrimination of the three *T. ferrooxidans* groups using the 16S *Rsa*I-ARDREA.

```
            P.457 (V3; helix 18)
T.f.23270 ...T.....................A...
T.f.21834 ...T.....................A...
TFSS4     ...T.....................A...  I
cl.22     ...T.....................A...
T.f.33020 ...C.....................G...  II
TFSS6     ...C.....................G...A
TFK2      ...C.....................A...›  III

            P.647 (between helices 21-1 and 22)
T.f.23270 ...T.T...
T.f.21834 ...T.T...|
TFSS4     ...T.T...|  I
cl.22     ...T.T...|
T.f.33020 ...C.G...   II
TFSS6     ...C.G...A
TFK2      ...C.C...›  III

            P.838 (V5; helix 27)
T.f.23270 ...TG..TA...
T.f.21834 ...TG..TA...|
TFSS4     ...TG..TA...|  I
cl.22     ...CG..TA...|
T.f.33020 ...TG..AC...   II
TFSS6     ...TG..AC...A
TFK2      ...TA..TA...›  III
```

Fig. 1: *T. ferrooxidans* type-specific 16S rRNA signatures.

As seen in Fig. 1, the clone 22 represents a strain belonging to type I. This clone possesses an additional transition from T to C in position 838 in front of the third signature. However, it cannot be ruled out that this difference is due to wrong incorporation of the nucleotide by direct amplification of the gene from the total soil DNA. Interestingly, the clone 22 was obtained from the same soil sample from which the group of natural isolates represented by the strain TFSS4, which also belongs to the type I, was recovered. The fact that both the 16S rDNA retrieval and the culturable method demonstrate the presence of 16S rDNA of type I in the same sample may be an indication that this type of *T. ferrooxidans* is dominating in the sample. As expected from the ARDREA analysis /2/, the strain 21384 possesses type I signatures.

The group of isolates belonging to type II, represented by the strain TFSS6, was recovered from another soil sample drawn from the surface of the uranium waste pile near Johanngeorgenstadt. This sample was three times less contaminated with heavy metals than the above-mentioned sample, which was abounded with type I and was drawn from a depth of 3 m.

At the moment the strain TFK2 is the only representative of type III. The sediment sample from which this strain was cultured was extremely contaminated with heavy metals /E. Ondruschka, personal communication/.

It is possible that the described 16S rDNA signatures reflect the genetic adaptation of the three particular *T. ferrooxidans* types to different concentrations of heavy metals, oxygen, and/or other compounds in their natural environments. It seems that these signatures correlate with heavy metal dependent growth rates of the strains (work in progress in our laboratory).

This is the first report on microdiversity between the strains of the species *Thiobacillus ferrooxidans*.

Acknowledgments

This work was supported by grants 7531.50-03-FZR/607 and 7531.50-04-844-99/4 from the Sächsisches Staatsministerium für Wissenschaft und Kunst, Dresden, Germany.

References

/1/ Selenska-Pobell, S., et al.; J. Appl. Microbiology **84**, 1085-1091 (1998)
/2/ Selenska-Pobell, S., et al.; Report FZR-218 (1998) p. 57-58
/3/ Kutschke, S., Selenska-Pobell, S., this report p. 54
/4/ Satschanska, G., Selenska-Pobell, S., Report FZR-247 (1999) p. 40

# DIRECT DETECTION AND DISCRIMINATION OF DIFFERENT *Thiobacillus ferrooxidans* TYPES IN SOIL SAMPLES OF A URANIUM MINING WASTE PILE

S. Selenska-Pobell, K. Flemming, G. Radeva [1]
[1] Institute of Molecular Biology, Bulgarian Academy of Sciences, 1113 Sofia, Bulgaria

*The presence of T. ferrooxidans strains with different 16S rDNA types was demonstrated in a large number of soil samples from two uranium waste piles in Saxony. We consider the observed coexistence of several ecotypes instead of one homogenous population an advantage for the survival of the species over a broader range of environmental conditions .*

Microdiversity is a newly recognized kind of bacterial diversity demonstrated for the strains of the same species which were isolated from different natural environments /1, 2, 3/. The 16S rRNA genes of such strains or ecotypes possess specific short sequence stretches named signatures which represent genetically distinct populations, adapted for optimal growth under different light, temperature, nutrient, and/or other environmental conditions. In some environments several ecotypes acclimatized to various past conditions may co-occur, due to factors which are favorable for all of them /1/.
In order to study the distribution of the three recently described *T. ferrooxidans* ecotypes /3/ in the uranium mining waste pile "Haberland Halde" near Johanngeorgenstadt and in the mill-tailing Gittersee/ Coschütz, the following strategy was developed and applied:
1) *T. ferrooxidans*-specific 16S rDNA fragments were amplified in total DNA recovered from a large number of soil samples drawn from various sites and depths (up to 5 m) of the pile. Two species specific primers $16S_{458F}$ and $16S_{1473R}$ were used for this /4/.
2) The resulting amplicons were then digested, using the frequently cutting endonuclease *Rsa*I. On the basis of the 16S rDNA sequences of the three ecotypes, three *Rsa*I patterns were predicted (see Fig. 1).

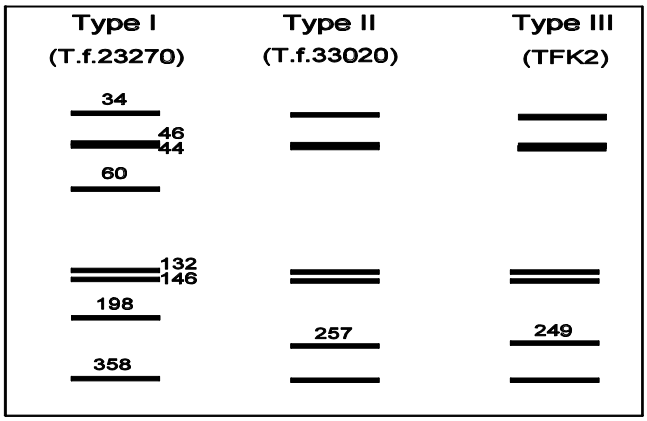


Fig. 1: RFLP-profiles of the three *T.ferrooxidans* types.

Several examples of direct molecular analysis of the soil samples are presented in Fig. 2. In many samples only one 16S rDNA type was demonstrated. There were samples in which two types co-occurred (see lanes 2 and 5 in Fig. 2), but one of them was always predominant. In 35 of 42 samples analyzed *T. ferrooxidans* was detected. In 24 samples type I was predominant and in 11 type II. In general, type I was found in samples from larger depths, which were more polluted with heavy metals, whereas type II was found in less contaminated samples from the surface.
In order to achieve better discrimination of the *T. ferrooxidans* types an analysis of the IGS of their *rrn* operons was started. It was demonstrated that the IGS of type I is 14 nucleotides longer than the IGS of type II. As expected, the sequence variability of the IGS is much higher than that of the 16S rDNA (see Fig. 3). Analysis of the IGS of type III is in progress.

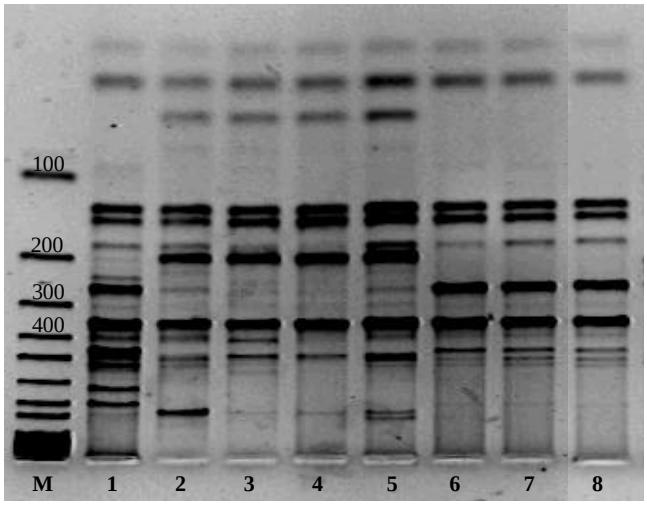


Fig. 2: *Rsa*I - RFLP types in the uranium waste samples
M:marker (bp), 1: JG-B 0-1, 2: JG-B 2-3, 3: JG-A 4-5, 4: JG-A 2-3, 5: JG-A 0-1, 6: Gitt.7, 7: Gitt.6, 8: Gitt.2

```
Type I  TTTAGGGTTTAGT-----GTG--TAGT-CTGAATAAC
Type II TGTAGGGTTGAGGATGTAGTGCGTAGTGCTGAATAAC

Type I  GCTTTAGGGATGTAGGAAGTAAG------GTGCTATT
Type II GCTTTAGGGATATAGGAAGTAAAAATAAAGTGCTATT

Type I  GATCACTGCCCACTCGGAAGATTGAGTGCGTTAGTTTG
Type II GATCACTGCCCACTCGGAAGGTCGAGTGTGTTAGTTCG
```

Fig. 3: A highly variable part of type I and type II IGS.

The strategy presented here is a straightforward way of analyzing of the structure and dynamics of the natural *T. ferrooxidans* populations. As the various types *of T. ferrooxidans* interact with uranium in various ways /5/ monitoring their distribution in polluted environments may be useful for modeling migration of this radionuclide.

Acknowledgments
This work was supported by grant 7531.50-03-FZR/ 607 from the Sächsisches Staatsministerium für Wissenschaft und Kunst, Dresden, Germany.

References

/1/ Moore, L.R., et al., Nature **393**, 464-467 (1998)
/2/ Prüß, B.M., et al., J. Bacteriol. **181**, 2624-2630 (1999)
/3/ Flemming, K., et al., this report p. 51
/4/ De Wulf-Durand, P., et al., Appl. Environ. Microbiol. **63**, 2944-2948 (1997)
/5/ Panak, P., et al., Report FZR-247 (1999) p. 46-47

## MICRODIVERSE TYPES OF *T. ferrooxidans* AND THEIR INTERACTIONS WITH URANIUM

M.L. Merroun, S. Selenska-Pobell

*The capability of representatives of the three recently described types of T. ferrooxidans to accumulate and tolerate uranium was investigated. Desorption studies demonstrated that sodium carbonate is able to recover up to 97% of the uranium bound.*

Recently, the presence of the three eco-types of *T. ferrooxidans* was demonstrated in the uranium mining waste pile “Haberlandhalde” near the city of Johanngeorgenstadt /1/.

The main objective of the present study was to determine if these three types differ on their capability to accumulate and tolerate uranium. In addition, the most potent desorbing agent for the accumulated uranium was selected.

The following strains were analysed: T.f. W1 belonging to type I, T.f. ATCC 33020 (type II) and T.f. D2 (type III). The strains D2 and W1 were kindly provided by Leo Leduc, University of Guelph, Guelph, Ontario, Canada.

The sorption studies (Fig. 1) showed that the strains from the three different types possess different capability to accumulate uranium. The rate of uranium biosorption gradually increased with increasing concentration of uranium at pH 1.5 and 4 and at room temperature. The amount of uranium bound to the biomass increases in the order *T. ferrooxidans* W1, D2 and ATCC 33020.

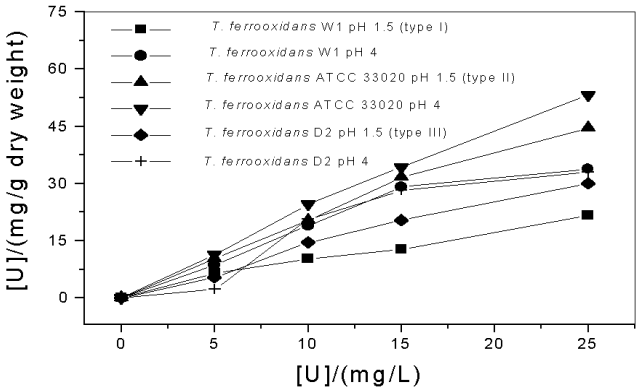


Fig. 1: Biosorption of uranium by the three types of *T. ferrooxidans*.

Interestingly, the strains W1 and D2 are resistant to 8 and 9 mM of uranium, respectively, wereas the strain ATCC 33020 does not tolerate more than 2 mM of uranium. The determination of the Minimum Inhibitory Concentrations (MICs) of uranium for the growth of the strains studied on solide media are summarized in Tab. 1.

| Strains | MICs of uranium (mM) |
|---|---|
| *T. ferrooxidans* W1(type I) | 9 |
| *T. ferrooxidans* D2 (type III) | 10 |
| *T. ferrooxidans* ATCC 33020 (type II) | 4 |

Tab. 1: MICs of uranium for the growth of *T. ferrooxidans* types.

On the basis of the results presented one may speculate that the strains of the type I and III are more resistant to uranium, probably because they possess a mechanism which limits the uranium binding below the letal amounts. This physiological diversity among the strains of *T. ferrooxidans* is very important because it allows fast selection and adaptation of the natural *T. ferrooxidans* populations to different leaching environments.

The desorption of uranium by EDTA, sodium carbonate and sodium citrate at different concentrations, are shown in Fig. 2.

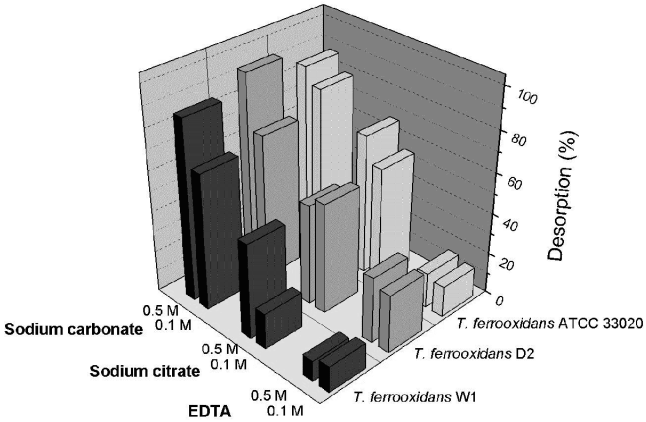


Fig. 2: Desorption of uranium accumulated by the three types of *T. ferrooxidans*.

The sodium carbonate was the most efficient desorbing agent tested, removing 97% of the uranium sorbed from the cells of *T. ferrooxidans* type III.

The desorption of uranium by the sodium carbonate treatment may be a result of the alkalization of the medium. Although an effect of the carbonate ion itself resulting in the formation of uranyl carbonate complexes, which might be stronger than the “bacterial-uranyl” ones cannot be ruled out. Approximately 12% of the bound metal ions were not removed from the cells of *T. ferrooxidans* type I and II by this treatment. It is not excluded that in these cases part of the uranium was complexed at sites with higher stability constants than those of the uranyl carbonate.

Sodium citrate, was the second best metal desorbing agent, and it removed uranium from *T. ferrooxidans* type II more effectively than from type I and III. EDTA could remove only between 10 and 30% of the accumulated uranium.

Acknowledgments

This work was supported by a grant (No. 4-7531.50-03-FZR/607) from the Sächsisches Staatministerium für Wissenschaft und Kunst, Dresden, Germany.

References

/1/ Flemming, K., et al., this report p. 51

# CLASSIFICATION AND GENOMIC FINGERPRINTING OF SEVERAL NATURAL *Thiobacillus ferrooxidans* ISOLATES RECOVERED FROM A URANIUM MINING WASTE PILE

S. Kutschke, S. Selenska-Pobell

*Six natural isolates of T. ferrooxidans were classified into two of the groups of this bacterial species. The genomic relationship between the strains studied was investigated by the use of random amplified polymorphic DNA analysis.*

Six *T. ferrooxidans* strains were recently recovered from two soil samples, contaminated to various degrees with heavy metals, from the uranium waste pile near Johanngeorgenstadt /1/. In the present work the strains were affiliated to the two recently described /2/ groups of the species *T. ferrooxidans* by the use of 16S amplified ribosomal DNA restriction enzyme analysis (16S-ARDREA) (see Fig. 1).

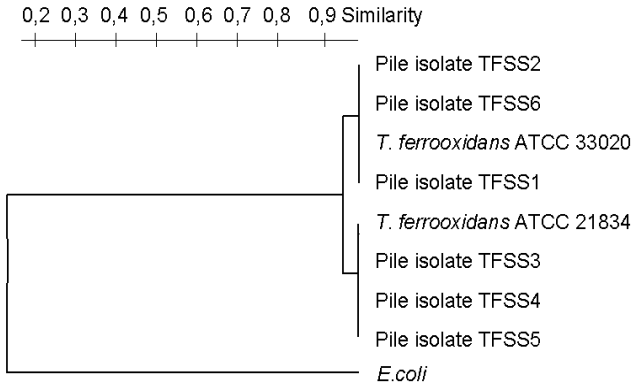


Fig. 1: Dendrogram showing the relationship between the natural *T. ferrooxidans* isolates and the reference strains as determinated by 16S- ARDREA

The reference strains of *T. ferrooxidans* were obtained from the American Type Culture Collection ATTC. The environmental *T. ferrooxidans* isolates were recovered and kindly provided to us by V. Groudeva, Department of Geomicrobiology, University of Sofia, Bulgaria. Total bacterial DNA was isolated by NucleoSpin C+T Kit (Machery-Nagel GmbH & Co. KG, Düren, Germany). The length polymorphism of the fingerprints was analyzed by the use of a software RFLP-Scan/Treecon (Scanalytics, Billerica, USA).

In order to study the interaction of the above-mentioned strains with heavy metals in natural environments it is important to distinguish and characterize them individually. Genomic analyses such as PGE or RAPD are powerful tools for discrimination and monitoring of individual bacterial strains /3/.

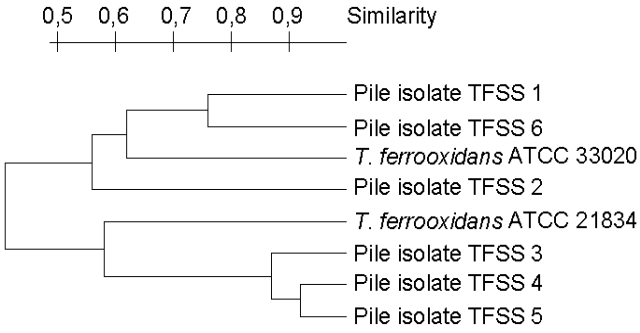


Fig. 2: Dendrogram showing the relationship between the natural *T. ferrooxidans* isolates and the reference strains as determined by RAPD

Using this method, see Figs. 2 and 3 it was possible to distinguish some individual characteristics of the strains and to evaluate their relatedness on the basis of the information derived from their whole genomes.

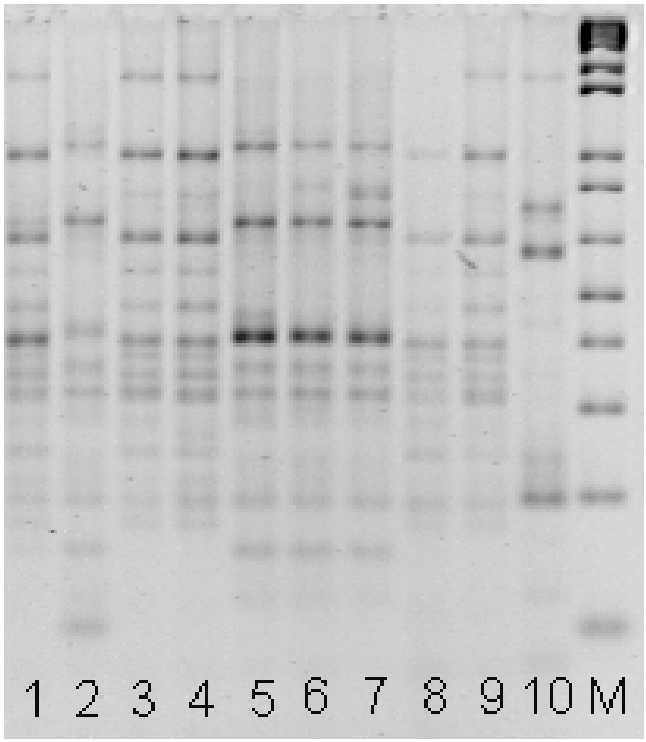


Fig. 3: Genomic RAPD fingerprints of the strains:1, ATCC 33020;2, ATCC 21834; 3, ATCC 19859; 4, pile isolate TFSS6; 5, pile isolate TFSS5; 6, pile isolate TFSS4; 7, pile isolate TFSS3; 8, pile isolate TFSS2; 9, pile isolate TFSS1; 10, *E.coli*; M, 1kb Plus DNA ladder

As expected the clusters of the pile isolates and the reference strains in the ARDREA and the RAPD dendrograms have the same structure (Fig. 1, Fig. 2). In the RAPD dendrogram, however, the homology between the strains is much lower due to the strain specific nature of the fingerprints derived by this method.

Acknowledgments

This work was supported by grant 7531.50-03-FZR/607 from the Sächsisches Staatsministerium für Wissenschaft und Kunst, Dresden, Germany.

References

/1/ Kutschke, S., et al., BMRI-1, Report FZR-252 (1998) p.10-11

/2/ Selenska-Pobell, S., et al., J. Appl. Bacteriol. **84**, 1085-1095 (1998)

/3/ Selenska-Pobell, S., et al., System. Appl. Microbiol. **18**, 425-438 (1995)

# PROTEOLYTICAL ANALYSIS OF THE S-LAYER PROTEINS OF THE URANIUM WASTE PILE ISOLATE *BACILLUS SPHAERICUS* JG-A 12 AND THE REFERENCE STRAIN *B. SPHAERICUS* NCTC 9602

J. Raff, M. Mertig [1], S. Selenska-Pobell, W. Pompe [1]
[1] Institute of Material Science, Technische Universität Dresden, 01062 Dresden, Germany

*The S-layer structures of the uranium mining waste pile isolate Bacillus sphaericus JG-A 12 and of the reference strain B. sphaericus NCTC 9602 were compared. Both S-layers have tetragonal (p4) symmetry with similar lattice constants. The primary structures of the two studied S-layer protein monomers, however, seems to be different.*

S-layers of bacteria are highly ordered protein or glycoprotein layers on the surface of the cell wall. These layers have a property to bind metals. Therefore they may be used as templates for fabrication of metal nanostructures /1/. In addition, the S-layer proteins may be suitable for bioremediation of heavy metal contaminated liquid wastes. In order to clear the mechanisms of metal binding by the S-layer proteins, we started studies on the primary structure of two such proteins - one from the uranium mining waste pile isolate *B. sphaericus* JG-A 12, and a second from the reference strain *B. sphaericus* NCTC 9602 /2, 3/. In that work we have demonstrated that the first 20 N-terminal amino acids of the two proteins are identical. In the present work a proteolytical analysis of both proteins was performed, in order to choose appropriate internal fragments for further protein sequencing and also to gain a preliminary information about the structure and stability of these two proteins.

Purified S-layer proteins were cleaved by the use of three proteases: trypsin, chymotrypsin and proteinase K. Digestions were accomplished in 50 mM $KH_2PO_4$/ $Na_2HPO_4$ buffer with 1 mM $MgCl_2$ and 3 mM $NaN_3$ at 4°C for 1 and 2 days, with a proteinase to S-layer protein ratio of 1 to 50. Received fragments were analyzed using SDS polyacrylamide gel electrophoresis (SDS-PAGE).

As shown in Fig. 1, the digestion patterns of the two proteins were different. In addition, the S-layer protein of the uranium mining waste pile isolate was more sensitive to the proteolytical enzymes. The fragment with a size of approximately 105 kDa (pointed by an arrow in the Fig.1) occurred also when a proteolytical treatment of intact cells was performed (not shown). In the case of the strain JG-A 12 this fragment was very unstable and it completely disappeared after a few hours of incubation with the proteinase K (see also lanes 13 and 14). The mentioned fragment was chosen and prepared for further sequence analyses of the proteins of both strains. On the basis of the amino acid sequences obtained, we will design reverse DNA primers for PCR amplifications of the N-terminal part of the S-layer proteins. The forwards primer for these amplifications will be designed on the basis of the sequences of the first N-terminal amino acids obtained in our previous work /2/. The expected size of the PCR products, which will cover the beginning of the S-layer genes is about 1000 bp. The amplicons resulted will be sequenced directly or after cloning into a TopoTA vector (INVITROGEN). Resulted DNA sequences will be than used to “reconstruct” the amino acid sequence of the N-terminal part of the S-layer proteins of the strains studied.

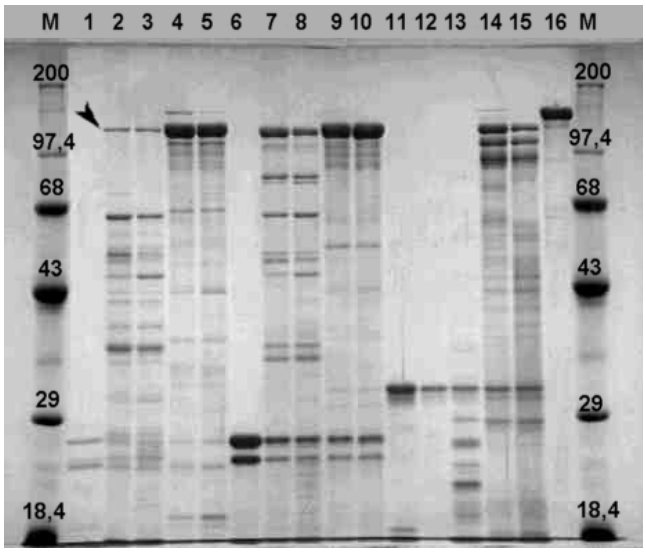


Fig. 1: SDS-PAGE proteolytical patterns of the S-layer proteins of the *B. sphaericus* strains, NCTC 9602 and JG-A 12.
**M**: GibcoBRL-standard (molecular weight in kDa), **1**: Trypsin (T), **2**: JG-A 12+T (1 day), **3**: JG-A 12+T (2 days), **4**: 9602+T (1 d), **5**: 9602+T (2 d), **6**: Chymotrypsin (C), **7**: JG- A 12+C (1 d), **8**: JG-A 12+C (2 d), **9**: 9602+C (1 d), **10** 9602+ C (2 d), **11**: Proteinase K (P), **12**: JG-A 12+P (1 d), **13**: JG-A 12+P (2 d), **14**: 9602 +P (1 d), **15**: 9602+P (2 d), **16**: S-layer (135 kDa)

Acknowledgments
This study was supported by grant 4-7531.50-03-0370/ 708 from Sächsisches Staatsministerium für Wissenschaft und Kunst, Dresden, Germany.

References

/1/ Pompe, W., et al.; Formation of Metallic Nanostructures on Biomolecular Templates. Zeitschrift für Metallkunde **90**, 1085-1091 (1999)
/2/ Raff, J., et al.; Report FZR-247 (1998) p. 45
/3/ Raff, J., et al.; The Surface Layer Protein of the *Bacillus sphaericus* Isolate JG-A 12 from a Uranium Waste Pile. 99th General Meeting of the ASM. 1999, Chicago, Illinois, USA, p. 398

# BACTERIAL DIVERSITY IN DRAIN WATERS OF SEVERAL URANIUM WASTE PILES

G. Radeva, S. Selenska-Pobell

*Bacterial diversity in drain waters from five uranium containing waste piles - three in Germany and two in the USA - was studied by the use of the 16S rDNA retrieval. Our results indicate significant differences in the composition of the bacterial communities in the water samples drawn from the different uranium waste piles.*

An extensive analysis of the composition of the natural bacterial communities was performed in drain waters drawn from three uranium mill-tailings, Schlema/ Alberoda, Gittersee/Coschütz (Germany) and Schiprock, New Mexico (USA), as well as in the drain waters from two uranium production disposal sites, Deponie B1/Weiße Elster (Germany) and Gunnison, Colorado (USA). For this the 16S rDNA retrieval was applied.

All samples were drawn under sterile and anaerobic conditions from depths of about 30 m below the surface of the uranium containing wastes studied.

A $16S_{63F\text{-}1387R}$ rDNA clone library was constructed and the 16S rDNA inserts of 480 clones, representing more than the half of the library were grouped in RFLP types by the use of the frequently cutting restriction endonucleases *Msp*I and *Hae*III (see Table 1).

| Geogr. Origin | Clones obtained | Clones analyzed | RFLP groups and individual RFLP types[1] |
|---|---|---|---|
| Schlema/ Alberoda I[2] | 106 | 50 | (31)*, (10)*, (2), and 7 individual |
| Schlema/ Alberoda II[3] | 142 | 132 | (11)*, (8), (7)*, ( 7)*, (7), (7), (5), (4)*, (4), (4), (4), (2), (2), (2), (2), and 20 individual |
| Gittersee/ Coschütz[2] | 69 | 63 | (8)*, (5)*, (3)*, (3), (3), (3), (2), (2), (2), (2), (2), (2), (2), and 24 individual |
| Schiprock, New Mex.[2] | 212 | 110 | (25)*, (24)*, (17)*, (5), (4)*, (4), (3)*, (2), and 1 individual |
| Gunnison, Colorado[2] | 223 | 88 | (42)*, (6)*, (5), (3), (3), (2), (2), (2), and 23 individual |
| Deponie B1[2] | 33 | 30 | (15)*, (11)*, and 4 individual |

[1]) in brackets the numbers of clones per RFLP type are given.
[2]) samples were stored under anaerobic conditions
[3]) samples were stored under aerobic conditions
*) one representative per group sequenced.

Tab. 1: RFLP- typing of the 16S rDNA clone library.

As one can see from the results presented in the Table 1, the bacterial populations in the studied five groundwater environments possess different grade of variability. The sequence analysis of the most abundant RFLP groups (marked with an asterisk in the Table 1) demonstrated that the predominant bacterial types in the samples studied are different. For example, in the Schlema/Alberoda I and in the Schiprock mill-tailing samples the main bacterial groups are belonging to δ-(*Nitrospina* - 31 and 10 closely related inserts) and to γ-Proteobacteria (*Pseudomonas* - 25, and *Frauteuria* -24 and 17 related inserts), respectively. In the case of the Gittersee/Coschütz mill-tailing water samples in which an extremely high diversity was found the predominant bacterial groups were affiliated to *Pseudomonas* -8 clones, *Geobacter* (γ-Proteobacteria) -5 clones, and to some uncultured clones of Cytophagales which were described in a deep sea hydrothermal vent by other authors /1/.

It is important to notice that the way of storage of the samples before their analysis strongly influences the structure of the bacterial communities. The sample Schlema/Alberoda II, which was taken simultaneously to the above mentioned Schlema/Alberoda I sample, but in contrast to the latter was kept at aerobic conditions, we have demonstrated that a significant shifting of the bacterial composition was induced by the presence of sterile air. As seen in the Table 1 the aeration of the sample did stimulate a propagation of a large number of different bacterial groups which in anaerobic conditions are below the limit of detection by the 16S rDNA approach used. As a result of this shifting the predominant bacterial types in the sample were also shifted from δ– (*Nitrospina*) to γ–Proteobacteria (*Pseudomonas*, 11 clones) and several noncultured bacterial types of *Holophaga/ Acidobacterium* phylum described for a hot spring in the Yellowstone caldera /2/. Clones possessing inserts representing bacteria related to the mentioned *Holophaga/Acidobacterium* groups were found in our initial analysis of a RISA clone library of the Schlema I sample /3/.

The bacterial diversity and the predominant bacterial groups in the two disposal sites studied were also different. As shown in the Table 1 the water samples of the Gunnison disposal site possess much higher amount of bacteria with extremely high diversity in comparisson to the samples from the Deponie B1. The predominant groups of the Gunnison site are estimated to be *Pseudomonas* (42 clones) and *Sphingobacterium* (6 clones). In the Deponie B1 *Acinetobacter* (15 and 11 clones) were mainly found.

Our results indicate that the composition of the bacterial communities in the studied environments is site-specific.

Acknowledgments

This work was supported by grant 7531.50-03-FZR/ 607 from the Sächsisches Staatsministerium für Wissenschaft und Kunst, Dresden, Germany.

References

/1/ Angert, E.R., et al., J. Am. Mineral. **83,** 1583-1592 (1998)
/2/ Hugenholtz, P., J. Bacteriol. **180**, 366-376 (1998)
/3/ Radeva, G., et al., this report p. 57

# MOLECULAR ANALYSIS OF BACTERIAL POPULATIONS IN GROUND WATER POLLUTED WITH HEAVY METALS

G. Radeva [1], K. Flemming, S. Selenska-Pobell
[1] Institute of Molecular Biology, Bulgarian Academy of Sciences, 1113 Sofia, Bulgaria

*An analysis of rDNA in the drain waters from the uranium mill-tailings Schlema/Alberoda, Gittersee/Coschütz, and the disposal site - Deponie B1 - Weiße Elster, and from the waste pile from a tin production mine demonstrated the presence of various bacterial species. Three predominant groups belonging to the Holophaga/Acidobacterium phylum, to the green-sulfur bacteria, and to a novel candidate phylum OP6 were found. Interestingly, the latter two were also found in another extreme lithotrophic environment - a hot spring in the Yellowstone National Park.*

The use of the 16S rDNA retrieval in bacterial ecology during the last decade has revealed a tremendous prokaryotic diversity, which was overlooked by traditional culture enrichment techniques /1/. One of the limitations of this technique is that the PCR amplicons derived from the environmental samples possess the same size due to the highly conservative nature of the 16S rRNA genes. Only after additional RFLP and sequence analysis, which are time-consuming and rather expensive, can the variety of members of the bacterial communities in the samples studied be judged.

Here we present an alternative molecular approach which provides information about bacterial diversity in a faster and more reliable way. The method is an extension of the so-named ribosomal intergenic spacer amplification (RISA) analysis and is based on direct amplification and cloning of enlarged RISA amplicons which, in addition to the IGS region, include about one third of the 16S rRNA gene (see Fig.1).


Fig. 1: Structure of the RISA amplicons.

Due to the great length and sequence variability of the IGS it is possible to evaluate immediately after amplification how abundant and diverse the bacterial populations present in the investigated environmental samples are (see Fig. 2).

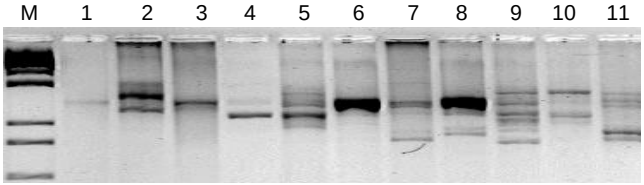


Fig. 2: RISA profiles of the samples: 1, R-2; 2, B-1G; 3, Gitt-33; 4, Gitt-39; 5, B-1U; 6, Schl-1; 7, Schl-2; 8, Schl-3; 9, Schl-4; 10, Schl-5; 11, Gitt-59.

By the additional sequence analysis of the RISA clones, which have about 570 bp from the 16S rDNA, it is possible to perform an exact affiliation of each amplicon. Even more, analyzing the 16S rDNA sequences obtained by the RISA approach in comparison with those derived by the traditional 16S rRNA retrieval, one may collect more exhausting information about the structure of the analyzed bacterial community, because the use of two different primer pairs makes it possible to overcome one of the biases of the PCR, the preferential amplification of particular sequences, which is strongly influenced by the template flanking regions /2/.

The above-described approach was used in the analysis of aquatic samples drawn from three uranium mill-tailings (Schlema-Alberoda /Schl/, disposal site Deponie B1 /B1/, Gittersee-Coschütz /Gitt/), and one tin mill-tailing near Rothschönberger /R/. As seen in the example presented in Fig. 2 the RISA profiles abounded with various DNA bands representing various bacterial groups in the water samples studied. 16S rDNA parts of nine of the 70 RISA clones constructed were sequenced and compared with the available databases by the use of BLAST (basic local alignment search tool) to determine phylogenetic affiliations. By this analysis two clones were affiliated to *Holophaga/ Acidobacterium* phyllum. Only a few organisms have so far been cultured from this division /3/. One of them, *Acidobacterium capsulatum*, an acidophilic chemo-organotroph, was recovered from an acidic mineral environment.

Two other pairs of 16S rDNAs of the RISA clone library were affiliated to the green-sulfur bacteria (strain OPS77), and to the candidate phyllum OP6 (strain OPS152). These two pairs of clones originate from an aquatic sample from Schlema/Alberoda which was drawn 20 m below the surface and had a temperature of 38°C. Interestingly, the two reference strains (OPS77 and OPS152) were recovered from a 75°C hot spring (Obsidian Pool-OP), which was described as fertile ground for the discovery of novel microbial diversity in communities based on lithotrophy /4/. The OP is surrounded by the Yellowstone caldera, which is rich in reduced iron and metal sulfides. The latter are present in the region of Schlema/Alberoda as well. From the same sample of this mill-tailing one additional clone was affiliated to delta-Proteobacteria (the closest species *Desulforhabdus amnigenus*), and another to the *Bacillus/Clostridium* group (*Melissococcus plutonius*).

The RISA clone of the Rothschönberg sample was affiliated to Brevibacteria (*Brevibacterium helvolum*). Our results demonstrate the presence of a large variety of bacteria in the drain waters of the mill-tailings studied. The predominant bacterial species are related to those recovered from other environments with similar mineral and geologic properties.

Acknowledgments

This work was supported by grants GRP/9816 from the European Science Foundation, and 7531.50-03-FZR/ 607 from the Sächsisches Staatsministerium für Wissenschaft und Kunst, Dresden, Germany

References

/1/ Pace, N.R., Science **275**, 734-740 (1997)
/2/ Hansen, M.C., FEMS Microbiol. Ecol. **26**, 141-149 (1998)
/3/ Ludwig, W., FEMS Microb. Lett. **153**, 181-190 (1997)
/4/ Hugenholtz, P., J. Bacteriol. **180**, 366-376 (1998)

# RECOVERY AND CHARACTERIZATION OF *Leptospirillum ferrooxidans* IN SOIL SAMPLES OF TWO URANIUM MINING WASTE PILES

T. Tzwetkova [1], K. Flemming, V. Groudeva [1], S. Selenska-Pobell
[1] Department of Geomicrobiology, University of Sofia, 1426 Sofia, Bulgaria

*Eighteen iron-oxidizing bacterial isolates recovered from soil samples from the uranium mining waste pile "Haberland Halde" and two isolates from a sediment sample from the uranium mill-tailing B1, Weiße Elster, were categorized as Leptospirillum ferrooxidans. A method for monitoring of L. ferrooxidans strains in environments polluted with heavy metals is suggested.*

For many years *Thiobacillus ferrooxidans* was considered to be the most important bacterium in commercial biooxidation of metals and their bioleaching. However, recently it was demonstrated by the use of PCR amplification directly in leachate plant samples that another bacterium - *Leptospirillum ferrooxidans* - is predominant there /1, 2/. Applying the immunofluorescent antibody microscopic count detection technique, Rawlings et al. /3/ demonstrated that in the continuous-flow biooxidation tanks from various bioleaching plants the proportion of bacterial types is: 48-57 % *Leptospirillum ferrooxidans*, 26-34 % *Thiobacillus thiooxidans*, and 10-17 % *T. ferrooxidans*.

The reason why *L. ferrooxidans* was "overlooked" for such a long time is that most procedures for isolation and purification of bacterial cultures from natural and commercial biooxidation samples are based on plating on solid media, and *L. ferrooxidans* has difficulty to grow on such media. Hence, classical recovery and analysis of bacteria from the bioleaching samples have resulted in a strong selection for *T. ferrooxidans* for years.

It was demonstrated that *L. ferrooxidans* strains are involved in the biooxidation of pyrite and other related ores /2,3/ and that they possess a higher affinity to ferrous iron than *T. ferrooxidans* /3/. The same authors demonstrated that, in contrast to *T. ferrooxidans, L. ferrooxidans* tolerates higher concentrations of ferric iron. They suggested that the domination of *L. ferrooxidans* in the industrial circulation bioleaching systems may be explained by the fact that the latter allow Fe(III) accumulation. In addition, the authors speculated that under natural leaching conditions *T. ferrooxidans* and not *L. ferrooxidans* is probably predominant, because of the constant renewal of the leaching solution and the washing of the ferric iron by the natural water percolation.

Our observations, however, are in contrast to the above-mentioned speculation. Using the natural soil samples drawn independently from the uranium mining waste pile near Johanngeorgenstadt and the uranium mill-tailing B1 we were able to culture a larger number of *L. ferrooxidans* than of *T. ferrooxidans* strains . The B1 strains were kindly supplied to us by E. Ondruschka and H. Seidel, UFZ Leipzig. By the use of the 16S ARDREA we demonstrated that both of the known *L. ferrooxidans* 16S *Rsa*I-RFLP types (type I and type II) are present in the samples studied (see Fig. 1). However, we cultured several other *Leptospirillum*-like strains which possess *Rsa*I profiles unrelated to the known types. An exact affiliation of the latter are in progress.

The sequence analysis of the 16S rRNA gene of one strain from the uranium mill-tailing B1 - Lf K4(B1),

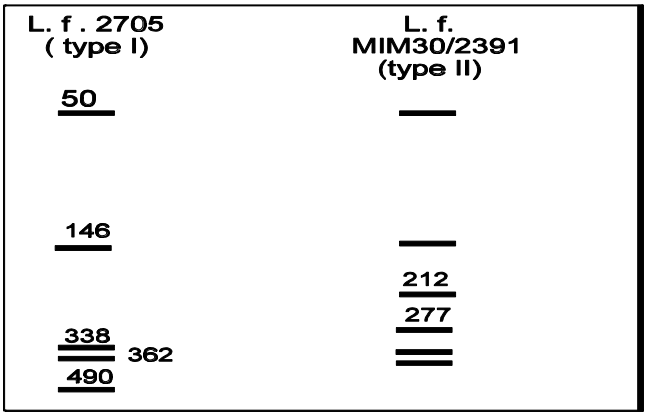


Fig. 1: 16S rDNA *Rsa*I-RFLP profiles of the two known *L. ferrooxidans* types.

which possesses an *Rsa*I-ARDREA profile of type I (see Fig. 1) demonstrated significant differences from the reference strain 2705 in one particular part of the gene, which corresponds to helix 18 of the variable region 3 (V3) (see Fig. 2). In the same region the highest variability was found between two strains of type II - Lf MIM30 and *Leptospirillum* sp. 2391 (see Fig. 2). Interestingly, one of the group-specific signatures of the strains of the species *T. ferrooxidans* which are also widely distributed in the heavy-metal-polluted samples, was found in the helix 18 /4/.

p. 465 (V3; helix 18)

```
L.f.K4(B1) A...GCGT.A...T.CGGCGCTT.
L.f.2705   A...ATAT.-...C.AATATCCC.
L.f.MIM30  G...GGGC.T...T.AGGTCACC.
L.sp.2391  A...ATGT.A...C.CGGCATTT.
```

Fig. 2: 16S rRNA signatures of the *Leptospirillum* strains.

The signatures presented in Fig. 2 can be used for direct detection and discrimination of *L. ferrooxidans* in the environments polluted with heavy metals. The high potential of these bacteria for interaction with metals makes their monitoring important for understanding the processes which occur in the uranium mining waste piles.

Acknowledgments

This work was supported by grants 7531.50-03-FZR/607 and 7531.50-04-844-99/4 from the Sächsisches Staatsministerium für Wissenschaft und Kunst, Dresden, Germany

References

/1/ DeWulf-Durand, P., et al.; Appl. Environ. Microbiol. **63**, 2944-2948 (1997)
/2/ Pizzaro, J., et al.; Appl. Environ. Microbiol. **62**, 1323-1328 (1996)
/3/ Rawlings, D., et al.; Microbiology **145**, 5-13 (1999)
/4/ Flemming, K., et al., this report p. 51

# Application of X-Ray Absorption Spectroscopy

# THE RADIOCHEMISTRY SAFETY SYSTEM AT THE ROSSENDORF BEAMLINE (ROBL)

H. Funke, G. Bernhard, V. Brendler, J. Claußner [1], G. Hüttig, K. Jansen [2], W. Oehme [1], T. Reich, D. Röllig [2]
[1] Department of Experimental Facilities and Information Technology
[2] Nuclear Engineering and Analytics Inc. (VKTA)

*The Radiochemistry Safety System is a necessary and independent part of the radiochemistry experimental station at ROBL. It was designed and built in collaboration with several FZR and VKTA groups.*

## Introduction

The Radiochemistry Hutch (RCH) at ROBL is a unique experimental endstation for X-ray spectroscopy with radioactive samples, including liquids. In addition to the usual X-ray safety regulations for synchrotrons it was necessary to have a safety system in accordance with all legal requirements for a radiochemical laboratory. The installation had to satisfy specific laws and regulations concerning environmental protection, personnel and nuclear safety. In addition, the transport and disposal of radioactive waste also had to satisfy requirements.

The regulations agreed upon ESRF are documented in the "Declaration of the ROBL Project" and have to be confirmed and controlled by the French control authority CIREA /1/. The legal basis for all procedures are the German and French laws on radionuclide laboratories as well as the EURATOM /2/ transport and storage regulations. Only specially trained staff are allowed to operate this experimental station.

## Nuclides

The safety regulations are determined by the allowed radionuclides. These are the actinides Th-nat, Pa-231, U-nat, Np-237, Pu-239, Pu-242, Am-241, Am-243 as well as Ra-226, Po-208, Po-209 and Tc-99 with a maximal activity of 185 MBq (5 mCi) of all samples at the same time. These elements have no stable isotopes which could be used for equivalent chemical studies. As far as possible the most stable, i.e., the least radioactive, isotopes of these elements are always chosen.

## Principles

The construction of the Radiochemical Safety System (RCSS) is based on the principles of multilayer containment of the samples and redundancy and automation of all safety components.

The radioactive compounds are heat-sealed in X-ray transparent polyethylene foils serving as the first barrier. For transport these samples are enclosed in a polyethylene "sample container". Outside the glovebox it must always be locked in a "working container" shielded with 1 cm lead walls to absorb all radiation up to 5 µSv/h. Outside the hall the working container is transported in certified "transport containers" made of steel. During experiments the second and third barriers are the glovebox and the RCH.

The RCH and the lockroom are made airtight by an inner wall of steel panels sealed with silicon. The floor is resistant compound filled with a tight epoxy resin layer.

An uninterruptible power supply (UPS) guarantees a controlled shutdown of the experiment in case of an electrical power cut.

## Ventilation

A separate ventilation system guarantees graduated negative pressure differences of about -10 Pa between the hall and the RCH and of -200 Pa between the RCH and the glovebox, where the samples are handled. The filtering system for the ingoing and outgoing air is equipped with high absorption absolute filters.

The filters and ventilators for the RCH and the glovebox as well as the vacuum valves around the glovebox exist in duplicate and work in an automatically controlled redundant regime.

Before the air leaves the hall, a final filter is inserted as a last barrier to the environment.

## Monitoring

The " - $ activity as well as the dose rate in the outgoing air are continuously controlled by an automatic aerosol monitoring system outside the RCH. 10% of the outgoing air is isokinetically separated to register the radioactive background and all possible deviations from it. A similar movable aerosol monitoring device constantly controls the air inside the RCH.

A (-spectrometer is incorporated into the glovebox floor. For a unique identification and documentation of the activity a (-spectrum has to be recorded for each individual sample.

The radiation monitoring equipment is complemented by a hand-foot monitor in the lockroom, movable " - $ - and dose rate monitors, and an " - $ measuring station, e.g., for analyzing wipe tests.

## Signaling

All safety-related data are collected in a signaling system which optically and acoustically indicates all changes, failures and deviations from standard values of the safety system. The worst case, an emergency, means either that the radiation limits have been exceeded, failure of the box-ventilation or fire. In case of an emergency in the RCH the signaling system will cause the beam shutter and the vacuum valves to close via the interlock system of the ESRF.

The combined status signals emergency, failure, warning, maintenance are given for the main components of the RCSS: ventilation, monitoring, count-gas supply, and UPS. Signaling boxes are installed in the control cabin, the RCH, and the lockroom. They allow a quick overview of the RCSS status.

## References

/1/ ESRF Safety Group, La Ligne de Lumiere Rossendorf BM20, Dossier CIREA, Grenoble 1998
/2/ EURATOM Regulation No. 1493/93

# EXAFS INVESTIGATIONS OF URANYL SULFATE COMPLEXES

H. Moll [1], T. Reich, C. Hennig, A. Roßberg, I. Grenthe [1]
[1] The Royal Institute of Technology (KTH), Stockholm, Sweden

*EXAFS analysis of uranyl sulfato complexes in solution indicate a bidentate coordination of sulfate to the linear uranyl unit.*

## Experimental

Samples were prepared by taking aliquots of an acidic $UO_2(ClO_4)_2$ stock solution to get a final uranyl concentration of 0.05M. The sulfate concentration in the acidic test solutions were adjusted using $H_2SO_4$ or $Na_2SO_4$. The solid, $UO_2SO_4 \cdot 2.5H_2O$, was prepared as described in /1/. The EXAFS spectra were recorded at the new Rossendorf Beamline (ROBL) at the ESRF in Grenoble. The transmission spectra were measured at room temperature using a cooled Si(111) double crystal monochromator of fixed-exit type (E= 5-35 keV). The higher harmonics were rejected by two Si and Pt coated mirrors. For energy calibration of the sample spectra, the spectrum from a Zr foil was recorded simultaneously. The ionization energy of the U $L_{III}$ electron, $E_0$, was arbitrarily defined as 17185 eV. The data were treated using the WinXAS software /2/. Theoretical backscattering phase and amplitude functions, $\Phi(k)$ and F(k), used in data analysis were calculated using the FEFF7 program /3/.

## Results

The isolated EXAFS oscillations and the corresponding Fourier transforms for samples A to D are shown in Fig. 1.

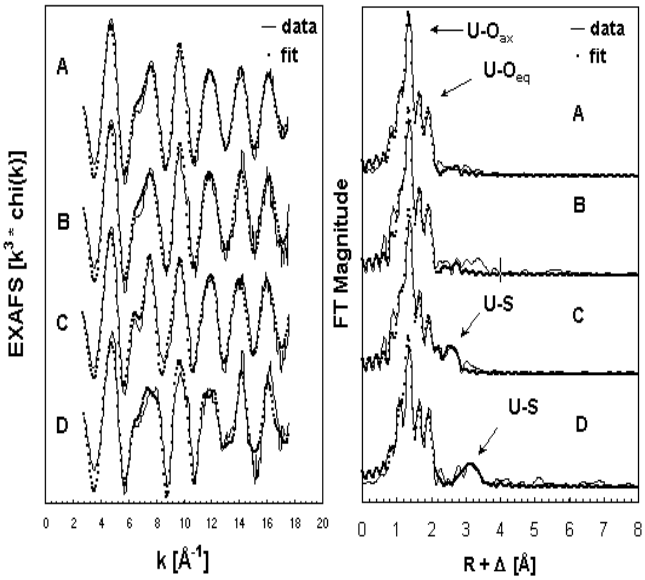


Fig. 1: Raw U $L_{III}$ edge $k^3$-weighted EXAFS data for samples A-D and corresponding FT's.

The FT peaks below 1.5 Å (without phase-shift) are artifacts of the spline removal and are not associated with any coordination distance. The obtained structural parameters are given in Tab. 1.

There are no EXAFS results about uranyl sulfate complexes published yet. In all samples uranium is surrounded by two $O_{ax}$ atoms at 1.77±0.01 Å. Approximately five $O_{eq}$ atoms are coordinated to the linear uranyl group at 2.39-2.41 Å in the equatorial plane. The large Debye-Waller (DW) factor observed for the third shell in samples A-B indicates the difficulties to localize the S backscatterer and may be due to a broad distribution of U-S distances. In sample C, where $UO_2(SO_4)_2^{2-}$ is the dominant species, approximately two sulfur atoms were measured at 3.11 Å. Blatov et al. reported an U-S distance of 3.07 Å in the solid $UO_2SO_4 \cdot 2CH_3CON(CH_3)_2$, where $SO_4^{2-}$ is bidentate coordinated to $UO_2^{2+}$ /4/. If sulfate is bridging and monodentate bonded to the uranyl ion, like in $UO_2SO_4 \cdot 2.5H_2O$, one expects a longer U-S distance. The EXAFS results confirm this assumption. And a U-S distance of 3.63 Å was measured. The structural parameter determined for $UO_2SO_4 \cdot 2.5H_2O$ are consistent with XRD measurements /5/.

| Sample | Shell | R [Å] | N | $\sigma^2$ [Å$^2$] |
|---|---|---|---|---|
| A<br>82% $UO_2SO_4$ (aq)<br>12% $UO_2^{2+}$ | U-$O_{ax}$ | 1.77 | 2f | 0.0014 |
| | U-$O_{eq}$ | 2.41 | 4.0 | 0.0071 |
| | U-S | 3.12f | 1f | 0.0105 |
| B<br>50% $UO_2SO_4$ (aq)<br>50% $UO_2(SO_4)_2^{2-}$ | U-$O_{ax}$ | 1.77 | 2f | 0.0013 |
| | U-$O_{eq}$ | 2.40 | 4.3 | 0.0068 |
| | U-S | 3.15 | 1f | 0.0083 |
| C<br>12% $UO_2SO_4$ (aq)<br>88% $UO_2(SO_4)_2^{2-}$ | U-$O_{ax}$ | 1.78 | 2f | 0.0013 |
| | U-$O_{eq}$ | 2.44 | 5.1 | 0.0110 |
| | U-S | 3.11 | 2.4 | 0.0075 |
| D<br>$UO_2SO_4 \cdot 2.5H_2O$ | U-$O_{ax}$ | 1.77 | 2f | 0.0016 |
| | U-$O_{eq}$ | 2.39 | 4.0 | 0.0048 |
| | U-S | 3.63 | 1.2 | 0.0021 |

f) parameter was kept constant during the fit.

Tab. 1: EXAFS structural parameters for uranyl sulfate complexes in solution and in $UO_2SO_4 \cdot 2.5H_2O$

By considering both previous structure information and the EXAFS data, we conclude that $SO_4^{2-}$ is bonded in a bidentate mode to the uranyl unit in solution. The results of these study provide necessary structural information to interpret ongoing reaction dynamic investigations in the binary uranyl sulfate system.

## Acknowledgments

This work was supported by the European Commission within the Training and Mobility of Researcher (TMR) Program under contract number ERBFMBICT972296.

## References

/1/ Cordfunke, E.H.P.; J. Inorg. Nucl. Chem. **31**, 1327-1335 (1969)
/2/ Ressler, T.; J. Synchrotron Rad. **5**, 118-122 (1998)
/3/ Zabinsky, S.I., Rehr, J.J., Ankudinov, A., Albers, R.C., Eller, M.J.; Phys. Rev. B **52(4)**, 2995-3008 (1995)
/4/ Blatov, V.A., Serezhkina, L.B., Serezhkin, V.N.; Zh. Struct. Khimii **31**, 131 (1990)
/5/ Brandenburg, N.P., Loopstra, B.O.; Cryst. Struct. Comm. **2**, 243 (1973)

# THE HYDROLYSIS OF DIOXOURANIUM(VI) INVESTIGATED USING EXAFS

H. Moll, T. Reich, C. Hennig, A. Roßberg, I. Grenthe [1]

[1] Department of Chemistry, The Royal Institute of Technology, Teknikringen 30, 10044 Stockholm, Sweden

*Polynuclear hydroxo species were identified by an U-U interaction at 3.80$_9$ Å in 0.05 M ($Me_4N$)-OH. The EXAFS data indicate the formation of $UO_2(OH)_4^{2-}$ at high pH [0.5 M ($Me_4N$)-OH].*

## Experimental

The test solutions A and C were prepared from appropriate amounts of $UO_2(NO_3)_2 \cdot 6H_2O$ (Merck, Germany) and tetramethylammonium hydroxide (TMA-OH, Sigma-Aldrich, Sweden) to get a final total concentration of 0.05 M $UO_2^{2+}$, and 0.05 M or 0.5 M TMA-OH, respectively. Sample B was precipitated from an aqueous solution of 0.05 M $UO_2^{2+}$ by adding 0.1 M TMA-OH at pH 7. The EXAFS data were recorded at the Rossendorf Beamline (ROBL) at the ESRF in Grenoble. The transmission spectra were measured at room temperature using a cooled Si(111) double-crystal monochromator of fixed-exit type (E = 5-35 keV). The higher harmonics were rejected by using the Pt coating of two mirrors.

## Results and Discussion

The hydrolysis reactions of uranium(VI) have been the subject of extensive study since 50 years. A comprehensive discussion and review of their thermodynamic data is published in /1/.

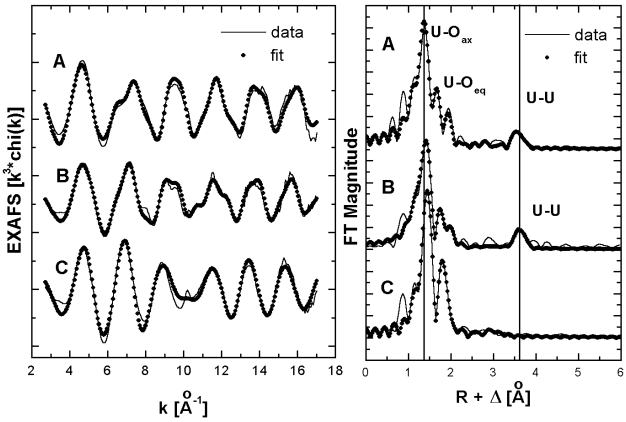


Fig. 1: Experimental EXAFS oscillations and corresponding Fourier transforms including the best theoretical fits.

Direct structure investigations of uranyl hydroxo complexes in solution are rare /2/. Recently, several attempts were made to characterize the structure of uranium(VI) species at high pH values using the TMA countercation, > 1 M, to prevent the precipitation of uranate salts /3, 4/. In contrast to these previous studies, we determined the structure of uranium(VI) at [($Me_4N$)-OH] below 1 M within pH 4 and 14. The isolated EXAFS oscillations and corresponding Fourier transforms for samples A to C are shown in Fig. 1. The obtained structural parameters are given in Tab. 1.

The speciation of uranium(VI) at a total concentration of 0.05 M is dominated by polynuclear complexes in slightly acidic (pH: 3 to 4) solutions. The major hydrolysis products in sample A are the (2,-2) and the (3,-5) complexes, where (3,-5) is the dominant species. This is clearly confirmed by the U-U interaction at 3.80$_9$ Å. The U-U distance gives evidence that the uranyl units are connected via oxo-bridges. The U-U distance should be longer (sample B) if the uranyl units are connected via OH bridges.

The precipitation of $UO_2(OH)_2$ compounds (Sample B) between pH 6 and 11 cannot be avoided using ($Me_4N$)-OH media. The structural parameters are similar to those published in /5/ indicating that the precipitate is schoepite.

| Sample | Shell | N | $F^2$ ($D^2$) | R (D) |
|---|---|---|---|---|
| A<br>10% $UO_2^{2+}$<br>30% $(UO_2)_2(OH)_2^{2+}$<br>60% $(UO_2)_3(OH)_5^{+}$<br>pH: 4.1 | U-$O_{ax}$ | 2.0±0.3 | 0,0012 | 1,79$_4$ |
| | U-$O_{eq}$ | 4.9±0.6 | 0,0114 | 2,41$_2$ |
| | U-U | 1.2±0.3 | 0,0056 | 3,80$_9$ |
| B<br>Precipitate at pH 7 | U-$O_{ax}$ | 2.0±0.3<br>(1.8) | 0.0021<br>(0.0019) | 1.81$_4$<br>(1.80) |
| | U-$O_{eq1}$ | 1.9±0.4<br>(2.7) | 0.0057<br>(0.0074) | 2.23$_0$<br>(2.27) |
| | U-$O_{eq2}$ | 1.8±0.4<br>(1.5) | 0.0097<br>(0.0059) | 2.37$_0$<br>(2.49) |
| | U-U | 1.6±0.5<br>(1.4) | 0.0062<br>(0.0052) | 3.87$_1$<br>(3.87) |
| C<br>100% $UO_2(OH)_4^{2-}$<br>pH: 14 | U-$O_{ax}$ | 1.8±0.3 | 0,001 | 1,83$_0$ |
| | U-$O_{eq}$ | 4.0±0.6 | 0,0048 | 2,26$_6$ |

Tab. 1: Fit parameters to the U $L_{III}$ edge EXAFS data. In parenthesis values from reference /5/.

The EXAFS measurements confirm the speciation calculations indicating that $UO_2(OH)_4^{2-}$ is the major species in the alkaline pH region. A detailed discussion of the structure of U(VI) in strong alkaline solutions is given in /4/. There are a few trends to be observed in the EXAFS data. The U-$O_{axial}$ bond lengths are 1.79, 1.81, and 1.83 Å moving from pH 4.1 to 14, whereas the average U-$O_{equatorial}$ bond length shows the opposite trend; 2.41, 2.30, and 2.26 Å, respectively. Similar trends were found for U(VI) oxide precipitates /5/.

## Acknowledgements

The financial support by the European Commission within the TMR Program under contract number ERBFMBICT972296 is greatly acknowledged.

## References

/1/ Grenthe, I., et al., *Chemical Thermodynamics of Uranium*, NEA OECD, 1992, p. 241

/2/ Dent, A.J., et al., J. Colloid Interface Sci. **150**, 45-60 (1992)

/3/ Clark, D.L., et al., Inorg. Chem. **38**, 1456-1466 (1999)

/4/ Wahlgren, U., et al., J. Phys. Chem. **A103**, 8257-8264 (1999)

/5/ Allen, P.G., et al., Radiochim. Acta **75**, 47-53 (1996)

## A STRUCTURAL COMPARISON OF URANYL PERCHLORATE IN SOLUTION AND SOLID PHASE

L. Sémon [1], I. Billard [1], I. Rossini [1], C. Hennig, K. Lützenkirchen[1], T. Reich, A. Roßberg
[1] Institut de Recherches Subatomiques, Université Louis Pasteur, F-67037 Strasbourg, France

*Uranyl perchlorate in solid and solution has been measured using EXAFS spectroscopy. In both cases outer-sphere complexes have been found.*

The aim of this investigations was to determine the coordination of uranyl perchlorate in solution. For comparison, a solid uranyl perchlorate sample was investigated.

Uranium $L_{III}$-edge extended X-ray absorption fine structure (EXAFS) spectra were measured in the transmission mode at the Rossendorf Beamline (ROBL) at the European Synchrotron Radiation Facility (ESRF) using a Si(111) double-crystal monochromator. The EXAFS spectra were analyzed according to standard procedures using the program EXAFSPAK and theoretical scattering phases and amplitudes calculated with the scattering code FEFF /1/.

Results and spectra of the EXAFS study are listed in Tab. 1 and shown in Fig. 1, respectively.

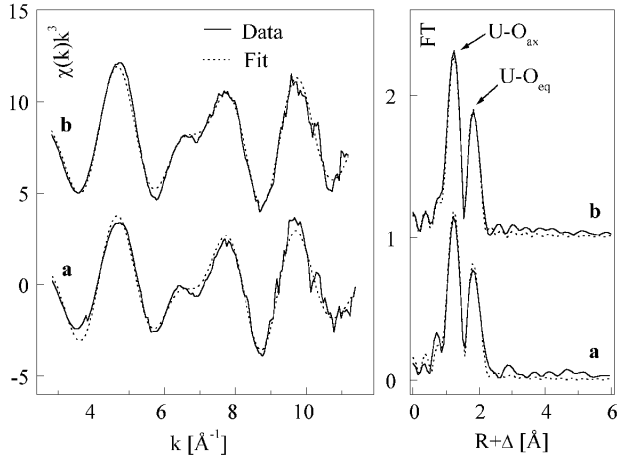


Fig. 1: $k^3$-weighted uranium $L_{III}$-edge EXAFS spectra (left) and the corresponding Fourier transform (right) of a uranyl perchlorate solid sample **a** and solution **b**.

| Sample | Shell | R[Å] | N | $F^2$[Å$^2$] |
|---|---|---|---|---|
| **a** | U-$O_{ax}$ | 1.76 | 2* | 0.002 |
| | U-$O_{eq1}$ | 2.36 | 2* | 0.004 |
| | U-$O_{eq2}$ | 2.47 | 3* | 0.004 |
| **b** | U-$O_{ax}$ | 1.76 | 2* | 0.0016 |
| | U-$O_{eq}$ | 2.41 | 4.6 | 0.0056 |

* value was kept constant

Tab. 1: EXAFS structural parameters for the solid samples **a** and solution **b**.

The uranium in the solid sample is surrounded by two axial oxygen atoms ($O_{ax}$) and five equatorial oxygen atoms ($O_{eq}$). The crystal structure of uranyl perchlorate heptahydrate /2/ shows five different distances for the bond lengths between uranium and the equatorial oxygen atoms with 2.36D, 2.38D, 2.48D, 2.51D and 2.55D. An identical crystal structure was assumed for the investigated solid sample. For the EXAFS analysis on the solid sample, these $O_{eq}$ bond lengths were split into two groups with fixed coordination numbers to obtain a stable fit. The resulting U-$O_{eq}$ distances for the solid sample **a** were determined as 2.36D and 2.47D.

In contrast, for the solution sample **b** ($10^{-4}$ M $UO_2^{2+}$ in 5 M $HClO_4$), the U-$O_{eq}$ bond length difference disappears. That means, that the U-$O_{eq}$ bond lengths are clearly uniform. Therefore, the U-$O_{eq}$ fine structure contribution was calculated only as one shell. In the case of the solid, 12 perchlorate tetrahedra are coordinated isolated from the uranium with U-Cl distances of 5.40-6.17D. Owing to these long distances, no chlorine scattering contribution is observed at room temperature EXAFS measurements.

Since the EXAFS of the solution also shows no indication of a chlorine scattering contribution, we conclude that uranium is coordinated by 5 water molecules and that the electrostatic interaction with the perchlorate ions takes place over longer distances.

References

/1/ Zabinsky, S.I., Rehr, J.J., Ankudinov, A., Albers, R.C., Eller, M.; J., Phys. Rev. **B52**, 2995 (1995)
/2/ Alcock, N.W., Esperas, F.F.S.; J. Chem. Soc., Dalton Trans. (1977) 893

# INVESTIGATION TO DETERMINE THE MAIN COMPLEX SPECIES IN THE AQUEOUS SYSTEM OF $UO_2^{2+}$ WITH PROTOCATECHUIC ACID BY EXAFS SPECTROSCOPY

A. Roßberg, T. Reich, C. Hennig, H. Funke, L. Baraniak, G. Bernhard, H. Nitsche

*Uranium $L_{III}$-edge EXAFS of aqueous uranium(VI) complexes with model compounds of wood degradation products was studied. According to the speciation in aqueous solution, uranium(VI) complexes with protocatechuic acid (3,4-dihydroxybenzoic acid, PCS) were studied as a function of pH by EXAFS. Uranium(VI) PCS EXAFS spectra above pH 6 were similar to those of 2-hydroxyphenol (BCT) complexes.*

## Experimental

The speciation of the complexes on ionic strength of 0.1 M ($NaClO_4$) and 25EC in the absence of $CO_2$ was calculated with the computer program RAMESES. The metal concentration was 1 mM $UO_2(ClO_4)_2$ and the PCS concentration was 50 mM. Uranium(VI) hydrolysis was taken into account in the calculations. The U $L_{III}$-edge spectra of the uranium(VI) complexes were measured at the Rossendorf Beamline using a Si(111) double-crystal monochromator in channel-cut mode. The fluorescence signal was measured with a 4-pixel germanium detector. The ionization potential of the U $L_{III}$-edge was defined as 17,185 eV. The weights of the four detector channels were calculated according to their statistical signal-to-noise ratios. The dead-time corrected EXAFS spectra were analyzed with the standard procedures using the suite of programs EXAFS PAK and the theoretical scattering phases and amplitudes calculated with the scattering code FEFF6 /1/.

## Results and Discussion

The raw $k^3$-weighted U $L_{III}$-edge EXAFS of the complex systems and their corresponding Fourier transforms (FT) are shown in Fig. 1 and the fit results in Tab. 1.

| $UO_2^{2+}$:L, %$UO_2^{2+}$:L | | U-X equatorial | | | |
|---|---|---|---|---|---|
| PCS(L) | pH | Atom | R | $F^2*10^{-3}$ | N |
| 1:1, 53% | 4.3 | O<br>C | 2.45<br>2.88 | 83 | 5.7<br>2.4 |
| 1:1, 46% | 4.45 | O | 2.4 | 12 | 7 |
| 1:1, 23%<br>1:2, 30% | 4.83 | O | 2.37 | 13 | 7.3 |
| 1:1, 10%<br>1:2, 65% | 5.04 | O | 2.38 | 10 | 6 |
| 1:2, 100% | 5.54 | O | 2.37 | 8 | 6 |
| 1:2, 100% | 6.03 | O | 2.36 | 9 | 6.4 |
| 1:2, 90% | 6.75 | O | 2.36 | 10 | 6.6 |

Tab. 1: Fit results for the second coordination shell (N - coordination number, R - radial distance in Å, $F^2$ - Debye-Waller factor in $Å^2$).

During the fitting procedure the coordination number (N) of the axial oxygen of the uranyl unit was kept constant at N = 2. The average of the radial U-$O_{ax}$ distance between uranium and axial oxygen is 1.79 ± 0.02 Å. The average Debye-Waller factor is 0.002 $Å^2$. The features in the k range from 6 $Å^{-1}$ to 8 $Å^{-1}$ and the radial distance of the equatorial oxygen change with

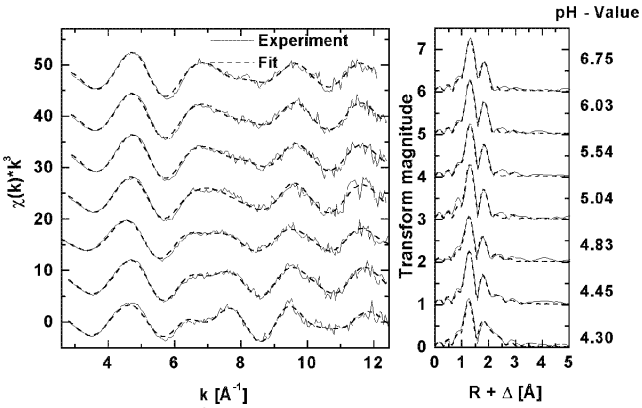


Fig. 1: Left: Raw $k^3$-weighted EXAFS spectra of PCS complexes sorted by pH values. Right: Corresponding Fourier- transforms without phase corrections.

the pH values (Fig. 1). The great distance of the equatorial oxygen of the 1:1 PCS complex at pH 4.3 indi cates that the carboxylic group coordinates with the uranyl cation in a bidentate fashion (Tab. 1). The coordination number of carbon in the PCS complex is 2.4 atoms, at pH 4.3. It is possible that at pH 4.3 two PCS ligands bind with the uranyl ion in a bidentate fashion. With increasing pH value, the bond distance of the equatorial oxygen decreases. At higher pH, the PCS ligands coordinate with the uranyl cation in an o-diphenolic bonding fashion and the carboxylic group is not involved in the complexation. The calculated speciation of the PCS systems shows at pH 4.8 the change from carboxylic to o-diphenolic coordination. At this pH, the Debye-Waller factor for the equatorial oxygen has a maximum (Tab. 1). The similarity of the EXAFS spectra and coordination parameters of the uranium(VI) PCS and BCT complexes increases with the pH /2/. The possible main complex species of PCA with the uranyl cation should be confirmed by principal component analysis of the EXAFS measurements. This can be used to validate the complexation constants for calculation of the speciation /3/.

## References

/1/ Zabinsky, S.I., Rehr, J.J., Ankudinov, A., Albers, R.C., Eller, M.J.; Phys. Rev. **B 52**, 2995 (1995)
/2/ Roßberg, A., et al., Report FZR-247 (1999) p. 53
/3/ Baraniak, L., et al., Report FZR-247 (1999) p. 31

# DETERMINATION OF THE SPECIATION IN THE AQUEOUS SYSTEM OF $UO_2^{2+}$ WITH PROTOCATECHUIC ACID BY EXAFS SPECTROSCOPY USING FACTOR ANALYSIS

A. Roßberg, T. Reich, C. Hennig, H. Funke, L. Baraniak, G. Bernhard

*Factor analysis (FA) was applied to a series of U $L_{III}$-edge EXAFS spectra to determine the number and relative concentration of structurally different species of uranium(VI) complexes with protocatechuic acid (PCS) as a function of pH. As a result of the FA, the EXAFS spectra of two complexes were extracted.*

## Experimental

In our previous report /1/ we presented the EXAFS structural parameters for seven carbonate-free aqueous solutions of uranium(VI) with PCS in the pH range from pH 4.3 to pH 6.75. The number of structurally different uranium(VI) species in these solutions contributing to each EXAFS spectrum is not known *a priori.* Factor analysis (FA) is a powerful mathematical method for determination of the number of components in the experimental data and of their relative weights /2/. For FA all experimental EXAFS spectra are collected in a data matrix [D]. Equation 1 describes the data matrix.

$$[D]=[R][C] \qquad (1)$$

The row matrix [R] contains the unknown EXAFS spectra of the main components. The concentration matrix [C] contains the concentration profiles of the main components. For the application of the FA we developed three computer program modules. The first program module contains an eigenanalysis procedure and yields the number of spectroscopic main components (eigenvectors) in the EXAFS spectra, using the Malinowski indicator function (IND function) /2/. The second program module performs the Kaiser orthogonal VARIMAX rotation of the abstract factor loadings /2/. Iterative target testing (ITT) with concentration-test vectors takes place in the third program module.

## Results and Discussion

An abstract solution of Eq. 1 was found by eigenanalysis. The IND function reaches a minimum when the correct number of main components is used for the abstract solution of Eq. 1.

| Eigenvector | 8 | IND•$10^3$ |
|---|---|---|
| 1 | 4935.83 | 16.20 |
| 2 | 226.41 | 15.05 |
| 3 | 44.90 | 20.82 |
| 4 | 26.71 | 34.35 |

Tab. 1: Results of eigenanalysis (8 - eigenvalue, IND - Malinowski indicator function)

Tab. 1 contains the first four eigenvalues (8) and the values of the IND function as a result of eigenanalysis. The eigenvalues indicate the relative spectroscopic importance of a possible main component. Based on the values in Tab. 1, we reduced the number of main components to two. The relative concentration of these two components as a function of pH (Fig. 1) and their EXAFS spectra (Fig. 2) are the result of the ITT procedure. The first component A has its maximal concentration at pH 4.3. With increasing pH the concentration of A decreases whereas the concentration of B increases. At pH 4.77 both complex species have equal concentrations. The error of concentration determined by FA is approximately ±3%. From the series of seven EXAFS measurements, FA yielded the U $L_{III}$-edge EXAFS spectra of the two structurally different components A and B (Fig. 2). Due to the species concentration in our system, we have the special case that the two derived EXAFS spectra are nearly identical with the experimental spectra at pH 4.3 and 6.03 (see Fig. 1 in /1/). The bidentate carboxylic coordination of complex A is characterized by U-$O_{eq}$ and U-C distances of 2.44 Å and 2.88 Å. In the complex species B, which has an ortho-diphenolic coordination of PCS, the U-$O_{eq}$ distance is 2.36 Å. In summary, EXAFS spectroscopy combined with FA is a powerful method for determination of speciation in complex mixtures according to the various structures of their main constituents. This approach is not limited to binary systems.

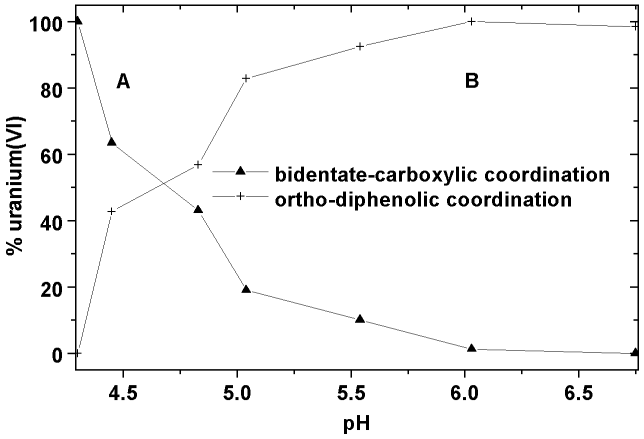


Fig. 1: Speciation of the pure complex species A and B.

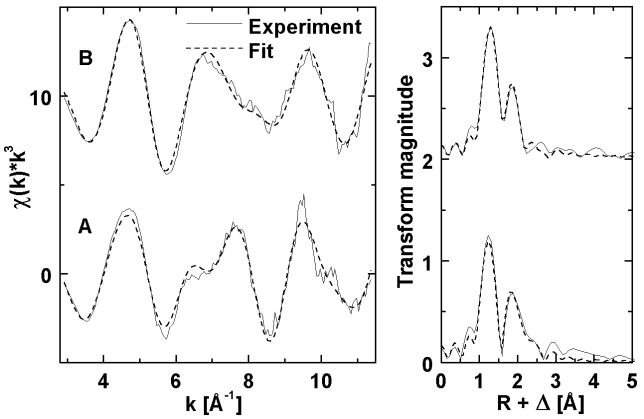


Fig. 2: The U $L_{III}$-edge $k^3$-weighted EXAFS from the pure complex species A and B (left) and the corresponding Fourier transforms (right).

## References

/1/ Roßberg, A., et al., this report, p. 63

/2/ Malinowski, E.R.: *Factor analysis in Chemistry.* Wiley, New York, 1980

# EXAFS STUDY OF THE INTERACTION OF URANIUM(VI) WITH HUMIC SUBSTANCES

K. Schmeide, S. Pompe, M. Bubner, T. Reich, A. Roßberg, C. Hennig, H. Funke, K.H. Heise, G. Bernhard

*The interaction of uranyl(VI) with humic substances was studied by means of extended X-ray absorption fine structure (EXAFS) analysis at room temperature to obtain information on the coordination structures of the complexes.*

## Introduction

The objective of this study was to obtain information about the binding of uranium(VI) onto functional groups of humic substances. Uranyl complexes of Kranichsee humic and fulvic acid (KHA and KFA: isolated from surface water of the mountain bog 'Kleiner Kranichsee' /1/), Aldrich humic acid (A2/97) as well as a synthetic HA type M42 /2/ were therefore investigated.

## Experimental

The samples were prepared according to /3/. The uranyl loading was between 18 and 19 % of the carboxylic group capacity of the humic substances. Complex formation was confirmed by IR spectroscopy. The samples were dispersed in Teflon and pressed as 1.3 cm diameter pellets. The U content of the resulting pellets was 11 to 22 mg U. The EXAFS measurements were carried out at the Rossendorf Beamline at the European Synchrotron Radiation Facility in Grenoble. Uranium $L_{III}$-edge X-ray absorption spectra were collected in transmission mode. The Si(111) double-crystal monochromator was used in the channel-cut mode.

## Results

The $k^3$-weighted EXAFS spectra and the corresponding Fourier transforms are shown in Figs. 1 and 2.

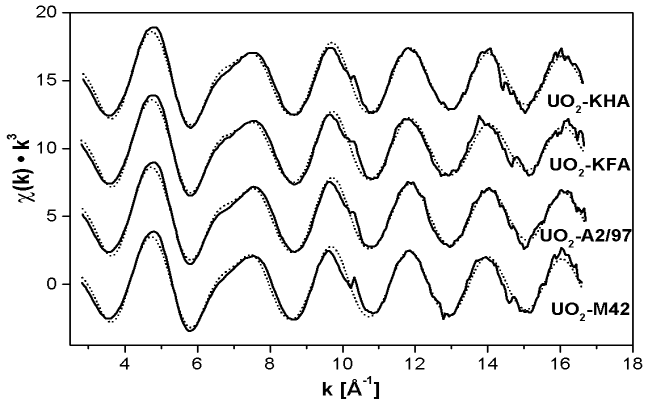


Fig. 1: $k^3$-weighted U $L_{III}$-edge EXAFS spectra of uranyl complexes with KHA, KFA, A2/97 and M42

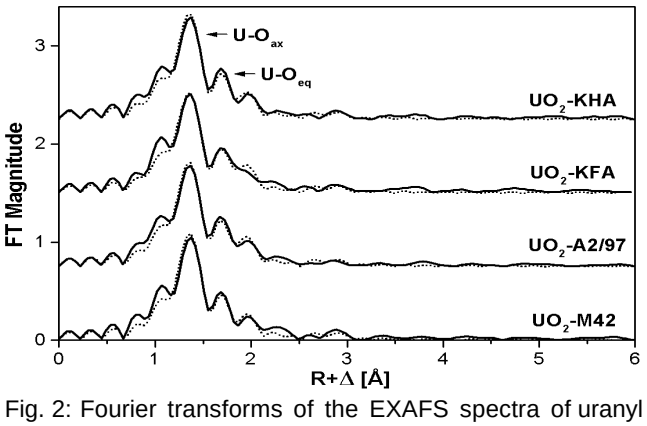


Fig. 2: Fourier transforms of the EXAFS spectra of uranyl complexes with KHA, KFA, A2/97 and M42

In both figures the solid lines represent the experimental data and the dotted lines the theoretical fit of the data. A two-shell fit to the experimental EXAFS data was used with oxygen atoms as backscatterers. The multiple scattering along the uranyl unit at 3.6 Å was also included in the fit. The coordination number (N) for the axial oxygen atoms and $\Delta E_0$ were kept constant at 2 and -13.6 eV. The EXAFS structural parameters of the uranyl humates are compiled in Tab. 1.

| Sample | U - $O_{ax}$ | | U - $O_{eq}$ | | |
|---|---|---|---|---|---|
| | R [Å] | $F^2$ [Å$^2$] | N | R [Å] | $F^2$ [Å$^2$] |
| $UO_2$-KHA | 1.78 | 0.001 | 5.2 | 2.39 | 0.012 |
| $UO_2$-KFA | 1.78 | 0.002 | 5.3 | 2.39 | 0.012 |
| $UO_2$-A2/97 | 1.78 | 0.001 | 5.3 | 2.40 | 0.012 |
| $UO_2$-M42 | 1.78 | 0.001 | 5.4 | 2.40 | 0.014 |

Error: N ± 10 %, R ± 0.02 Å

Tab. 1: Structural parameters of the uranyl humates

Axial U-O bond lengths (R) of 1.78 Å were determined for all uranyl humates. In the equatorial plane approximately five oxygen atoms were found at a mean distance of 2.40 Å. Since carboxylic groups are generally considered the main functional groups of the humic substances involved in the complexation of metal ions at pH#4, the results of this EXAFS study were compared with the mean values of the bond distances found for crystalline uranyl carboxylate complexes of known structures given in /4/. It turned out that the mean bond distance of 2.40 Å in the equatorial plane determined for the humates is the same as that found for the carboxylates where the uranyl ions are bound monodentately.

## Conclusion

Both for natural humic substances (KHA, KFA, A2/97) and for the synthetic HA type M42 comparable structures of uranyl complexes were found with predominantly monodentate coordination of the humic acid carboxylic groups onto uranium(VI) ions.

## Acknowledgments

This work was supported by the EC Commission under contract no. F14W-CT96-0027.

## References

/1/ Schmeide, K., et al., Report FZKA 6124, Forschungszentrum Karlsruhe (1998) p. 161
/2/ Pompe, S., et al., Radiochim. Acta **82**, 89 (1998)
/3/ Bubner, M., et al., this report p. 30
/4/ Denecke, M., et al., Radiochim. Acta **79**, 151 (1997)

# EXAFS MEASUREMENTS AT LOW TEMPERATURE

C. Hennig, T. Reich, M. Rutsch, A. Roßberg, H. Funke, S. Dienel [1], U. Strauch [2], W. Oehme [1], G. Bernhard
[1] Department of Experimental Facilities and Information Technology, [2] ROBL Project Group

*A helium cryostat was build at ROBL for measurements at temperatures down to 15 K. The As K-edge and U $L_{III}$-edge EXAFS spectra on uranyl arsenate samples were measured at low temperature and compared to room temperature measurements.*

Thermal oscillations led to damping effects in the EXAFS amplitude. Low temperature reduces this damping and allows measurements at higher k range.

The safety regulations for the radiochemistry hutch at ROBL prohibit a water circulation with the surroundings outside of the experimental station. Therefore, we combined an air-cooled helium compressor (CTI-Cryogenics) with a specially designed helium cryostat (OXFORD Instruments) to a noncommercial arrangement. Based on an intelligent temperature controller module (OXFORD Instruments), a temperature control software was written and extensively tested.

EXAFS measurements were taken on hydrogen uranyl arsenate hydrate $H[UO_2AsO_4]\ 4H_2O$ as an example for a highly ordered crystal structure. The EXAFS spectra obtained at room temperature and at low temperature are shown in Fig. 1 for the As K-edge and in Fig. 2 for the U $L_{III}$-edge. The curve fitting results for the low temperature measurements are given in Tab. 1 and Tab. 2.

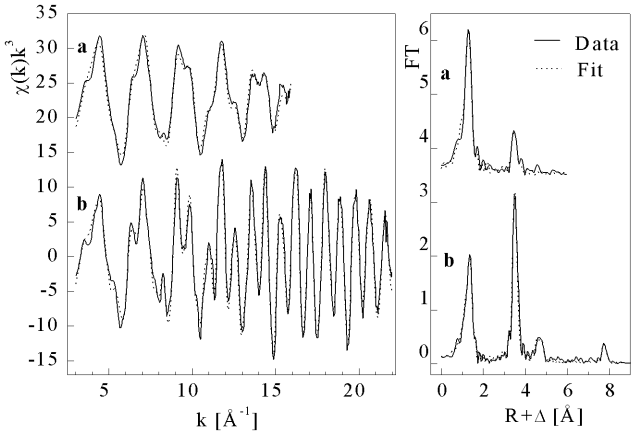


Fig. 1: Arsenic K-edge $k^3$-weighted EXAFS spectra (left) and the corresponding Fourier transform (right) of hydrogen uranyl arsenate at T=293 K (a) and T=41K (b)

The Fig. 1 and Fig. 2 show that the upper limit of the EXAFS k-range increases from 16 $Å^{-1}$ at room temperature to 22 $Å^{-1}$ at low temperature. Therefore, the scattering contributions from higher shells are obtainable in the Fourier transforms. Because the EXAFS signal is $k^3$ weighted, the requirements on the beam stability are very high. The bond lengths determined at room temperature /1/ and those found at low temperature are in good agreement. Temperature depended bond length variations are in the range of the experimental error. The largest bond lengths of a heavy translational symmetric atom (for example U-$U_2$) are in the range of the lattice constants.

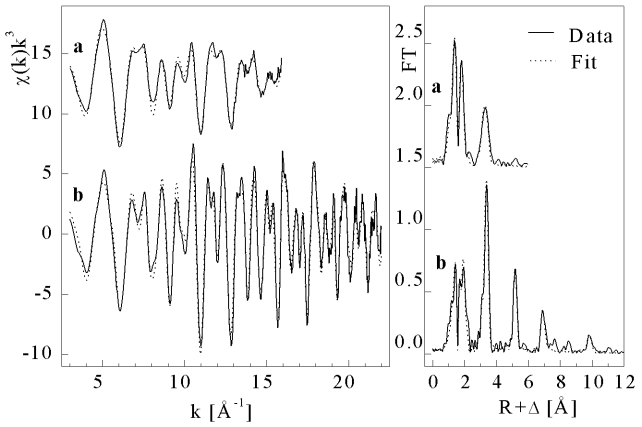


Fig. 2: Uranium $L_{III}$-edge $k^3$-weighted EXAFS spectra (left) and the corresponding Fourier transform (right) of hydrogen uranyl arsenate at T=293 K (a) and T = 15 K (b).

| Shell | R [Å] | N | $F^2$ [$Å^2$] | ) E [eV] |
|---|---|---|---|---|
| As-$O_{eq}$ | 1.69 | 3.8(1) | 0.0017 | -5.1 |
| As-$U_1$ | 3.71 | 4.2(1) | 0.0021 | -9.7 |
| As-$As_1$ | 5.06 | 3.7(1) | 0.0029 | -6.6 |
| As-$U_2$ | 8.04 | 9.8(4) | 0.0045 | -16.5 |

R-bond length, N-coordination number with standard deviation, $F^2$ -Debye-Waller factor, ) E-energy shift

Tab. 1: EXAFS parameters for the As K-edge

| Shell | R [Å] | N | $F^2$ [$Å^2$] | ) E [eV] |
|---|---|---|---|---|
| U-$O_{ax}$ | 1.78 | 2.2(1) | 0.0036 | 6.2 |
| U-$O_{eq}$ | 2.31 | 3.8(2) | 0.0018 | 2.4 |
| U-$As_1$ | 3.70 | 3.9(1) | 0.0018 | 0.8 |
| U-$U_1$ | 5.41 | 5.0(1) | 0.0029 | 1.7 |
| U-$U_2$ | 7.19 | 6.3(3) | 0.0029 | -9.1 |

R-bond length, N-coordination number with standard deviation, $F^2$ -Debye-Waller factor, ) E-energy shift

Tab. 2: EXAFS parameters for the U $L_{III}$-edge

References

/1/ Hennig, C., et al., Report FZR-247 (1999) p. 55

# FIRST XANES AND EXAFS MEASUREMENTS OF TECHNETIUM MODEL COMPOUNDS AT THE ROSSENDORF BEAMLINE ROBL

T. Reich, H. Funke, C. Hennig, A. Roßberg, H.-J. Pietzsch [1], S. Seifert [1], J.-U. Künstler [1], G. Bernhard
[1] Institute of Bioinorganic and Radiopharmaceutical Chemistry

*Technetium K-edge EXAFS measurements on model compounds demonstrate the superb quality of the radiochemistry endstation of ROBL for x-ray absorption spectroscopy.*

## Experimental

The structure of novel Tc complexes has been studied successfully in the framework of a collaboration between the Institute of Radiochemistry and the Institute of Bioinorganic and Radiopharmaceutical Chemistry over the last few years /1,2/.

In order to evaluate the possibilities of the new Rossendorf Beamline (ROBL) for Tc EXAFS studies, we prepared four samples for a first experiment with $^{99}$Tc at ROBL. The samples were 127 mMol/L $NaTcO_4$(aq), 1.3 mMol/L $NaTcO_4$(aq), $KTcO_4$(s), and $TcO_2 \cdot nH_2O$(s). Except for the 1.3 mMol/L Tc solution, the amount of Tc in the samples yielded an edge jump of ~1 across the Tc K absorption edge at 21 keV. These samples were measured in transmission mode at ROBL using the Si(111) double-crystal monochromator in fixed-exit mode with an additional feedback system to minimize beam intensity fluctuations. The Tc K-edge EXAFS spectrum of the dilute solution was recorded using a four pixel Ge fluorescence detector. The energy scale of the XANES scans was calibrated with a Mo metal foil (Mo K edge at 20004.3 eV). For the EXAFS analysis, the first inflection point of the pre-edge absorption peak for the $NaTcO_4$(aq) sample was defined as 21044 eV /3/.

## Results and Discussion

Fig. 1 displays the raw Tc K-edge $k^3$-weighted EXAFS spectrum of $NaTcO_4$(aq). The spectrum of the 127 mMol/L Tc solution was recorded in a single sweep up

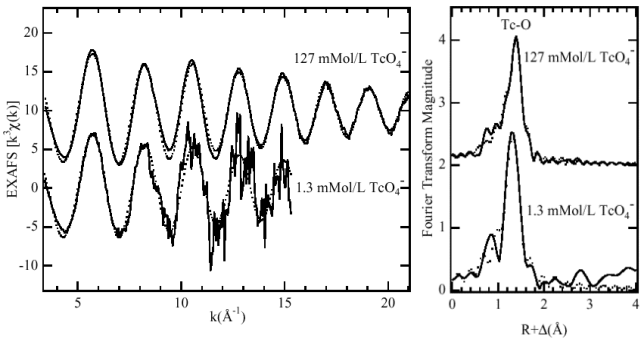


Fig. 1: Raw $k^3$-weighted Tc K-edge EXAFS spectra (left) and corresponding Fourier transforms (right) of experimental data (solid line) and theoretical fits (dots) for 127 mMol/L $NaTcO_4$(aq) (top) and 1.3 mMol/L $NaTcO_4$(aq) (bottom)

to k=21 Å$^{-1}$. During this sweep the counting time per data point was gradually increased from 2 to 20 sec. To our knowledge, this is the first Tc EXAFS spectrum of a liquid sample where it was possible to observe the fine structure of the x-ray absorption spectrum over an energy range of 1700 eV. In addition, this spectrum is an impressive demonstration of the superb quality and stability of all beamline components. It follows from the best theoretical fit to the data (Fig. 1) that Tc is surrounded by 4 oxygen atoms (N=4.1±0.1) at a distance of 1.72±0.01Å ($F^2$=0.0013±0.0004Å$^2$). The EXAFS spectrum of the 100 times more dilute $NaTcO_4$(aq) sample is also shown in Fig. 1 and represents an average of four sweeps measured in fluorescence mode. The intensity of the Tc K" fluorescence line was $1.2 \cdot 10^5$ counts/sec. The total count rate processed by the fluorescence detector was $6.4 \cdot 10^5$ counts/sec. Under these conditions, it was possible to analyze the Tc K-edge $k^3$-weighted EXAFS spectrum of the 1.3 mMol/L Tc solution up to k=15 Å$^{-1}$. The structural parameters obtained are the same as for the $TcO_4^-$ ion in the concentrated solution, i.e., N=3.9±0.2, R=1.72 ±0.01 Å, and $F^2$= 0.0016±0.0003 Å$^2$. Our structural parameters agree with a previous Tc K-edge EXAFS measurement of a 0.2 Mol/L $NH_4TcO_4$(aq) sample /3/.

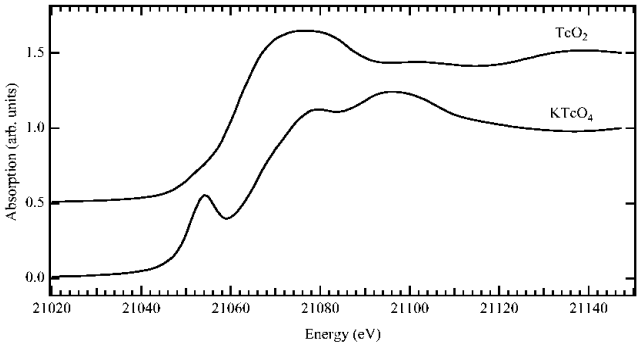


Fig. 2: Raw Tc K-edge XANES spectra of $TcO_2 \cdot nH_2O$(s) (top) and $KTcO_4$(s) (bottom)

Fig. 2 displays the Tc K-edge XANES spectra of $KTcO_4$(s), and $TcO_2 \cdot nH_2O$(s). The energy of the main absorption edge defined by the first-derivative method increases from 21061.6 eV to 21065.8 eV as the Tc valence increases from IV to VII. This energy shift of 4.2 eV is in qualitative agreement with previous measurements /3/. The shape of the Tc K-edge XANES spectra reflects the symmetry of the oxygen atoms surrounding Tc. The most distinct feature of the $TcO_4^-$ ion, which has $T_d$ symmetry, is the pre-edge peak at 21050.8 eV. The XANES features can been used as a probe to determine the Tc speciation as it has been shown, for example, in cement waste forms /3/.

In summary, the Tc K-edge x-ray absorption measurements on Tc model compounds showed that high-quality data can be obtained for liquids and solids at the new Rossendorf Beamline. We conclude that ROBL provides excellent experimental conditions to study the structure of Tc complexes with a large variety of organic and inorganic ligands covering a Tc concentration range of at least two orders of magnitude.

## References

/1/ Johannsen, B., et al.; Appl. Radiat. Isot. **48**, 1045 (1997)
/2/ Jankowsky, R., et al.; J. Inorg. Biochem. **70**, 99 (1998)
/3/ Allen, P.G., et al. Radiochim. Acta **76**, 77 (1997)

# EXAFS ANALYSIS OF A TECHNETIUM(I) CARBONYL COMPLEX

H. Funke, S. Seifert [1], J.-U. Künstler [1], A. Roßberg, C. Hennig, T. Reich, B. Johannsen [1]
[1] Institute of Bioinorganic and Radiopharmaceutical Chemistry

*EXAFS analysis was successfully used to determine the structure of Tc(I) carbonyl thioether complexes in solid and liquid samples. In connection with other methods, the behavior of these complexes in aqueous solution was studied.*

## Introduction

The (-emitting radionuclide technetium-99m plays the dominant role in diagnostic nuclear medicine because of its optimal nuclide properties. As a result of the extremely small amount of technetium present in $^{99m}$Tc radiopharmaceuticals ($10^{-6}$ - $10^{-8}$ M), XAS studies as well as chemical investigations employ the long-lived isotope $^{99}$Tc as surrogates.
In continuation to the previous considerations of rhenium carbonyl complexes /1/, the stability of the Tc(I) carbonyl complex $[TcCl(CO)_3L]$ (L = bidentate thioether ligand) in aqueous solution was studied.
Besides chromatographic methods for the characterization of the no-carrier-added Tc complexes and their reaction products, EXAFS and mass spectrometry were used for the identification of the $^{99}$Tc congeners. An extended description of the presented results will be published in /2/.

## Experimental and results

The Tc K-edge EXAFS spectra were measured under the same experimental conditions as in /1/ for two complexes: Tc1, dissolved in methanol/saline, and Tc1a, dissolved in methanol/water. Both complexes and reaction scheme are described in Fig. 1.

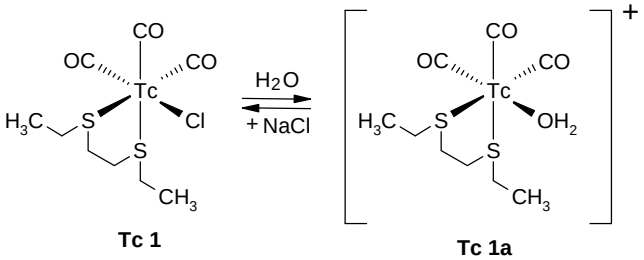


**Tc 1** **Tc 1a**

Fig. 1: Reaction scheme for the reversible Cl-substitution reaction of complex Tc1 in aqueous solution.

In aqueous medium, complex Tc1 exchanges its $Cl^-$ with a water molecule and forms the cationic Tc(I) carbonyl complex Tc1a. This exchange is impossible in methanol/saline medium. Therefore, the EXAFS spectra of Tc1 as solid and in solution are the same (Fig. 2). The EXAFS spectrum and Fourier Transform of complex Tc1a differ from those of complex Tc1 (Fig. 2). The exchange of $Cl^-$ by the lighter O atom ($H_2O$) is clearly detected by the decreased intensity of the second FT peak centered at 2 Å. As expected, the EXAFS fit results (Tab. 1) show a significant difference in bond length for Tc-Cl (2.49Å) in Tc1 and Tc-O (2.19Å) in Tc1a.
It was found that Tc complexes containing a bidentate thioether ligand are able to react with water by exchange of the chloride ion, which results in the formation of a cationic complex. This exchange is shown in a direct way by EXAFS analysis in agreement with conclusions from chromatographic, electrophoretic and mass spectrometric investigations.

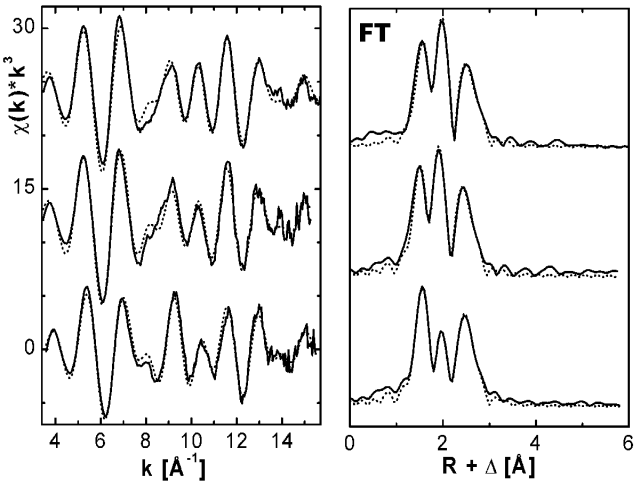


Fig. 2: Tc K-edge $k^3$-weighted EXAFS spectra and the corresponding Fourier transforms of Tc1 and Tc1a.
From above: Tc1 solid sample, Tc1 dissolved in saline/methanol, Tc1a dissolved in water/methanol. (Solid line: experimental data, dotted line: fit).

| | Tc 1(solid/liquid) | | | Tc 1a (liquid) | | |
|---|---|---|---|---|---|---|
| PATH | N | R[Å] | F² [1)] | N | R[Å] | F² [1)] |
| Tc-C | 4.0 | 1.92 | 3.1 | 3.3 | 1.92 | 2.2 |
| Tc-Cl | 1.3 | **2.49** | 5.1 | - | - | - |
| Tc-O | - | - | - | 1.2 | **2.19** | 2.2 |
| Tc-S | 2.7 | 2.49 | 5.1 | 2.5 | 2.49 | 5.6 |
| Tc-C-O (3 legs) | 2.8 [2)] | 3.06 | 3.0 | 2.5 | 3.06 | 3.1 |
| Tc-C-O (4 legs) | 2.8 | 3.06 | 3.0 | 2.5 | 3.06 | 3.1 |

[1)] Debye Waller factors in $10^{-3}$ Å²
[2)] The degeneracy of 2 was taken into account

Tab. 1: EXAFS structural parameters for Tc 1 and Tc 1a

## References

/1/ Funke, H., et al., this report p. 69
/2/ Seifert, S., et al. Radiochimica Acta, in press

# EXAFS ANALYSIS OF A RHENIUM(I) CARBONYL COMPLEX

H. Funke, S. Seifert [1], J.-U. Künstler [1], A. Roßberg, C. Hennig, T. Reich, G. Bernhard, B. Johannsen [1]
[1] Institute of Bioinorganic and Radiopharmaceutical Chemistry

*First experiments with rhenium carbonyl complexes were performed to prepare future measurements on Tc complexes. The EXAFS spectra of Re and Br as central atoms are compared with X-ray diffraction results of similar compounds.*

## Introduction

First EXAFS measurements of a rhenium(I) carbonyl complex were performed using the Rossendorf beamline (ROBL) at the European Synchrotron Radiation Facility(ESRF) Grenoble. Being a collaboration between the Institutes of Radiochemistry and Bioinorganic and Radiopharmaceutical Chemistry this analysis serves as a stepping stone into preparing future EXAFS experiments with $^{99}$Tc carbonyl complexes.
Rhenium and technetium carbonyl complexes with the general formula $[M(CO)_3XL]$ (M = Re, Tc; X = $Br^-$, $Cl^-$; L = bidentate thioether or Schiff base ligand) are at present under study for the development of neutral receptor-affine complexes which are able to cross the blood-brain barrier and to bind to receptors of the central nervous system. Some of the rhenium carbonyl thioether complexes are fully characterized by X-ray analysis and other chemical methods, whose data may be used for comparison with EXAFS results.

## Experimental

The EXAFS spectra of the Re $L_{III}$ - and Br K-edges of the same sample were measured in transmission mode using the Si(111) double-crystal monochromator in fixed-exit mode. The sample consists of 20 mg of the following rhenium complex:

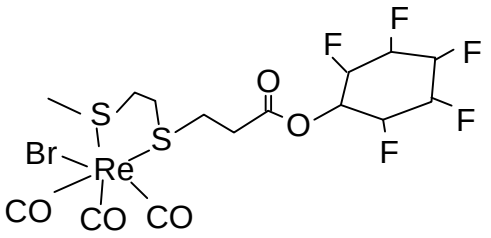


(1)

mixed with Teflon powder as matrix material and pressed into a pellet. The EXAFS spectra were evaluated using the program package EXAFSPAK, and phases and amplitudes were calculated with the scattering code FEFF6.

## Results

To obtain a satisfactory fit-result for the Re spectra, the single scattering paths Re-C, Re-S, and Re-Br and the multiple-scattering path along the carbonyl group, i.e., Re-C-O, have to be included (see Fig. 1, Tab. 1).
The EXAFS scan of the same compound with bromine as the central atom gives a more complicated spectrum, which is dominated by the heaviest possible back-scatterer rhenium. Apart from the main scattering path Br - Re, the nearly linear multiple scattering paths Br - Re - C and Br - Re - C - O yield the most important contributions to the radial distribution function. The evaluated bond length Br - Re is 2.60 Å.

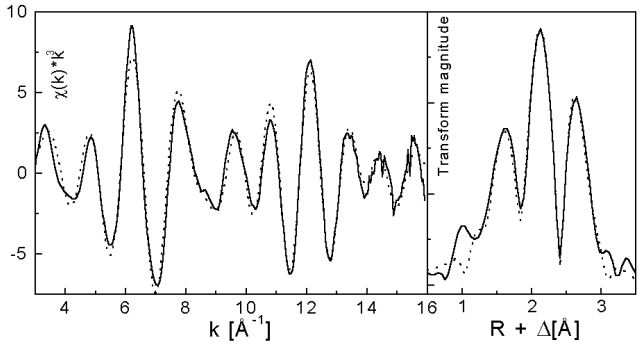


Fig. 1: Re $L_{III}$ edge EXAFS spectrum and Fourier-transform of the Rhenium(I) carbonyl complex (1)
(solid line: experimental data, dotted line: fit)

| | EXAFS | | | XRD[1)] | XRD[2)] |
|---|---|---|---|---|---|
| PATH | N | F[23)] | R [Å] | R [Å] | R [Å] |
| Re - C1<br>Re - C2<br>Re - C3 | 2.7 | 1.8 | 1.92 | 1.92<br>1.90<br>1.90 | 1.98<br>1.94<br>1.92 |
| Re - Br | 0.9 | 3.3 | 2.62 | 2.64 | 2.61 |
| Re - S1<br>Re - S2 | 2.4 | 3.6 | 2.49 | 2.47<br>2.46 | 2.54<br>2.53 |
| Re-C-O<br>(3 legs) | 2.7[4)] | 3.0 | 3.07 | 3.07 | no data |
| Re-C-O<br>(4 legs) | 2.7 | 3.0 | 3.06 | 3.07 | |

[1)] $Re(CO)_3Br(CH_3\text{-}S\text{-}C_2H_4\text{-}S\text{-}CH_3\text{-}CCH)$ /1/
[2)] $Re(CO)_3Br(Cl\text{-}C_2H_4\text{-}S\text{-}C_2H_4\text{-}S\text{-}C_2H_4\text{-}Cl)$ /2/
[3)] Debye Waller factors in $10^{-3}$ Å$^2$
[4)] The degeneracy of 2 was taken into account

Tab. 1: Comparison of bond distances obtained by EXAFS measurement and X-ray analysis data (XRD) of similar complexes ( ) $R_{EXAFS} < 0.02$ Å)

Measurements of the inner coordination spheres of rhenium carbonyl complexes which differ in dithioether ligands using X-ray crystal structure methods, lead to Re - Br distances between 2.61 and 2.64 Å /1,2/. The presented EXAFS results are consistent with these data.

## References

/1/ Reisgys M.; Dissertation, FZR/FWB, 1998
/2/ Alberto R., et al.; Trans. Met. Chem. **22**, 597 (1997)

## EXAFS INVESTIGATION OF U(VI) COMPLEXES WITH BACILLUS STRAINS

C. Hennig, P. Panak, T. Reich, A. Roßberg, S. Selenska-Pobell, G. Bernhard, H. Nitsche

*The average bond length of U(VI) complexes of four bacillus strains and their spores was measured by uranium $L_{II}$-edge EXAFS.*

Bacteria in soil, sediment, and water have a significant influence on the transport of radionuclides and other heavy metals in nature. Certain bacterial strains can selectively take up various metal ions from aqueous systems and are therefore important for the regulation of environmental pollution and for remediation purposes. Because of the high resistance of their spores, bacilli are found in a large variety of natural habitats. Recently two bacillus strains (JG-A30 and JG-A12) were isolated from a uranium mining waste pile in Saxony, Germany, and classified as *B. cereus* and *B. sphaericus* /1/. The bacterial strains were grown with intensive aeration in 300 mL nutrient medium (8 g/L nutrient broth, Difco) at 30ºC and harvested by centrifugation. For preparation of the EXAFS samples, thoroughly washed biomass was treated for two days at pH 5 with 50 mL 0.9 % NaCl solution containing $10^{-4}$ mol/L U(VI). After washing with 5 mL 0.9 % NaCl solution, most of the solution was removed by centrifugation. The samples were cells from: *B. cereus* 4415 **a**, *B. cereus* JG-A30 **b**, *B. sphaericus* 9602 **c**, *B. sphaericus* JG-A12 **d**, and spores from: *B. cer.* 4415 **e**, *B. cer.* JG-A30 **f**, *B. sph.* 9602 **g** and *B. sph.* JG-A12 **h**. Uranium $L_{II}$-edge EXAFS spectra of wet paste samples were measured in fluorescence mode at the Stanford Synchrotron Radiation Facility.
The spectra are shown in Fig.1.

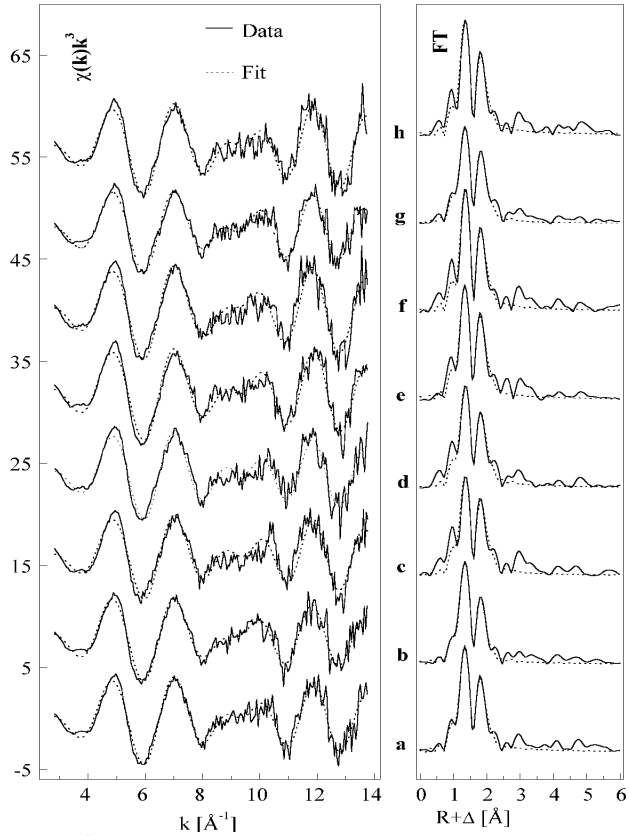


Fig. 1: $k^3$-weighted U $L_{II}$-edge EXAFS spectra (left) and the corresponding Fourier transforms (right).

The results of the data analysis are listed in Tab. 1.

| Sample | Shell | R[Å] | N | $F^2$[Å$^2$] |
|---|---|---|---|---|
| **a** | U-$O_{ax}$ | 1.79 | 2 | 0.0015 |
| | U-$O_{eq}$ | 2.27 | 3.9 | 0.0034 |
| **b** | U-$O_{ax}$ | 1.79 | 2 | 0.0017 |
| | U-$O_{eq}$ | 2.29 | 3.7 | 0.0039 |
| **c** | U-$O_{ax}$ | 1.79 | 2 | 0.0019 |
| | U-$O_{eq}$ | 2.28 | 3.0 | 0.0017 |
| **d** | U-$O_{ax}$ | 1.79 | 2 | 0.0018 |
| | U-$O_{eq}$ | 2.28 | 3.7 | 0.0027 |
| **e** | U-$O_{ax}$ | 1.79 | 2 | 0.0011 |
| | U-$O_{eq}$ | 2.28 | 3.7 | 0.0023 |
| **f** | U-$O_{ax}$ | 1.79 | 2 | 0.0005 |
| | U-$O_{eq}$ | 2.29 | 3.8 | 0.0030 |
| **g** | U-$O_{ax}$ | 1.79 | 2 | 0.0021 |
| | U-$O_{eq}$ | 2.29 | 3.1 | 0.0019 |
| **h** | U-$O_{ax}$ | 1.78 | 2 | 0.0008 |
| | U-$O_{eq}$ | 2.28 | 3.6 | 0.0026 |

Tab. 1: EXAFS structural parameters for samples **a-h**.

In all samples the uranium is coordinated by two axial oxygen atoms ($O_{ax}$) at a distance of 1.79 Å. The distance between uranium and the equatorial oxygen atoms ($O_{eq}$) is 2.27-2.29 Å. The coordination number for $O_{eq}$ is approximately four. This may be indicative of monodentate complex formation of uranium on the bacterial surface. The short U-$O_{eq}$ bond length and its low Debye-Waller factor point to a strong interaction with the substrate. No significant structural differences were observed between the vegetative cells and the spores. An additional weak peak appears in the Fourier transform at approximately 3 Å (Fig. 1). This peak cannot result from a U-$O_{ax}$ multiple scattering interaction because for this case the theoretical R value is shorter than the ones observant. The peak can be modeled as a U-P interaction giving a U-P bond length of 3.62 Å. Both the U-$O_{eq}$ and the U-P bond lengths agree with the corresponding bond lengths observed in uranyl phosphates. Similarly short U-$O_{eq}$ bonds as for the bacteria were observed for uranium after its uptake by plants /2/. For a better understanding of the obtained structural parameters EXAFS studies on model systems are needed.

References

/1/ Selenska-Pobell, S., et al., FEMS Microbiol. Ecol. **29**, 59 (1999)
/2/ Günther, A., et al., Report FZR-247 (1999) p. 54

# FIRST EXAFS MEASUREMENT OF NEPTUNIUM SOLUTIONS AT ROBL

T. Reich, G. Geipel, H. Funke, C. Hennig, A. Roßberg, G. Bernhard

*This is a report on our first Np $L_{III}$-edge EXAFS measurements of Np(IV), Np(V), and Np(VI) solutions in acid media at the new Rossendorf Beamline ROBL.*

## Experimental

Two series of aqueous solutions containing 50 and 5 mMol/L neptunium in three different oxidation states were prepared for EXAFS measurements at the new Rossendorf Beamline (ROBL) at the European Synchrotron Radiation Facility (ESRF) in Grenoble, France. Solution 1 consisted of 50 mMol/L Np(IV) in 0.1 M $HNO_3$ and 2 M $H_2SO_4$. The composition of solutions 2 and 3 was 50 mMol/L Np(V) and Np(VI), respectively, in 0.1 M $HNO_3$. Solutions 4 – 6 were identical to solutions 1 – 3 except for the lower Np concentration of 5 mMol/L. The starting material for the sample preparation was solid $NpO_2(NO_3)$ (AEA Technology, QSA GmbH). It was dissolved in 0.1 M $HNO_3$. The different oxidation states of Np were obtained by electrochemical oxidation/reduction in a conventional H-formed electrolysis cell with a diaphragm between anode and cathode. The oxidation state of neptunium and its stability with time were determined for the 5 mMol/L Np solutions by UV-Vis spectroscopy using the characteristic absorption bands of Np(IV), Np(V), and Np(VI) at 967 nm, 980 nm, and 1223 nm, respectively /1/.

For the measurements, 4 ml of the solution were filled in a polyethylene cuvette, which was sealed and put in a polyethylene bag. Multiple scans of the Np $L_{III}$-edge EXAFS of solutions 1 – 6 were collected in transmission mode at room temperature at ROBL using the Si(111) double-crystal monochromator in fixed-exit mode. The energy scale was calibrated using the first inflection point of the absorption spectrum of a Zr foil (17998 eV). The scattering phases and amplitudes where calculated for hypothetical clusters of $NpO_8S_2$, $NpO_2O_4$, and $NpO_2O_5$ using FEFF6.

## Results

The raw EXAFS data and the best theoretical fit for solutions 1 – 3 are shown in Fig. 1.

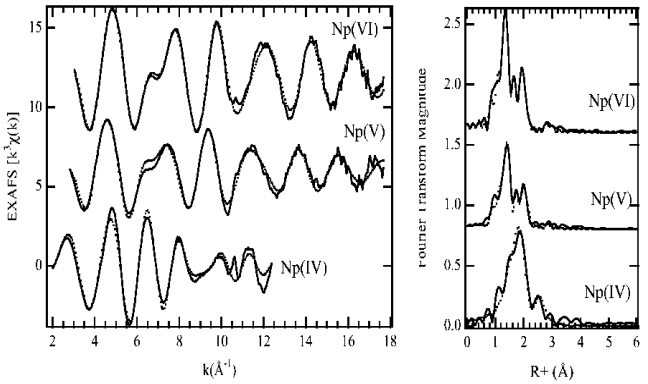


Fig. 1: Raw Np $L_{III}$-edge $k^3$-weighted EXAFS spectra (left) and corresponding Fourier transforms (right) of 50 mMol/L Np solutions.
Solid line – experiment; dots – theoretical fit.

The obtained structural parameters are given in Tab. 1.

| Sample | Shell | R(Å) | N | $F^{2\ a)}$ |
|---|---|---|---|---|
| 1 Np(IV) | Np-O | 2.39 | 11.3(4) | 1.18 |
| | Np-S | 3.07 | 2.2(3) | 0.70 |
| 2 Np(V) | Np-$O_{ax}$ | 1.82 | 1.9 | 0.23 |
| | Np-$O_{eq}$ | 2.49 | 3.6(2) | 0.61 |
| 3 Np(VI) | Np-$O_{ax}$ | 1.75 | 2.0 | 0.15 |
| | Np-$O_{eq}$ | 2.42 | 4.6(2) | 0.56 |

a) $F^2$ in units of $10^{-2}$ $Å^2$

Tab. 1: EXAFS structural parameters for 50 mMol/L Np solutions.

In solution 1 Np(IV) is surrounded by 11 oxygen atoms at a distance of 2.39 Å. In the second coordination sphere we observed two sulfur atoms with a Np-S distance of 3.07 Å. This distance corresponds to a bidentate coordination of the $SO_4^{2-}$ ion to the Np. Using the Np-O distance of 2.39 Å and the structural parameters of the $SO_4^{2-}$ unit (S-O = 1.51 Å, angle O-S-O = 109° /2/), the calculated Np-S distance of 2.93 Å is in good agreement with the measured value.

Both Np(V) and Np(VI) solutions 2 and 3 show the structural parameters of the actinyl ion. In case of Np(V), the distance to the axial oxygen atoms, $O_{ax}$, is 1.82 Å. In the equatorial plane the Np is surrounded by 4 water molecules with a Np-$O_{eq}$ distance of 2.49 Å. The increase of the Np oxidation state from Np(V) to Np(VI) leads to a shortening of the axial and equatorial oxygen bonds by 0.07 Å and an increase of the number of water molecules attached to the neptunyl from four to five. The bond distances Np-$O_{ax}$ and Np-$O_{eq}$ of the Np(VI) solution are 1.75 Å and 2.42 Å, respectively.

The analysis of the 5 mMol/L Np solutions 4 – 6 gave results (not shown here) similar to the 50 mMol/L solutions. There is only a small increase of the coordination number of sulfur from 2.2 to 2.8 when going from 50 mMol/L to 5 mMol/L Np(IV).

The observed structural parameters for the Np-O bond distances of Np(IV) and Np(V) are in good agreement with the values reported for 5 mMol/L Np in chlorine solution /3/. The structural parameters for Np(IV) sulfate and Np(VI) hydrate given in Tab. 1 are reported for the first time.

## References

/1/ Keller, C.: *The Chemistry of the Transuranium Elements*. Verlag Chemie GmbH, Weinheim, 1971, p. 294

/2/ Hollemann, A.F.: *Lehrbuch der anorganischen Chemie*. 101th Ed., Walter de Gruyter 1995, p. 585

/3/ Allen, P.G., et al., Inorg. Chem. **36**, 4676 (1997)

# FIRST XANES AND EXAFS MEASUREMENTS OF PLUTONIUM SOLUTIONS AT ROBL

T. Reich, G. Geipel, H. Funke, C. Hennig, A. Roßberg, G. Bernhard

*This is a report of our first Pu $L_{III}$-edge XANES and EXAFS measurements of Pu(III) and Pu(VI) hydrates at the Rossendorf Beamline ROBL.*

## Experimental

The hydrate is the simplest chemical form of plutonium in aqueous solution. The knowledge of the structural parameters of the hydration sphere is important for the interpretation of EXAFS results on complicated aqueous plutonium complexes where the water molecules are partly or fully replaced by other ligands. Plutonium(VI) hydrate was prepared by dissolution of highly purified $PuO_2$ (Pu-242, AEA Technology, QSA GmbH) and electrochemical oxidation. Part of this solution was reduced to Pu(III) in an electrochemical cell. The Pu(III) and Pu(VI) hydrates were in perchloric and nitric media (1 M acidic solution), respectively. The final Pu concentration was 50 mol/L. The Pu oxidation states were confirmed by UV/vis spectroscopy. For the measurements 4.7 mL of solution (7.5 MBq) was filled and sealed in polyethylene cuvettes. The samples were measured at the Rossendorf Beamline ROBL at the European Synchrotron Radiation Facility (ESRF), Grenoble, France within 48 hours after their preparation.

Multiple scans of the Pu $L_{III}$-edge EXAFS were collected in transmission mode at room temperature using the Si(111) double-crystal monochromator in fixed-exit mode /1/. The energy scale was calibrated using the first inflection point of the absorption spectrum of a Zr foil (17998 eV). The scattering phases and amplitudes where calculated for hypothetical clusters of $PuO_8$, and $NpO_2O_5$ using FEFF6.

## Results

As one can see from the XANES spectra given in Fig. 1, the $L_{III}$ absorption edge of Pu(VI) is shifted by 4 eV toward higher energy as compared to that of Pu(III).

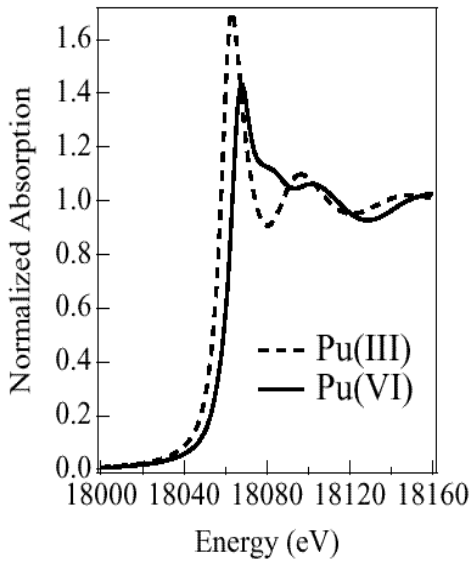


Fig. 1: Pu $L_{III}$-edge XANES spectra Pu(III) and Pu(VI) hydrates.

The energy shift and the distinct XANES features of these two Pu hydrates can be used for the determination of the Pu oxidation states /2/. The different electronic and molecular structures of Pu(III) and Pu(VI) hydrates are also reflected in the EXAFS shown in Fig. 2.

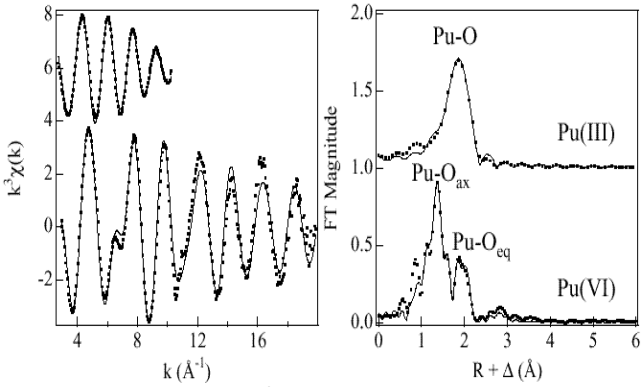


Fig. 2: Raw Pu $L_{III}$-edge $k^3$-weighted EXAFS spectra (left) and corresponding Fourier transforms (right) of 50 mMol/L Pu hydrates. Solid line – theoretical fit; dots – experiment.

The coordination sphere of Pu(III) hydrate can be written as $Pu(H_2O)_8^{3+}$ with an average Pu-O bond distance of 2.48 Å. The Fourier transform corresponding to the EXAFS of Pu(VI) hydrate shows two coordination shells. The Pu(VI) forms a plutonyl ion $PuO_2(H_2O)_{4\text{-}5}^{2+}$. The axial and equatorial Pu-O bond distances are 1.74 and 2.42 Å, respectively. The structural parameters of Pu(VI) hydrate are nearly identical to those of U(VI) and Np(VI) hydrates (see Tab. 1), which were measured recently at ROBL /3/.

| Sample | Shell | R(Å) | N | $\sigma^{2}$ a) |
|---|---|---|---|---|
| Pu(III) | Pu-O | 2.48 | 7.6(2) | 1.02 |
| Pu(VI) | Pu -$O_{ax}$ | 1.74 | 1.9 | 0.12 |
| | Pu -$O_{eq}$ | 2.42 | 4.4(2) | 0.50 |
| Np(VI) | Np-$O_{ax}$ | 1.75 | 2.0 | 0.15 |
| | Np-$O_{eq}$ | 2.42 | 4.6(2) | 0.56 |
| U(VI) | U-$O_{ax}$ | 1.76 | 1.9 | 0.12 |
| | U-$O_{eq}$ | 2.41 | 4.9(2) | 0.61 |

a) $\sigma^2$ in units of $10^{-2}$ Å$^2$

Tab. 1: EXAFS structural parameters for 50 mMol/L Pu hydrates and comparison with 50 mMol/L Np(VI) and U(VI) hydrates.

## References

/1/ Matz, W., et al., J. Synchrotron Rad. **6**, 1076 (1999)
/2/ Conradson, S.D., et al., Polyhedron **17**, 599 (1998)
/3/ Reich, T., et al., Radiochim. Acta (accepted for publication).

# Behavior of Colloids

# A SEPARATION AND DETECTION SCHEME FOR ENVIRONMENTAL COLLOIDS

H. Zänker

*A separation and detection scheme for submicron particles applicable to a wide range of environmental samples was developed.*

The presence of colloids is one of the reasons for the discrepancies between experimental findings and theoretical predictions of contaminant transport via the water path. The scheme of separation and detection of colloids developed at our group is aimed at minimizing outside influences on the samples and maximizing the unambiguity of measurements. Separation steps are performed as mildly as practicable or, if possible, avoided altogether. Separation procedures are centrifugation and mild filtration. Detection methods are scattered light intensity measurements, photon correlation spectroscopy (PCS), ICP-MS, AAS, TOC analysis and imaging by scanning electron microscopy (SEM), i.e., non-invasive as well as invasive methods. An important element of this scheme is the parallel application of as many complementary methods as possible, which increases the probability that artifacts are recognized.

Our first step in tackling a colloid characterization problem is a non-invasive particle size measurement of the raw sample by PCS. The next step is PCS of a 5 µm filtrate. Filtration through 5 µm Nuclepore filters improves the counting statistics for PCS but has only little influence on the colloids. Particles of 100 to 300 nm, which are typical of environmental samples, can also be easily visualized by SEM on a filter. Examples from an acid rock drainage (ARD) sample are given in this report /1/. Particles from a mine drainage water sample, a bog water sample and a backwater sample from a sanitary landfill are given in Figures 2, 4, and 5 of /2/. In all these samples we found good agreement between the PCS results and the SEM particle sizes. Whereas it is not possible to decide solely on the basis of the SEM micrographs if the micron-sized aggregates visible on the filters also exist in the solutions, the in-situ measurements by PCS prove that these aggregates are formed in the filtration process. The nanoparticles of the 100 to 300 nm size range usually move freely in the unperturbed solution. The minimum colloid concentration detectable by PCS for particles of about 100 nm is 10 to 100 µg/L. The chemical composition of such particles can be determined by filtration and by ICP-MS and EDX of the filter cakes.

A much more difficult problem is the non-invasive or only slightly invasive determination of particles of only few nanometers diameter. The minimum concentration detectable by PCS is much higher for such particles because they scatter very little light. The presence of only a few larger particles prevents PCS because they optically mask the small particles. The small particles can be unmasked by removing the larger particles using filtration or centrifugation. An unmasking experiment on an ARD sample is shown in this report (Fig. 1 of /3/). Light scattering intensity measurements, PCS, and chemical analyses by ICP-MS, TOC analysis etc. should be combined to identify the colloid inventories and the colloid composition / mineralogy of such complex colloid mixtures in centrifugation or filtration experiments, and one should always be aware of the artifacts that can be caused by centrifugation and especially by filtration (self-coagulation, clogging, adsorption etc.). Fig. 7 of /2/ demonstrates the particle size characterization of organic particles in a bog water sample down to about 1 nm by ultrafiltration. Extremely fine iron oxyhydroxide particles in ARD and fine particles in wood degradation products and in lignin solutions were also characterized by ultrafiltration /2/. The visualization of particles of less than 10 nm in size is possible by transmission electron microscopy (TEM) and atomic force microscopy (AFM). However, sample preparation is tedious for these methods; the techniques, although challenging and very promising, are hardly routine techniques. An example (visualization of individual humic acid molecules by AFM) is given in Fig. 8 of /2/.

A real challenge to our separation and detection scheme is the investigation of extremely fine, low-concentration colloids (of few nanometers and few mg/L). Particle size determination by PCS is not possible in such cases because of poor counting statistics due to low scattered light intensities and also due to masking problems. Ultrafiltration is often disturbed by adsorption problems at the filter membranes. For inorganic particles (Fe and Al oxyhydroxide particles) we reached the lowest detection limits by centrifugation. Using centrifugal accelerations of up to 46,000 g and centrifugation times of up to 10 hours, we classified colloidal particles down to about 5 nm in diameter at concentrations of about 0.5 mg/L /2/. Fortunately, low-concentration colloids do not usually play an important role in contaminant transport via the water path as was demonstrated, for instance, for ground water from crystalline rock formations in Switzerland /4/. Compared with the available rock surface, the total surface area of the particles of low-concentration colloids is too small to have any real influence. Extremely fine particles in particular tend to be low concentrated in nature due to their high instability, unless they are electrostatically stabilized (as it is the case in humic acid solutions or in ARD solutions). This instability is caused by the very fast coagulation kinetics of environmental particles of the lowest nanometer size range (<50 nm) /5/.

References

/1/ Richter, W., Zänker, H., Hüttig, G., this report p. 75
/2/ Zänker, H.: Internet homepage of FZR, Jan. 2000 (www.fz-rossendorf.de/FWR/COLL/Coll_2.html)
/3/ Zänker, H., Richter, W., Brendler, V., Kluge, A., Hüttig, G., this report p. 77
/4/ Degueldre, C. A., Report PSI 94-21, Paul Scherrer Institut Villigen (1994)
/5/ Fillela, M., Buffle, J., Colloids Surf. A **73**, 255 (1993)

# CHEMICAL MODELING OF COLLOIDS IN MINE WATERS

V. Brendler, H. Zänker, W. Richter

*Comparison of mine water colloid analysis with geochemical speciation modeling showed, that Pb is quantitatively bound in anglesite, Si is not colloidally bound due to equilibrium with amorphous silica, Fe is partly bound to colloids with the exact chemical nature of the precipitate still being unclear, either as a hydrogen-jarosite phase, ferrihydrite or schwertmannite.*

The understanding of the formation, composition, stability and reactions of colloids is essential for risk assessment and the planning of restoration measures for contaminated water supplies. This study should explore to which degree thermodynamic speciation modeling is able to predict colloids in mine water systems. Acidic, highly mineralized water samples from the "Himmelfahrt Fundgrube" mine in Freiberg/Saxony were investigated. The respective analytical results and the colloid characterization are presented in the previous paper.

The EQ3/6 /1/ geochemical speciation software was used for the modeling. The modeling was based on the chemical analysis of the unfiltered ARD sample. Assumptions are that the colloid concentration is small in the particle size range between ion size and 1.3 nm, and that the sample is not far from thermodynamic equilibrium. All thermodynamic constants are taken from the "COM" database accompanying EQ3/6, assuming the solubility of colloidal particles being equal to that of macroscopic ones. However, several extensions proved to be necessary, including the addition of solid phases such as hydrous ferric oxide, hydronium jarosite, schwertmannite, and scorodite /2-4/.

EQ3NR computations revealed oversaturation of the minerals anglesite ($PbSO_4$), various $SiO_2$ modifications, Fe minerals such as schwertmannite, jarosite, ferrihydrite, hematite, goethite, and $Th(SO_4)_2$.

In a second step, EQ6 computations took mineral precipitations into account. The modeled, nearly complete precipitation of Pb as anglesite was in good agreement with the findings for the colloid compositions. With regard to Si, the system was in equilibrium with amorphous silica, the formation of thermodynamically more stable $SiO_2$ phases obviously being kinetically hindered, as found from the colloid observations. Finally, with regard to the Fe speciation, several scenarios had to be considered to account for uncertainties in phase composition and precipitation kinetics. This also influences the arsenic speciation through Fe-arsenates and aqueous Fe/As complexes. Common to all models is the assumption of an oxidizing environment, open to the air.

*Scenario 1:* Only ferrihydrite, jarosite and Na-jarosite are allowed to precipitate.
*Scenario 2:* In addition to scenario 1, schwertmannite is allowed to precipitate.
*Scenario 3:* In addition to scenario 2, H-jarosite is allowed to precipitate.
*Scenario 4:* In addition to scenario 3, scorodite is allowed to precipitate.

Moreover, there are ranges of the solubility products log $K_{sol}$ of schwertmannite and jarosite in the literature. The differences for schwertmannite are only reflected in scenario 2a with log $K_{sol}$ = 20.5 and 2b with log $K_{sol}$ = 15.5, in all the other models schwertmannite does not occur. And the two extremes in log $K_{sol}$ for jarosite (ranging from -12.5 to -9.21) change the Fe speciation only slightly, with the higher value resulting in the formation of about 0.5 % jarosite at the maximum. The results for the Fe speciation for the scenarios as discussed above are shown in Fig. 1. Scenario 4 is in closest agreement with the experimental findings (XRD) that jarosite-like phases may be the major precipitate.

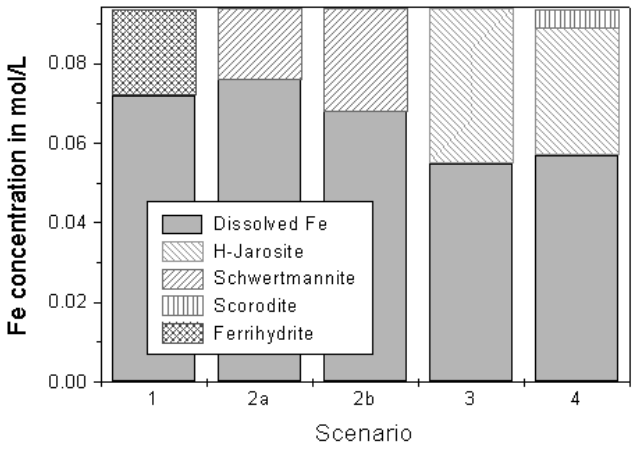


Fig. 1: Fe distribution in colloidal solutions, computed with EQ3/6

The speciation of the dissolved Fe fraction is dominated by only three species: $FeSO_4$(aq) with mole fractions between 42 and 55 %, $Fe^{2+}$ (between 28 and 42 %), and $Fe^{3+}$ (between 2 and 16 %). It means that most of the dissolved iron is present in the reduced form. The sum of all aqueous Fe-As-complexes does not exceed 4 %. These general speciation patterns are independent of the considered model scenario.

The modeling also correctly reflected the steadily drifting of the pH from the measured pH 2.7 of the fresh solution to a value of 2.4 after several months. The models predict a final equilibrium pH between 2.05 and 2.25. The redox potential Eh is predicted to be between +620 and +690 mV, close to the experimental value.

References

/1/ Wolery, T.J.; Report UCRL-MA-110662 Part I, Lawrence Livermore National Laboratory, Livermore (1992)
/2/ Cornell, R.M., Schwertmann, U., *The iron oxides. Structures, properties, reactions, occurrences and uses.* VCH, Weinheim, 1996, p. 573
/3/ Bigham, J.M., Schwertmann, U., Traina, S.J., Winland, R.L., Wolf, M., Geochim. Cosmochim. Acta **60**, 2111-2121 (1996)
/4/ Robins, R.G., American Mineralogist **72**, 842-844 (1987)

# CHARACTERIZATION OF COLLOID PARTICLES IN ACID ROCK DRAINAGE FROM THE MINE AT FREIBERG, SAXONY

W. Richter, H. Zänker, G. Hüttig

*Significant fractions (> 20 mass %) of the heavy metals in the acid rock drainage sample studied occur as colloid particles of 1 to 5 nm. Colloids, obviously, play an important role in acid rock drainage waters.*

## Introduction

Gangues of clay minerals (so-called “Letten”) that are impregnated with finely-divided sulphide ores play a key role in the sulphide oxidation and water mineralization process in abandoned ore mines. Highly mineralized, red-colored solutions are formed in the pores of these gangues. They result in acid rock drainage (ARD) /1/. Solutions of pH values of 0.7 to 2.5 that are in equilibrium with products of sulphide oxidation such as jarosite and scorodite have been observed in the pores of clay mineral gangues at Freiberg /2/. The ARD (“Lettenwasser”) often gathers in pools in front of the clay gangues. We took a sample from an ARD pool at a clay gangue in the Himmelfahrt Fundgrube mine at Freiberg and investigated it for its colloid content. The sample had a pH of 2.7 and contained 39.5 g/L of sulphate, 4.5 g/L of Fe, 4.8 g/L of Zn, 2.1 g/L of Mg, 1.3 g/L of Al, 470 mg/L of As, 13 mg/L of Pb, 14 mg/L of Cd, and a variety of further heavy metals.

## Experimental

The sample was filtered through Nuclepore filters of the pore sizes 5 µm and 50 nm and through ultrafilters of molecular weight cutoffs of 100 kD, 30 kD, 10 kD, and 3 kD (geometrical pore sizes of about 5 nm, 2.2 nm, 1.6 nm, and 1.2 nm). The filtrates were investigated for their particle sizes (photon correlation spectroscopy) and heavy metal concentrations (ICP-MS and/or AAS). The filter cake of a 5µm Nuclepore filter was washed three times, dried, coated with carbon and examined with SEM and EDX.

## Results

*Photon correlation spectroscopy (PCS)*

It indicates the presence of particles from 70 to 250 nm. After the removal of these particles by filtration through a 50nm filter, PCS still indicates the presence of particles of < 10 nm.

*SEM and EDX*

SEM confirms that there is a small fraction of particles in the size range from 70 to 250 nm (Fig.1). The agglomerate visible in the micrograph was probably formed from the nanoparticles on the filter membrane during the filtration process (self-coagulation) /3/. PCS shows that micron-sized agglomerates do not exist in solution. Fig. 1 also gives an EDX spectrum of the particles. Fe and As are identified as the main constituents, which is in accordance with the ICP-MS/AAS results. The high carbon peak in Fig. 1 is caused by the filter material and thus an artifact. The sulphur peak can probably be attributed to the sulphate ion. We suppose that the particles contain sulphate minerals such as jarosite or schwertmannite.

*Ultrafiltration*

The ultrafiltration experiments show that significant fractions of the elements Fe, As and Pb occur as colloid particles of < 10 nm in size. The 3-kD filter retains 25-30 mass % of the Fe, 60 mass % of the As and 90 mass % of the Pb.

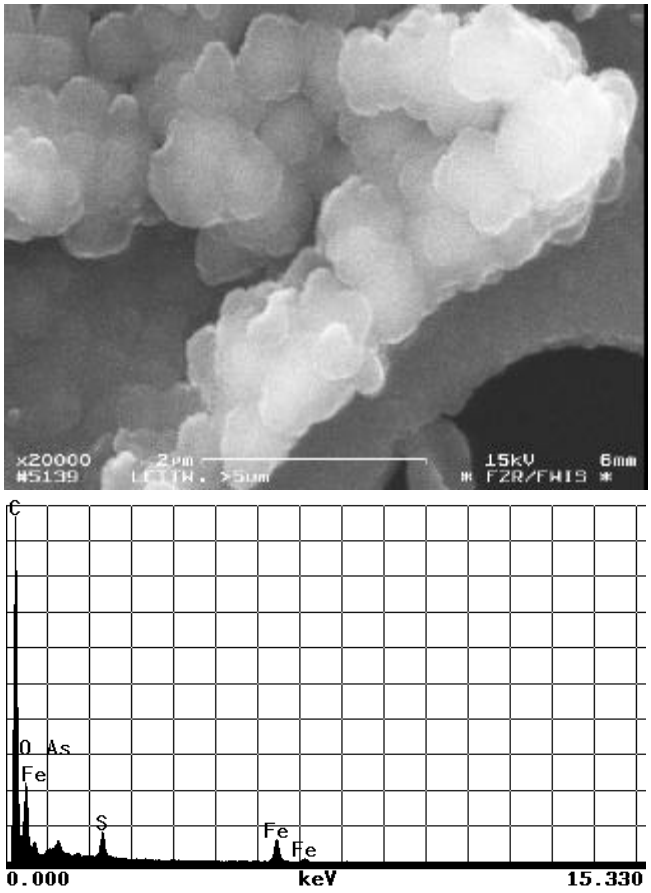


Fig. 1: SEM micrograph and EDX spectrum of a particle agglomerate on a 5-µm Nuclepore filter

## Conclusions

Very small fractions of the constituents of the ARD sample (< 0.5 mass % of the heavy metals) occur as relatively coarse nanoparticles of 70 to 250 nm in diameter. However, significant fractions of the constituents exist in the form of very fine colloids. The major components of these fine colloids are iron minerals. About 25 to 30 mass % of the sample’s iron are colloid particles in the size range from 1.2 to 5 nm. These particles carry most of the As and Pb. The experiment demonstrates that colloids in flooded mines are not only formed by precipitation processes in the bulk of the mine water /4/. They obviously play an important part already at the first stage of mining water mineralization, i.e. during the formation of ARD.

## References

/1/ Geller, W., Klapper, H., Salomons, W. (Eds.): *Acidic Mining Lakes*. Springer 1998

/2/ Haubrich, F., et al.: GUG Schriftenreihe “Geowissenschaften + Umwelt”, 1999

/3/ Buffle, J., Leppard, G.G.; Environ. Sci. Technol. **29**, 2176 (1995)

/4/ Zänker, H., Brendler, V., Richter, W., Nitsche, H.; Report FZR-247 (1999) p. 62

# THE ADSORPTION OF URANIUM TO THE COLLOIDS OF A MINING WATER

H. Zänker, W. Richter, V. Brendler, G. Hüttig, U. Schulte-Ebbert [1]
[1] Institut für Wasserforschung GmbH Dortmund, Zum Kellerbach 46, 58239 Schwerte

*Carbonato and aquo complexes prevent the uranyl from being adsorbed to the colloids of the gallery water. Acidification destroys these complexes: up to 50 mass % of the uranyl is attached to the colloids in the slightly acidic pH region. Further acidification, however, makes the uranyl "non-colloidal" again.*

The water of the main drainage gallery of the Freiberg mining area contains above all dissolved sulfates and carbonates of Ca, Mg, and Na /1/. The pH of this water is 7.3; the electrical conductivity is 1,000 to 1,100 µS/cm. As we showed in /1/, there are also colloids in this mining water. Their concentration is about 1 mg/L; their size is 100 to 300 nm. They consist of a matrix of Fe and Al compounds (probably ferrihydrite and alumogel or alkaline aluminum sulfate) that bears trace elements such as As, Pb, and Cu. Almost 100% of the As and Pb is colloid-borne. An element that showed strictly "non-colloidal" behavior was uranium. This was somewhat surprising uranium normally has a pronounced tendency to adsorb onto ferrihydrite /2/. We wanted to test the behavior of uranium in the gallery water under the influence of pH variations. Thus, we acidified the water step by step with nitric acid. The rationale behind this experiment was elucidation of uranium behavior in the acidic mining waters in Saxony.

We investigated the behavior of 25 elements by filtration and ICP-MS/AAS.

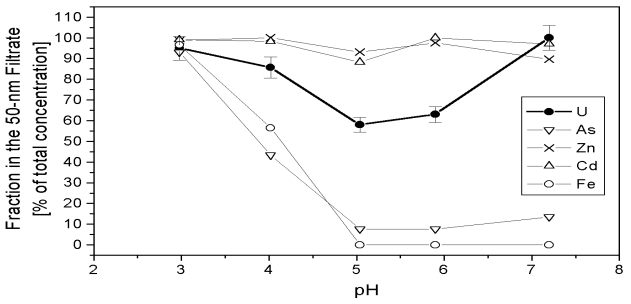


Fig. 1: Influence of pH on the colloid-borne fraction of several heavy metals. Error bars: 2F confidence intervals of the measured uranium concentration

Fig. 1 shows 5 examples. Given are the fractions of the elements that passed through a 50 nm Nuclepore filter versus pH. Most of the elements behaved like Cd and Zn: they were "non-colloidal" over the whole pH range. For the "colloidal" elements, as represented by Fe and As, the tendency to occur as colloids decreased with an increasing degree of acidification. This is obviously due to both the disappearance of the colloidal particles by dissolution of the colloid matrix and the decrease in the adsorption affinity of the trace elements in the acidic region.

Uranium shows a specific behavior. The fraction of uranium that is not filterable by a 50 nm filter has a minimum in the slightly acidic pH region (Fig. 1). We explain this minimum by the occurrence of competing processes: changes in the uranyl speciation and in the average electrovalency of the uranyl compounds, on the one hand, and changes in the electrical surface charge and the chemical solubility of the colloid particles, on the other.

Fig. 2 shows the calculated uranyl speciation in the gallery water as a function of pH and Fig. 3 the course of the particles' measured zeta potential on acidification.

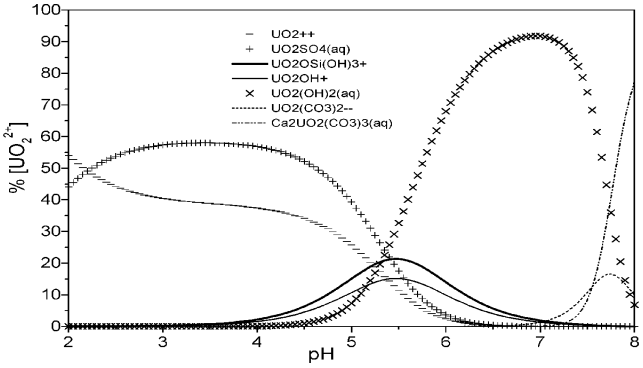


Fig. 2: Uranyl speciation in water of the mining gallery for varying pH values. Computed with EQ3/6 /3/

It becomes obvious from Fig. 2 that neutral and negatively charged uranyl species prevail in the original water (pH 7.3). Here the charge of the colloid particles is negative; a zeta potential of -13 mV was measured. Adsorption of uranyl is obviously prevented in the original water by a lack of attractive forces.

On acidification positive uranyl species play an increasing part (Fig. 2). In the slightly acidic region a significant fraction of the U is adsorbed to particles due to opposite electrical charges. Up to 50 mass % of the uranium is attached to the colloids.

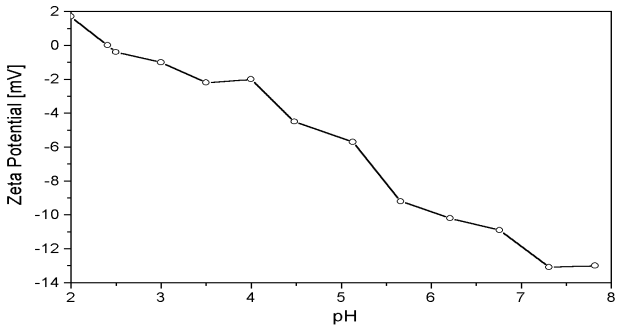


Fig. 3: Zeta potential of the colloidal particles in the gallery water for varying pH. (Laser Doppler electrophoresis)

When pH decreases further, the negative charge of the particles disappears (Fig. 3), i.e., the attractive forces vanish. The colloid particles are moreover dissolved in the more acidic pH region. The uranyl species again lose their "colloidal" properties in this region.

References

/1/ Zänker, H., et al.: Report FZR-247 (1999) p. 62
/2/ Waite, T. D., et al.: Geochim. Cosmochim. Acta **58**, 5465 (1994)
/3/ Wolery, T.J.: Report UCRL-MA-110662, Part I, Lawrence Livermore National Laboratory (1992)

# ULTRAFINE COLLOID PARTICLES IN ACID ROCK DRAINAGE (ARD)

H. Zänker, W. Richter, V. Brendler, A. Kluge [1], G. Hüttig
[1] TU Bergakademie Freiberg, Institut für Mineralogie

*Ultrafine particles of 1 to 5 nm were the major colloidal component in an ARD sample. They consist of iron oxyhydroxides, anglesite and possibly scorodite.*

In /1/ we have demonstrated that the highly mineralized ARD sample from the abandoned Freiberg Zn-Pb-Ag ore mine contains a small amount (<50 mg/L) of easily-detectable submicron particles of 70 to 250 nm. However, it turned out that these particles form only the minor colloid component. This can also be deduced from the photon correlation spectroscopy (PCS) results in Fig. 1. Whereas the larger submicron particles dominate in the raw sample and the first two filtrates, particles of <10 nm appear after the filtration through a 50-nm filter. The larger particles have been removed by the 50-nm filtration which makes the ultrafine particles detectable by PCS (the detection of extremely small colloid particles by PCS is prevented in the presence of large submicron particles due to optical masking which results from the $r^6$ dependence of the scattered light intensity on the particle radius r in the particle size range of Rayleigh scattering).

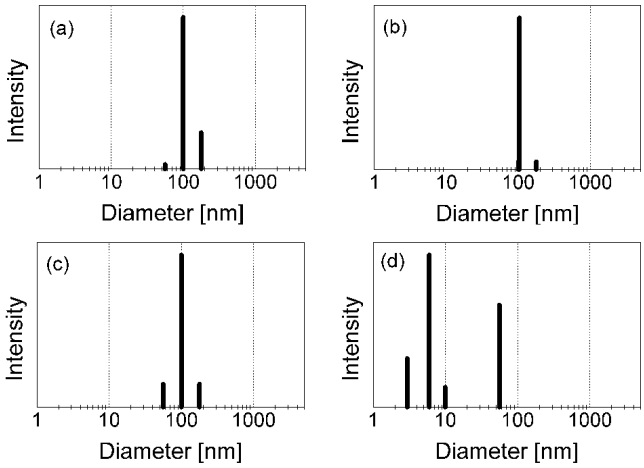


Fig. 1: Particle size distribution in the ARD sample according to PCS. (a) Raw sample. (b) 5-µm filtrate. (c) 400-nm filtrate. (d) 50-nm filtrate.

The <10 nm particles were investigated more thoroughly by ultrafiltration through Amicon YM filters (molecular weight cutoffs: 3, 10, 30, and 100 kD). Tab. 1 gives the retention of important chemical elements at the 3-kD ultrafilter. Most of the elements show percentage retentions between 7.5 and 13.2 mass%. This group includes elements such as Li, Mg, Cu or Zn which are typically ionogenic in acidic sulfate solutions. Therefore, we suppose that the retention of these elements is not due to particle filtration. Reverse osmosis may be the reason for this retention. However, three chemical elements fall unambiguously outside this group: Fe, As, and Pb. Assuming that the "nonparticular retention" is about 10 %, we can conclude that at least 15 % of the Fe, 50 % of the As and 80 % of the Pb occur as particles of 1.3 to 5 nm in diameter (the geometric sizes of the 3-kD and the 100-kD filter pores, respectively). This corresponds to a colloid concentration of at least 680 mg/L Fe, 230 mg/L As and 20 mg/L Pb in the ARD sample. No information is available about colloids of the particle size range between ion size and 1.3 nm. However, it is plausible to expect also particles in this size region.

| Element | Raw sample concentration [mg/L] | Retention >3 kD | |
|---|---|---|---|
| | | [mg/L] | [%] |
| Li | 3.55 | 0.25 | 7.5 |
| Si | 72.0 | 7.9 | 10.1 |
| Ca | 501 | 48.5 | 9.7 |
| Mg | 2065 | 197 | 9.5 |
| Al | 1330 | 175 | 13.2 |
| Fe | 4530 | 1150 | 25.4 |
| Mn | 1230 | 117 | 9.5 |
| Cu | 95.4 | 9.1 | 9.5 |
| Zn | 4830 | 450 | 9.3 |
| As | 468 | 290 | 62.0 |
| Cd | 30.7 | 2.8 | 9.1 |
| Pb | 26.7 | 24.2 | 90.2 |

Tab. 1: Raw sample analysis and retention of several chemical elements at the 3-kD ultrafilter (3kD • ca.1.3 nm).

We tried to identify the mineralogy of the ultrafine particles by comparison with geochemical speciation modeling with EQ3/6 the details of which are given in the following paper. The experimental findings for lead coincide with the model prediction of nearly quantitative precipitation of anglesite ($PbSO_4$). Also the detected concentration of iron colloids is close to the model output. Here, however, several mineral phases are possible, depending on the solubility data set applied for schwertmannite, ferrihydrite, and various jarosite phases. Finally, the large fraction of colloidal arsenic must be interpreted as, probably metastable, scorodite ($FeAsO_4 \cdot 2H_2O$). Another hypothesis is a substantial adsorption of arsenic onto iron oxyhydroxides. These ambiguities concerning the nature of the iron and arsenic phases will be the focus of future studies, namely by EXAFS experiments.

Acknowledgments
This work has been funded by the Deutsche Forschungsgemeinschaft.

References
/1/ Richter, W., Zänker, H., Hüttig, G.: this report p. 75

# LONG-TERM BEHAVIOR OF AN ACID ROCK DRAINAGE (ARD) SOLUTION FROM THE MINE AT FREIBERG

H. Moll, H. Zänker

*A relatively coarse precipitate evolved in the sample which consists primarily of H-jarosite and which binds significant amounts of As and Pb.*

In /1,2/ we have shown that the ARD sample taken in the mine at Freiberg in February 1999 had relatively high concentrations of Fe, Zn, Mg, Al, Mn, and As, that the main anion was sulfate and that the pH was 2.7. A remarkable portion of the Fe, As, and Pb exists as colloids. The size of most of the colloidal particles is very small (<5 nm); the concentration of these ultrafine particles is about 1 g/L. Not much is known about the composition/mineralogy of these ultrafine particles. They consist of iron oxyhydroxides (jarosite, H-jarosite, schwertmannite, or ferrihydrite), anglesite and possibly scorodite /2/. We hope that EXAFS experiments will provide further elucidation of the ultrafine particles' mineralogy. The sample was not in full thermodynamic equilibrium. This can be concluded from a decrease in the pH from 2.7 to 2.4, from a decrease in the Fe, As, and Pb concentrations during the time after sampling (Tab. 1) and from the formation of a relatively coarse precipitate during the months after sampling.

| Component | Concentration [mMol/L] | |
|---|---|---|
| | One day after sampling | Ten months after sampling |
| As | 5.95 | 5.27 |
| Cu | 1.43 | 1.43 |
| Fe | 77.9 | 69.3 |
| K | 0.02 | 0.002 |
| Na | 0.06 | 0.006 |
| Pb | 0.065 | 0.0092 |
| U | 0.007 | 0.008 |

Tab. 1: Concentration of selected elements in the 5-µm filtrates of the ARD sample after two aging times.

We were interested in the processes proceeding in the ARD solution after sampling, in particular in the nature of the precipitated solid. The metal contents of the precipitate, calculated in two different ways, are given in Tab. 2. The following secondary minerals come into question as the constituents of the solid: scorodite ($FeAsO_4 \cdot 2H_2O$), jarosite ($KFe_3(SO_4)_2(OH)_6$), H-jarosite ($HFe_3(SO_4)_2(OH)_6$), schwertmannite ($Fe_{16}O_{16}(OH)_{10}(SO_4)_3 \cdot 10H_2O$), ferrihydrite ($Fe_5OH_8 \cdot 4H_2O$), anglesite ($PbSO_4$), and plumbojarosite ($Pb[Fe_3(SO_4)_2(OH)_6]$). Scorodite can not have bound more than one fifth of the iron because the theoretical molar Fe/As ratio of scorodite is 1 (cf. Tab. 2). Thus, most of the iron must be bound as one of the other iron minerals between which cannot be further differentiated from the results of Tab. 2. By EDX on the precipitate we measured a molar Fe/S ratio of 2.0. The theoretical molar Fe/S ratio is 1.5 for jarosite and 8.0 for schwertmannite. Therefore, the sulfate-rich mineral jarosite should be the main constituent of the precipitate. This jarosite should be primarily H-jarosite since the content of potassium is too low to explain the presence of larger amounts of common jarosite. The arsenic may be bound as scorodite or adsorbed (surface complexation). The small amount of lead may be in the form of anglesite or plumbojarosite.

| Component | Concentration [mMol/g] | |
|---|---|---|
| | According to the decrease of the solution concentrations | According to direct chemical analysis on the precipitate |
| Fe | 8.6 | 5.8 |
| As | 0.68 | 1.1 |
| Pb | 0.056 | 0.071 |
| K | 0.02 | 0.1 |

Tab. 2: Metal composition of the precipitate that evolved in the ARD sample within 10 month.

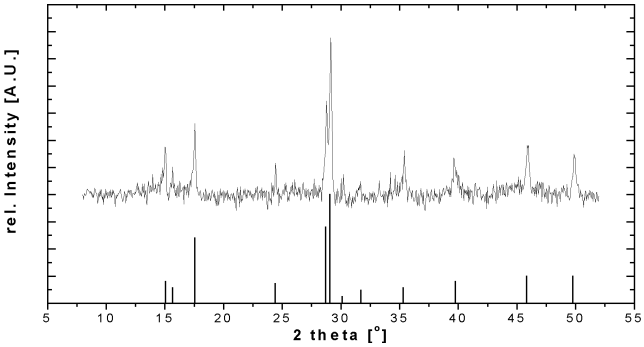


Fig. 1: XRD powder diagram of the precipitate and the major reflexes of $(K, H_3O)Fe_3(SO_4)_2(OH)_6$ /3/.

The XRD analysis of the solid (Fig. 1) clearly shows that jarosite of the general formula $(K,H_3O)Fe(SO_4)_2(OH)_6$ /3/ is the major component (>90 %). Because of the deficiency in potassium, this jarosite should be H-jarosite. No indications of scorodite could be found. No lead minerals were detected. However, the presence of small amounts of poorly crystalline phases (schwertmannite) cannot be excluded.
The detected ultrafine particles (<5 nm; cf. /2/) in ARD may be an intermediate in the precipitate formation process of H-jarosite. If so, the mineralogy of the precipitate could possibly give clues as to the mineralogy of the ultrafine colloid particles.

Acknowledgments
This work has been funded by the Deutsche Forschungsgemeinschaft (IIC6-Ni210/4-1).

References
/1/ Richter, W., et al., this report p. 75
/2/ Zänker, H., et al., this report p. 77
/3/ *Powder Diffraction File*, International Center of Diffraction Data, Newtown Square, Pennsylvania, U.S.A., Diffraction Data Card No. 36-427 (1991)

# ADSORPTION OF HEAVY METALS BY ENVIRONMENTAL COLLOIDS EXAFS MODEL COMPOUNDS PART I: SCORODITE

H. Moll, H. Zänker, G. Schuster

*$FeAsO_4x2H_2O$ was synthesized with a high phase purity and yields of 95 %. The powder has a surprisingly narrow particle size distribution of 10.5 ± 0.5 µm.*

Motivation

Previous studies /1/ showed that colloid particles in mining waters (Rothschönberger Stolln, Lettenwasser Freiberg) mainly consist of iron and/or aluminum compounds, e.g. oxidhydroxides. These waters contain As in a broad concentration range from $10^{-7}$ to $10^{-2}$ M. An interesting question is how the arsenic interacts with the iron oxidhydroxide colloid particles. In principle two possibilities exist: a) adsorption and surface complexation and b) formation of secondary phases. XAS measurements of such mining waters are suited to answer the question which mechanism may occur. This requires first the preparation and XAS characterization of model compounds. One of those is scorodite, $FeAsO_4$ $x2H_2O$, a mineral phase found also in nature /2/ and a model compound for case b.

Experimental

Aqueous solutions (0.1 M) of iron chloride and sodium arsenate were combined in stoichiometric amounts /3/. Samples were prepared at pH 2.1 (sample B) and at pH 4 (sample C). The amorphous precipitate was aged for 11 days in the mother liquor at 105 EC. The resulting powder was washed with Milli-Q water to remove unreacted starting materials. The final products were identified and analyzed by XRD, AAS, thermoanalysis and SEM. The results are compared to those obtained on scorodite found in Utah, USA, (sample A).

Results and Discussion

After mixing of the reactants, the precipitation of a light, tan-colored product was immediately observed. In the case of the pH 2.1 experiment, this precipitate changed into a light green substance after a reaction time of 6 days at 105EC. The XRD patterns of the powders are summarized in Fig. 1.

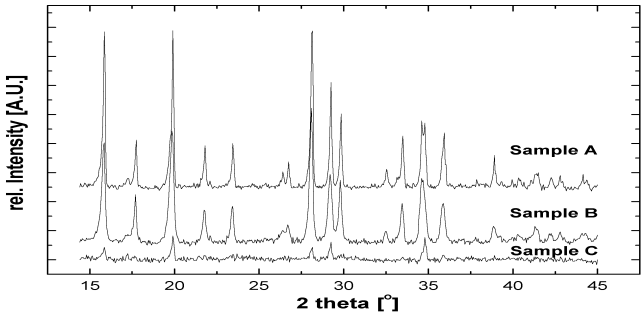


Fig. 1: XRD powder diagrams of different scorodite samples; A: mineral, B: sample at pH 2.1, C: sample at pH 4.

The main component in all samples is scorodite of orthorhombic structure (cf. /4/). Amorphous material was present in sample C. The lattice constants of samples A and B were calculated from all clearly identifiable reflections. The following values were obtained: a = 8.951, b = 10.310, c = 10.027 nm, and V = 925.22 $nm^3$. The lattice constants determined by our analyses are in fair agreement with the literature values. We only observed slightly smaller a and b values (0.016 nm) in comparison with the published data /4/.

Iron arsenate with the proposed formula of $FeAsO_4$ $x2H_2O$ theoretically contains 24.2 wt% Fe, 32.5 wt% As, and 15.6 wt% structural water and has a stoichiometric ratio *n(Fe)/n(As)* = 0.745. All samples contain 24.3 ± 0.2 wt% Fe, and 30.2 ± 0.8 wt% As. The measured Fe and As contents correspond well to the theoretical values. Our products have a stoichiometric ratio *n(Fe)/n(As)* = 0.804 ± 0.02.

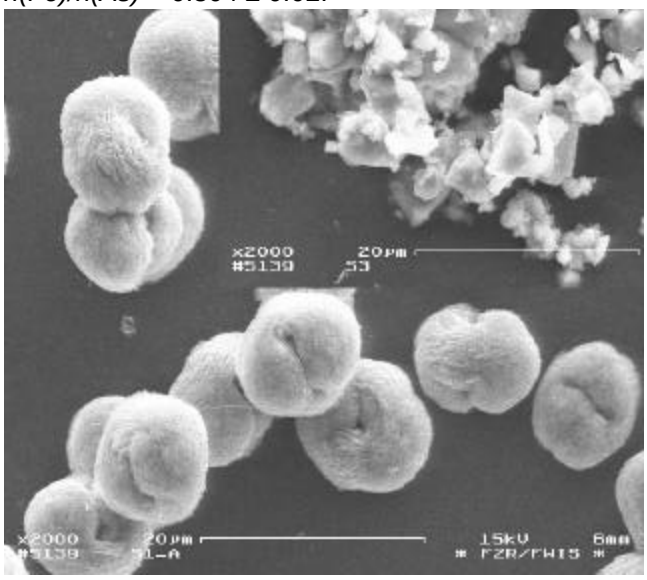


Fig. 2: SEM images of synthetic scorodite (sample B, large) and the mineral (sample A, small).

SEM investigations on sample B revealed a very narrow particle size distribution (Fig. 2). The particle size is 10.5 ± 0.5 µm. The picture is completely different for samples A and C. Many different particle shapes exist with a broad size distribution from 4 to 130 µm and larger agglomerates of up to 600 µm. It follows from the XRD and the SEM investigations on sample C that a mixture of scorodite and amorphous iron oxidhydroxides may be formed or the scorodite particles may have a coating of iron oxidhydroxides as proposed in /3/. The thermoanalytical investigations on sample C showed similarities to those obtained for pure iron oxidhydroxides which supports this hypothesis. The content of structural water is clearly increased for sample C (18.6 % compared with 15.8 % for samples A and B). All three samples will be used as reference materials in the EXAFS experiments on the mining water colloids.

Acknowledgments

This work has been funded by the Deutsche Forschungsgemeinschaft (IIC6-Ni210/4-1).

References

/1/ Richter, W., et al., Report FZR-247 (1999) p. 61

/2/ Haubrich, F., et al., GUG-Schriftenreihe “Geowissenschaften und Umwelt” 1999

/3/ Dove, P.M., Rimstidt, J.D., Am. Mineral. **70**, 838-844 (1985)

/4/ Hawthorne, F., Acta Cryst. **B32**, 2891-2892 (1976)

# AEROSOL FORMATION BY UV IRRADIATION OF SILOXANE VAPORS

D. Rettig, R. Adam [1], P. Merker
[1] TOPAS GMBH Dresden

*The recently observed phenomenon of the photolytically induced formation of silicon-containing aerosol particles in wet gases is demonstrated to originate from a minute contamination of the gases with polydimethylsiloxane vapors. This process is used for stable long-term aerosol generation.*

We recently noticed the formation of spheric particles during UV irradiation of humid nitrogen, argon, helium or air in a flow-through reaction vessel of fused silica with a low-pressure mercury lamp /1/. The detection of silicon in the aerosols led us to the erroneous hypothesis that a photolytic decomposition of hydrated silicic acid from the quartz surface of the vessel had taken place. In that first interpretation we overlooked that the gases where conducted along stainless steel tubing which had been contaminated by mineral oil or silicones.

To simulate the observed particle production, we introduced alkanes and silicone oils (polydimethylsiloxanes) into clean gases at concentrations between $10^{-5}$ and $10^{-11}$ parts per volume and studied the photolytically formed aerosols /2/. Here we discuss the reactions of the wax n-eicosane $C_{20}H_{42}$, low viscous silicone oil $(CH_3)_3SiO[Si(CH_3)_2O]_{\sim 13}Si(CH_3)_3$, and octamethylcyclotetrasiloxane (see formula), the latter being one of the depolymerization products of siloxanes.

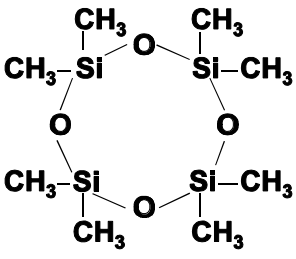

The high-energetic UV radiation of 185 nm (low pressure mercury lamp) is necessary to induce the decomposition of the substances in the humid gases. There is absolutely no particle production from alkanes and siloxanes in the dry gas mixtures (<20 vpm $H_2O$) nor in synthetic air ($N_2$ + $O_2$).

Water vapor absorbs the 185 nm radiation to form hydroxyl radicals. In the first reaction step, the hydroxyl radicals abstract hydrogen from the compounds under study to form alkyl radicals /3/. These may undergo a wide variety of secondary reactions. Intermediate reaction products which nucleate and coagulate as particles are formed in short periods of irradiation (<1 sec; cf. Fig.1). Dicarboxylic acids and demethylated hydroxyl-substituted siloxanes can be assumed to be the low-volatile intermediate products. During longer periods of irradiation (> 1 sec; cf. Fig. 1) the intermediate products are increasingly further oxidized and decomposed to their final reaction products. Aerosols from alkanes and from siloxanes show a significant difference under these conditions. Alkanes form gaseous $CO_2$ and $H_2O$ and the particle concentration decreases whereas silicones leave the hydroxylated skeletons of -Si-O-Si- chains or rings, which are generally termed silica. These findings enable us to identify the contaminant observed in /1/ as siloxane. This conclusion is confirmed by similar results of SEM, TEM, XRD, XRF, EDX, ICPMS and AFM analysis of filtered particles obtained from the runs with the unknown contaminant /1/ and from those with siloxane addition /2/. Vibration bands of the Si-O-Si configuration were found as doublets at 1037 and 902 $cm^{-1}$ in IR analysis.

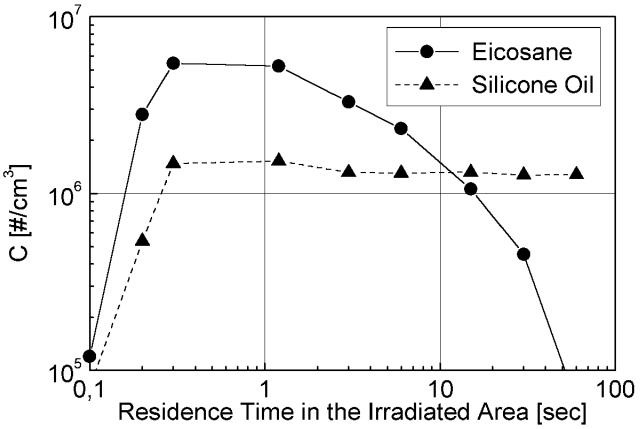


Fig. 1: Dependence of the particle concentration C in flowing humid nitrogen saturated with vapor of the wax eicosane or of a low viscous silicone oil on the residence time in the irradiated area of the vessel. (The area exposed to the light is controlled by shielding)

The rapid photolytically induced gas-to-particle conversion of siloxanes combined with subsequent filtration may be an effective method for cleaning gases from siloxanes and taking samples for siloxane analysis in air monitoring. Counting nanometer-sized particles with a condensation particle counter, as was done in this work, may be a sensitive method for siloxane detection. A detection limit as low as $10^{-11}$ parts per volume can be reached in online measurement. With this low detection limit, we were able to pinpoint the reasons for the particle formation in our experimental setup where the carrier gases had presumably been in contact with silicone resin, rubber or oil /1/.

The gas-to-particle conversion of siloxanes is used in a particle generator consisting of a siloxane source, a humidification unit, a reaction vessel of fused silica with a low-pressure mercury lamp and gas-flow regulating and cleaning devices. An aerosol of silica was produced from octamethylcyclotetrasiloxane. The production rate was stable over a period of 30 days with a number concentration of $6.2 \cdot 10^6$ $cm^{-3}$ (±3%=2F) and a median particle diameter of 27 nm (±4%=2F) at a gas flow rate of 40 L/h. The particle diameter can be varied between 5 and 150 nm by gas flow regulation.

References

/1/ Rettig, D., et al., J. Aerosol Sci. **29**, Suppl.1, S921 (1998), and Report FZR-218, p.80 (1998)
/2/ Rettig, D., et al., Last Minute Poster at the European Aerosol Conference 1999, 6-10 Sept., Prague
/3/ Sommerlade, R., et al., Environ. Sci. Technol. **27** 2435 (1993)

# Chemistry of the Heaviest Elements

# ACTINIDE SEPARATION BY THERMOCHROMATOGRAPHY ON METAL COLUMNS

A. Vahle, S. Hübener, S. Taut, K. Gregorich [1], U. Kirbach [1], C. Laue [1], H. Nitsche [1]
[1] Lawrence Berkeley National Laboratory

*The separation of the metallic trivalent actinide Bk from the metallic divalent actinide Fm under the conditions of a real Lr experiment was studied by thermochromatography. A decontamination factor of about $10^6$ was determined.*

## Introduction

In continuation of our thermochromatographic adsorption studies of the heavy actinides we started to investigate Lr, the last member of the actinide series.
$^{261}$Lr, a spontaneously fissioning isotope with a half-life of 39 min, is regarded as the Lr nuclide best suited for thermochromatographic off-line experiments. (The longer-lived $^{262}$Lr would be even more convenient if it could be produced in sufficient quantities.) We propose to produce $^{261}$Lr by the $^{249}$Bk($^{18}$O, $\alpha$2n) reaction. The $^{261}$Lr production cross section was estimated to be about 8 nb. In order to measure it by fission counting, spontaneously fissioning nuclides like $^{256}$Fm have to be completely separated from the Lr. Separation procedures based on ion exchange chromatography or extraction chromatography are usually employed to isolate actinide products. On the condition that Lr is adsorbed onto metals in the metallic trivalent state and not in the divalent state as expected from theoretical considerations involving relativistic effects, thermochromatography on metal columns should be very well suited as a separation technique. Separations can be completed within a short time with a high decontamination factor for the separation of metallic divalent actinides from the trivalent actinides. The pieces of the column can serve as samples for alpha spectroscopy without further preparation operations.
This work should show whether or not the separation is sufficient for an unambiguous determination of $^{261}$Lr by fission counting, which is a precondition not only for the cross section measurements but also for the adsorption studies of Lr.

## Experimental

Actinide isotopes were produced at the LBNL 88-Inch cyclotron by bombarding a $^{249}$Bk/$^{249}$Cf target (0.67 mg/cm $^{249}$Bk) with an $^{18}$O beam (93 MeV on target).
The recoil nuclei of the nuclear reactions were caught in 4 µm Zr foils. These catcher foils were used as thermochromatographic samples.
The experimental setup is similar to the one described in /1/. Thermochromatographic columns were made of Nb and Ta foils. A sapphire column served as a support tube. The apparatus was preconditioned at working temperature for about one hour before each experiment. Then the Zr catcher foil, attached to a small Ta boat, was inserted into the antechamber of the apparatus. After flushing the antechamber with 50 mL/min of purified He for 3 minutes, the sample boat was pushed into the thermochromatography starting position at 1930 K as necessary for an Lr experiment. This was considered the starting point of the thermochromatographic process. After 15 minutes the gradient oven heating was switched off, thus terminating the chromatographic process. The nuclide distribution along the column was determined off-line by $\alpha$-spectroscopy of 2 cm column pieces. 15 to 30 minutes were needed to prepare the samples.

## Results

The main alpha activities were caused by $^{248}$Cf and $^{250}$Cf which are the decay products of $^{248}$Bk and $^{250}$Bk formed by transfer reactions, thus representing the Bk distribution. Bk served as a model element for the metallic trivalent actinides. It was almost completely separated from the simultaneously produced Fm. On Nb, both Bk isotopes were deposited at the oven position 30-38 cm, corresponding to a deposition temperature of about 1630 K. Fig. 1 shows the sum spectrum of this column section. An alpha resolution of 30 keV (FWHM) was achieved.

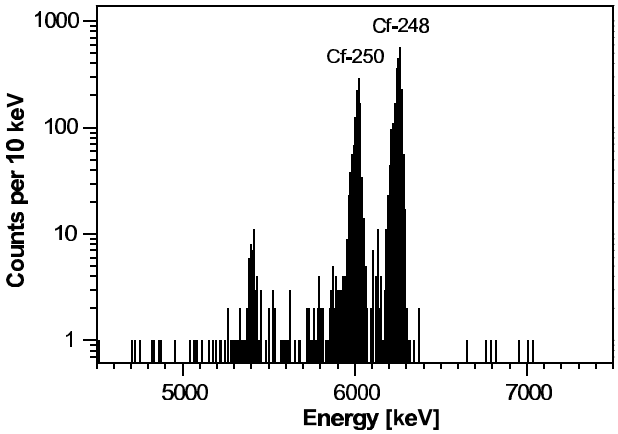


Fig. 1: Sum spectrum of an Nb column at the position of the Bk peak (30 - 38 cm)

Fm was deposited at significantly lower temperatures than Bk /2/. Only 3 decay events were detected in the energy range of 7.02 ± 0.1 MeV which is characteristic of $^{252}$Fm and $^{255}$Fm. A decontamination factor of about $10^6$ was obtained from a comparison with the total amount of Fm as evaluated from the cross sections given in /3, 4/. This is large enough to unambiguously assign the fission events to $^{261}$Lr.
The excellent separation of Fm from the metallic trivalent Bk encourages us to continue our efforts to characterize Lr, using thermochromatography.

## Acknowledgments

The support by the DFG under contract Hu 642/1-2 is gratefully acknowledged.

## References

/1/ Taut, S., et al., Radiochim. Acta **78**, 33 (1997)
/2/ Taut, S., et al., J. Alloys Comp. **271-273**, 316 (1998)
/3/ Gäggeler, H., et al., internal EIR report (1987)
/4/ Lee, D., et al., Phys. Rev. **C 27**, 2656 (1983)

# THERMOCHROMATOGRAPHIC ADSORPTION STUDIES OF BERKELIUM

S. Hübener, S. Taut, A. Vahle, B. Eichler [1], N. Trautmann [2], J.R. Peterson [3]
[1] PSI Villigen, [2] Universität Mainz, [3] University of Tennessee, Knoxville

*The adsorption of $^{250}$Bk atoms on niobium was studied thermochromatographically at temperatures as high as 1850 K at the starting position of the column. The trivalency in the adsorbed state is concluded from the adsorption behavior.*

In continuation of thermochromatographic adsorption studies of the heavy actinides /1,2/ and envisaging experiments with the heaviest actinide element lawrencium the goal of the present studies was to measure adsorption enthalpies for berkelium on niobium and to test the experimental setup at temperatures as necessary for studying lawrencium.

The experimental setup used in the present studies resembles the one described in /1/. We chose a temperature of 1850 K at the starting position in the column and a sapphire support tube for the thermochromatographic columns made of niobium foils. $^{254}$Es electroplated on tantalum was used as the $^{250}$Bk source. The $^{250}$Bk source was placed at the starting position into the column. Then the column was flushed with helium used as the carrier gas at a flow rate of 50 cm$^3$ per minute. To start chromatography the hot oven was moved into working position. In this work we used a mobile oven whereas the sapphire tube was stationary. After 30 min thermochromatography time the thermochromatogram of berkelium was measured with a resolution of 1 cm by gamma ray spectrometry of the $^{250}$Bk 989 keV and 1022 keV lines.

Fig. 1 shows a decay-corrected thermochromatogram of $^{250}$Bk ($t_{1/2}$ = 3.217 h). The position with the maximum berkelium concentration determines the deposition temperature which was found to be 1535 K in two identical experiments.

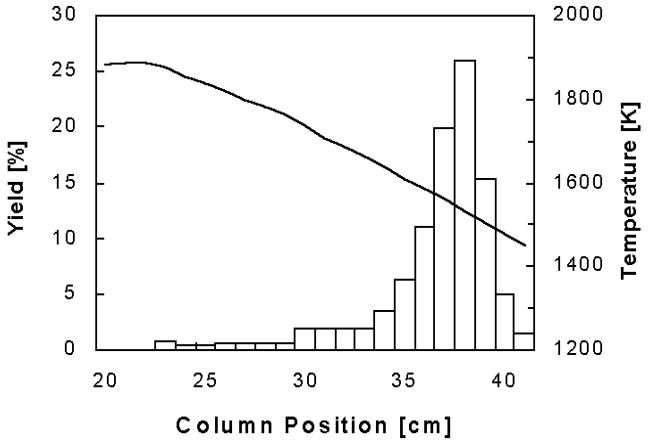


Fig.1: Thermochromatogram of $^{250}$Bk on a Nb column

The standard enthalpy of adsorption, $-H^0_{ads}$, was calculated from the deposition temperature and the experimental parameters as described in /1/. To calculate the standard entropy of adsorption, $-S^0_{ads}$, the period of oscillation of the adatom, $J_0$, was taken to be $0.81 \cdot 10^{-12}$ s as determined for the adsorption of Es on niobium /3/. We obtained $-H^0_{ads}$ = -332 kJ/mol and $-S^0_{ads}$ = -152 J/(K·mol).

As seen from Fig. 2, there is a regular trend in the adsorption enthalpies from berkelium to californium and to the divalent actinides einsteinium, fermium, and nobelium. In analogy to the electronic properties of the actinide metals we interpret the value of the adsorption enthalpy of berkelium having the [Rn]5f$^9$7s$^2$ ground state with an adsorption on niobium in the trivalent 5f$^8$6d$^1$7s$^2$ state.

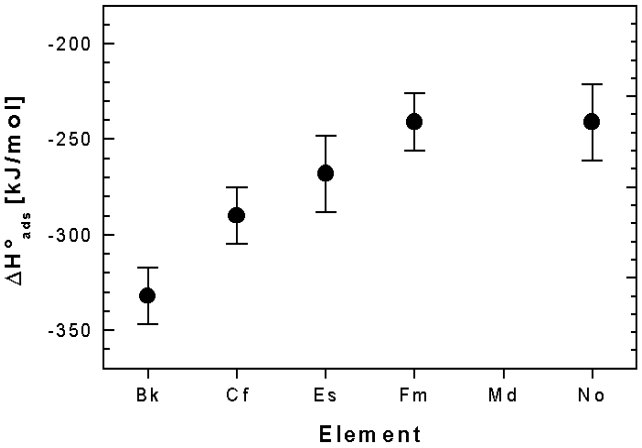


Fig. 2: Adsorption enthalpies on niobium. Values for Cf, Es, Fm, and No from /2/

Acknowledgments
The authors are indebted for the use of $^{254}$Es to the Office of Basic Energy Sciences, U.S. Department of Energy, through the transplutonium element production facilities at the Oak Ridge National Laboratory, managed by Lockheed Martin Energy Research corporation. The support by the DFG under contract Hu 642/1-2 is gratefully acknowledged.

References

/1/ Taut, S., et al., Radiochim. Acta **78**, 33 (1997)
/2/ Taut, S., et al., J. Alloys Comp. **271-273**, 316 (1998)
/3/ Taut, S., et al., Report FZR-218 (1998) p. 84

# THERMOCHROMATOGRAPHY OF CURIUM AND BERKELIUM ON NIOBIUM COLUMNS

S. Taut, A. Vahle, S. Hübener, B. Eichler [1], D. T. Jost [1], A. Türler [1]
[1] Paul Scherrer Institut Villigen

*The adsorption of elemental curium and berkelium onto metallic niobium was measured by thermochromatography. Adsorption enthalpies of -392±15 kJ/mol (curium) and -349±15 kJ/mol (berkelium) were determined.*

## Introduction

In the past years we have studied the adsorption of the metallic divalent actinides einsteinium, fermium, and nobelium in their elemental states on several metals /1, 2, 3/.

Recently, we extended our research to berkelium /4/ and curium. This is a preparation of the planned adsorption study of lawrencium, the last member of the actinide series. The adsorption behavior of lawrencium is expected to be very similar to that of Cm.

## Experimental

We used a similar experimental setup as described in /2/ with a sapphire support tube instead of the tantalum tube.

The chromatographic samples were obtained in the following way: A $^{248}$Cm target (0.7 mg/cm$^2$) was irradiated with an $^{18}$O beam (about 2 × 10$^{12}$ s$^{-1}$) at the PSI Philips cyclotron. The reaction products and curium which were sputtered from the target material during the bombardment was caught in zirconium catcher foils behind the target. These foils were used as samples without further preparation.

The samples were transferred into the cold chromatographic column. After flushing the column with purified helium we adjusted the helium flow rate to 50 cm$^3$/min and moved the hot gradient furnace over the column. The temperature in the starting position was 1890 K. After 10 or 20 minutes the heating was switched off. This stopped the chromatographic process due to the immediate cooling of the column. Finally, the column was cut in 1-cm sections. These pieces were counted off-line in an alpha spectrometer.

## Results

Fig. 1 shows the distribution of curium and berkelium along a niobium column.

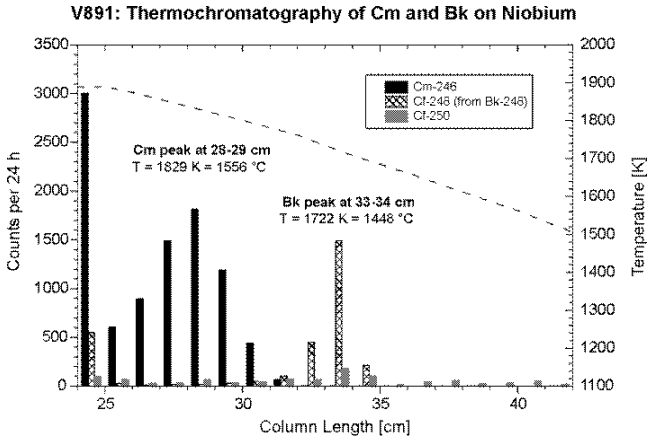


Fig. 1: Thermochromatogram of curium and berkelium on a niobium column

We assign the $^{248}$Cf to the daughter activity of $^{248}$Bk for two reasons:

It is known from previous experiments /2/ that the Cf deposition temperature under similar conditions is about 1200 K, far below the range covered in this experiment.

$^{252}$Cf, as the main californium transfer product of the used nuclear reaction /5/, is not present. The $^{248}$Cf is therefore the decay product of the short-lived $^{248}$Bk and represents the Bk chromatographic peak.

Fig. 2 shows the experimentally determined adsorption enthalpies /6/ of berkelium and curium on niobium in comparison to earlier experimental data /1, 2, 3, 4/ and EICHLER-MIEDEMA model calculations.

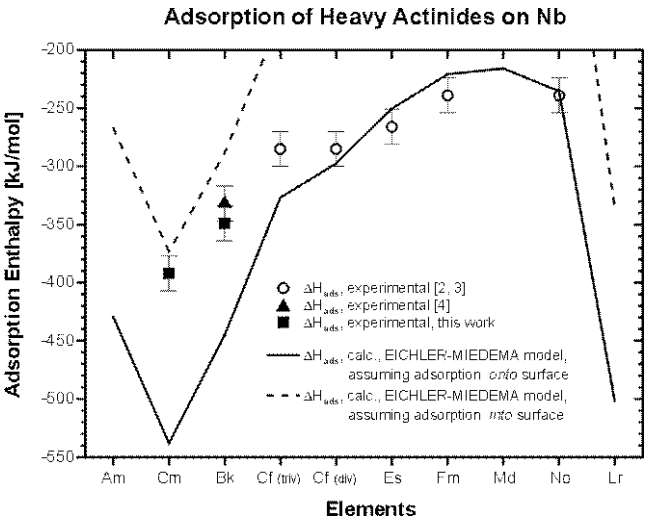


Fig. 2: Adsorption enthalpies of actinides on niobium and EICHLER-MIEDEMA model calculations /7/

## Acknowledgments

The support of Deutsche Forschungsgemeinschaft, contract Hu 642/1-2 is gratefully acknowledged.

## References

/1/ Taut, S., et al., Radiochimica Acta **78**, 33 (1997)
/2/ Taut, S., et al., J. Alloys. Comp. **271**, 316 (1998)
/3/ Taut, S., et al., Report FZR-218 (1998) p.84
/4/ Hübener, S., et al., this report p. 82
/5/ Lee, D., et al., Phys. Rev. **C 27**, 2656 (1983)
/6/ Eichler, B., et al., Radiochimica Acta **30**, 233 (1982)
/7/ Eichler, B., Report ZfK-396 (1979)

# HITGAS EFFICIENCY IN THE SEABORGIUM OXIDE HYDROXIDE EXPERIMENT

S. Taut, R. Dressler, A. Vahle, S. Hübener, D. Jost [1], A. Türler [1]
[1] Paul Scherrer Institut Villigen (CH)

*The chemical efficiency of the high temperature gas chromatography apparatus HITGAS in the seaborgium oxide hydroxide experiment is calculated with the spectra from tungsten isotopes which are produced as monitor nuclides during the seaborgium experiment.*

## Introduction

A first determination of the chemistry efficiency of the high temperature gas chromatography apparatus HITGAS /1/ for the group 6 oxide hydroxide system was carried out in /2/. We obtained 53 % and 63 % efficiency for $^{166}$W and $^{168}$W, resp., for 1350 K isothermal temperature.
Unfortunately, this approach requires similar pressures in the target chamber in both experiment parts of /2/ because the attachment of the nuclear reaction products onto aerosols is pressure dependent. This could not be adjusted in our seaborgium experiment /1/.

## Algorithm

We estimated the HITGAS efficiency from on-line gamma spectra with the following quantities:

| | |
|---|---|
| $fh; r$ | indices indicating filter holder and ROMA |
| $\dot{n}$ | nuclide production rate |
| $n_0$ | number of atoms collected during $t_{coll,r}$ |
| $\lambda$ | nuclide decay constant |
| $t_{coll,x}$ | sample collection period; $x$ = $fh$, $r$ |
| $t_{jet}$ | gas jet transport time |
| $t_{step}$ | duration of ROMA step movement |
| $t_{int}$ | ROMA step interval length; $t_{int} = t_{coll,r} + t_{step}$ |
| $\varepsilon_{det,x}$ | detection efficiency; $x$ = $fh$, $r$ |
| $\varepsilon_{jet}$ | gas jet efficiency |
| $\varepsilon_{hitgas}$ | chemistry efficiency of HITGAS |
| $J$ | number of ROMA detection places |
| $J+1$ | number of ROMA deposition places |
| $K$ | actual ROMA detector place |
| $L$ | number of ROMA wheel rotations during $t_{coll,r}$ |
| $N$ | number of ROMA deposition places which were counted $N$ times |
| $J+1-N$ | number of ROMA deposition places which were counted $(N-1)$ times |
| $D_x$ | number of detections during $t_{coll,x}$; $x$ = $fh$, $r$ |

In a first step, the production rate of the nuclide under study is determined with a catcher foil experiment.
In a following direct-catch experiment, the gas jet is directed to a glass fiber filter holder which activity is counted during the nuclide collection. Eq. 1 expresses the measured number of nuclide detection events. A simple rearrangement gives the gas jet efficiency.

$$D_{fh} = \dot{n} \cdot e^{-\lambda \cdot t_{jet}} \cdot \left( t_{coll,fh} - \frac{1 - e^{-\lambda \cdot t_{coll,fh}}}{\lambda} \right) \cdot \varepsilon_{det,fh} \cdot \varepsilon_{jet} \qquad (1)$$

Finally, the nuclide accumulation on the ROMA wheel is detected on-line during a HITGAS experiment. Eq. 2 describes the number of collected atoms in one ROMA deposition place during one sample collection period:

$$n_0 = \dot{n} \cdot \frac{1 - e^{-\lambda \cdot t_{coll,r}}}{\lambda} \cdot e^{-\lambda \cdot t_{jet}} \cdot \varepsilon_{jet} \cdot \varepsilon_{hitgas} \qquad (2)$$

This unknown number can be calculated from the number of detection events which are measured in the ROMA over a longer period (L wheel rotations) with eq. 3 and the abbreviations *a*, *b*, and *c*:

$$D_r = n_0 \cdot a \cdot [N \cdot b + (J + 1 - N) \cdot c] \qquad (3)$$

$$a = \frac{e^{-\lambda \cdot t_{step}} \cdot e^{-(K-1) \cdot \lambda \cdot t_{int}} \cdot (1 - e^{-\lambda \cdot t_{coll,r}}) \cdot \varepsilon_{det,r}}{1 - e^{-(J+1) \cdot \lambda \cdot t_{int}}} \qquad (4)$$

$$b = L - \frac{1 - e^{-L \cdot (J+1) \cdot \lambda \cdot t_{int}}}{e^{+(J+1) \cdot \lambda \cdot t_{int}} - 1} \qquad (5)$$

$$c = L - 1 - \frac{1 - e^{-(L-1) \cdot (J+1) \cdot \lambda \cdot t_{int}}}{e^{+(J+1) \cdot \lambda \cdot t_{int}} - 1} \qquad (6)$$

The HITGAS chemistry efficiency remains as the only unknown in eq. 2 and can be calculated easily.

## Results

The results are shown in the table below. The efficiency for $^{168}$W agrees very well with that determined in /2/. The low efficiency for $^{166}$W indicates a HITGAS dwell time between 10 and 20 seconds. This was already obtained with a yield curve Monte Carlo simulation in /2/. However, all tungsten peaks in the on-line gamma spectra of the seaborgium experiment /1/ had a poor signal-to-noise ratio. Therefore, we consider our results from /2/ to be more precise.

| Nuclide | Half Life [s] | HITGAS Efficiency |
|---|---|---|
| $^{166}$W | 18.8 | 30 % |
| $^{168}$W | 51 | 60 % |
| $^{169}$W | 76 | 40 % |
| $^{171B}$W | 642 | 50 % |

## Acknowledgments

We gratefully acknowledge the support by both the BMBF, contract 06DR 824, and GSI, contract DRNITK.

## References

/1/ Hübener, S., et al., PSI Annual Report 1998, Annex IIIA, 9
/2/ Vahle, A., et al., Radiochimica Acta **84**, 43 (1999)

# CHEMICAL INVESTIGATION OF BOHRIUM (Bh, ELEMENT 107)

R. Eichler, Ch. Düllmann, H.W. Gäggeler (Univ. Bern & PSI), B. Eichler, D.T. Jost, D. Piquet, L. Tobler, A. Türler, P. Zimmermann (PSI); T. Häfeli, V.M. Lavanchy (Univ.Bern); K.E. Gregorich, D.C. Hoffman, U. Kirbach, C.A. Laue, H. Nitsche, J. Patin, D. Strellis, P. Wilk (UCB & LBNL); R. Dressler (TU Dresden), S. Hübener, S. Taut, A. Vahle (FZR); W. Brüchle, M. Schädel (GSI); Y. Tsyganov, A.B. Yakushev (JINR)

*Neutron-rich nuclides of bohrium were produced in the reaction 249Bk(22Ne,4n-5n)266,267Bh at the PSI Philips cyclotron. Bh was separated from other reaction products in a remotely controlled low temperature OLGA III set-up in the form of volatile oxychloride. The detection of genetically linked α-decay chains of 267Bh was accomplished using the ROMA detection system.*

The neutron-rich $^{266,267}$Bh have been discovered in spring of 1999 in a joint experiment performed at the Lawrence Berkeley National Laboratory /1/. These Bh nuclides were formed in the heavy ion induced "hot" fusion reaction $^{249}$Bk($^{22}$Ne;4,5n)$^{267,266}$Bh. The half-life of ~17 s for $^{267}$Bh and the production cross section of about 50 pb make $^{267}$Bh an ideal candidate to be used for gas phase chemical studies.

Assuming Bh to be a member of group 7 in the Periodic Table, a suitable chemical isolation procedure was developed in several model experiments using various nuclides of Tc and Re /2,3,4/. In thermochromatography experiments with trace amounts of $^{101,104}$Tc and $^{183,184}$Re in the reactive gas mixture $HCl/O_2$ in quartz columns the formation of only one single volatile compound was observed, which was interpreted as the formation of $MO_3Cl$ (M = Tc, Re) molecules. Volatile oxychlorides were formed also on-line with short-lived nuclides $^{108}$Tc ($t_{½}$ = 5.2 s) and $^{169}$Re ($t_{½}$ = 16 s), Fig.1.

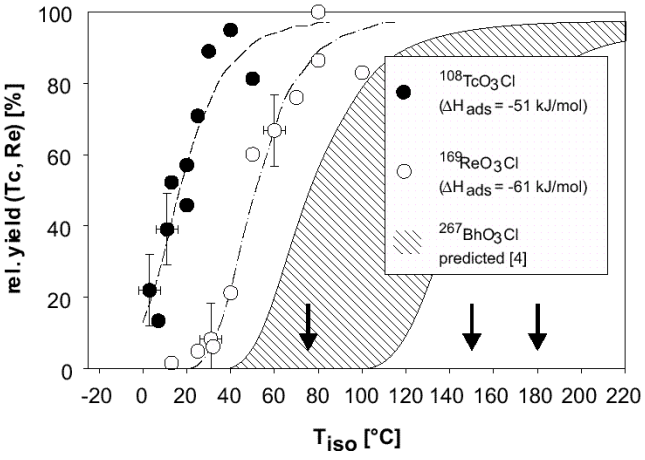


Fig. 1: Rel. yield vs. $T_{iso}$ for $^{108}TcO_3Cl$ and $^{169}ReO_3Cl$. The arrows indicate isothermal temperatures, at which the retention behavior of Bh-oxychloride was studied.

Between August 20th and September 26th a 670 mg/cm$^2$ $^{249}$Bk target, prepared by LBNL, was irradiated with a total beam dose of 3.02*10$^{18}$ $^{22}Ne^{6+}$ particles at a beam energy of 118 MeV and an average intensity of about 250 pnA. The recoiling reaction products were thermalised and transported with a 1 l/min He/C aerosol gas jet to the reaction oven of the 3 m distant remotely controlled /5/ low temperature OLGA III setup. A reactive gas mixture of 50 ml/min HCl and 50 ml/min $O_2$ was added in order to oxidise the C aerosols and to form oxychloride compounds. Volatile compounds were separated from less volatile compounds in the adjoining isothermal section (1.5 m length, 1.5 mm i.d.) of the quartz chromatography column depending on their adsorption behaviour and half-life of the nuclide. This section was kept at three different isothermal temperatures (Tab.1, $T_{iso}$). After passing the column the isolated products were re-attached to a 1 l/min He/CsCl gas jet in the recluster chamber and transported to the ROtating wheel Multidetector Analyser (ROMA). The aerosol particles were impacted in vacuum (~5 mbar) on thin (30-40 mg/cm$^2$) polyethylene foils, which were mounted on the circumference of the wheel. The stepping time was 10 s. Each of the collected samples was then measured between 12 pairs of PIPS-detectors for α- and sf-decays. Since the target contained 100 mg/cm$^2$ $^{159}$Tb, $^{176}$Re was also produced, serving as a yield monitor for the chemical separation. The overall yield of the whole separation process from thermalisation of the recoiling $^{176}$Re to the collection of the CsCl aerosols in the ROMA setup was determined to be about 16%.

The detection efficiency for an α- or sf-decay was about 70%. Six correlated decay chains, which are directly linked to the decay of $^{267}$Bh /6/, were detected.

Table 1: Experimental conditions.

| $T_{iso}$ [°C] | Beam dose *10$^{18}$ $^{22}Ne^{6+}$ | Samples (measured foils) |
|---|---|---|
| 180°C | 1.02 | 62285 |
| 150°C | 1.00 | 57652 |
| 75°C | 1.00 | 57740 |

Acknowledgments

We are indebted to the US DOE for making the $^{249}$Bk target material available through the transplutonium element program at Oak Ridge National Laboratory. We thank the staff of the PSI Philips cyclotron for providing intense beams of $^{22}$Ne.

References

/1/ Wilk, P., et al., PSI-Annual Report 1999
/2/ Eichler, R. et al., PSI-Scient. Report 1998 (1999) p.123
/3/ Eichler, R., et al., submitted to Radiochimica acta
/4/ Eichler, R., et al., PSI-Annual Report 1999, p. 10
/5/ Jost, D.T., et al., PSI-Annual Report 1999, p. 15
/6/ Eichler, R., et al., PSI-Annual Report 1999, p. 3

# RESULTS OF A PRELIMINARY ANALYSIS OF THE BOHRIUM EXPERIMENT

R. Eichler, Ch. Düllmann, H.W. Gäggeler (Univ. Bern & PSI), B. Eichler, D.T. Jost, D. Piquet, L. Tobler, A. Türler, P. Zimmermann (PSI);T. Häfeli, V.M. Lavanchy (Univ.Bern);K.E. Gregorich, D.C. Hoffman, U. Kirbach, C.A. Laue, H. Nitsche, J. Patin, D. Strellis, P. Wilk (UCB & LBNL); R. Dressler (TU Dresden), S. Hübener, S. Taut, A. Vahle (FZR;) W. Brüchle, M. Schädel (GSI); Y. Tsyganov, A.B. Yakushev (JINR)

*With the observation of 6 decay chains, starting with the decay of $^{267}$Bh after chemical separation, we conclude that Bh forms a volatile oxychloride, presumably $BhO_3Cl$. Bh behaves therefore like a typical member of group 7 of the Periodic Table. From the yield observed at three different isothermal temperatures $BhO_3Cl$ appears to be less volatile than its lighter homologues $TcO_3Cl$ and $ReO_3Cl$. A standard adsorption enthalpy on quartz surface $Dh_{ads}(BhO_3Cl)$ = -77 (+10 -8) kJ/mol was evaluated from the experimental data.*

The nuclide $^{267}$Bh was produced at the PSI Philips cyclotron in the reaction $^{249}$Bk($^{22}$Ne;4n)$^{267}$Bh and chemically isolated as volatile oxychloride using the On-line Gas Chromatography Apparatus OLGA /1/.

A total of 6 correlated decay chains attributed to the decay of $^{267}$Bh were observed and listed in Tab.1 together with the evaluated number of expected random events (NR).

Tab. 1: Correlated decay chains related directly to the decay of $^{267}$Bh detected after the chemical separation

| $T_{iso}$ [°C] | beam dose: $^{22}Ne^{6+}$ | Decay chain | $E_{\alpha1}$ [MeV] | $t_1$ [s] | $E_{\alpha2}$ [MeV] | $\Delta t_2$ [s] | $E_{\alpha3}$ [MeV] | $\Delta t_3$ [s] | Decay assignment | $N_R$ |
|---|---|---|---|---|---|---|---|---|---|---|
| 180°C | $1.02*10^{18}$ | 1 | 8.84 | 26.7 | 8.35 | 73.4 | | | $^{267}$Bh → $^{263}$Db or $^{259}$Lr | 1.2 |
| | | 2 | 8.72 | 2.9 | 8.40 | 29.9 | | | $^{267}$Bh → $^{263}$Db or $^{259}$Lr | |
| | | 3 | 8.81 | 18.4 | 101 | 16.3 | | | $^{267}$Bh → $^{263}$Db or $^{259}$Lr | |
| | | | | | 86 | | | | | 0.1 |
| | | 4 | 8.91 | 10.5 | 8.37 | 0.8 | 8.41 | 14.6 | $^{267}$Bh → $^{263}$Db → $^{259}$Lr | 0.001 |
| 150°C | $1.00*10^{18}$ | 5 | 8.81 | 24.5 | 82 | 21.1 | | | $^{267}$Bh → $^{263}$Db or $^{259}$Lr | 0.1 |
| | | 6 | 8.85 | 34.4 | 46 | 98.9 | | | $^{267}$Bh → $^{263}$Db or $^{259}$Lr | |
| 75°C | $1.00*10^{18}$ | - | - | - | - | - | - | - | - | |

At 180°C and 150°C isothermal temperature ($T_{iso}$) 4 and 2 events were detected, respectively. At 75°C no event was registered. The unambiguous identification of Bh after chemical separation allows to conclude that Bh like its lighter homologues forms a volatile oxychloride compound, presumably $BhO_3Cl$ and behaves like a typical member of group 7 of the Periodic Table.

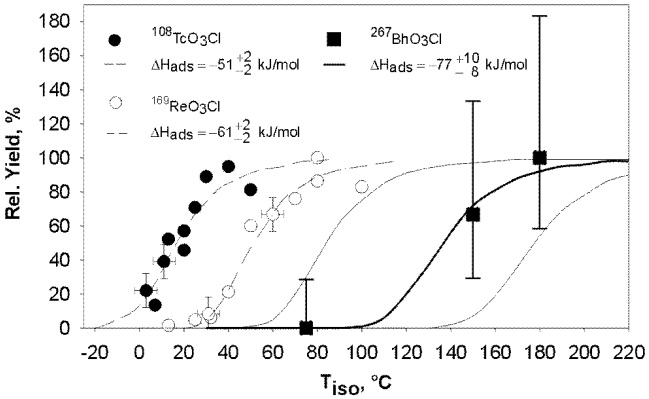


Fig. 1: Yield vs. isothermal temperature curves for the oxychlorides of $^{108}$Tc ($t_{½}$=5.2 s), $^{169}$Re ($t_{½}$=16 s), and $^{267}$Bh ($t_{½}$=17 s).
Symbols: experimental data with 1σ error bars. Lines: Monte Carlo model /2/ with 1σ error range (thin lines).

The relative yields of Bh are shown in Fig. 1 together with the yield vs. isothermal temperature curves of the corresponding compounds of Tc and Re. Assuming the Bh compound to be $BhO_3Cl$ and applying a microscopic model of the adsorption process developed by Zvara /2/, we evaluated the standard adsorption enthalpy of $BhO_3Cl$ on the quartz surface $\Delta H_{ads}(BhO_3Cl) = -77\ (+10\ -8)$ kJ/mol (68%c.i.).
The series of the adsorption enthalpies of group 7 oxychlorides $MO_3Cl$ (M – Tc, Re, Bh) on quartz yields the sequence Tc > Re > Bh. This sequence can also be expected from stability trends in the Periodic Table. In our experiment $BhO_3Cl$ was reclustered with CsCl. This is an additional indication that $BhO_3Cl$ is more similar to $ReO_3Cl$ than to $TcO_3Cl$ since $TcO_3Cl$ could only be reclustered with $FeCl_2$-aerosol particles /3/.

Acknowledgments
We are indebted to the US DOE for making the $^{249}$Bk target material available through the transplutonium element program at Oak Ridge National Laboratory. We thank the staff of the PSI Philips cyclotron for providing intense beams of $^{22}$Ne. This work was supported by the Swiss National Science Foundation.

References
/1/ Eichler, R., et al., this report p. 85
/2/ Zvara, I., Radiochimica Acta **38**, 95 (1982)
/3/ Eichler, R., et al., PSI-Annual Report 1999, p. 10

# II. PUBLICATIONS, PATENTS, LECTURES AND POSTERS

## PUBLICATIONS


Abram, U., Dilworth, J.R.
Technetium Complexes with 2-Mercaptomethyltetrazolate
Z. Anorg. Allg. Chem. **625**, 609 (1999)

Abram, U., Schmidt-Brücken, B., Ritter, S.
Reactions of [ReN(Cl)($Me_2PhP$)$_2$($HEt_2tcb$)] with Lewis Acids. Characterization and Structures of [Re($NBBr_3$)$Br_2$($Me_2PhP$)$_3$], [Re{$N(C_6F_5)_3$}Cl($Me_2PhP$)$_2$($HEt_2tcb$)] and [Re($NGaCl_3$)Cl($Me_2PhP$)$_2$($H_2Et_2tcb$)][$GaCl_4$] ($H_2Et_2tcb$ = N,N-diethylthiocarbamoylbenzamidine)
Polyhedron **18**, 831 (1999)

Abram, U.
[Re{$NB(C_6F_5)_3$($Et_2dtc$)$_2$]$_2$ – Dimerisierung als Folge der Ausbildung einer Nitridobrücke
Z. anorg. allg. Chem. **625**, 839 (1999)

Abram, U.
[Re($NBH_2SBH_3$)($Me_2PhP$)($Et_2dtc$)]$_2$ – A Novel Rhenium Dimer with the Unusual Bridging $(NBH_2SBH_3)^{4-}$ Ligand
Inorg. Chem. Communications **2**, 227 (1999)

Abram, U., Bonfada, E., Schulz-Lang, E.
Bis{2-[1-(thiosemicarbazono)ethyl]pyridinium}hexakis(nitrato-O,O')thorate(IV)tetramethanol solvate
Acta Cryst. **C55**, 1479 (1999)

Abram, U., Alberto, R., Ortner, K., Yifan Zheng, Dilworth, J.R.
Technetium and Rhenium Complexes with Diphenyl(pyridyl)phosphine
Polyhedron **18**, 1995 (1999)

Arnold, T., Zorn, T., Bernhard, G.
Modelling sorption of uranyl onto quartz and muscovite. In: Mineral/Water Interactions Close to Equilibrium.
Report FZKA 6291, Forschungszentrum Karlsruhe, (1999) p. 155-159

Alberto, R., Schibli, R., Waibel, W., Abram, U., Schubiger, A.P.
Basic Aqueous Chemistry of $[M(OH_2)(CO)_3]^+$ (M = Re, Tc) Directed Towards Radiopharmaceutical Application
Coord. Chem. Rev. **190-192**, 901 (1999)

Alberto, R., Schibli, R., Schubiger, A.P., Abram, U., Pietzsch, H.-J., Johannsen, B.
First Application of *fac*-[$^{99m}Tc(OH_2)(CO)_3]^+$ in Bioorganometallic Chemistry: Design, Structure, and in Vitro Affinity of a 5-$HT_{1A}$ Receptor Ligand Labelled with $^{99m}Tc$
J. Am. Chem. Soc. **121**, 6076 (1999)

Alberto, R., Schibli, R., Egli, A., Schubiger, A.P., Abram, U., Kaden, T.A.
A Novel Organometallic Aqua Complex of Technetium for the Labelling of Biomolecules: Synthesis of [$^{99m}Tc(OH_2)(CO)_3]^+$ from [$^{99m}TcO_4]^-$ in Aqueous Solution and Its Reaction with a Bifunctional Ligand
J. Am. Chem. Soc. **120**, 7987 (1998)

Baraniak, L., Thieme, M., Bernhard, G., Nitsche, H.
Sorption Behaviour of Radium on Sandy and Clayey Sediments of the Upper Saxon Elbe River Valley
J. Radioanal. Nucl. Chem. **241**, No. 3 (1999)

Bolano, S., Bravo, J., Carballo, R., Garcia-Fontan, S., Abram, U., Vazquez-Lopez, E.
Synthesis and Characterization of the Bromo and Hydrido Derivatives of Rhenium(I) 1,2-bis(diphenylphosphito) ethane Complexes
Polyhedron **18**, 1431 (1999)

Bonfada, E., Maichle-Mößmer, C., Strähle, J., Abram, U.
Synthese, Charakterisierung und Struktur von Carbonyl- und Hydrido-Isocyanatokomplexen des Rutheniums
Z. anorg. allg. Chem. **625**, 1327 (1999)

Carballo, R., Cabaleiro, S., Garcia-Fontan, S., Abram, U., Vazquez-Lopez, E.M.
Synthesis, Characterization and Crystal and Molecular Structures of the Novel Rhenium(IV) Complexes *trans*-[$ReCl_4${$PPh_2$(OMe)}$_2$], *trans*-[$ReCl_4${$PPh_2$(OEt)}$_2$] and *trans*-[$ReCl_4(OPPh_3)_2$]
Polyhedron **18**, 1431 (1999)

Dressler, R., Eichler, B., Jost, D.T., Pignet, D., Türler, A., Düllmann, Ch., Eichler, R., Gäggeler, H.W., Gärtner, M., Schädel, M., Taut, S., Yakushev, A.B.
Production of $^{262}Db$ (Z = 105) in the Reaction $^{248}Cm$ ($^{19}F$, Sn)
Phys. Rev. C **59**, 3433 (1999)

Funke, H., Reich, T., Bernhard, G., Brendler, V., Claussner, J., Hüttig, G., Matz, W., Neumann, W., Oehme, W.
The radiochemistry experimental station at the Rossendorf Beamline

Proceedings Workshop: “Speciation, Techniques and Facilities for Radioactive Materials at Synchrotron Light Sources”, Grenoble; France, 4-6 October 1998, OECD/NEA Paris, France, p.181-187 (1999)

Hennig, C., Nolze, G.
Characterization of the preferred orientation in EXAFS-samples using Bragg-Brentano x-ray diffraction
Proceedings Workshop: “Speciation, Techniques and Facilities for Radioactive Materials at Synchrotron Light Sources”, Grenoble; France, 4-6 October 1998, OECD/NEA Paris, France, p.235-243 (1999)

Hennig, C., Hallmeier, K.-H., Zahn, G., Tschwatschal, F., Hennig, H.
Conformational Influence of Dithiocarbazinic Acid Bishydrazone Ligands on the Structure of Zinc(II) Complexes: A Comparative XANES Study
Inorg. Chem. **38**, 38 (1999)

Hennig, C., Nolze, G.
Texture Analysis of EXAFS-Samples using the Rietveld Method (Abstract)
Z. Krist. Suppl. **16**, 157 (1999)

Hennig, C., Reich, T., Roßberg, A., Funke, H., Rutsch, M., Geipel, G., Nitsche, H., Bernhard, G.
Local Structure Analysis of Uranium Phosphates and Arsenates using EXAFS Spectroscopy (Abstract)
Z. Krist. Suppl. **16**, 158 (1999)

Hudson, E.A., Terminello, L.J., Viani, B.E., Denecke, M., Reich, T., Allen, P.G., Bucher, J.J., Shuh, D.K., Edelstein, N.M.
The structure of $U^{6+}$ sorption complexes on vermiculite and hydrobiotite
Clays and Clay Minerals **47**, 439-457 (1999)

Jackson, D., Wragg, S.K., Bousher, A., Zeevaert, T., Stiglund, Y., Brendler, V., Hedemann Jensen, P., Nordlinder, S.
Establishing a method for assessing and ranking restoration strategies for radioactively contaminated sites and their close surroundings
Nuclear Energy **38**, 223-231(1999)

Kramer, A., Alberto, R., Egli, A., Novack-Hofer, I., Hegetschweiler, K., Abram, U., Bernhardt, P.V., Schubiger, P.A.
Derivatives of 1,3,5-Triamino-1,3,5-trideoxy-cis-inositol as Versatile Pentadentate Ligands for Protein Labeling with Re-186/188. Prelabeling, Biodistribution and X-Ray Structural Studies.
J. Bioconjugate Chem. **9**, 691 (1998)

Legin, A.V., Selenzev, B.L., Rudnitskaya, A.M., Vlasov, Yu.G., Mack, B., Abraham, A., Arnold, T., Baraniak, L., Nitsche, H.
Multisensor System for Determination of Iron(II), Iron(III), Uranium(VI) in Complex Solutions
Czech. J. Physics **49**, 679-685 (1999)

Lukens, W.W., Allen, P.G., Bucher, J.J., Edelstein, N.M., Hudson, E.A., Shuh, D.K., Reich, T., Andersen, R.A.
Structures of substituted-cyclopentadienyl uranium(III) dimers and related uranium metallocenec deduced by EXAFS
Organometallics **18**, 1253 (1999)

Matz, W., Schell, N., Bernhard, G., Prokert, F., Reich, T., Claußner, J., Oehme, W., Schlenk, R., Dienel, S., Funke, H., Eichhorn, F., Betzl, M., Pröhl, D., Strauch, U., Hüttig, G., Krug, H., Neumann, W., Brendler, V., Reichel, P., Denecke, M.A., Nitsche, H.
ROBL - a CRG beamline for radiochemistry and materials research at the ESRF
Journal of Synchrotron Radiation **6**, 1076-1085 (1999)

Mertig, M., Klemm, D., Pompe, W., Zänker, H., Böttger, M.
Scanning Force Microscopy of Spin-Coated Humic Acid
Surface and Interface Analysis **27**, 426-432 (1999)

Miteva, V., Selenska-Pobell, S., Mitev, V.
Random and repetitive primer amplified polymorphic DNA analysis of *Bacillus sphaericus*
J. of Appl. Microbiology **86**, 928-936 (1999)

Nebelung, C., Nitsche, H.
Stillegung und Rückbau: Direktmessung alpha-aktiver Nuklide in Bauschutt zur Freigabeentscheidung
Schlußbericht zum Fördervorhaben BMBF 02 S 7655 / 02 S 7655A
Rossendorf 1999

Nitsche, H., Silva, R.J., Brendler, V., Geipel, G., Reich, T., Teterin, Y.A., Thieme, M., Baraniak, L., Bernhard, G.
Modern Speciation Techniques Applied to Environmental Systems

in: D.T. Reed, S. Clark and L. Rao (Eds).: "Actinide Speciation in High Tonic Strength Media"
Plenum Publishing Corp., New York, 1999, p.11-38

Nitsche, H., Reich, T., Hennig, C., Roßberg, A., Geipel, G., Denecke, M.A., Baraniak, L., Panak, P., Abraham, A., Mack, B., Selenska-Pobell, S., Bernhard, G.
Application of synchrotron radiation techniques to radionuclide studies
Proceedings Workshop: “Speciation, Techniques and Facilities for Radioactive Materials at Synchrotron Light Sources”, Grenoble; France, 4-6 October 1998, OECD/NEA Paris, France, p.15-27 (1999)

Oppermann, H., von Woedtke, F., Reich, T., Denecke, M.A., Nitsche, H., Doerr, M.
Phase relations in the system V/Nb/$O_2$: V. Investigation of mixed crystals $V_{1-x}Nb_xO_2$
Fresenius J. Anal. Chem. **363**, 202 (1999)

Ortner, K., Hilditch, L., Dilworth, J.R., Abram, U.
Stabilisation of gold(I) and gold(III) in the same complex molecule by a tridentate phosphinothiolate ligand. Structures of [$Au^{III}LCl$] and [$Au^{I}L_2Au^{III}$] [L = {$PhP(C_6H_3$-S-2-$SiMe_3$-3)$_2$}$^{2-}$]
Inorg. Chem. Commun. **1**, 469 (1998)

Ortner, K., Abram, U.
Gold(III) complexes with Diphenylthiocarbazonate. Synthesis and Structures of [Au(Hdamp-$C^1$){PhNHNC(S) NNPh}Cl]Cl x $H_2O$ and [Au(Hdamp-$C^1$){PhNNC(S)NNPh}(Smetetraz)] (Hdamp-$C^1$ = 2-(dimethylaminomethyl) phenyl, Sme tetraz = 2-methylmercaptotetrazolate)
Polyhedron **18**, 749 (1999)

Panak, P., Selenska-Pobell, S., Kutschke, S., Geipel, G., Bernhard, G., Nitsche, H.
Complexation of uranium with the cells of *Thiobacillus ferrooxidans* and *Thiomonas cuprina*.
Radiochim. Acta **84**, 183-186 (1999)

Pompe, S., Artinger, R., Schmeide, K., Heise, K.H., Kim, J.I., Bernhard, G.
Investigation of the Migration Behavior of Uranium in an Aquifer System Rich in Humic Substances: Laboratory Column Experiments.
Report FZKA 6324, Forschungszentrum Karlsruhe, S.219-243 (1999)

Pompe, S., Bubner, M., Schmeide, K., Heise, K.H., Bernhard, G., Nitsche, H.
Influence of Humic Acid on the Migration Behavior of Radioactive and Non-Radioactive Substances under Conditions Close to Nature. Synthesis, Radiometric Determination of Functional Groups, Complexation.
Final Report BMBF Project No. 02E88150 (1999)

Reich, T., Moll, H., Arnold, T., Denecke, M.A., Hennig, C., Geipel, G., Bernhard, G., Nitsche, H., Allen, P.G., Bucher, J.J., Edelstein, N.M., Shuh, D.K.
An EXAFS study of uranium(VI) sorption onto silica gel and ferrihydrite
J. Electron Spectrosc. Related Phenom. **96**, 237 (1998)

Reich, T., Moll, H., Arnold, T., Denecke, M.A., Hennig, C., Geipel, G., Bernhard, G., Nitsche, H., Allen, P.G., Bucher, J.J., Edelstein, N.M., Shuh, D.K.
EXAFS studies of uranium(VI) sorption on mineral surfaces
Proceedings Workshop: “Speciation, Techniques and Facilities for Radioactive Materials at Synchrotron Light Sources”, Grenoble; France, 4-6 October 1998, OECD/NEA Paris, France, p.83-92 (1999)

Reich, T., Brendler, V., Denecke, M.A., Bubner, M., Pompe, S., Nitsche, H.
Structural analysis of the interaction of uranium(VI) with humic acid and simple carboxylic acids using EXAFS
Proceedings Workshop: “Speciation, Techniques and Facilities for Radioactive Materials at Synchrotron Light Sources”, Grenoble; France, 4-6 October 1998, OECD/NEA Paris, France, p.277-283 (1999)

Reich, T.
Euroconference and NEA Workshop Actinide-XAS-98
ESRF Newsletter **32**, 7 (1999)

Rutsch, M., Geipel, G., Brendler, V., Bernhard, G., Nitsche, H.
Interaction of uranium(VI) with arsenate(V) in aqueous solution studied by time-resolved laser-induced fluorescence spectroscopy
Radiochimica Acta **86**, 135-141 (1999)

Schmeide, K., Zänker, H., Hüttig, G., Heise, K.H., Bernhard, G.
Complexation of Aquatic Humic Substances from the Bog “Kleiner Kranichsee” with Uranium(VI)
Report FZKA 6324, Forschungszentrum Karlsruhe, S.177-197 (1999)

Schmeide, K., Jander, R., Heise, K.H., Bernhard, G.
Effect of Humic Acid on the Uranium(VI) Sorption onto Phyllite and its Mineralogical Constituents
Report FZKA 6324, Forschungszentrum Karlsruhe, S.199-218 (1999)

Schulz-Lang, E., Abram, U., Strähle, J., Vazquez-Lopez, E.M.
Synthesis and Structure of $(NH_4)_2[(AuI_4)(MI_4)]$ (M = Ga, In)
Z. Anorg. Allg. Chem. **625**, 359 (1999)

Schulz-Lang, E., Dahmer, M., Abram, U.
Tetraphenylphosphonium tetra(1-methyl-1,2,3,4-tetrazole-5-thiolato)aurate(III)hemihydrat
Acta Cryst. **C55**, 854 (1999)

Schulz-Lang, E., Fernandez Jr., R.M., Silveira, E.T., Abram, U., Vazquez-Lopez, E.
Structures of Iodophenyltellurium(II) and Diiododi-($-naphtyltellurium(IV)
Z. anorg. allg. Chem. **625**, 1401 (1999)

Selenska-Pobell, S., Panak, P., Miteva, V., Boudakov, I., Bernhard, G., Nitsche, H.
Selective accumulation of heavy metals by three indigenous *Bacillus* strains, *B. cereus, B. megaterium* and *B. sphaericus,* from drain waters of a uranium waste pile
FEMS Microbiology Ecology **29**, 59-67 (1999)

Teterin, Yu.A., Nefedov, V.I., Teterin, A.Yu., Lebedev, A.M., Dementjev, A.P., Utkin, I.O., Bubner, M., Reich, T., Pompe, S., Heise, K.H., Nitsche, H.
Investigation of the interaction of the uranyl group $UO_2^{2+}$ and Fe(III) with natural humic acid in aqueous solution by x-ray photoelectron spectroscopy (in Russian)
Zh. Neorg. Khimii **44**, 593-597 (1999)

Teterin, Yu.A., Teterin, A.Yu., Lebedev, A.M., Dementjev, A.P., Utkin, I.O., Nefedov, V.I., Bubner, M., Reich, T., Pompe, S., Heise, K.H., Nitsche, H.
X-ray Photoelectron Spectroscopy Investigation of the Interaction of UVI) and Fe(III) with Natural Humic Acid in Aqueous Solutions
J. Prakt. Chem. **341**, 773 (1999)

Türler, A., Brüchle, W., Dressler, R., Eichler, B., Gäggeler, H.W., Gärtner, M., Glatz, J.-P., Gregorich, K.E., Hübener, S., Jost, D.T., Lebeder, V.Y., Pershina, V.G., Schädel, M., Taut, S., Timokhin, S.N., Trautmann, N., Vahle, A., Yakusher, A.B.
Erste experimentelle Bestimmung einer thermochemischen Größe einer Seaborgiumverbindung
Angew. Chemie **111**, 2349 (1999); Angew. Chem. Int. Ed. **38**, 2212 (1999)

Vahle, A., Hübener, S., Funke, H., Eichler, B., Jost, D.T., Türler, A., Brüchle, W., Jäger, E.
Gas Chromatographic Studies of Oxide and Hydroxide Species of Tungsten - Model Experiments with Respect to the Physico-Chemical Characterization of Seaborgium (Element 106)
Radiochim. Acta **84**, 43-51 (1999)

Voigt, A., Abram, U., Böttcher, R., Strauch, P., Kirmse, R.
X-Band, Q-band EPR and EHT-MO calculations on $[Re^{II}(NO)Cl_2(OPPh_3)_3][ReO_4]$
Inorg. Chem. Communications **1**, 389 (1998)

Voigt, A., Abram, U., Kirmse, R.
Zur Existenz von $[ReNCl_{4-n}F_n]$- (n = 1-3) Nitridorhenat(VI)-Gemischtligandkomplexen - eine EPR-Untersuchung
Z. Naturforsch. **53b**, 1183 (1998)

Voigt, A., Abram, U., Kirmse, R.
Darstellung, Strukturen, und EPR-Spektren der Rhenium(II)-Thionitrosylkomplexe *trans*-$[Re(NS)Cl_3(MePh_2P)_2]$ und trans-$[Re(NS)Br_3(Me_2PhP)_2]$
Z. Anorg. Allg. Chem. , 1658 (1999)

Waibel, R., Alberto, R., Willuda, J., Finnern, R., Schibli, R., Stichelberger, A., Egli, A., Abram, U., Mach, J.-P., Plückthun, A., Schubiger, P.A.
Stable one-step technetium-99m labeling of His-tagged recombinant proteins with a novel Tc(I)-carbonyl complex
Nature Biotechnology **17**, 897 (1999)

Wragg, S.K., Jackson, D., Bousher, A., Zeevaert, T., Stiglund. Y., Nordlinder, S., Brendler, V., Jensen, P.H.
Remediation Strategies for Radioactively Contaminated Sites and their Close Surroundings (RESTRAT)
Southport International Symposium - Achievements & Challenges: Advancing Radiation Protection into the 21st Century
Society for Radiological Protection Conference Proceedings, Southport, 1999

Zänker, H., Mertig, M., Böttger, M., Hüttig, G.
The Colloidal States of Humic Acid
Report FZKA 6324, Forschungszentrum Karlsruhe, S.155-175 (1999)

Zimmermann, Th., Schmidt, K., Abram, U.
Ring Transformations of Heterocyclic Compounds. XVI [1]. Spiro[cyclohexadiene-dihydroacridines] - A Novel

Class of Spirodihydroacridines by Ring Transformation of Pyrylium Salts with 9-Methylacridine and ist Quarternary Salts
J. Heterocyclic Chem. **35**, 787 (1998)

## LECTURES

Arnold, T., Zorn, T., Bernhard, G.
Modelling Sorption of Uranyl onto Quartz and Muscovite
Münster Workshop on Mineral Surface Science
Münster, Germany, 22.-24.03.1999

Arnold, T., Zorn, T., Zänker, H., Bernhard, G., Nitsche, H.
Sorption Behavior of U(VI) on Phyllite: Experiments and Modeling
Migration '99, 7th International Conference on the Chemistry and Migration Behavior of Actinides and Fission Products in the Geosphere
Lake Tahoe, Nevada/California, USA, 26.09.-01.10.1999

Bernhard, G.
Die Bestimmung der Speziation des Urans in erzbergbautypischen Wässern
Kolloquium "Anthropogen veränderte geologisch-biologische Stoffflüsse, untersucht an der ostthüringischen Uranbergbauregion"
Friedrich Schiller Universität
Jena, Germany, 12.01.1999

Bernhard, G.
Das Institut für Radiochemie im Überblick -Forschungsprofil-Struktur-Forschungsergebnisse -
Wissenschaftlicher Beirat des FZR
Rossendorf, Germany, 12.02.1999

Bernhard, G., Heise, K.H., Pompe, S.
Arbeiten des Instituts für Radiochemie zur Komplexierung von Actiniden mit Huminsäuren
Projekttreffen der Projektträger PTE
Leipzig, Germany, 02.06.1999

Bernhard, G.
Radionuklidmigration und ökologische Konsequenzen für Mensch und Umwelt
5. Symposium "Mensch - Umwelt"
Erfurt, Germany, 04.06.1999

Bernhard, G.
Vorkommen, Speziation und Transfer von Radionukliden in der Geo- und Biosphäre
Tharandter Biologisch-ökologische Kolloquien
TU Dresden, Institut für Allgemeine Ökologie und Umweltschutz
Tharandt, Germany, 17.06.1999

Bernhard, G.
Radioökologische Umweltforschung
Tagung Wissenschaftsgemeinschaft Gottfried Wilhelm Leibniz (WGL), Sektion E, Umweltwissenschaften
Berlin-Potsdam, Germany, 21.-22.06.1999

Bernhard, G.
Institute of Radiochemistry, Profile-Structure-Results
Meeting Bulgarian Academy of Science - Forschungszentrum Rossendorf
Sofia, Bulgaria, 01.11.1999

Brendler, V., Geipel, G., Reich, T., Rutsch, M., Pompe, S., Baraniak, L., Bernhard, G.
Radionuclide Speciation at Trace Levels: Laser & X-Ray Spectroscopies.
4th International Conference on Environmental Radioactivity in the Arctic / Pre-conference Workshop
Edinburgh, Scotland, 18.-19.09.1999

Brendler, V., Stiglund, Y., Nordlinder, S., Arnold, T., Bernhard, G.
Coupling geochemical speciation to risk assessment codes.
4th International Conference on Environmental Radioactivity in the Arctic
Edinburgh, Scotland, 20.-23.09.1999

Bubner, M., Pompe, S., Schmeide, K., Amayri, S., Reich, T., Nefedov, V.I., Heise, K.H., Bernhard, G.
Untersuchungen zur Bildung fester Metall-Huminsäure-Komplexe
Arbeitstagung der Deutschen Gesellschaft für Moor- und Torfkunde e.V.
Bad Elster, Germany, 07.-08.10.1999

Geipel, G.
Neue Komplexverbindungen des Urans -Uranylarsenatspezies-
Wissenschaftlicher Beirat des FZR
Rossendorf, Germany, 12.02.1999

Geipel, G., Bernhard, G., Brendler, V., Nitsche, H.
Complex Formation of Uranium(IV) with Phosphate studied by Laser Induced Photoacoustic Spectroscopy
Migration '99, 7th International Conference on the Chemistry and Migration Behavior of Actinides and Fission Products in the Geosphere
Lake Tahoe, Nevada/California, USA, 26.09.-01.10.1999

Heise, K.H., Nicolai, R., Pompe, S., Bubner, M., Klöcking, R., Bernhard, G.
FTIR-Untersuchungen zur Komplexierung von Uran(VI) durch Huminsäuren
Arbeitstagung der Deutschen Gesellschaft für Moor- und Torfkunde e.V.
Bad Elster, Germany, 07.-08.10.1999

Hennig, C., Nolze, G.
Texture Analysis of EXAFS-Samples using the Rietveld Method
DGK-Tagung
Leipzig, Germany, 08.-10.03.1999

Hübener, S.
Physico-Chemical Characterization of Seaborgium as Oxide Hydroxide
1st Int. Conf. On the Chemistry and Physics of the Transactinide Elements
Seeheim, Germany, 26.-30.09.1999

Nebelung, C., Henniger, J.
Actiniden Direktmessung im Beton zur Freigabeentscheidung - Fortschrittsbericht
Workshop "Freimessung und Verwertung von Beton"
Karlsruhe, Germany, 15.12.1999

Nitsche, H., Bernhard, G., Geipel, G., Rutsch, M., Heise, K.H., Pompe, S., Schmeide, K., Bubner, M., Arnold, T., Zorn, T., Baraniak, L., Abraham, A., Mack, B., Reich, T., Roßberg, A., Brendler, V., Zänker, H., Panak, P., Selenska-Pobell, S.
Uranium speciation in the aquatic environment: Convergence between modeling results and laboratory and field measurements
217th American Chemical Society National Meeting
Anaheim, CA, USA, 21.-25.03.1999

Panak, P., Raff, J., Selenska-Pobell, S., Geipel, G., Hennig, C., Reich, T., Bernhard, G., Nitsche, H.
Complex formation of U(VI) with bacillus isolates from a uranium mining waste pile
Migration '99, 7th International Conference on the Chemistry and Migration Behavior of Actinides and Fission Products in the Geosphere
Lake Tahoe, Nevada/California, USA, 26.09.-01.10.1999

Pompe, S., Bubner, M., Schmeide, K., Heise, K.H., Bernhard, G.
Einfluß von Huminstoffen auf das Migrationsverhalten radioaktiver und nichtradioaktiver Schadstoffe unter naturnahen Bedingungen. Überblick zu den Ergebnissen des Teilprojekts des Instituts für Radiochemie (Förderkennzeichen 02 E8815).
Fachgespräch zu FuE-Projekten zur Huminstoffkomplexierung von Radionukliden und Schwermetallen
IIF
Leipzig, Germany, 02.06.1999

Pompe, S., Artinger, R., Schmeide, K., Heise, K.H., Bernhard, G., Kim, J.I.
Investigation of the Migration Behavior of Uranium in an Aquifer System Rich in Humic Substances - Column Experiments
Workshop EU Projekte im Institut für Radiochemie, FZ Rossendorf e.V.
Rossendorf, Germany, 07.07.1999

Pompe, S., Schmeide, K., Bubner, M., Geipel, G., Heise, K.H., Bernhard, G., Nitsche, H.
Investigation of Humic Acid Complexation Behavior with $UO_2^{2+}$ Ions Using Modified Synthetic and Natural Humic Acids
Migration '99, 7th International Conference on the Chemistry and Migration Behavior of Actinides and Fission Products in the Geosphere
Lake Tahoe, Nevada/California, USA, 26.09.-01.10.1999

Pompe, S., Schmeide, K., Bubner, M., Geipel, G., Reich, T., Heise, K.H., Bernhard, G.
Untersuchungen des Einflusses phenolischer OH-Gruppen auf das Komplexierungsverhalten von Huminsäuren mit Uran(VI)

Arbeitstagung der Deutschen Gesellschaft für Moor- und Torfkunde e.V.
Bad Elster, Germany, 07.-08.10.1999

Pompe, S., Schmeide, K., Bubner, M., Geipel, G., Heise, K.H., Bernhard, G.
Study of the Influence of Phenolic OH Groups on the Complexation Behavior of Humic Acids with $UO_2^{2+}$ Ions Using Modified Humic Acids with Blocked Phenolic OH Groups and Preliminary Results of NMR Investigations on Humic Acids
Group Meeting, Florida State University, Department of Chemistry
Tallahassee, Florida, USA, 06.12.1999

Reich, T.
Environmental Radiochemistry at the Rossendorf Beam Line at ESRF
Paul Scherrer Institut
Villigen, Switzerland, 15.01.1999

Reich, T.
EXAFS-Strukturuntersuchungen an Uranylkomplexen von Huminsäure- und Lignin-Modellverbindungen
Wissenschaftlicher Beirat des FZR
Rossendorf, Germany, 12.02.1999

Reich, T.
X-Ray absorption spectroscopy of radionuclides at the Rossendorf Beamline
3rd Russian-German Seminar on Electron and X-ray Spectroscopy
Yekaterinburg, Russia, 15.-19.9.1999

Reich, T., Bernhard, G., Geipel, G., Funke, H., Hennig, C., Rossberg, A., Matz, W., Schell, N., Nitsche, H.
The Rossendorf Beamline ROBL – a dedicated experimental station for XAFS measurements of actinides
Migration '99, 7th International Conference on the Chemistry and Migration Behavior of Actinides and Fission Products in the Geosphere
Lake Tahoe, Nevada/California, USA, 26.09.-01.10.1999

Reich, T.
Scientific activities of the ROBL facility at the European Synchrotron Radiation Facility (ESRF)
Lawrence Berkeley National Laboratory, The Glenn T. Seaborg Center
Berkeley, CA, USA, 6.10.1999

Richter, W., Zänker, H., Brendler, V.
Kolloidchemische Untersuchungen an Wasser aus dem Hauptentwässerungsstollen des Freiberger Bergbaureviers
5. Kolloquium der DFG "Geochemische Prozesse mit Langzeitfolgen im anthropogen beeinflußten Sickerwasser und Grundwasser"
Bad Herrenalb, Germany, 25.-26.03.1999

Rutsch, M., Geipel, G., Bernhard, G.
Zeitaufgelöste Laserinduzierte Fluoreszenzspektroskopie zur Bestimmung der Komplexverbindungen des Urans am Beipiel der Uranylarsenatkomplexierung
Fresenius Analytische Tage Dresden
Dresden, Germany, 28.04.1999

Schmeide, K., Pompe, S., Bubner, M., Heise, K.H., Bernhard, G.
Uranium and Humic Acid Sorption onto Ferrihydrite and Phyllite in the Absence and Presence of Sulfate
Sixth EC Project Meeting 'Effects of Humic Substances on the Migration of Radionuclides: Complexation and Transport of Actinides', Forschungszentrum Karlsruhe, INE
Karlsruhe, Germany, 23.-24.11.1999

Schuster, G., Bubner, M., Henkel, K., Pompe, S., Schmeide, K., Jander, R., Heise, K.H., Bernhard, G.
Anwendung der thermischen Analyse zur Charakterisierung natürlicher und synthetischer Huminsäuren und ihrer Eisen(III)- und Uran(VI)-Komplexverbindungen
Arbeitstagung der Deutschen Gesellschaft für Moor- und Torfkunde e.V.
Bad Elster, Germany, 07.-08.10.1999

Selenska-Pobell, S.
Bakterien aus uranhaltigen Abfallhalden und ihre Wechselwirkung mit Uran
Wissenschaftlicher Beirat des FZR
Rossendorf, Germany, 12.02.1999

Selenska-Pobell, S.
Bacterial diversity and activity in soil and water samples of uranium mining waste piles
International Symposium on Bacterial Genetics and Ecology

Florence, Italy, 19.-24.06.1999

Selenska-Pobell, S., Flemming, K., Kutschke, S., Panak, P., Satschanska, G.
Bacterial diversity and activity in uranium waste piles
4th International Symposium on Subsurface Microbiology
Vail, Colorado, USA, 22.-27.08.1999

Selenska-Pobell S.
Molecular analysis of the natural bacterial communities in uranium wastes
Microbiologia Balcanica`99
Plovdiv, Bulgaria, 05.-09.10.1999

Taut, S.
Gas Chemical Characterization of Seaborgium as Oxide Hydroxide
SHEIKS Group Meeting, LBNL Berkeley
Berkeley, USA, 12.04.99

Zänker, H., Richter, W., Brendler, V.
Charakterisierung der Kolloidpartikel im Hauptentwässerungsstollen des Freiberger Bergbaureviers (Rothschönberger Stolln).
Jahrestagung der GDCh-Fachgruppe Wasserchemie
Regensburg, Germany, 10.-12.05.1999

Zänker, H., Mertig, M., Böttger, M., Hüttig, G., Pompe, S.
Photon Correlation Spectroscopy and Scanning Force Microscopy on Humic Acid
Arbeitstreffen EU-Projekt “Effects of Humic Substances on the Migration of Radionuclides: Complexation and Transport of Actinides” (Projekt Nr. FI4W-CT96-0027)
Rossendorf, Germany, 17.-19.05.1999

Zänker, H., Richter, W., Brendler, V.
Colloid-Borne Uranium and Other Heavy Metals in the Water of a Mine Drainage Gallery
Migration ’99, 7th International Conference on the Chemistry and Migration Behavior of Actinides and Fission Products in the Geosphere
Lake Tahoe, Nevada/California, USA, 26.09.-01.10.1999

Zorn, T., Arnold, T., Bernhard, G.
Sorption von Uran(VI) an das Gestein Phyllit - Experiment und Modellierung
Fresenius Analytische Tage in Dresden, XI. Radiochemische Methoden in der Analytik
Dresden, Germany, 26.04.1999

## POSTERS

Arnold, T., Zorn, T., Bernhard, G.
Modelling sorption of uranyl onto quartz and muscovite
Workshop “Mineral/Water Interactions Close to Equilibrium”, FZ Karlsruhe
Speyer, Germany, 25.-26.03.1999

Baraniak, L., Abraham, A., Mack, B., Geipel, G., Bernhard, G., Nitsche, H.
Reducing Behaviour of Natural Organic Matter and its Influence on the Uranium Moobility in Flooded Mines
Migration ’99, 7th International Conference on the Chemistry and Migration Behavior of Actinides and Fission Products in the Geosphere
Lake Tahoe, Nevada/California, USA, 26.09.-01.10.1999

Bernhard, G., Friedrich, H., Nitsche, H.
A new Radiochemistry Building for the Institute of Radiochemistry of the Research Center Rossendorf
-Construction and Radiation Protection Aspects-
Jahrestagung Kerntechnik ´99
Karlsruhe, Germany, 18.-20.05.1999

Geipel, G., Bernhard, G., Brendler, V., Rutsch, M., Nitsche, H.
Spectroscopic properties of Uranium(VI) Minerals studied by Time-Resolved Laser Induced Fluorescence Spectroscopy (TRLFS)
Migration ’99, 7th International Conference on the Chemistry and Migration Behavior of Actinides and Fission Products in the Geosphere
Lake Tahoe, Nevada/California, USA, 26.09.-01.10.1999

Giacomini, A., Struffi, P., Selenska-Pobell, S., Tola, E., Venramin, E., Dazzo, F., Casella, S., Nuti, M., Squartini, A.
Evidences for the proposal of a new species of *Rhizobium* nodulating *Hedysarum coronarium*

9th International Congress on Molecular Plant-Microbe Interactions
Amsterdam, The Netherlands, 25.-30.07.1999

Hennig, C., Reich, T., Roßberg, A., Funke, H., Rutsch, M., Geipel, G., Hitsche, H., Bernhard, G.
Local Structure Analysis of Uranium Phosphates and Arsenates using EXAFS Spectroscopy
DGK-Tagung
Leipzig, Germany, 08.-10.03.1999

Krawczyk-Bärsch, E., Schmeide, K., Arnold, T., Heise, K.H., Bernhard, G.
Untersuchung zur Sorption von Huminsäure und Uran(VI) an den Kristallflächen des Schichtsilikates Muskovit
Workshop „Radiochemische Analytik beim Betrieb und Rückbau kerntechnischer Anlagen, der Deklaration von Abfällen und im Strahlenschutz"; VTKA Rossendorf
Dresden, Germany, 06.-07.09.1999

Kutschke, S., Selenska-Pobell, S.
Molecular characterization of *Thiobacillus* strains recovered from uranium mining waste piles
Jahrestagung 1999 der Vereinigung für Allgemeine und Angewandte Mikrobiologie
Göttingen, Germany, 07.-10.03.1999

Kutschke, S., Selenska-Pobell, S.
Molecular characterization of *Thiobacillus* strains recovered from uranium mining waste piles
International Symposium on Bacterial Genetics and Ecology
Florence, Italy, 19.-24.06.1999

Moll, H., Reich, T., Hennig, C., Rossberg, A., Szabó, Z., Grenthe, I.
Solution coordination chemistry of uranium in the binary $UO_2^{2+}$ - $SO_4^{2-}$ and the ternary $UO_2^{2+}$ - $SO_4^{2-}$ - $OH^-$ system
Migration '99, 7th International Conference on the Chemistry and Migration Behavior of Actinides and Fission Products in the Geosphere
Lake Tahoe, Nevada/California, USA, 26.09.-01.10.1999

Raff, J., Kirsch, R., Kutschke, S., Mertig, M., Selenska-Pobell, S., Bernhard, G., Pompe, W.
The surface layer protein of *Bacillus sphaericus* isolate JG A-12 from a uranium waste pile
99th General Meeting of American Society for Microbiology
Chicago, USA, 30.05.-03.06.1999

Rettig, D., Adam, R., Merker, P.
Aerosol formation by UV irradiation of paraffine and silicone vapors
EAC '99 European Aerosol Conference 1999
Prague, Czech Republic, 06.-10.09.1999

Richter, W., Hüttig, G., Zänker, H.
Charakterisierung der Kolloidpartikel im Entwässerungsstollen des Freiberger Bergbaureviers (Rothschönberger Stolln)
5. Kolloquium DFG Schwerpunktprogramm "Geochemische Prozesse mit Langzeitfolgen im anthropogen beeinflußten Sickerwasser und Grundwasser"
Bad Herrenalb, Germany, 25.-26.03.1999

Roßberg, A., Baraniak, L., Reich, T., Hennig, C., Bernhard, G., Nitsche, H.
EXAFS structural analysis of aqueous uranium(VI) complexes with wood degradation products
Migration '99, 7th International Conference on the Chemistry and Migration Behavior of Actinides and Fission Products in the Geosphere
Lake Tahoe, Nevada/California, USA, 26.09.-01.10.1999

Rutsch, M., Geipel, G., Pompe, S., Schmeide, K., Bernhard, G.
Zeitaufgelöste Laserinduzierte Fluoreszenzspektroskopie mit Ultrakurzen Pulsen: Experimentelles Setup und Anwendungsbeispiele
ANAKON, GDCh-Fachtagung Analytische Chemie
Konstanz, Germany, 07.-10.04.1999

Rutsch, M., Geipel, G., Baraniak, L., Bernhard, G., Nitsche, H.
Time-Resolved Laser-Induced Fluorescence Spectroscopy with Pico- and Femtosecond Excitation Pulses: Studies of Complex Formation of U(VI) and Lignin Degradation Products
Migration '99, 7th International Conference on the Chemistry and Migration Behavior of Actinides and Fission Products in the Geosphere
Lake Tahoe, Nevada/California, USA, 26.09.-01.10.1999

Schmeide, K., Pompe, S., Bubner, M., Heise, K.H., Bernhard. G.
Einfluß von Huminsäure auf die Uranyl(VI)-Sorption an Phyllit und seinen mineralischen Bestandteilen

Workshop ‘Radiochemische Analytik beim Betrieb und Rückbau kerntechnischer Anlagen, der Deklaration von Abfällen und im Strahlenschutz’
Dresden, Germany, 06.-07.09.1999

Schmeide, K., Pompe, S., Bubner, M., Heise, K.H., Bernhard. G., Nitsche, H.
Effect of Humic Acid on the Uranium(VI) Sorption onto Phyllite and its Mineralogical Constituents
Migration ’99, 7th International Conference on the Chemistry and Migration Behavior of Actinides and Fission Products in the Geosphere
Lake Tahoe, Nevada/California, USA, 26.09.-01.10.1999

Taut, S.
CORA - A News Control Program for the ROMA Detection System
1st Int. Conf. on the Chemistry and Physics of the Transactinide Elements
Seeheim, Germany, 26.-30.09.1999

Wober, J., Flemming, K., Hard, B., Pietsch, K., Selenska-Pobell, S.
Classification of *Desulfovibrio* isolates recovered from a uranium mining waste pile
Jahrestagung 1999 der Vereinigung für Allgemeine und Angewandte Mikrobiologie
Göttingen, Germany, 07.-10.03.1999

Wober, J., Flemming, K., Selenska-Pobell, S.
Characterisation of *Desulfovibrio* isolates recovered from a uranium mining waste pile
International Symposium on Bacterial Genetics and Ecology
Florence, Italy, 19.-24.06.1999

# III. SEMINARS, CONFERENCES AND WORKSHOPS

## INSTITUTE SEMINARS

Prof. Dr. Renate Klöcking
Friedrich-Schiller-Universität Jena, Institut für Antivirale Chemotherapie
Biologische Wirkungen von Huminsäuren - Indizien für ein einheitliches chemisches Strukturprinzip
28.01.1999

Dr. Fritz Neuweiler, Dr. Andreas Reimer
Georg-August-Universität Göttingen, Institut und Museum für Geologie und Paläontologie
Die geohistorische Bedeutung mariner Huminsubstanzen bei der Bildung mikrokristalliner Karbonate - eine Projektskizze (SFB 468)
04.03.1999

Dr. habil. Wolfgang Dedek
Universität Leipzig
Geschichte der radioaktiven Elemente: Die Entdeckung von Radium und Polonium im Jahre 1898
25.03.1999

Dr. Wolfgang Seidel
FZ Rossendorf
Projekt eines “Freie-Elektronen-Lasers” im FZR und mögliche Anwendungen
15.04.1999

Dr. Galina Radewa
Bulgarian Academy of Science, Institute of Molecular Biology, Sofia, Bulgaria
Molecular Analysis of Natural Bacterial Populations in Uranium Contaminated Wastes
02.06.1999

Dr. Silvia Roßbach
Western Michigan University, Department of Biological Sciences, Kalamazoo, Michigan, USA
Heavy Metal-Regulated Gene Expression in Soil Bacteria
05.08.1999

Dr. Richard Ankerhold
Carl Zeiss Jena GmbH, European Competence Center - ECC
SM 510 - Neue Strategien in der Konfokalen Laser Scanning Mikroskopie
14.09.1999

Prof. Dr. David Balkwill
Florida State University, Tallahassee, USA
Characterization of Bacteria that Can Interact with Organic and Inorganic Contaminants in Subsurface Environments
17.09.1999

Prof. Dr. Max Mergeay
Laboratory of Microbiology, Radioactive Waste & Clean-up Division, SCK/CEN, Mol, Belgium
Metal-Risistant Soil Bacteria Belonging to the Ralstonia Genus: From Molecular Biology to Environmental Biotechnology
23.09.1999

Dr. habil. Wolfgang Dedek
Universität Leipzig
Uran und Radium im Sächsisch-Böhmischen Erzgebirge
26.10.1999

Prof. Dr. Yu.A. Babanov
Institute of Metal Physics, Russian Academy of Sciences, Yekaterinburg, Russia
EXAFS study of disordered Ni-Mn alloys
Rossendorf Beamline, ESRF, Grenoble, France
04.11.1999

Dr. Thilo Hoffmann
Universität Mainz, Institut für Geowissenschaften
Kolloidaler Stofftransport: Relevanz für die künstliche Grundwasseranreicherung
16.11.1999

## **INTERNAL SEMINARS** (open for the public)

S. Kutschke
Phylogenetische und genomische Charakterisierungsmethoden
15.03.1999

W. Richter
Kolloidchemische Untersuchungen an Wasser aus dem Hauptentwässerungsstollen des Freiberger Bergbaureviers
18.03.1999

M. Horn (TU BA Freiberg)
Mikroskopische Untersuchungen an Eibenstocker Granit hinsichtlich Uransorptionsbestimmungen (Praktikumsbericht)
31.03.1999

T. Zorn
Adsorption von Uran an Phyllit
26.04.1999

K. Jantsch, VKTA
Vorstellung des Radiochemischen Labors des VKTA Rossendorf e.V. für stilllegungsbegleitende Aufgaben
06.05.1999

H. Zänker
Charakterisierung der Kolloidpartikel im Hauptentwässerungsstollen des Freiberger Bergbaureviers (Rothschönberger Stolln)
07.05.1999

M. Merroun
Cellular localization of heavy metals and radionuclides accumulated by *Myxococcus xanthus* and toxicity of lead on this bacterium using flow cytometry
10.06.1999

K. Nakata (University of Tokyo)
Sorption of Np(V) on Iron Oxides
08.09.1999

E. Krawczyk-Bärsch
Chemische und strukturelle Charakterisierung der Verwitterungsprozesse von mittelalterlichen Gläsern - Eine elektronenmikroskopische Studie
02.11.1999

## **CONFERENCES / WORKSHOPS** (organized by Institute of Radiochemistry)

5$^{th}$ EU PROJECT MEETING
Effects of Humic Substances on the Migration of Radionuclides: Complexation and Transport of Actinides (Project No.: FI4W-CT96-0027)
Rossendorf, Germany, 17.-19.05.1999

K. Schmeide, S. Pompe, M. Bubner, K.H. Heise, G. Bernhard
Effects of Humic Substances on the Migration of Radionuclides: Complexation and Transport of Actinides - Summary of the Contribution from the Institute of Radiochemistry to the EC Project No. FI4W-CT96-0027

K. Schmeide, S. Pompe, M. Bubner, K.H. Heise, G. Bernhard,
Effect of Humic Substances on the Uranium Sorption onto Phyllite - Kinetic Studies of the Uranium and Humic Acid Sorption

K. Schmeide, S. Pompe, T. Reich, M. Bubner, K.H. Heise, G. Bernhard
EXAFS Study of the Interaction of Uranium(VI) with Humic Substances

K. Schmeide, G. Geipel, K.H. Heise, G. Bernhard
Case-Study: Uranium-Mining Rock Pile No. 250 in the Region Schlema/Alberoda (Saxony, Germany)

H. Zänker, M. Mertig, M. Böttger, G. Hüttig, S. Pompe
Photon Correlation Spectroscopy and Scanning Force Microscopy on Humic Acid

GERMAN-CZECH WORKSHOP ON ENVIRONMENTAL PROBLEMS OF URANIUM SITES
Forschungszentrum Rossendorf, Institut für Radiochemie
Nuclear Research Institute (NRI) Ì eñ, Waste Disposal Department

VKTA Rossendorf, Fachbereich Analytik
Rossendorf, Germany, 04.05.1999

*Lectures*

Dr. P.Lietava, NRI Rez
Risk Assessment Model for the Evaluation of Environmental Remediation Options at the Straz Underground Uranium Leaching Site

P. Franta, NRI Rez
Basic Technologies Used for ISL Remediation at the Straz Site

R. Knappik, K. Fleischer, VKTA Rossendorf
Investigations of Hydrochemical Processes during the Flooding of the Uranium Mines Schlema, Alberoda, and Pöhla

K.-H.Heise, FZ Rossendorf
Synthetic Humic Acid - a Tool to Study Environmental Problems

*Posters*

J. Slovak, P. Franta, NRI Rez
Elimination of Hazardous Elements and Compounds from the ISL Uranium Mining in the Czech Republic

G. Geipel, M. Thieme, G. Bernhard, FZ Rossendorf
Distribution of Natural Radionuclides in a Mine Tailing Pile from Uranium Mining in Schlema and the Release of Seepage Water

L. Baraniak, M. Thieme, H. Funke, G. Bernhard, K. Nindel, J. Schreyer
FZ Rossendorf and Wismut GmbH, Chemnitz
Radium Adsorption on Sediments of the Upper Saxonian Elbe River Basin

L. Baraniak, G. Bernhard, H. Nitsche, K. Jelen, R. Schiene, K. Fischer
FZ Rossendorf and TU Dresden
Hydrothermal Mine Wood Decomposition and Influence of the Degradation Products on Metamorphic Rocks and Sediments

WORKSHOP: EU-PROJEKTE IM INSTITUT FÜR RADIOCHEMIE
Rossendorf, Germany, 06.07.1999

H. v. Maravic (EC)
The Fifth Frame Work Programe

K. Schmeide, S. Pompe, M. Bubner, K.H. Heise, G. Bernhard
Effects of humic substances on the migration of radionuclides: Complexation and transport of actinides - Summary of the contribution from the Institute of Radiochemistry to the EC project no. FI4W-CT96-0027

S. Pompe, R. Artinger, K. Schmeide, K.H. Heise, G. Bernhard, J.I. Kim
Investigation of the migration behavior of uranium in an aquifer system rich in humic substances: column experiments

H. Zänker, M. Mertig, M. Böttger, G. Hüttig
Photonenkorrelationsspektroskopie und Rasterkraftmikroskopie an Huminsäure

V. Brendler
Überblick und Ergebnisse zu den EU-Projekten: JETDEM und RESTRAT

# IV. PERSONNEL

# PERSONNEL

## Director

Prof. Dr. G. Bernhard (acting, since November 1, 1998)

## Administrative Staff

G. Kreusel*
A. Nagel
H. Pospischil

## Scientific Staff

Prof. Dr. U. Abram
Dr. T. Arnold*
Dr. L. Baraniak
Prof. Dr. G. Bernhard
DC D. Birnstein
Dr. V. Brendler+
Dr. M. Böttger*
Dr. M. Bubner
Dr. H.-J. Engelmann
Dr. E. Förster*
Dr. H. Funke
Dr. G. Geipel
Dr. A. Günther*
Dr. K.H. Heise
Dr. C. Hennig+
Dr. S. Hübener
Dr. E. Krawczyk-Bärsch
Dr. K. Krogner
Dr. G. Mainka+
Dr. P. Merker
Dr. M. Merroun+
DC C. Nebelung
DI K. Nicolai*
Dr. S. Pompe*
Dr. C. Puers+
Dr. T. Reich
Dr. D. Rettig*
Dr. W. Richter*
Dr. S. Selenska-Pobell
Dr. K. Schmeide*
Dr. G. Schuster*
Dr. S. Taut*
Dr. A. Vahle*
Dr. W. Wiesener
DBC J. Wober*
Dr. H. Zänker

## Technical Staff

DI(FH) B. Barz*
DI(FH) C. Eckardt
B. Eisold
DBC K. Flemming*
J. Falkenberg
DI(FH) H. Friedrich
Ch. Fröhlich
Dl(FH) G. Grambole
G. Heinz
S. Heller*
DI(FH) K. Henkel
B. Heschel
H. Heyne
B. Hiller
DI(FH) G. Hüttig
DI(FH) R. Jander
P. Kluge
DI(FH) M. Meyer
Ch. Müller
H. Neubert
A. Rumpel
R. Ruske
DI(FH) U. Schaefer

## Graduate Students

DC A. Abraham
DC S. Amayri
DBT S. Kutschke
DB J. Raff
DC A. Roßberg
DC M. Rutsch
DBC G. Sachanska*
DC B. Schmidt-Brücken
DC T. Zorn

## Trainee

K. Berger
A. Grenner
C. Heidel
M. Horn
P. Jährig
C. Reichelt
S. Wallner

+ post doc
* term contract

DC: Dipl.-Chem.
DI: Dipl.-Ing.
DBC: Dipl.-Biochem.
DBT: Dipl.-Biotech.
DB: Dipl.-Biol.

## Guest Scientists

| | |
|---|---|
| Prof. Dr. David Balkwill | Department of Biological Science, Florida State University, Tallahassee, Florida, USA |
| Prof. Dr. Yuri A. Babanov | Institute of Metal Physics, Russian Academy of Sciences, Yekaterinburg, Russia |
| Dr. Julio Benitez | University of Montevideo, Uruguay |
| DC Anatoly Chernyshev | Institute of Biochemistry and Physiology of Plants and Microbiology, Russian Academy of Science, Saratov, Russia |
| Dr. Anna Doytcheva | Department of Geomicrobiology, University of Sofia, Sofia, Bulgaria |
| Gwendolyn Drake | Department of Biological Science, Florida State University, Tallahassee, Florida, USA |
| Dr. Oksana Fomina | Institute of Biochemistry and Physiology of Plants and Microbiology, Russian Academy of Science, Saratov, Russia |
| Dr. Veneta Groudeva | Department of Geomicrobiology, University of Sofia, Sofia, Bulgaria |
| Dr. Konstantin Guerman | Institute of Physical Chemistry, Russian Academy of Sciences, Moscow, Russia |
| Prof. Dr. Max Mergeay | Laboratory of Microbiology, Radioactive Waste & Clean-up Division, SCK/CEN, Mol, Belgium |
| DC Kotaro Nakata | University of Tokyo, Department of Quantum Engineering and Systems Science, Tokyo, Japan |
| Dr. Fritz Neuweiler | Universität Göttingen, Institut und Museum für Geologie und Paläontologie, Göttingen, Germany |
| Dr. Galina Radeva | Institute of Molecular Biology, Bulgarian Academy of Sciences, Sofia, Bulgaria |
| Dr. Silvia Rossbach | Western Michigan University, Department of Biological Sciences, Kalamazoo, USA |
| Dipl.-Biol. Galina Satschanska | Institute of Molecular Biology, Bulgarian Academy of Sciences, Sofia, Bulgaria |
| Dipl.-Biol. Irena Tzvetkova | Department of Geomicrobiology, University of Sofia, Sofia, Bulgaria |
| Dipl.-Biol. Tzvetelina Tzvetkova | Department of Geomicrobiology, University of Sofia, Sofia, Bulgaria |
| Dr. Andreas Voigt | Universität Leipzig, Institut für Anorganische Chemie, Leipzig, Germany |
| Dr. Christopher White | University of Dundee, Department of Biological Sciences, Dundee, United Kingdom |
| Dr. Ping Yong | School of Biological Sciences, University of Birmingham, Edgbaston Birmingham, United Kingdom |

# V. ACKNOWLEDGMENTS

## ACKNOWLEDGMENT OF FINANCIAL SUPPORT

The Institute is part of the Forschungszentrum Rossendorf e.V., which is financed in equal parts by the Federal Republic of Germany and the Free State of Saxony.

Seven projects were supported by the Bundesministerium für Bildung, Wissenschaft, Forschung und Technologie (BMBF):

- Stillegung und Rückbau: Direktmessung "-aktiver Nuklide in Bauschutt zur Freigabeentscheidung.
  Contract No. BMBF 02 S 7655 A8
- Stillegung und Rückbau: Schnelles Freimeßverfahren für "-aktive Nuklide in Bauschutt durch Direktmessung von großflächigen dünnen Meßpräparaten - Automatisierung des Verfahrens -
  Contract No. BMBF 02 S 7768
- Chemie der schwersten Elemente: Hochtemperaturgaschromatographie der Elemente 106 und 107
  Contract No. BMBF 06 DR 824 (2)
- Influence of humic acids on migration behavior of radioactive and non-radioactive heavy elements under natural conditions.
  Contract No. BMBF 02 E 88150
- Biosorption of uranium by bacillus for remediation of uranium wastes
  Contract No. DRL: BUL-014-97
- **S** Abtrennung von Uran aus Sicker- und Grundwässern mit uranophilen Calixarenen
  Contract No. UTRP 01722599
- **S** Untersuchung über die Komplexierung und die Migration von Actiniden und nichtradioaktiven Stoffen mit Huminsäuren unter geogenen Bedingungen - Komplexierung von Huminsäuren mit Actiniden in der Oxidationsstufe IV, Th, U, Np
  Contract No. PTE 02E92999

Four projects were supported by Commission of the European Communities:

- Restoration Strategies for Radioactive Contaminated Sites and their Close Surroundings (RESTRAT).
  In collaboration with:
  SCK-CEN Mol, Belgium; Studsvik Ecosafe AB, Sweden; Riso National Laboratory, Danmark; Westlakes Scientific Consulting, Great Britain
  Contract No. F14P-CT95-0021
- Cooperative Network Matching EU and FSU Activities in the Field of Nuclear Fission Safety (NETWORK/NNFS).
  In collaboration with:
  JRC Ispra, Italy; SIEVERT Moscow, Russia; UIOP Kiew, Ukraine; INTERPROJECT Minsk, Weißrußland
  Contract No. F14C-CT96-0016
- Effects of Humic Substances on the Migration of Radionuclides: Complexation and Transport of Actinides.
  In collaboration with:
  FZ Karlsruhe, Inst. f. Nukleare Entsorgungstechnik, Germany; British Geological Survey, Nottingham, United Kingdom; Centre d' Etudes des Saclay, CEA, France; Katholicke Universiteit Leuven, Labor voor Colloidchemie, Heverlee, Belgium; Loughborough University, Dept. of Chemistry, Leicestershire, United Kingdom; University of Manchester, Dept. of Chemistry, Manchester, United Kingdom; National Environmental Research Institute, Roskilde, Denmark; GSF Forschungszentrum für Umwelt und Gesundheit, Oberschleißheim, Germany; Université de Nantes, Laboratorie de Biochimie at Radiochimie, Nantes, France
  Contract No. F14W-CT96-0027
- Joint European Thermodynamic Database for Environmental Modeling (JETDEM).
  In collaboration with:
  FZ Karlsruhe, Germany; RCM Environmental Ltd., United Kingdom; Kungliga Tekniska Hogskolan, Department of Chemistry, Sweden; University of Aberdeen, Department of Chemistry, United Kingdom; Quantisci, Spain; Uppsala University, Institute of Earth Sciences, Sweden
  Contract No. F14W-CT96-0029

The Sächsisches Staatsministerium für Wissenschaft und Kunst provided support for the following projects:

- Mine-water Induced Wood Decomposition and Influence of the Degradation Products on Radionuclide Speciation, Sorption and Migration.
  Contract No. SMWK 4-7541.83-FZR/402

- Influence of Natural Water-borne Organic Substances on the Valency of Radionuclides and Toxic Heavy Metals.
  Contract No. SMWK 4-7541.88-FZR/512
- Soil-Plant Transfer Factors for Uranium.
  Contract No. SMWK 4-7531.50-03-VKTA/601
- Wechselwirkung von Mikroorganismen mit Uran und ausgewählten Radionukliden: Charakterisierung der Biosorption und ihrer genetischen Grundlagen mit Hinblick auf Ausbreitungsverhalten und Bioremedation.
  Contract No. SMWK 4-7531.50-03-FZR/607
- Charakterisierung und Klassifizierung von Bakterien aus uranhaltigen Halden mit Hinblick auf Bioremediation: Bakterielle Diversität, Populationsdynamik und Bioakkumulation von Uran und ausgewählten Radionukliden durch Bakterien. (Fortsetzung)
  Contract No. SMWK 4-7531.50-03-FZR/607
- Wechselwirkung zwischen Proteinen und Metalloberflächen. Teilvorhaben C: Wechselwirkung von bakteriellen Zellhüllenproteinen mit Metallclustern.
  Contract No. SMWK 4-7531.50-03-0370/708
- Untersuchung der Bildung von kolloidalen organischen Partikeln in Bergwerkswässern.
  Contract No. SMWK 4-7533.70-FZR/704
- Natural acidophillic bacterial populations in uranium wastes.
  Contract No. SMWK 4-7531.50-04-844-99/4
- Chemical conversion of $^{14}C$-labeled products to [$^{14}C$]Barium carbonate for long-time disposal.
  Contract No. SMWK 4-7581.312/20
- Vortragstagung der GDCh-Fachgruppe Nuklearchemie
  Contract No. SMWK 4-7531.50-05-98/35
- Sequence analysis of the 16S rDNA from *Pseudomonas "vanadiumreductans"* and *Pseudomonas "isachenkovii"*
  Contact Fellowship from the HSP-III

One project was supported by Sächsisches Staatsministerium für Wirtschaft und Arbeit:

- Festelektrolytsensoren für die Messung von Verunreinigungen in flüssigem Stahl.
  In cooperation with Herbst GmbH Wärmekeramik, Dürrröhrsdorf.
  Projekt Nr. 1500/309

Nine projects were supported by Deutsche Forschungsgemeinschaft (DFG):

- Experimentelle Untersuchung der Eigenschaften schwerer Actinoide im elementaren Zustand mittels chromatographischer Methoden.
  Contract No. DFG HU 642/1-2
- Identifizierung und Charakterisierung von Komplexierungsprodukten des U(VI) in Pflanzen.
  Contract No. DFG BE 2234/1-1

**S** Komplexierung von Uranyl- und Neptunylionen mit phenolischen Monomeren des natürlichen Ligninabbaus als Grundlage für die Beschreibung der Radionuklidausbreitung
Contract No. DFG BE 2234/3-1

**S** Heterogene Reaktionsmechanismen und deren Kinetik an Schichtsilikatoberflächen
Contract No. DFG BE 2234/4-2

- Nitridobrücken zwischen Übergangsmetallen und Hauptgruppenelementen.
  Contract No. DFG AB 67-4/1
- Nitridobrücken zwischen Rhenium und Elementen der 3. Hauptgruppe.
  Contract No. DFG AB 67-4/2
- Charakterisierung der Kolloidpartikel in den Wasserfließsystemen stillgelegter sächsischer Bergwerke
  Contract No. DFG ZA 238/1-3
- Untersuchungen zur Sorption von Uranylionen an Huminsäurebioschichten auf Phyllit und seinen mineralischen Bestandteilen
  Contract No. DFG NI 210/5-1
- Untersuchung der Sorptionsmechanismen von Uran(VI) auf Gesteins- und Mineraloberflächen. Identifizierung und Modellierung der sorbierten Oberflächenspezies auf molekularer Ebene.
  Contract No. DFG NI 210/6-1

Seven projects were supported by the following sponsors:

- Development of experimental arrangements and methods for on-line high temperature gas-chromatography of the heaviest elements.
  In cooperation with GSI.
  GSI DRNIK.
- INTAS: Spectroscopic study of particles emitted by nuclear fuel under different accident scenarios.
  Contract No. INTAS 96-1927
- Fundamental Technetium, Rhenium and Gold Chemistry.
  Contract No. DAAD ARC-XI-97/1
- Molecular analysis of natural bacterial communities in uranium wastes.
  ESF scientific programme: “Ground water pollution”
  Contract No. Gpoll/9816
- Euroconference “Speciation, techniques, and facilities for radioactive materials at synchrotron light sources”
  Contract No. EU/ERBFMMACT98-0331
- Euroconference “Bacterial-Metal/Radionuclide Interaction: Basic Research and Bioremediation”
  Contract No. EU/ERBFMMACT98-0339
- NATO Collaborative Research Grant “Speciation of radionuclides in environmentally relevant systems by XAFS spectroscopy”
  Contract No. SA.5-2-05(CRG.971641)